Novel pleiotropic regulators of gas vesicle biogenesis in *Serratia*.

Alex Armando Quintero Yanes

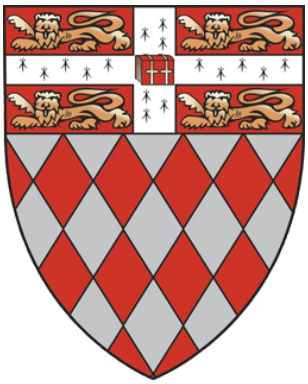

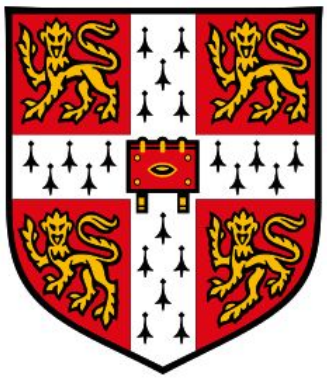

Department of Biochemistry

Fitzwilliam College, University of Cambridge

September 2018

This dissertation is submitted for the degree of Doctor of Philosophy

Novel pleiotropic regulators of gas vesicle biogenesis in *Serratia*

Alex Armando Quintero Yanes

Summary

Serratia sp. ATCC 39006 (S39006) is known for producing carbapenem and prodiginine antibiotics; 1-carbapen-2-em-3-carboxylic acid (car) and prodigiosin. It displays different motility mechanisms, such as swimming and swarming aided by flagellar rotation and biosurfactant production. In addition, S39006 produces gas vesicles to float in aqueous environments and enable colonization of air-liquid interfaces. Gas vesicles are thought to be constructed solely from proteins expressed from a gene cluster composed of two contiguous operons, *gvpA1-gvpY* and *gvrA-gvrC*. Prior to this study, three cognate regulators, GvrA, GvrB, and GvrC, encoded by the right hand operon were known to be essential for gas vesicle synthesis. Post-transcriptional regulators such as RsmA-*rsmB* were also known to be involved in the inverse regulation of gas vesicles and flagella based motility. Furthermore, gas vesicle formation, antibiotic production, and motility in S39006 were affected by cell population densities and de-repressed at high cellular densities through a quorum sensing (QS) system. The aim of this research study was to identify novel regulatory inputs to gas vesicle production. Mutants were generated by random transposon mutagenesis followed by extensive screening, then sequencing and bioinformatic identification of the corresponding mutant genes. After screening, 31 mutants and seven novel regulatory genes impacting on cell buoyancy were identified. Phenotypic and genetic analysis revealed that the mutations were pleiotropic and involved in cell morphology, ion transport and central metabolism. Two new pleiotropic regulators were characterized in detail. Mutations in an ion transporter gene (*trkH*) and a putative transcriptional regulator gene *(floR*) showed opposite phenotypic impacts on flotation, flagella-based motility and prodigiosin, whereas production of the carbapenem antibiotic was affected in the transcription regulator mutant. Gene expression assays with reporter fusions, phenotypic assays in single and double mutants, and proteomics suggested that these regulatory genes couple different physiological inputs to QS and RsmA-dependent and RsmA-independent pathways.

Declaration

This dissertation is the result of my own work and includes nothing which is the outcome of work done in collaboration except as declared in the Preface and specified in the text.

It is not substantially the same as any that I have submitted, or, is being concurrently submitted for a degree or diploma or other qualification at the University of Cambridge or any other University or similar institution except as declared in the Preface and specified in the text. I further state that no substantial part of my dissertation has already been submitted, or, is being concurrently submitted for any such degree, diploma or other qualification at the University of Cambridge or any other University or similar institution except as declared in the Preface and specified in the text

It does not exceed the 60,000 world limit set by the Degree Committee for the Faculty of Biology.

Alex Armando Quintero Yanes

September 2014.

Acknowledgements

First and foremost, I "*give thanks to the LORD, for his love endures for ever*" (*Psalm 136*).

My thanks to Professor George Salmond, my PhD supervisor, for his support and for the way he has always encouraged me to be critical and independent as a scientist. This started with his support for my application to undertake a PhD in Biochemistry at the University of Cambridge, and continued with his letters of recommendation enabling me to receive grants of the Cambridge Philosophical Society, Cambridge trust and Microbiology Society. I will not forget our conversations about such diverse topics as gas vesicles, bacterial genetics and physiology, synthetic biology, politics, religion and history – greatly enriching my time in Cambridge. Working under his mentorship has contributed greatly to the formation of my approach to the many unknowns of the world of microbiology. Thank you, George – many, many thanks.

Thanks to my funding body, the Cambridge Trust for awarding me with the Cambridge International Scholarship and being attentive to my development throughout my studies. Also, for giving me an extension that eased my life during the last year of my studies. Many thanks.

I am grateful to the members of the Salmond Lab: specially to Alison Rawlinson for her technical support and for her friendly smiles and patient conversation when I made mistakes. To be able to pick up our friendship is one of the things I most hope to do once the PhD is behind me. Thanks to Dr. Rita Monson for her technical supervision of my PhD experiments, for her comments on this document and for her advice on how best to enjoy my time in Cambridge. Thank you for sharing your good judgement both inside and outside the lab. Thanks to Bihe Chen from whom I caught a spirit of commitment and hard work – I learnt a lot from you. Ray Chai, Sam Magaziner, Dr. Chin Mei Lee and Andy Day were always ready to listen to me when I needed to discuss my experiments and to offer their own critical perspectives. And thanks to Ziyue Zeng and Megan Booth, for their friendship and for always showing concern for my wellbeing.

Thanks to Dr. Chin Mei Lee from the Salmond Lab, and Dr. Mike Deery and Dr. Marco Chiapello from the Cambrigde Centre for Proteomics (CCP) for their collaboration with the proteomics experiments and advices on data analysis. The proteomics experiments were done in conjunction with Dr. Chin Mei Lee to save cost on the analysis of mutations studied in this project and Dr. Lee's PhD project. All the experimental procedures specified in the Appendix sections 7.1-7.4 were performed by the CCP scientific staff.

My thanks to all in the Welch Lab and the Hee Jong Lab: to Dr. Martin Welch for all his contributions to my research during group meetings – his critical input helped to shape my research. Thanks to Ash for his friendliness and encouragement, to Ahir for his cheerfulness and good humour, to Larson for those times when we left the routine of the lab to enjoy a beer and watch a game of football, and to Stephen and Yasmin for their technical help and their good humour as we discussed protein expression experiments.

I would like to thank the administrative personnel in the Department of Biochemistry, especially Ming, Lyang, Sue, Shanon, Clova, Maurice, Janet, Steph and Latika. Thank you for your hard work and friendliness, and for the smiles every time our paths crossed. You added to the joy I felt at the start of each working day.

Thanks to my friends in Fitzwilliam: to the college and its staff in general for providing a suitable space for students from all over the world to live together harmoniously; and to my friends Ante, Ardi, Chinedu and Mohamed for all our conversations. You made my social life in Cambridge into an opportunity for growth, both intellectually and as a human being.

Thanks to the Christian community which provided a home during my time in Cambridge, specially to my friends in the Chrisitan Graduate Society, CENTI and Saint Matthew's. To Ben, Bruno, Godwin and Kevin for those conversations "salted" with understanding, humility and fellowship. From you I learnt that "*there are friends who stick together closer than a brother*" (*Proverbs 18:24*). To Bartow and Marianne, thanks for your listening ear and advice, and for including my wife and me in your lives with such love. To Carlos, Deydamia, Ruben and Victor,

thanks for the trust you placed in me, and for the sacrificial and affectionate way you cared for my wife and me. And to Emiliy Nicolic, for her comments on this document.

Thanks to my parents and other family members. To my Father for his example in overcoming obstacles and for the pride he showed in my Cambridge studies. Thank you for battling on – every time I hear or see you my heart is filled with joy. To my Mother for her sacrifice and support in all I have undertaken. Your example saved my life. Thank you for your persistence and your dedication, for putting my education ahead of luxuries for yourself, and for your daily prayers for me. And thanks to my uncles and aunts, standing in for my parents in supporting when it was necessary.

To my wife, Diana Herrera, thank you for leaving everything to be at my side in the last part of my studies. Thank you for the way you listened with interest to the daily ups and downs of my research. Thank you for your patience when I arrived home late at night after long days in the lab, and even during the write-up of this thesis. Thank you for making our house into a home where I always wanted to return after a day in the lab. Thank you for softening my life with your love. I love you.

Once again, thank you all.
Alex.

Contents

List of Figures

List of Tables

Abbreviations

A	
Amp	ampicillin
Amp^R	ampicillin resistance
APS	ammonium persulphate
ATCC	american tissue culture collection
A_{xxx}	absorbance, wavelength denoted by $_{xxx}$
B	
BHL	n-butanoyl-$_L$-homoserine lactone
bp	base pair
C	
Car	1-carbapenen-2-em-3-carboxylic acid
cfu	colony forming units
Cm	chloramphenicol
cm	centimetre
Cm^R	chloramphenicol resistance
D	
DAPA	diaminopimelic acid
dH_2O	deionised water
DNA	deoxyribonucleic acid
dNTPs	deoxyribonucleoside triphosphate
DTT	dithiothreitol
E	
EDTA	ethylenediaminetetraacetic acid
Em	erythromycin
Em^R	erythromycin resistance
F	
FloR	Flotation regulator
G	
g	gram
g	gravity force

H

h	hours
His	histidine

I

IPTG	isopropyl β-d-1-thiogalactopyranoside

K

Kbp	kilo base pair
KDa	kilo daltons
Km	kanamycin
Km^R	kanamycin resistance

L

l	litre
LB	luria broth
LC-MS/MS	liquid chromatography–mass spectrometry
LPS	lipopolysaccharide

M

M	molar
min	minutes
mg	milligram
ml	millilitre
mM	millimolar
mRNA	messenger ribonucleic acid

N

NEB	new england biolabs
ng	nanogram
nl	nanolitre

O

O.N.	over night
OD_{xxx}	optical density, wavelength denoted by $_{xxx}$

P

PCM	pahse contrast microscopy

PCR	polymerase chain reaction
prodigiosin	2-methyl-3-pentyl-6-methoxyprodigiosin
Q	
QS	quorum sensing
R	
RFU	relative fluorescence units
RNA	ribonucleic acid
RP PCR	random primed pcr
Rpm	revolutions per minute
S	
S39006	*Serratia* sp. ATCC 39006
SDS	sodium dodecyl (lauryl) sulphate
SDS-PAGE	sodium dodecyl sulphate-polyacrilamyde gel electrophoresis
Sm	streptomycin
Sp	spectinomycin
Sp^R	spectinomycin resistance
T	
Tc	tetracycline
Tc^R	tetracycline resistance
TEM	trasmision electron microscopy
TEMED	tetramethylethylenediamine
V	
v/v	volume/volume
W	
w/v	weight/volume
WT	wild type
μg	microgram
μl	microlitre

Chapter 1
Introduction

1.1 *Serratia* sp. ATCC 39006

Serratia sp. strain ATCC 39006 (S39006) is a rod-shaped Gram-negative bacterium. It was initially found as a free-living organism and associated with roots and stems of halophytic bushes in salt marshes, and it became of clinical interest for producing antibiotic, immunosuppressive, and anticancer compounds (Parker *et al.,* 1982; Williamson *et al.,* 2007). S39006 is also a pathogen that affects potato tubers by producing cellulases and pectate lyases, and kills the microscopic worm *Caenorhabditis elegans* through yet unknown mechanisms (Coulthurst *et al.,* 2004; Fineran *et al.,* 2007). S39006 displays different mechanisms for moving and persisting in different environments; it swims and floats in liquid cultures, and swarms over semi-solid surfaces. S39006 is a model for understanding how bacteria use multiple genetic pathways to respond and adapt to the environment. This chapter describes some of the most important genetic and physiological features of S39006 related to the research on cell buoyancy and pleiotropic regulation presented in this thesis.

1.2 Cell buoyancy and gas vesicle production

S39006 is the only enterobacterium reported to produce gas filled proteinaceous structures (gas vesicles), which naturally allow bacteria and archaea to float in static liquid columns (Ramsay *et al.,* 2011; Pfeifer, 2012). Gas vesicles are intracellular hollow chambers permeable to any gas surrounding the cytoplasm but impermeable to water. Many aquatic prokaryotes produce gas vesicles to lower the cellular density, allowing them to float and to reach the air-liquid interface. Some photosynthetic bacteria use gas vesicles to reach the upper liquid column and optimize light harvesting (Pfeifer, 2012). In addition, flotation has been suggested as a cost-effective strategy for cell and population migration, compared to flagellar motility (Walsby *et al*., 1994). Although gas vesicles limit bacterial movement to a vertical plane they facilitate migration without the need to invest high amounts of energy.

The exact components of mature S39006 gas vesicles are still unknown. Nonetheless, multiple genetic and structural analyses in other bacteria suggest that the small hydrophobic protein GvpA is the main constituent (Walsby *et al*., 1994; Pfeifer, 2012). Other proteins also found in S39006 seem to play important structural roles in cyanobacterial gas vesicles, such as the hydrophilic GvpC, the amphipathic GvpG and the acidic GvpF (Englert *et al.,* 1992; Buchholz *et al*., 1993; Shukla & DasSarma, 2004; Xu *et al.*, 2014). Solid-state NMR and structure prediction algorithms suggest that GvpA aggregates in rib structures forming antiparallel β-sheets to construct the biconical basal nanostructure (Figure 1.1.A-B) (Sivertsen *et al.*, 2010; Pfeifer, 2012).

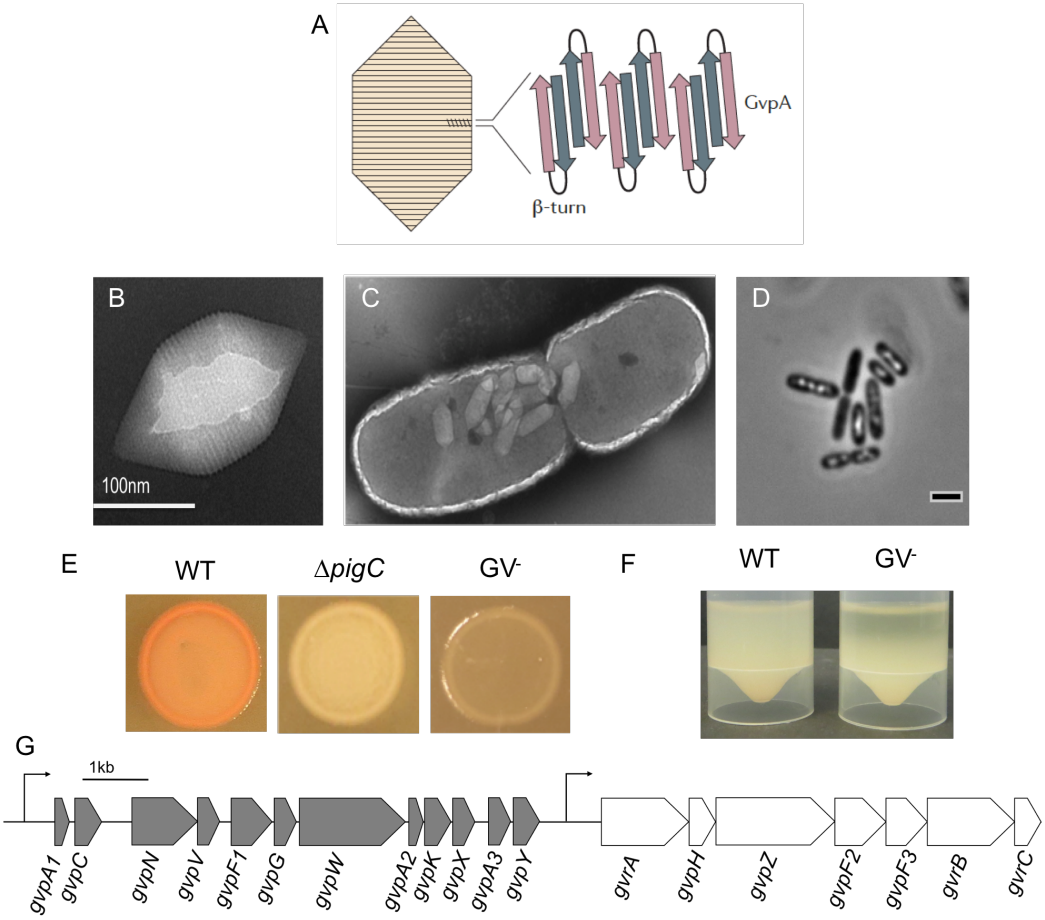

Figure 1.1. Gas vesicle phenotype and gene cluster. A. Structural model for gas vesicle assembly. Antiparallel β-sheets are represented as purple and blue arrows (Image taken from Pfeifer, 2012). (**B**) Transmission electron microscopy (TEM) images of single gas vesicle from S39006 showing the GvpA ribs and (**C**) a single WT cell with clustered gas vesicles. **D.** Phase contrast microscopy (PCM) image of WT cells with and without phase bright structures (gas vesicles). Scale bar in the PCM image corresponds to 1 μm. **E.** Patch morphology of WT, prodigiosin (Δ*pigC*) and gas vesicles mutant (GV$^-$) cells. **F.** Flotation assay with WT and GV$^-$ cells. **G.** Gas vesicle gene cluster. Left-hand (grey) and right-hand (white) operons are under control of the *gvpA1* and *gvrA* promoters, respectively.

In the cyanobacterium *Aphanizomenon flos-aquae* immunodetection in cell lysates and with purified gas vesicles allowed the identification of other structural components, such as GvpC. Amino acid sequencing of proteolytic residues from gas vesicles revealed that GvpC and GvpA are present in a molar ratio of 1:25 (Buchholz *et al*., 1993). GvpC covers the outer layer and strengthens the overall structure to resist external pressure inputs (see detailed information on section 1.3), while GvpA is on the inner gas-exposed surface probably interacting with GvpF, as revealed by tomography in intact and fragmented gas vesicles (Xu *et al.*, 2014).

Gas vesicles are found as small bicones in early stages of growth, but later develop into larger spindle-shaped or cylindrical structures (Pfeifer, 2012). During the exponential phase of growth gas vesicles occupy more space and can cluster in the cytoplasm (Figure 1.1.C). The aggregated gas vesicles (gas "vacuoles") give a distinctive phase brightness to individual cells, and opacity to S39006 colonies (Figure 1.1.D-E) (Ramsay *et al.,* 2011). Light scattering in gas vacuolated bacteria is an important feature because gas vesicle-defective colonies appear transparent and do not float (Figure 1.1.E-F); this morphological feature facilitates their isolation and identification in mutagenesis screening.

Gas vesicles in S39006 are synthesized from a 16.7 kb cluster composed of 19 genes that is divided into two operons, *gvpA1-gvpC* and *gvrA-gvrC* (Figure 1.1.G). The genetic arrangement of the S39006 gas vesicle cluster is unique among gas vacuolated microorganisms (Figure 1.2). However, all its open reading frames are homologues with genes from other gas vesicle clusters found in proteobacteria, cyanobacteria, firmicutes, actinobacteria and archaea (Figure 1.2) (Tashiro *et al.,* 2016). The *gvpA1-gvpY* operon contains both genes that are known to be essential for structural assembly and shape, and genes of unknown function. The structural components in this operon are three *gvpA* homologues (*gvpA1*, *gvpA2* and *gvpA3*), *gvpC*, a *gvpF* homologue (*gvpF1*) and *gvpG*. Two more genes have been found to affect gas vesicle shape: TEM images of Δ*gvpN* and Δ*gvpV* mutants show that deletions of these genes result in spindle-like gas vesicles. GvpN and GvpV might act as chaperones involved in cylindrical structure maturation in S39006 (Tashiro *et al.,* 2016). Among the genes of unknown function, *gvpW*, *gvpX* and *gvpY* when disrupted do not affect cell buoyancy or gas vesicle formation, whereas *gvpK* is essential for gas vesicle production. Nonetheless, there is no evidence of GvpK being present in the bicones.

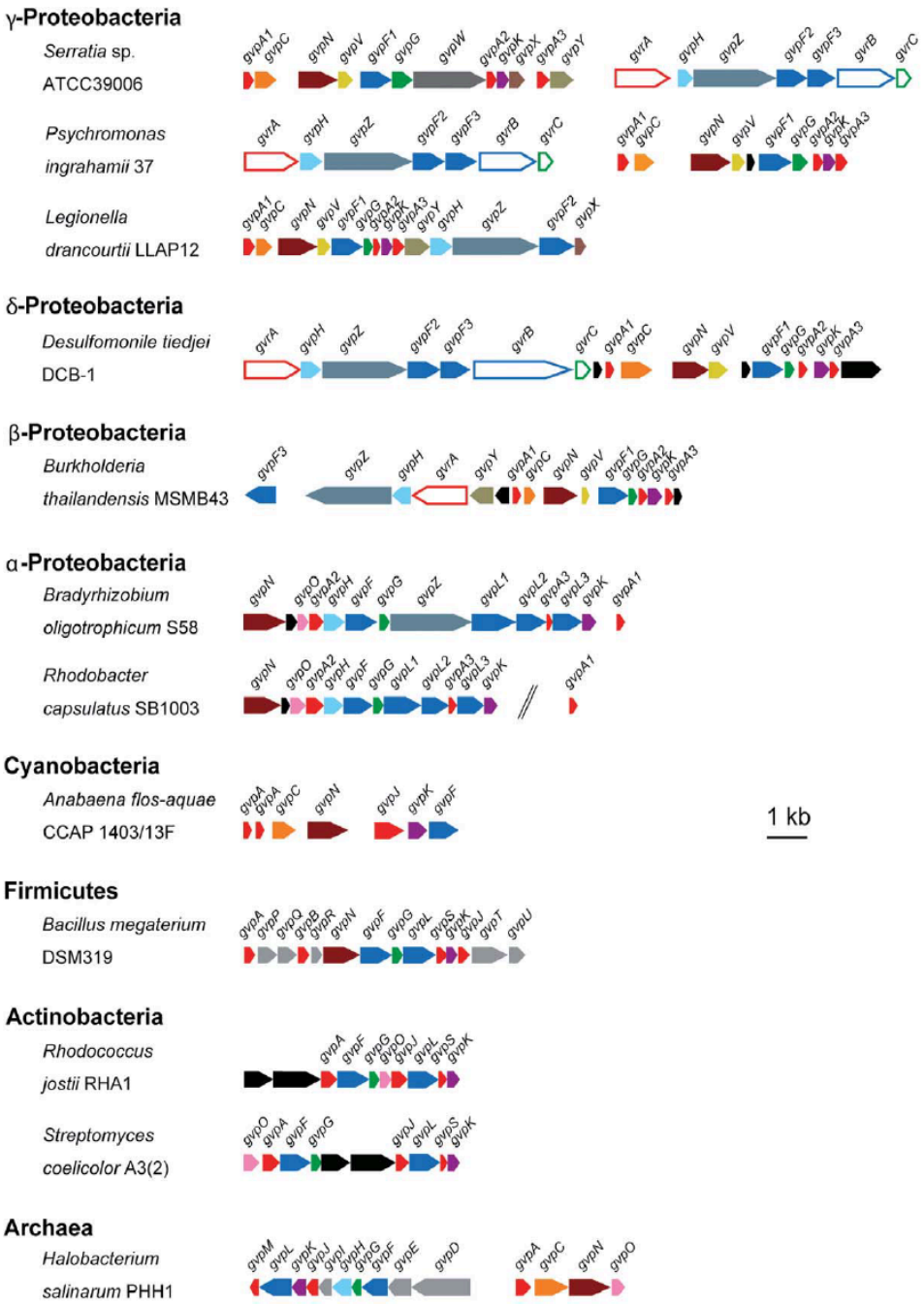

Figure 1.2 Organization of gas vesicle genetic clusters in bacteria and archaea (image taken from Tashiro *et al.,* 2016). Homologous genes are highlighted with the same colours. Solid arrows indicate genes predicted to encode structural proteins, whilst hollow arrows indicate genes predicted to encode regulatory proteins.

The *gvrA-gvrC* operon contains two essential genes which are *gvpF* homologues (*gvpF2* and *gvpF3*), two genes with undetermined function (*gvpH* and *gvpZ*) and three regulatory genes (*gvrA*, *gvrB* and *gvrC*) (Monson *et al.,* 2016; Tashiro *et al.*, 2016). Homologues of *gvpH* are present in all proteobacterial and archaeal gas vesicle genetic clusters, whilst *gvpZ* is present

only in proteobacteria (Tashiro *et al.*, 2016). Cells with Δ*gvpH* and Δ*gvpZ* mutations still produce gas vesicles and remain buoyant in liquid cultures. Likewise, Δ*gvpH* mutants in the archaeon *Halobacterium salinarium* PHH1 maintain gas vesicle production, but the structures seem to be less stable than in wild type (WT) samples (Offner *et al.*, 2000). A previous study of the genes essential for gas vesicle formation in the archaeon *Halobacterium halobium* NRC-1 reported that *gvpH* mutants reduce significantly, but do not abolish completely, the construction of gas vesicles (DasSarma *et al.,* 1994). However, this phenotype might be caused by polar effects of the inserted cassette on downstream genes.

GvrA, GvrB and GvrC regulate the transcription of the *gvpA1-gvpY* operon (Ramsay *et al.,* 2011; Tashiro *et al.,* 2016). These regulators are not related to genes studied previously in other gas vesicle producing organisms, but homologues are found in some proteobacteria (Figure 1.2). Protein BLAST predicts that GvrA belongs to the NtrC family, which is composed of transcriptional response regulators dependent on the σ54 initiation factor (RpoN), whereas GvrB is predicted to be a homologue of the sensor histidine kinase NtrB. GvrC contains a phosphorylation receiver domain homologue of the chemotaxis transducer CheY that could be involved in gas vesicle and flagella regulation. Cells with Δ*gvrA* and Δ*gvrB* mutations fail to make gas vesicles in liquid and solid cultures. Intriguingly, although Δ*gvrC* mutants from liquid cultures do not produce gas vesicles, cells grown in plates show some moderate production (Tashiro *et al.,* 2016). The regulatory components GvrA, GvrB and GvrC in the gas vesicle cluster, along with others detected in mutant screening, indicate that cell buoyancy is tightly controlled by multiple environmental cues and genetic regulatory pathways.

1.3 Collapse pressure and gas vesicles as molecular tools to measure turgor pressure

Gas vesicles are compartments that maintain pressure inside (p_g) in equilibrium with the exterior (Walsby, 1994). It has been reported that the hydrophobic protein GvpC binds to the outer surface of the gas vesicles and strengthens the overall structure. Nevertheless, rapid changes in external pressure cause gas vesicle collapse and, consequently, cell precipitation (Walsby, 1994; Tashiro *et al.,* 2016) (Figure 1.3). Gas pressure in the environment (p_f) and cell turgor pressure (p_t) are important external factors contributing to the net pressure on gas vesicles (Figure 1.3.A).

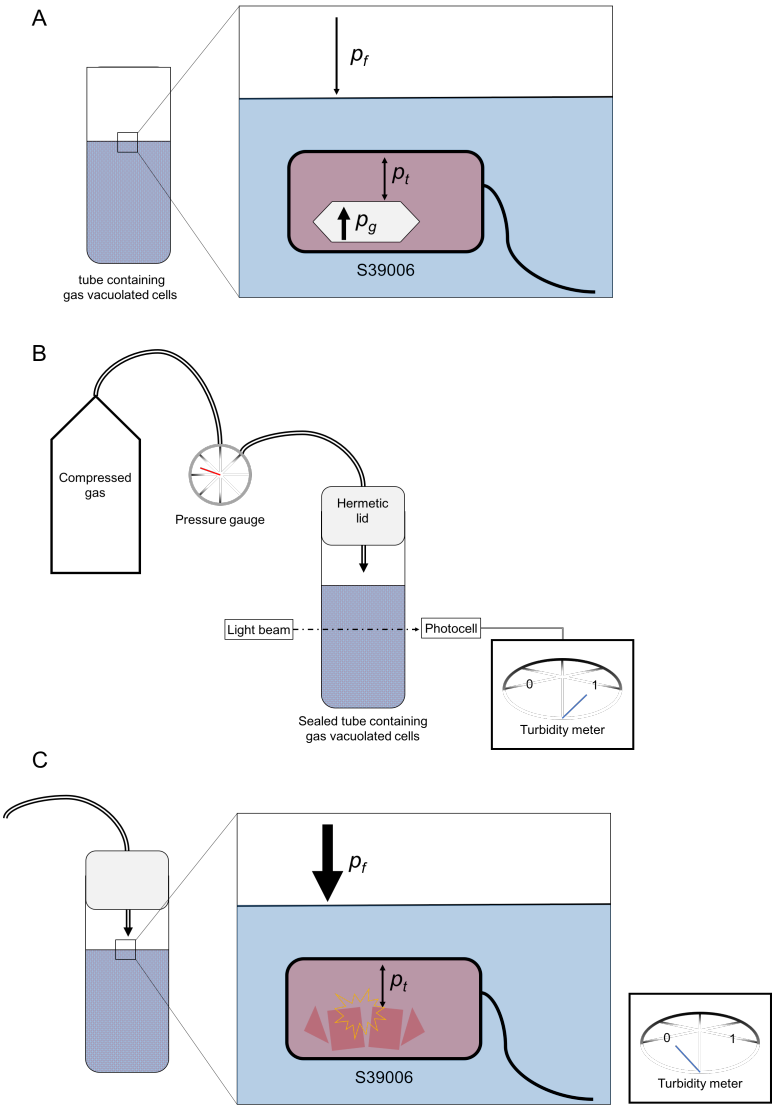

Figure 1.3. Net pressure components on S39006 gas vesicles and pressure nephelometry. The collapse of S39006 gas vesicles and turgor pressure are analysed in cultures grown in 5 ml of either diluted or turgid media in universal tubes, which lead to an insignificant hydrostatic pressure. **A.** In these conditions the GvpC coating, external gas (p_f), turgor(p_t) and internal gas (p_g) pressures are the main factors impacting on gas vesicle collapse. **B.** Pressure nephelometry measures changes in turbidity due to loss of gas vesicles by controlled injection of compressed gas. Before increasing the external gas pressure, the turbidity meter is set to 1 (100% gas vesicles intact). **C.** Thereafter, changes in light transmittance are recorded as external gas pressure (p_f) rises and gas vacuoles collapse.

Since gas vesicles are light-scattering structures, changes in sample turbidity (nephelometry) related to injection of compressed gas (e.g. N_2) is used to determine the external pressure (p_c) required to collapse gas vesicles (Walsby, 1971) (Figure 1.3.B-C). Hydrostatic pressure is an important factor in samples analysed *in situ*, such as deep sea and lake columns, but it is

insignificant in laboratory conditions where up to 5 ml cultures are analysed. The effect of turgor pressure on gas vesicles can be suppressed by adding sucrose to the medium, creating a hypertonic environment that allows quantification of the pressure needed to collapse gas vesicles.

Pressure nephelometry also facilitates measurement of cell turgor pressure (Walsby, 1994; Tashiro *et al.,* 2016). Turgor pressure (p_t) in prokaryotes can be defined as the osmotic pressure from the cytoplasmic contents pushing out the inner cell membrane, but also pushing on intracellular aggregates, such as gas vesicles (Figure 1.3.A). Turgor pressure can be calculated in gas vesicle-producing microorganisms by measuring the difference between collapse pressure in turgid (hypotonic) and non-turgid (hypertonic) conditions, as follows:

$$p_t = p_c \text{ hypotonic} - p_c \text{ hypertonic}$$

Turgor pressure is the main force driving cellular growth, morphology and penetration into hard surfaces (Money, 2008; Osawa & Erickson, 2018; Rojas & Huang, 2018). Changes in membrane morphology due to turgor pressure fluctuations can be sensed by the cell and can induce expression of osmoregulatory genes (Csonka*,* 1989; Walderhaug *et al.*, 1992). Controlled gas vesicle collapse has been recognized as a simple, robust and effective technique to measure turgor pressure compared to other methods that use complex micromechanical instruments or stop-flow measurements on predried cell samples (Arnoldi *et al.,* 1999; Deng *et al.,* 2011; Tashiro *et al.,* 2016). However, use of this technique is restricted to gas vesicle-producing bacteria.

1.4 Genetic regulation of gas vesicles

The development of molecular genetic techniques in enterobacteria, such as *in vivo* mutagenesis with transposable elements, phage transduction, and mutant screening based on colony opacity led to the identification of gas vesicle genetic regulators in S39006 (Ramsay *et al.,* 2011; Lee *et al.,* 2017). The genetic regulation of gas vesicle production involves, as mentioned above, three cognate regulators (GvrA, GvrB and GvrC) encoded by the gas vesicle gene cluster (Figure 1.1.G). Furthermore, other regulators located at different loci have been

identified as controlling cell buoyancy. These non-cognate gas vesicle regulators are discussed in the following sections.

1.4.1 SmaI/SmaR: cell buoyancy under quorum sensing control

Many bacteria control gene expression through quorum sensing (QS) (Atkinson & Williams, 2009). The QS mechanism includes LuxI-like proteins synthesizing diffusible acyl-homoserine lactones (AHLs) and sensing the diffusible molecules in a cell density-dependent manner via LuxR-like allosteric transcription factors (Whitehead *et al.,* 2001; Ng & Bassler, 2009; Tsai & Winans*,* 2010). This auto-induction system permits the synchronization of entire cell populations and communities to turn gene expression on or off.

S39006 has a LuxI/LuxR homologue system, SmaI/SmaR, that uses *N*-butanoyl-$_L$-homoserine lactone (BHL) as the signalling molecule (Thomson *et al.,* 2000). SmaI/SmaR regulation does not work like most AHL-based QS systems, in which the QS receptor (LuxR-homologue) enhances the transcription of target genes after AHL binding. In contrast, S39006 QS circuitry works through a derepression mechanism. This means that SmaR binds to target promoters and represses gene expression at low cell densities, but at higher cellular densities BHL binds to SmaR to release promoters and facilitate transcription activation (Slater *et al.,* 2003; Tsai & Winans*,* 2010).

Flotation assays using static liquid cultures with *smaI* and *smaR* mutants, and complementation of cell buoyancy in *smaI* mutants supplemented with BHL, confirmed that QS regulates gas vesicle production in S39006 (Ramsay *et al.*, 2011). Transcription assays using *gvpA1* and *gvrA* reporter fusion strains revealed that QS affects the expression of both *gvpA1-gvpY* and *gvrA-gvrC* gas vesicle operons. Moreover, quantification of *gvpA1* and *gvrA* promoter activity under heterologous expression (in *E. coli*) of SmaR suggested that QS regulates directly the gene expression of the *gvpA1-gvpY* operon*,* whilst the *gvrA-gvrC* operon indirectly through other regulators (Figure 1.4) (Tashiro *et al.*, 2016).

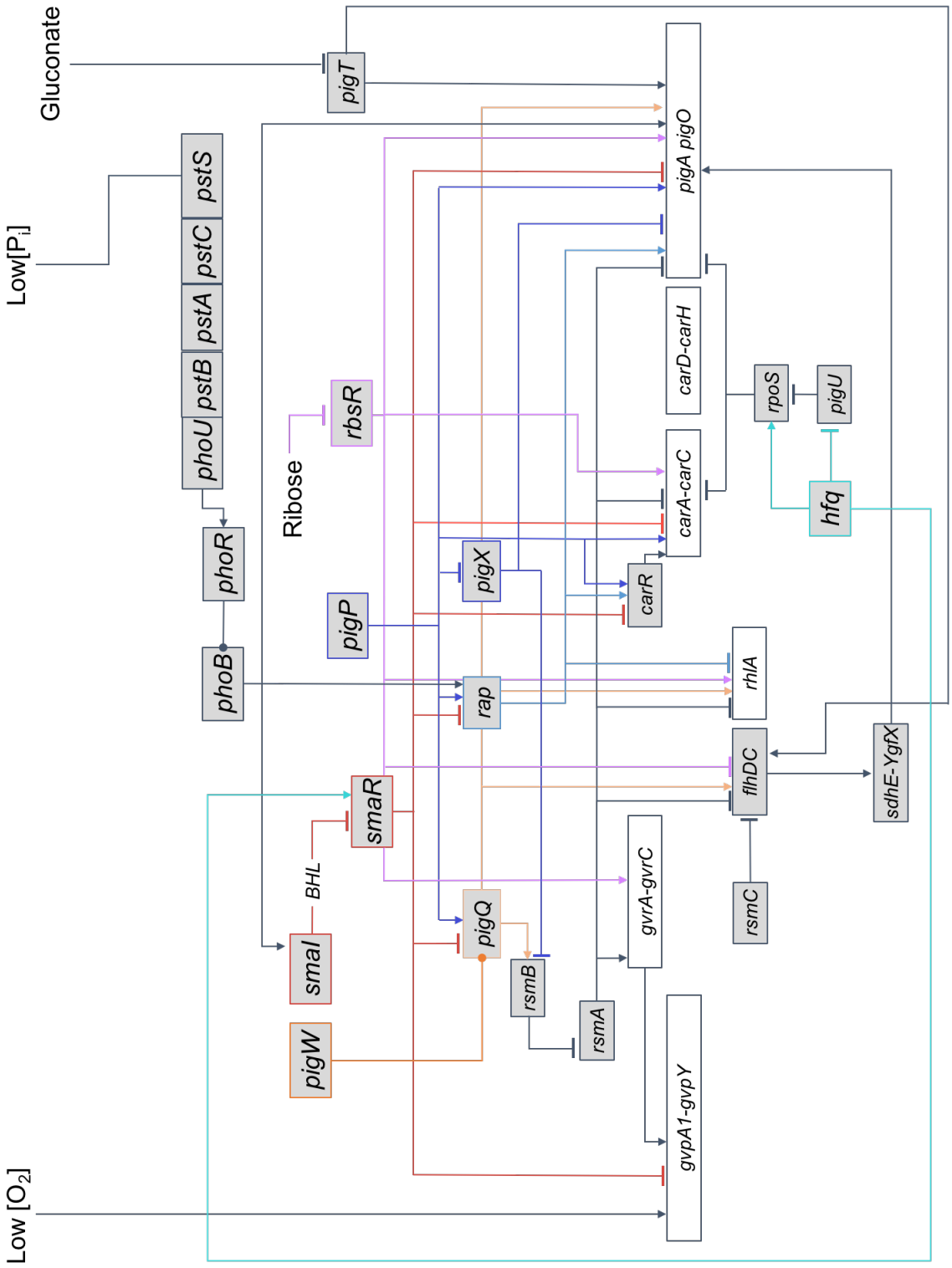

Figure 1.4 Model of hierarchical regulation in S39006 for gas vesicles, flagellar motility, carbapenem and prodigiosin production. Coloured lines were included to facilitate reader accessibility to the multiple pathways shown. Grey boxes indicate regulatory genes, white boxes indicate either the gas vesicle, bio-surfactant, carbapenem or prodigiosin operons. Arrows and perpendicular lines indicate activation and inactivation, respectively. Lines ending in a solid circle indicate regulation through phosphorylation. See description in text for detailed information.

1.4.2 PigQ: a GacA-homologue and receptor of PigW signalling

PigQ and PigW are homologues of a two-component system conserved among Gram-negative bacteria: the GacS and GacA regulators, respectively (Heeb & Haas, 2001). GacS-like proteins contain two transmembrane sensor domains, connected through a periplasmic loop, in the N-terminal domain, and amphipathic flexible residues (linkers) that facilitate conformational changes in the C-terminal domain. GacS folds, presumably after signal sensing, and autophosphorylates a histidine residue. Phosphotransfer of aspartate and histidine residues across the C-teminal end leads to phosphorylation of an aspartate residue in the response regulator GacA. Thereafter, the activated GacA undergoes a conformational change that allows DNA binding and gene expression activation.

GacS/A-like two-component systems regulate diverse phenotypes in bacteria, such as antimicrobial production, virulence, and QS signals, among others (Heeb & Haas, 2001). The impact of PigW on gas vesicles has not been determined. Nonetheless, *pigQ* mutants show small but significant overexpression of the gas vesicle operons (Ramsay *et al.,* 2011) (Figure 1.4). This suggests that the PigW/Q system is a negative regulator of gas vesicle gene expression.

1.4.3 PigX: a composite GGDEF and EAL protein

Another flotation regulator is the predicted inner membrane protein PigX. In contrast to PigQ, *pigX* mutants down-regulate the expression of the *gvpA1-gvpY* and *gvrA-gvrC* operons (Ramsay *et al.,* 2011) (Figure 1.4). PigX is a homologue of CsrD in *E. coli*, and contains GGDEF and EAL domains which are involved in the synthesis and hydrolysis, respectively, of 3´, 5´-cyclic diguanylic acid (c-di-GMP). c-di-GMP has been reported as an intracellular signalling molecule controlling multiple phenotypes in bacteria, including flagellar motility in other enterobacteria (Jenal & Malone, 2006; Wolfe & Visick, 2008). Nonetheless, neither synthesis nor degradation of c-di-GMP seems to be associated with CsrD gene regulation activity (Leng *et al.,* 2016).

1.4.4 PigQ-PigX-RsmA-*rsmB* system: pleiotropic post-transcriptional regulation

GacA and CsrD-like proteins, such as PigQ and PigX, control the transcription of untranslated regulatory RNAs, such as the small RNA (sRNA) *csrB*, to govern multiple metabolic pathways in *Pectobacterium carotovorum* (Cui *et al.,* 2001; Hyytiäinen *et al.,* 2001). In *E. coli*, phosphorylated GacA promotes the expression of *csrB*, which is an antagonist of the mRNA chaperone CsrA (carbon storage regulator A). In contrast, CsrD (PigX homologue) inhibits the production of *csrB* to facilitate CsrA activity (Suzuki *et al.,* 2006; Potts *et al.,* 2018). In *Vibrio chlorae*, CsrD interacts via its EAL domain with an unphosphorylated glucose- dependent protein, $EIIA^{Glc}$, to induce, through an unknown mechanism, *csrB* decay via nucleases RNase E and PNPase (Leng *et al.,* 2016). CsrA has been classified as an important global regulator, sequestering numerous mRNAs to control central and secondary metabolism, motility and virulence. RsmA (repressor of stationary phase metabolites A) is the CsrA homologue in S39006, and it is known to promote gas vesicle production through transcriptional regulation of both *gvpA1-gvpY* and *gvrA-gvrC* operons (Ramsay *et al.,* 2011) (Figure 1.4). Similar to other bacteria, the *csrB* homologue (*rsmB*) is an antagonist of RsmA activity in S39006.

Experiments in *E. coli* revealed that CsrA (RsmA) is a small protein that binds to conserved GGA motifs in the 5'UTR of target mRNAs to promote transcription termination, their transition into RNA-decay or translation (Liu & Romeo, 1997; Romeo, 1998; Wei *et al.,* 2001; Patterson-Fortin *et al.,* 2013; Figueroa-Bossi *et al.,* 2014). One single unit of the non-coding RNA *csrB* (*rsmB)* binds to 18 units of CsrA to antagonize its activity. Expression assays suggest that the CsrA-*csrB* complex is still active in regulating the translation of CsrA mRNA targets. Moreover, the Δ*csrA* phenotype is reproduced only after overexpression of *csrB*. This suggests that CsrA-*csrB* complex stoichiometry plays an important role in regulation.

1.4.5 RbsR: a ribose repressible transcription factor

RbsR is a LacI-like transcription factor that represses the ribose operon, including the expression of the ribose mutarotase and ribose kinase RsbD and RbsK. S39006 *rbsR* mutants are impaired for flotation and down-regulated for *gvpA1* and *gvrA* transcription (Lee *et al.,* 2017). As with other carbon metabolism repressors, RbsR activity is inhibited by allosteric

binding of effectors related to the pathways under their control (in this case ribose) (Mauzy & Hermodson, 1992; Lee *et al.,* 2017). Thus, it has been suggested that ribose is an important negative modulator of cell buoyancy through inhibition of RbsR transcription.

1.5 Other phenotypes affected by gas vesicle regulators in S39006

S39006 is also known to produce antimicrobials, such as the the β–lactam antibiotic Car (1-carbapen-2-em-3-carboxylic acid) and the red tripyrrole pigment, prodigiosin. In addition, it is motile by means of flagellar rotation. The QS system SmaI/SmaR, the two-component system PigW/PigQ, the transcription factor RbsR, and the post-transcriptional regulators RsmA/*rsmB* regulate flagella-based motility and antimicrobial production, in addition to gas vesicle production, in S39006 (Figure 1.4). Interestingly, the overexpression of GvrA and GvrB led to increased production of prodigiosin, suggesting that the cognate gas vesicle regulators are tightly controlled in S39006. Given the connection, through common regulatory pathways, of cell buoyancy, motility and secondary metabolism for antimicrobial production, the production of carbapenem, prodigiosin and flagellar-based motility will be discussed in the following sections.

1.5.1 Carbapenem production

Car is a β–lactam antibiotic and a member of the carbapenem class (Coulthurst *et al.,* 2005). It is composed of a pyrroline-carboxylate moiety and the characteristic β–lactam ring (Figure 1.5.A). Carbapenem antibiotics have been used for treatment against both Gram-positive and Gram-negative pathogenic bacteria (Bradley *et al.* 1999). Their spectrum of activity includes bacteria with extended resistance due to β–lactamase production (Livermore. 1998).

The S39006 car genetic cluster (Figure 1.5.B) is a homologue of the one in *Pectobacterium carotovorum*; it contains five genes that encode the biosynthetic enzymes CarA, CarB, CarC, CarD and CarE. Mutations in genes *carA, carB* and *carC* completely abolish antibiotic synthesis, while S39006 *carD* and *carE* mutants have significantly, but not completely, reduced antibiotic production (McGowan *et al.,* 1996). Metabolic engineering for heterologous production of carbapenem in *E. coli* showed that expression of *carD* and *CarE*

increased the antibiotic production significantly (Shomar *et al.,* 2018). This suggests that CarD and CarE are not essential but important for carbapenem synthesis.

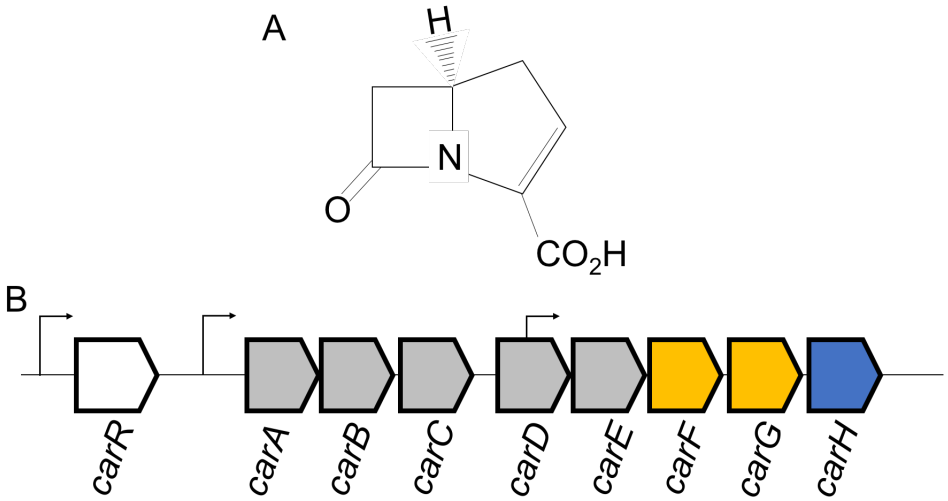

Figure 1.5. Car structure and genetic cluster. A. 1-carbapen-2-em-3-carboxylic acid (Car) structure. **B.** Genetic cluster for regulation, biosynthesis and resistance of Car. It contains a transcriptional regulator (white), biosynthetic genes (grey), intrinsic resistance genes (yellow) and a gene with unknown function (blue). Black thin arrows represent *carR* and *carA* promoters, and *carD* internal promoter. See description in text for detailed information.

The car genetic cluster also contains four additional genes *carF, carG, carH* and *carR*, which do not encode biosynthetic enzymes (Figure 1.1.B). Expression of *carF, carG* and *carH* occurs via an internal promoter in the carbapenem operon, located within *carD* (McGowan *et al.,* 2005). CarF and CarG provide intrinsic resistance to car through as yet unknown mechanisms. These proteins are predicted to be located in the periplasm, and both are required for resistance in *P. carotovorum* and S39006 (McGowan *et al.,* 1996; Tichy *et al.*, 2014; Tichy *et al.,* 2017) The role of CarH in antibiotic synthesis, resistance or regulation is unknown. Homologues are found only in other Car producing bacteria such as *P. carotovorum* and *Photorhabdus luminescens* (Coulthurst *et al.,* 2005). CarR is a LuxR-like transcriptional activator that is regulated by the quorum sensing system SmaI/SmaR (Figure 1.4) (Thomson *et al.,* 2000; Slater *et al.,* 2003). In *P. carotovorum*, CarR binds to its own promoter and the promoter controlling the expression of the car operon, upstream of CarA, but not the *carD* internal promoter (Coulthurst *et al.,* 2005; McGowan *et al.,* 2005). Interestingly, in contrast to other homologues, CarR does not need a signal inducer to activate expression of the car operon in S39006 (Cox *et al.,* 1998; Slater *et al.,* 2003).

1.5.2 Prodigiosin production

Prodigiosin (2-methyl-3-pentyl-6-methoxyprodigiosin) belongs to a family of tripyrrole pigments known as prodiginines. These molecules have a wide range of antimicrobial activity: they have been reported as effective antifungal, antibacterial and antiprotozoal compounds; and they have been shown to act as anticancer agents and immunosuppressants (Berg, 2000; Williamson *et al*., 2007; Pandey *et al*., 2009; Papireddy *et al*., 2011; Danevčič *et al.,* 2016; Wang *et al.,* 2016; Numan *et al.,* 2018). Prodigiosin confers a red appearance on S39006 WT cells, whilst mutants appear white, opaque (Figure 1.6.A). Thus, prodigiosin production mutants can be easily identified in mutagenesis experiments. S39006 is a useful model for understanding the regulatory and biosynthetic pathways of Gram-negative prodiginines.

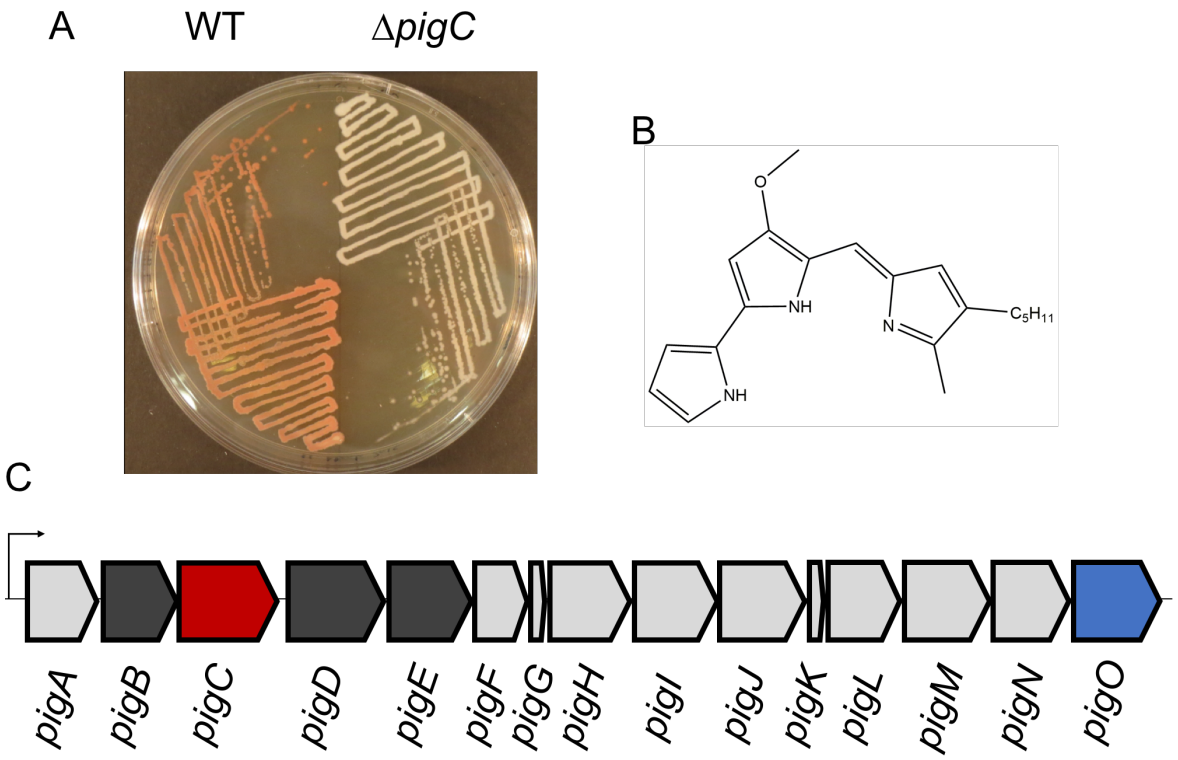

Figure 1.6. Prodigiosin phenotype, structure and genetic cluster. A. WT colonies are red-pigmented while prodigiosin negative mutants appear white. **B.** 2-methyl-3-pentyl-6-methoxyprodigiosin (prodigiosin) structure. **C.** Genetic cluster for biosynthesis of prodigiosin. Genes encoding proteins involved in MCB (light grey) and MAP (dark grey) biosynthesis and MBC-MAP condensation (red). The *pigA* promoter is represented by a black thin arrow. See description in text for detailed information.

Most prodiginines are found as cyclic compounds, but prodigiosin and undecylprodigiosin are composed of linear chains of three pyrrole rings with alkyl substituents (Figure 1.6.B) (Williamson *et al.,* 2006). The prodigiosin operon contains all genes necessary for its synthesis (Figure 1.6.C). Prodigiosin synthesis is the result of two separate metabolic pathways that converge in a final condensation reaction carried out by PigC (Williamson *et al.,* 2006). The first pathway involves the production of 2-methyl-3-n-amyl-pyrrole (MAP) from 2-octenal (a derivative of unsaturated fatty acid oxidation) by three enzymes; PigD, PigE and PigB. The second pathway comprises a larger number of enzymes, including PigI, PigL, PigG, PigA, PigJ, PigH, PigM, PigF and PigN in that order for chemical reactions, to produce 4-methoxy-2-2'-bipyrrole-5-carbaldehyde (MBC) from proline. The functions of PigK and PigO are unknown; mutations in *pigK* and *pigO* do not affect pigment production (Williamson *et al*., 2005).

1.5.3 Flagellar motility

Flagellar rotation facilitates swimming in liquid cultures and, aided by bio-surfactant molecules to reduce cell-surface tension, swarming across semi-solid surfaces (Williamson *et al.,* 2008). Flagellar motility is a well-studied mechanism for ecological adaptation. In general, it has been suggested as a strategy for fast and coordinated colonization of new environments and to escape from predators (Kearns, 2010).

In addition to movement, the secretion of bio-surfactants in S39006 has been reported to be an important mechanism of defence facilitating the localized secretion of prodigiosin and other virulence factors (Williamson *et al.,* 2008). Random transposon mutagenesis and screening for swarming-defective strains allowed the identification and characterization of a gene involved in rhamnolipid surfactant production in S39006 (Williamson *et al.,* 2008). This gene (*rhlA*) is involved in 3-(3-hydroxyalkanoyloxy) alkanoic acid (HAA) synthesis. HAA is a precursor of rhamnolipids and is essential for swarming motility in *Pseudomonas aeruginosa*. Interestingly, HAA is an effective surfactant on its own and it is commonly found in bacterial extracellular extracts (Deziel *et al.,* 2003). It is likely that HAA works as a biosurfactant in S39006.

S39006 carries 35 genes for flagellar assembly and function. Although all of them are in a cluster in the genome, they are distributed across different operons. Previous studies in *Escherichia coli* demonstrated that multiple operons involved in flagellar assembly and chemotaxis are under the control of the master transcriptional regulation complex FlhDC (Liu & Matsumura, 1994). Likewise, *flhC* controls swimming and swarming motility in S39006 (Williamson *et al.,* 2008). FlhDC and motility genes are under the control of RsmA in S39006 (Wilf *et al.*, 2013; Hampton *et al.,* 2016) (Figure 1.4).

1.6 Other genetic regulators studied in S39006

Over the last two decades, environmental cues and proteins involved in signal reception and transduction, transcriptional and post-transcriptional control for the regulation of carbapenem production, prodigiosin production, and swimming and swarming motility, have been identified in S39006. However, knowledge of gene regulation for cell buoyancy is limited due to the fact that the discovery of gas vesicles in S39006 is relatively recent, and due to the paucity of molecular tools for the study of gas vesicles in other systems, such as cyanobacteria and archaea (Ramsay *et al.,* 2011). As mentioned above, the regulatory components reported so far for gas vesicle production in S39006 are pleiotropic and support the idea that flotation is a dynamic process connected to environmental sensing and intracellular response regulation. The following section discusses the different pleiotropic regulatory components and pathways characterized in S39006 for carbapenem, prodigiosin, and flagellar motility. Such regulatory components are not yet characterized for gas vesicle production.

1.6.1 Regulator of antibiotic production: Rap, a *slyA* homologue

The first regulator studied in S39006 was identified in a screen of non-pigmented mutants obtained after random mutagenesis with ethyl methanesulfonate (EMS) (Thomson *et al.,* 1997). A mutation in a gene predicted to encode a SlyA-like transcriptional regulator disrupted prodigiosin and carbapenem production. Thus, the gene was named after "regulation of antibiotic and production" (rap). SlyA-like proteins contain a winged helix DNA-binding motif, and positively and negatively regulate the expression of multiple genes, including virulence factors, in pathogenic bacteria of the Enterobacteriaceae family (Thomson

et al., 1997; Spory *et al.,* 2002; Wu *et al.,* 2003). Later studies in S39006 showed that Rap promotes antibiotic production by inducing transcription of the prodigiosin biosynthetic cluster and the carbapenem intrinsic regulator CarR, while down-regulating bio-surfactant production and swarming motility (Slater *et al.,* 2003; Fineran *et al.,* 2005(a)) (Figure 1.4). Interestingly, *rap* mutants swarm more than WT cells, but neither *rhlA* nor *flhC* transcription is affected (Williamson *et al.,* 2008). This suggests that Rap may affect the expression of post-transcriptional regulators for motility control.

1.6.2 The stationary phase-dependent sigma factor RpoS

Sigma factors bind to RNA polymerase (RNAP) to facilitate specific promoter recognition for transcription. Notably, sigma factors such as RpoD and RpoS allow differential gene expression during population growth. RpoD is active during the growth phase, whilst RpoS is expressed during stationary phase. RpoS competes with RpoD for the same RNAP binding core, hence it also inhibits the expression of RpoD-regulated genes in stationary phase (Farewell *et al.,* 1998). RpoS is an important factor that regulates the expression of stress-response genes for survival under starvation, high temperature and oxidative conditions (Battessi *et al.,* 2011). In S39006, *rpoS* is essential for survival in minimal media conditions (without essential amino acids) (Wilf *et al.,* 2012). In addition, *rpoS* mutants are hyper-motile and are hyper-producers of prodigiosin and car, whilst attenuated for virulence in worms.

1.6.3 PigU: A HexA homologue

The LysR family transcriptional regulator known as LhrA represses *rpoS* expression in *E. coli* (Peterson *et al.,* 2006). The LhrA homologue in *P. carotovorum* (HexA) down-regulates QS and *rsmB*, in addition to *rpoS* (Mukherjee *et al.,* 2000). S39006 has a HexA homologue, known as PigU, which is QS independent and stimulates prodigiosin, carbapenem and cellulase production (Fineran *et al.,* 2005(a)). Proteomic analysis suggests that PigU also regulates *rpoS* in S39006 (Figure 1.4) (Wilf *et al.,* 2013).

1.6.4 PigT: a gluconate sensor controlling motility and prodigiosin production

Besides PigX and RbsR, another transcription factor connects carbon metabolism with the production of antibiotics and motility in S39006: the GntR family protein PigT (Fineran *et al.,* 2005(b)). GntR-like proteins control the expression of gluconate catabolic genes and are susceptible to gluconate-dependent inactivation (Tong *et al.,* 1996). Experiments with S39006 confirm that gluconate is an important environmental signal repressing prodigiosin expression by inactivating PigT (Figure 1.4). Although swarming motility is also affected in *pigT* mutants, the role of gluconate in flagellar synthesis was not assessed (Fineran *et al.,* 2005(b)). Ribose and gluconate, and perhaps many other carbon sources, differentially modulate secondary metabolism, motility and morphology in S39006 through allosteric transcription factors.

1.6.5 YgfX: a pleiotropic regulator previously known as PigV

YgfX is an inner membrane protein initially identified as PigV and found in prodigiosin mutant screens (Fineran *et al.,* 2005(a)). This protein is highly conserved among different enterobacteria and it has been shown to form a complex with SdhE, a protein involved in flavinylation and activation of enzymes involved in the TCA cycle (McNeil *et al.,* 2012; McNeil *et al.,* 2014). *ygfX* and *sdhE* are part of the same operon and are thought to form a two-component system (Paterson *et al.,* 2013). Recently, it was found that *ygfX* is a pleiotropic regulator, controlling prodigiosin and flagellar motility, and that RsmA represses *ygfX* transcription via inhibition of the flagellar master regulator FlhDC (Figure 1.4) (Hampton *et al.,* 2016). Given that RsmA is a post-transcriptional regulator and is known to repress flagellar motility, it is likely that RsmA inhibits *ygfX* and *shdE* expression by sequestering *flhDC* mRNA.

1.7 Master regulators

Studies in S39006 showed that different "master" pleiotropic regulators control gene expression indirectly, through some of the subordinate regulators that were discussed earlier. For instance, the transcription factor PigP, the phosphate uptake and response system PstSCAB-PhoU, and the RNA-binding protein Hfq act as major hierarchical regulators. These

components induce or repress the transcription of multiple genes to determine the conditions in which antibiotic production, swimming and swarming motility occur in S39006 (Thomson *et al.,* 2000; Williamson *et al.,* 2008; Ramsay *et al.,* 2011; Wilf *et al.,* 2012) (Figure 1.4).

1.7.1 PigP

PigP was initially discovered in screens for Car and prodigiosin mutants (Fineran *et al*., 2005(a)). Amino acid sequence analysis showed that PigP contains a helix-turn-helix (HTH) DNA binding domain similar to XRE (xenobiotic response element) transcriptional regulators. Homologues of *pigP* are present in closely related enterobacteria, such as the carbapenem and prodiogiosin producers *P. luminescens* and *Serratia marcescens*. Further studies revealed that PigP is a highly pleiotropic regulator, controlling not only secondary metabolism, but also motility and virulence. Ectopic expression in mutants suggests that PigP is a positive regulator of carbapenem and prodigiosin, while also being a negative regulator of flagellar motility (Fineran *et al.,* 2005(a); Fineran *et al.,* 2007; Williamson *et al.*, 2008).

PigP also acts indirectly, regulating the transcription of proteins involved in DNA binding and signal synthesis, reception, transduction, and degradation (Fineran *et al.,* 2005(a)). For instance, PigP controls the production of plant cell wall-degrading enzymes, such as cellulases and pectate lyases, production of prodigiosin, flagellar motility and, possibly, gas vesicles through PigQ and PigX (Fineran *et al.,* 2005(a); Fineran *et al.,* 2007, Ramsay *et al.,* 2011). Interestingly, *pigQ* and *pigX* mutants have opposite regulatory effects on the phenotypes mentioned above, suggesting that PigP is a dynamic regulator sensing multiple environmental cues or depending on other major regulators.

1.7.2 PstSCAB-PhoU and PhoBR: connecting phosphate uptake and gene expression

Phosphate depletion is an important environmental signal modulating bacterial ecology, behaviour and gene expression (Wanner, 1993; Wanner, 1996; Fuller *et al.,* 2005; Martiny *et al.,* 2006; Chekabab *et al.,* 2014). Extracellular inorganic orthophosphate (P_i) is crucial for bacterial systems because it is the main source of cellular phosphate. In *E. coli*, P_i is

transported, when present in high concentrations, by the low affinity transporter Pit and by the membrane complex and ABC (**A**TP **b**inding **c**assette) transporter PstSCAB, whilst P_i is exclusively sensed and transported at low concentrations by PstSCAB. At high P_i concentrations, PstSCAB and the chaperone PhoU inhibit the activation of the sensory histidine kinase and integral membrane protein PhoR. When activated (that is, at under low P_i concentrations), PhoR phosphorylates the response regulator and transcription factor PhoB to induce the expression of multiple genes, including *phoB*, in a positive feedback loop mechanism (Hsieh & Wanner, 2010).

Likewise, S39006 uses the *pstSCAB-phoU* operon for high affinity phosphate transport and signal transduction via PhoBR to control antibiotic production and flagellar motility (Slater *et al.,* 2003; Gristwood *et al.,* 2009). Furthermore, at low phosphate concentrations PstSCAB-PhoU and PhoBR induce overproduction of BHL. This means that the phosphate regulon induces SmaR derepression and the transcription of other QS-dependent regulators, such as *rap* (Gristwood *et al.,* 2009) (Figure 1.4). Given that QS regulates gas vesicle production it is likely that phosphate levels may also affect cell buoyancy.

1.7.3 Hfq: A post-transcriptional master regulator

In addition to RsmA, another RNA binding protein was identified in the regulation of antibiotic production, motility and virulence. The Sm-like protein, Hfq, positively controls prodigiosin and carbapenem production, as well as plant and animal invasion (Wilf *et al.,* 2011). Hfq is a ring-shaped hexameric protein that binds to uracil rich sequences to promote sRNA-mRNA interactions and protect them from RNase E cleavage (Valentin-Hansen *et al.,* 2004). Hfq was initially identified in *E. coli* as a factor required for the activity of the Qβ RNA bacteriophage replicase (Franze de Fernandez *et al.,* 1968). Later, the *hfq* gene was identified and implicated in the regulation of cell division and morphology (Tsui *et al.,* 1994).

Transcriptomic and proteomic profiles in S39006 *hfq* mutants confirm that this protein plays highly pleiotropic physiological roles (Wilf *et al.,* 2013). Binding to different sRNAs and mRNA targets, Hfq expands its activity on global gene regulation through other pleiotropic transcriptional regulators. For instance, S39006 Hfq promotes the expression of *rpoS* aided

by two sRNAs, *dsrA* and *rprA*, and through inhibition of *pigU* (Wilf *et al.,* 2012; Wilf *et al.,* 2013) (Figure 1.4). Accordingly, *rpoS* Hfq-dependent control seems to be conserved among different enterobacteria (Brown and Eliot, 1996; Tsui *et al.,* 1997; Matilla *et al.,* 2015).

Hfq is also a positive regulator of the QS receptors CarR and SmaR (Wilf *et al.,* 2011) (Figure 1.4). This implies that Hfq inhibits indirectly the transcription of some of the mRNAs that it later helps to translate. Although this process seems contradictory, it is known that SmaR represses transcription at low cell densities, prior to BHL titration, whilst Hfq promotes protein synthesis during stationary phase aided by RpoS. This suggests that Hfq stimulates *smaR* expression to guarantee that antibiotic production and virulence occur only at high cell-densities.

1.8 Aims of this project

The transcriptional and post-transcriptional regulatory network for flagellar motility, and antibiotic and pigment production is complex and has been widely studied in S39006 (Figure 1.4). Nevertheless, limited information is available on how environmental and physiological stimuli, along with biochemical and genetic mechanisms, are involved in the control of gas vesicle production. This project aims to (i) identify novel genetic regulators of gas vesicle production; (ii) study whether defects in those elements have pleiotropic effects; and (iii) investigate the mechanisms by which these new regulators induce or inhibit gas vesicle production.

This study describes the identification of seven novel regulators in S39006 after a comprehensive screening of gas vesicle mutants. Most of these mutants display different phenotypes in motility and antibiotic production when compared with WT cells (Chapter 3). Most of the research performed was focused on two mutants with opposite gas vesicle phenotypes (Chapters 4 and 5). The first mutant studied had an insertion in an uncharacterized transcriptional regulator (Chapter 4). The second had a mutation in a gene encoding an ion transporter (Chapter 5). All regulatory components were previously unknown in gas vesicle regulation and showed differential pleiotropic effects. Moreover, they were

shown to act through different regulatory pathways and could potentially respond to different environmental stimuli.

Chapter 2.
Materials and methods.

2.1 Growth conditions

All bacterial strains are listed in Table 2.1. S39006 and *Pectobacterium carotovorum* strains were grown at 30 ^{o}C in either LB for 16 h, minimal media with different potassium concentrations for 24 h, or on solid medium for 48h (See media contents in Table 2.3). *E. coli* strains were grown in LB at 37 ^{o}C. *E. coli* β2163 cultures were supplemented with erythromycin (Em) and diaminopimelic acid (DAPA) (see Table 2.3 for concentrations). Seed cultures were grown from single colonies inoculated into 30 ml sealed universal tubes containing 5 ml of LB and aerated on tube rollers for overnight (O.N.) growth (14 h - 16 h). Cells were preserved by mixing 1 ml of fresh O.N. cultures and 0.5 ml 50 % glycerol and stored at -80 ^{o}C until needed.

Growth assays were done in 250 ml flasks containing 25 ml of either LB or minimal media with different potassium concentrations. Cultures were inoculated to an initial density of 0.05 OD_{600}, incubated at 30 ^{o}C, and aerated by shaking at 215 rpm. Flotation assays were performed with cell cultures inoculated to an initial density of 0.05 OD_{600} and grown for 24 h in tube rollers. Then, the tubes were set upright and static for between 2 to 15 days, as indicated. Complementation experiments were performed by inducing ectopic gene expression with 0.2% arabinose and plasmid selection with ampicillin (Amp).

2.2 Random Transposon Mutagenesis

Fresh O.N. cultures of β2163 (pKRCPN1) (donor) and Δ*pigC* (recipient) were mixed at different donor to recipient volume ratios (1:1, 2:1, 3:1, 1:2) and spotted, using 30 μl of co-culture, onto LBA plates with DAPA (see Table 2.3 for concentrations). The spots were dried at room temperature for 30 minutes and incubated at 30 ^{o}C O.N. The grown patches were resuspended in 1 ml of LB and serially diluted to 10^{-3}, and 100 μl of each dilution was spread on LBA plates with kanamycin (without DAPA) O.N. for growth. The transparent, hyper-

opaque, bull's-eye transparent and bull's-eye opaque colonies were picked and colony purified by streaking onto LB plates.

Table 2.1. Bacterial Strains and phage used in this study.

Name, code (name in this document)	Genetic Information	Reference
	Serratia sp. ATCC 39006 (S39006)	
S39006	Strain acquired from the ATCC	Parker *et al.,* 1982
WT	Lac$^-$ (LacA), laboratory strain referred to as wild type	Thomson *et al.,* 2000
NWA19	LacA, Δ*pigC*	Ramsay *et al.,* 2011
GPA1 (*gvpA1*::*uidA*)	LacA, *gvpA1*::TnDS1028-*uidA*, Cm^R	Ramsay *et al.,* 2011
GRA (*gvrA*::*uidA*)	LacA, *gvrA*::TnDS1028-*uidA,* Cm^R	Ramsay *et al.,* 2011
LIS (*smaI*::LacZ)	LacA, *smaI*::miniTn*5*Sm/Sp, Sp^R	Thomson *et al.,* 2000
SP19	LacA, *smaI*::mini-Tn*5*Sm/Sp, *pigX*::Tn-DS1028, *pigZ*::miniTn*5*lacZ1, Sp^R, Cm^R, Km^R	Poulter *et al*., 2010
MCA54 (*carA*)	LacA, *carA*::miniTn5lacZ1, Km^R	Thomson *et al.,* 2000
LC13 (*smaI*::*lacZ*)	LacA, *smaI*::miniTn*5lacZ1*, Km^R	Thomson *et al.,* 2000
HSPIG17 (*pigQ*::*lacZ*)	LacA, *pigQ*::miniTn*5lacZ1*, Km^R	Fineran *et al.,* 2005(a)
HSPIG23 (*pigR*::*lacZ*)	LacA, *pigR*::miniTn*5lacZ1*, Km^R	Fineran *et al.,* 2005(a)
HSPIG26 (*pigS*::*lacZ*)	LacA, *pigS*::miniTn*5lacZ1*, Km^R	Fineran *et al.,* 2005(a)
HSPIG46* (*ygfX*::*lacZ*)	LacA, *ygfX*::miniTn*5lacZ1*, Km^R,	Fineran *et al.,* 2005(a)
HSPIG62 (*pigP*::*lacZ*)	LacA, *pigQ*::miniTn*5lacZ1*, Km^R	Fineran *et al.,* 2005(a)
HSPIG67 (*pigP*::*lacZ*)	LacA, *pigP*::miniTn*5lacZ1*, Km^R	Fineran *et al.,* 2005(a)
MAS1 (*rap*)	LacA, *rap*::miniTn*5*Sm/Sp, Sp^R	Thomson *et al.,* 2000
MCP2L (*pigA*::*lacZ*)	LacA *pigA*::miniTn*5lacZ1*, Km^R	Slater *et al.,* 2003
NW64 (*rsmA*::*uidA*)	LacA, *rsmA*::TnDS1028-*uidA,* Cm^R	Hampton *et al.,* 2016
NMW25 (*rpoS*::*uidA*)	LacA, *rpoS*::TnDS1028-*uidA,* Cm^R	Wilf *et al.,* 2005
PIG62S (*pigW*)	LacA, *pigW::*mini-Tn5Sm/Sp, Sp^R	Fineran *et al.,* 2005(a)
SP21 (*smaR*::*lacZ*)	LacA, Δ*pigC*, *smaR*::*lacZ*	Wilf *et al.,* 2011

Table 2.1. Continued.

Name, code	Genetic Information	Reference
	S39006	
rsmB::*uidA*	LacA, *rsmB*::TnDS1028-*uidA,* Cm^R	Laboratory stock
AQY44	LacA, Δ*pigC, gvpF1*::TnKRCPN1, Km^R	This study
AQY54	LacA, Δ*pigC, gvpV*::TnKRCPN1, Km^R	This study
AQY74	LacA, Δ*pigC, gvpA2*::TnKRCPN1, Km^R	This study
AQY75	LacA, Δ*pigC, rbsk*::TnKRCPN1, Km^R	This study
AQY102	LacA, Δ*pigC, Ser39006_1186*::TnKRCPN1, Km^R	This study
AQY103	LacA, Δ*pigC, Ser39006_0591*::TnKRCPN1, Km^R	This study
AQY107	LacA, Δ*pigC, trkH::*TnKRCPN1, Km^R	This study
trkH	LacA*, trkH::*TnKRCPN1, Km^R	This study
trkH pigW	LacA*, trkH::*TnKRCPN1 LacA, *pigW::*mini-Tn*5*Sm/Sp, Km^R, Sp^R	This study
gvpA1::*uidA, trkH*	LacA, *gvpA1*::TnDS1028-*uidA*, *trkH::*TnKRCPN1, Km^R,Cm^R	This study
gvrA::*uidA, trkH*	LacA, *gvrA*::TnDS1028-*uidA, trkH::*TnKRCPN1, Km^R, Cm^R	This study
gvpA1::*uidA*, *trkH, pigW*	LacA*, gvpA1*::TnDS1028-*uidA*, *trkH::*TnKRCPN1, *pigW::*mini-Tn*5*Sm/Sp, Cm^R, Km^R, Sp^R	This study
rsmA::*uidA, trkH*	LacA, *rsmA*::TnDS1028-*uidA, trkH::*TnKRCPN1, Cm^R, Km^R	This study
rsmB::*uidA, trkH*	LacA, *rsmB*::TnDS1028-*uidA, trkH::*TnKRCPN1, Cm^R, Km^R	This study
AQY108	LacA, Δ*pigC, gvpF1*::TnKRCPN1, Km^R	This study
AQY110	LacA, Δ*pigC, crp*::TnKRCPN1, Km^R	This study
AQY112	LacA, Δ*pigC, gvpN*::TnKRCPN1, Km^R	This study
AQY113	LacA, Δ*pigC, pigP*::TnKRCPN1, Km^R	This study
AQY115	LacA, Δ*pigC, Ser39006_0591*::TnKRCPN1, Km^R	This study
AQY117	LacA, Δ*pigC, gvpN*::TnKRCPN1, Km^R	This study
AQY118	LacA, Δ*pigC, Ser39006_1185*::TnKRCPN1, Km^R	This study
AQY119	LacA, Δ*pigC, gvpZ*::TnKRCPN1, Km^R	This study
AQY120	LacA, Δ*pigC, gvpA*::TnKRCPN1, Km^R	This study
AQY121	LacA, Δ*pigC, Ser39006_3885* (*floR*)*::*TnKRCPN1, Km^R	This study
floR	LacA*,* Ser39006_3885 (*floR*)*::*TnKRCPN1, Km^R	This study
gvpA1::*uidA, floR*	LacA, *gvpA1*::TnDS1028-*uidA*, Ser39006_3885 (*floR*)*::*TnKRCPN1, Km^R, Cm^R	This study
gvrA::*uidA, floR*	LacA, *gvrA*::TnDS1028-*uidA,* Ser39006_3885 (*floR*)*::*TnKRCPN1, Km^R, Cm^R	This study

Table 2.1. Continued.

Name, code	Genetic Information	Reference
	S39006	
rsmA::*uidA, floR*	LacA, *rsmA*::TnDS1028-*uidA, floR*::TnKRCPN1, Cm^R, Km^R	This study
rsmB::*uidA, floR*	LacA, *rsmB*::TnDS1028-*uidA, floR*::TnKRCPN1, Cm^R, Km^R	This study
rpoS::*uidA, floR*	LacA, *rpoS*::TnDS1028-*uidA, floR*::TnKRCPN1, Cm^R, Km^R	This study
rap, floR	LacA, *rap*::miniTn*5*Sm/Sp, *floR*::TnKRCPN1, Sp^R, Km^R	This study
AQY122	LacA, Δ*pigC, gvrA*::TnKRCPN1, Km^R	This study
AQY123	LacA, Δ*pigC, rsbK*::TnKRCPN1, Km^R	This study
AQY 124	LacA, Δ*pigC, tufA*:: TnKRCPN1, Km^R	This study
AQY125	LacA, Δ*pigC, Ser39006_3817*::TnKRCPN1, Km^R	This study
AQY126	LacA, Δ*pigC, Ser39006_1185*::TnKRCPN1, Km^R	This study
AQY131	LacA, Δ*pigC, Ser39006_3885* (*floR*)::TnKRCPN1, Km^R	This study
AQY136	LacA, Δ*pigC, pigP*::TnKRCPN1, Km^R	This study
AQY138	LacA, Δ*pigC, gvpV*::TnKRCPN1, Km^R	This study
AQY142	LacA, Δ*pigC, gvpW*::TnKRCPN1, Km^R	This study
AQY143	LacA, Δ*pigC, pigP*::TnKRCPN1, Km^R	This study
AQY149	LacA, Δ*pigC, gvpN*::TnKRCPN1, Km^R	This study
AQY150	LacA, Δ*pigC, rph*::TnKRCPN1, Km^R	This study
AQY158	LacA, Δ*pigC, rph*::TnKRCPN1, Km^R	This study
	Escherichia coli	
β2163	(F^-) RP4-2-Tc::Mu Δ*dapA::(erm-pir)*, Em^R	Demarre *et al.,* 2005
DE3	*E. coli* BL21 derivative, pRare2, Cm^R	Tegel *et al.,* 2010
DH5α	F^- Ø80*lacZ*ΔM15 Δ(*lacZYA−argF*) U169 *recA1 endA1 hsdR17* (rK−, mK+) *phoA supE*44 λ− *thi-1*	Laboratory stock
ESS	β-lactam supersensitive strain	Bainton *et al.,* 1992
	Pectobacterium carotovorum	
ATTn10	ATCC39048::Tn10	McGowan *et al.,* 1996
SM10	ATCC39048::Tn10 Δ*carRABCDEFGH*	McGowan *et al.,* 1996
	Phage	
φOT8	Transducing phage for S39006, flagellum-dependent	Evans *et al.,* 2010

* *ygfX* was initially annotated as *pigV* (Fineran *et al.,* 2005 (a)), but changed recently (Paterson, 2013)

Table 2.2. Plasmids and primers used in this study.

Name, code	Genetic Information	Reference
	Plasmids	
pKCPRN1	Derivative of pDS1028. This plasmid contains a composite transposon, Tn-KRCPN1, with *kan*^{R} and a promoterless *lacZ*, Km^R, Tc^R	Monson *et al.*, 2015
pQE80*oriT*	Derivative of pEQ80, Amp^R	Ramsay *et al*., 2011
pBAD30	Expression vector under control of the *araBAD* promoter, Amp^R	Guzman *et al.*, 1995
pRW50	Promotorless *lacZ* plasmid, Tc^R	Lodge *et al.*, 1992
pTA14	*rap* promoter fusion in pRW50, Tc^R	Gristwood *et al.*, 2009
pTA17$^+$	*smaR* promoter fusion in pRW50, Tc^R	Salmond Lab stock
pTA21$^+$	*pigQ* promoter fusion in pRW50, Tc^R	Salmond lab stock
pTA24$^+$	*pigX* promoter fusion in pRW50, Tc^R	Salmond lab stock
pET19b	Derivative of pET19m, Amp^R	Dolan *et al.*, 2017
pAQY1	pBAD30 with *trkH* , Amp^R	This study
pAQY2	pBAD30 with *floR,* Amp^R	This study
pAQY3	pQE80*oriT* with *floR*, Amp^R	This study
pAQY4	pET19b with *floR*, Amp^R	This study
	Primers (5'sequence, description)	
MAMV1	GGAATTGATCCGGTGGATG F transposon specific primer	Matilla *et al.*, 2012
MAMV2	GCATAAAGCTTGCTCAATCAATCAC F transposon specific primer	Matilla *et al.*, 2012
PF106	GACCACACGTCGACTAGTGCNNNNNNNNNNAGAG Random primed PCR primer 1	Fineran *et al.*, 2005(b)
PF107	GACCACACGTCGACTAGTGCNNNNNNNNNNACGCC Random primed PCR primer 2	Fineran *et al.*, 2005(b)
PF108	GACCACACGTCGACTAGTGCNNNNNNNNNNGATAC Random primed PCR primer 3	Fineran *et al.*, 2005(b)
PF109	GACCACACGTCGACTAGTGC Random primed PCR primers PF106, PF107 and PF108 aptamer specific primer	Fineran *et al.*, 2005(b)
oAQ1	ACGGTAACGCCAAAAATCGAA F Ser39006_1186 specific primer	This study.
oAQ2	ACCGCGATTCACATCACCAA R Ser39006_1186 specific primer	This study
oAQ3	TTCCAGGATGGTTATTCTGCAT F Ser39006_0591 specific primer	This study
oAQ4	GCTAAGCATTGTTCACTCCGC R Ser39006_0591 specific primer	This study

Table 2.2 continued.

Name, code	Genetic Information	Reference
	Primers (5'sequence, description)	
oAQ5	AGCTGAGATGAGGTTGCGTG F *trkH* specific primer	This study
oAQ6	AGAGATGGGCAAACGAGATCG R *trkH* specific primer	This study
oAQ9	GCGATTGGCGTGAAACTGAG F *tufA* specific primer	This study
oAQ10	CTGGAAAGAGCACGGGATCA R *tufA* specific primer	This study
oAQ11	AAAGGTTTGCTCGATGCTGT F Ser39006_3817 specific primer	This study
oAQ13	TAAGACAGCATATTGACGGGCTT R Ser39006_3817 specific primer	This study
oAQ14	GGGCGAGATGGTGGATGAAT F Ser39006_1185 specific primer	This study
oAQ15	TCCAACTTGTCTTTCGCCACT R Ser39006_1185 specific primer	This study
oAQ16	CGGCACGGCGTTTGATATTG F Ser39006_3885 (*floR*) specific primer	This study
oAQ17	GCAACCGGTGACCATCTACT R Ser39006_3885 (*floR*) specific primer	This study
oAQ32	GATGAGCTCGGGCAAACATTGAGTGA F Ser39006_3885 (*floR*) specific primer with *Sac*I restriction sequence	This study
oAQ33	CTACTGCAGTCAACGGAAATTAACATC R Ser39006_3885 (*floR*) specific primer with *Pst*I restriction sequence	This study
oAQ44	GATGAGCTCAAGGAAGGCATCTGTAATGCAC F *trkH* specific primer with *Sac*I restriction sequence	This study
oAQ45	CTATCTAGATTATTCCCGCCAAAAAG R *trkH* specific primer with *Xba*I restriction sequence	This study
oAQ46	GATGAGCTCTCAGGATAACTGGGTAAACGG F Ser39006_3885 (*floR*) specific primer with *Sac*I restriction sequence	This study
oAQ47	CTATCTAGATCAACGGAAATTAACATCCAC R Ser39006_3885 (*floR*) specific primer with *Xba*I restriction sequence	This study
oAQ52	AAAAAACATATGGGGCAAACATTGAGTGATG F Ser39006_3885 (*floR*) specific primer with *Nde*I restriction sequence	This study
oAQ53	ACGCGGATCCTCAACGGAAATTAACATCCACCA R Ser39006_3885 (*floR*) specific primer with *Bam*HI restriction sequence	This study

[+]These plasmids were constructed by Pete Fineran and are part of the Salmond lab plasmid repository.
*All primers were purchased from Sigma. F: forward, R: reverse. Underlined nucleotides correspond to restriction sites for the enzymes specified.

Table 2.3. Media, buffers, solutions, antibiotics and supplements.

Name	Composition	Reference
	Media	
Lysogeny Broth (LB)	• 10 g l^{-1} Tryptone • 5 g l^{-1} Yeast extract • 5 g l^{-1} NaCl	Miller, 1972
Minimal medium (pH 7.0)	• 5.4 g l^{-1} Na_2HPO_4 • 3.34 g l^{-1} NaH_2PO_4 • 0.1 % NH_4SO_4* • 0.41 mM $MgSO_4$* • 0.2 % glucose*	This study
Minimal medium with potassium phosphate salts (pH 7.0)	• Minimal medium • 7 g l^{-1} K_2HPO_4 • 2 g l^{-1} KH_2PO_4	This study
LB agar (LBA)	• Same as LB Broth, but with 15 g l^{-1} of Agar	Miller, 1972
Minimal medium agar	• Same as minimal medium broth, but with 15 g l^{-1} of agarose	This study
Tryptone swimming agar	• 10 g l^{-1} Tryptone • 5 g l^{-1} NaCl • 3 g l^{-1} Agar	Williamson *et al.,* 2008
Eiken swarming sgar	• Same as LB Broth, but with 7.5 g l^{-1} of Eiken Agar	Williamson *et al.,* 2008
LB top lawn agar (LB molten agar)	• Same as LB Broth, but with 7 g l^{-1} of Agar	Poulter *et al*., 2010
	Buffers and solutions	
50% glycerol	• 50 % glycerol • 50 % dH_2O	
10% glycerol	• 10 % glycerol • 90 % dH_2O	
50X TAE buffer	• 242 g l^{-1} Tris • 18.61 g l^{-1} ethylenediaminetetraacetic acid (EDTA) • 0.0571 % (v/v) glacial acetic acid	
Blocking buffer	• 5% dried skimmed milk (Marvel) in Wash buffer	
CHAPS lysis buffer	• 8 M Urea • 4 % (3-[(3-cholamidopropyl) dimethylammonio]-1-propane-sulphonate) CHAPS • 5 mM magnesium acetate • 10 mM Tris-HCl (pH 8.0)	
Electrode Buffer (pH:8.3) (10X)	• 150 g glycine in 600 ml dH_2O • 30 g Tris • Adjust pH with HCl • dH_2O to 1 l	

Table 2.3 continued.

Name	Composition	Reference
Buffer and solutions		
Lysis buffer	• 50 mM Tris HCl (pH 8) • 0.2 M NaCl • 10 % glycerol • 1 mM Imidazole	
PBS	• 8 g l^{-1} NaCl • 0.2 g l^{-1} KCl • 1.15 g l^{-1} Na_2HPO_4 • 0.2 g l^{-1} KH_2PO_4	
PBS LacZ buffer	• 250 μg ml^{-1} 4'-Methylumbelliferyl-β-D-galactopyranose (Melford laboratories) • 20 mg ml^{-1} lysozyme (Sigma) • PBS	
PBS UidA buffer	• 250 μg ml^{-1} 4'-Methylumbelliferyl-β-D-glucuronide (Melford laboratories) • 20 mg ml^{-1} lysozyme (Sigma) • PBS	
Resolving gel (15% Acrylamide)	• 20 ml 30% Acrylamide stock • 20 ml stock running gel buffer • 0.2 ml 20% sodium dodecyl sulphate (SDS) • 0.4 ml 80 mg ml^{-1} ammonium persulphate (APS) (freshly prepared) • 25 μl TEMED	
SDS-PAGE sample buffer solution A	• 240 mM Tris HCl (pH: 6.8) • 8 % SDS • 40 % glycerol • 50 mM EDTA • 0.4 % bromophenol blue	
SDS-PAGE sample buffer (to 5 ml 4X)	• 4 ml SDS-PAGE sample buffer solution A • 1ml 1 M dithiothreithol (DTT)	
Stacking gel (6 %)	• 6 % (v/v) acrylamide stock • 10 % (v/v) Stock stacking gel buffer	
Stock running gel buffer (pH: 8.3)	• 90.86g Tris in 0.8 l dH_2O • Adjust pH with HCl • dH_2O to 1 l	
Stock stacking gel buffer (pH: 6.8)	• 151.46 g Tris in 0.6 l • Adjust pH with HCl • dH_2O to 1 l	
Transfer buffer	• 14.4 g Glycine • 3.03 g Tris base • 150 ml Methanol • dH_2O to 1 l	

Table 2.3 continued.

Name	Composition	Reference
Buffer and solutions		
Wash Buffer	• PBS • 0.1 % (v/v) Tween 20	
Antibiotics and supplements (Working concentrations)$^{+}$		
Ampicillin (Amp)	50 μg ml^{-1}	
Arabinose	0.2%	
Chloramphenicol (Cm)	50 μg ml^{-1}	
Diaminopimelic acid (DAPA)	0.3 mM	
Erythromycin (Em)	200 μg ml^{-1}	
Kanamycin (Km)	25 μg ml^{-1}	
IPTG	0.5 mM	
Spectinomycin (Sp)	50 μg ml^{-1}	
Streptomycin (Sm)	50 μg ml^{-1}	
Tetracycline (Tc)	15 μg ml^{-1}	

*Stocks of each of these components were autoclaved separately and added to the final solution concentrations indicated. $^{+}$All antibiotics and supplements were sterilized using 0.22 μm filters. Also, they were dissolved in dH_2O, except Em which was dissolved in 99.6 % ethanol.

2.3 Random Primed PCR

The transposon insertion site in transparent, hyper-opaque and bulls-eye mutants were identified using random primed PCR (RP-PCR) and DNA sequencing. Reagents and conditions for RP-PCR are listed in Table 2.4. All reactions were performed in a Veriti Thermal Cycler. A first round of touchdown PCR was performed using random primers (PF106, PF107 and PF108) tagged with a known sequence at the end (aptamer), and a transposon-specific primer (MAMV1). Colonies of S39006 mutants were used as the source of the DNA template in the first round. Sequentially, a second round was done to amplify sequences synthesised from the first round using a transposon-specific primer (MAMV2) and PF109. PF109 is a complementary oligonucleotide to the known sequence at the end of the first-round random primers (aptamer). The PCR products were run in 1X TAE with 1 % agarose and against 5 μl 0.2-1Kb marker (Bioline Hyperladder).

Table 2.4. Random PCR conditions

Reagent	Round 1 Volume (μl)		Round 2 Volume (μl)
10X PCR Buffer (Bioline®)		2.5	
50mM $MgCl_2$		0.375	
2mM dNTPs		2.5	
10μM MAMV1	1.25		-
10μM MAMV2	-		1.25
10μM PF106	0.425		-
10μM PF107	0.425		-
10μM PF108	0.425		-
10μM PF109	-		1.25
Taq pol (Bioline)		0.5	
Colony	+		-
DNA from 1st round	-		2.5
dH_2O	16.85		14.375
Total Volume per reaction	**25**		**25**

Cycles	Temperature and time Round 1	Round 2
1X	94 °C x 3min	
6X and the annealing temperature was increased * 1°C each cycle.	94 °C x 15s 42 °C* x 30sec 72 °C x 3min	
25 X	94 °C x 15sec 55 °C x 30sec 72 °C x 3min	94 °C x 15sec 60 °C x 30sec 72 °C x 3min
1X	72 °C x 7min	
1X	12 °C	

2.4 DNA Sequencing

DNA products were resolved in 1X TAE on 1% agarose gels containing 0.5 μg ml^{-1} ethidium bromide. Bands showing DNA were cut and purified from the gel using the GeneJet Gel Extraction Kit from Thermo Fisher Scientific and DNA quantified using the NanoDrop. Samples of 10 μl containing 1 μM of forward primer (MAMV2 in the case of random primed PCR products) and 7.5ng μl^{-1} either PCR or plasmid product were sequenced at the GATC Company.

2.5 Bioinformatic analysis

The quality of the sequencing chromatograms was analysed using SnapGene Viewer. The software Artemis 16.0 (Carver *et al.,* 2011) was used for identification of the transposon

insertion sites. This information was obtained through nucleotide alignment with the genome sequence of S39006 (Genome provided by Dr. Rita Monson) (Fineran *et al.* 2013). The predicted amino acid sequences encoded by the genes were identified and analysed for conserved domains using the protein-protein BLAST algorithm from NCBI (Boratyn *et al.,* 2012).

2.6 Transduction with φOT8 phage

2.6.1 Determination of the phage titre

Transduction of mutations into different S39006 strains was performed following the methodology published by Evans and co-workers (2010). First, the phage titre necessary for transduction was determined by spotting 10 μl of serial dilutions (down to 10^{-7}) of a φOT8 phage stock on an LBA plate containing a top lawn of S39006. The top lawn was prepared using 4 ml of molten LB Top Lawn Agar (Table 2.3) with 100 μl of bacteria before pouring onto LBA plates and allowing to set for 20 minutes. After 16 h of incubation at 30°C, plates were analysed and the spot showing semi-confluent lysis (this is a plate with phage plaques overlapping each other) determined the dilution used for phage infection in subsequent steps.

2.6.2 Transduction of gas vesicle mutants

Phage lysates carrying the transposon mutations were obtained using a LB Top Lawn Agar containing 100 μl of bacteria (strains AQY102, AQY103, AQY107, AQY121, AQY124, AQY125 and AQY126) and 10 μl of φOT8 dilution determined as explained in the previous section. The mixtures were immediately poured onto LBA plates and incubated at 30 °C O.N. The top-lawns showing semi-confluent lysis were harvested and transferred to a 20 ml glass universal with 500 μl of $NaHCO_3$-saturated chloroform. The contents in the universals were mixed vigorously using a vortex mixer for 2 min and centrifuged at 4 °C and 2,219 *g* for 20 min. The upper liquid phase obtained was transferred to a 5 ml glass bijoux and stored at 4 °C.
Fresh O.N. cultures of recipient host (i.e. strains NWA19, LacA, *gvpA1*::*uidA*, *gvrA*::*uidA*) were pelleted at 4 °C and 2,219 *g* for 10 min. The supernatant was discarded and the pellet was

resuspended in 1 ml with 100 μl of phages lysates obtained from the transposon mutants. The phage-bacteria mix was incubated at 30 ^{o}C for 20 min, then transferred to a 1.5 ml Eppendorf tube and centrifuged at 2,000 *g* for 1 min. The supernatant was discarded and the pellet was washed three times with 1 ml of LB. The bacteria were incubated at 30 ^{o}C for 20 min, pelleted at 2,000 *g* for 1 min and resuspended in 250 μl of LB. Finally, up to 100 μl were spread on LB plates containing either Km, Cm, Sm, Sp (Table 2.3) or in combination, and incubated at 30 ^{o}C for 48 h.

2.7 Confirmation of phenotypes by transduction into S39006 (clean backgrounds)

The transposon insertion sites in *Ser39006_1186*, *Ser39006_0591*, *trkH*, *tufA*, *Ser39006_3817*, *Ser39006_1185* and *Ser39006_3885* were confirmed, after transduction, by PCR with oligonucleotides specific for their open reading frames (ORF) (Table 2.2). PCR conditions are listed in Table 2.5. PCR reactions were performed in a Veriti Thermal Cycler as indicated in Table 2.5 and purified DNA samples were used to confirm sequence as described in section 2.4.

Table 2.5. PCR conditions

Reagent	**Volume (μl)**	
DNA source	colony	Purified DNA (2.5)
10X PCR Buffer (Sigma®)	2.5	
50mM $MgCl_2$	0.375	
2mM dNTPs	2.5	
Forward primers	1.25	
Reverse primers	1.25	
Taq pol (Sigma)	0.5	
dH_2O	16.85	14.375
Total Volume per reaction	**25**	**25**
Cycles	**Temperature and time**	
1X	94 ^{o}C x 3min	94 ^{o}C x 1min
35 X	94 ^{o}C x 15s 55-63 ^{o}C* x 30sec 72 ^{o}C x 15sec	
1X	72 ^{o}C x 3min	
∞	4 ^{o}C	

*Temperature varied depending on the Tm of primers.

2.8 Cell and Colonial morphology, swarming and swimming motility assays

S39006 strains were spotted using 10 μl of normalized (OD_{600} 1.0) cultures, and assessed for patch morphology on LB agar, and for flagellar motility in tryptone swimming agar and Eiken swarming agar (Table 2.3). The effect of extracellular potassium on cell morphology was assessed in minimum media plates with different potassium concentrations (Table 2.3) for 16 h at 30 ^{o}C to observe the colonial morphology.

2.9 Prodigiosin measurement

1 ml samples from either fresh overnight cultures normalized to OD_{600} 1.0, or growth assays samples taken at different time points were pelleted at 12,000 *g* and 4 ^{o}C for 10 min. Cell pellets were kept at -80^{o}C until assayed. Later, samples were thawed at room temperature, solubilized with 1 ml of acidified (4 % 1 M HCl) ethanol and vortex mixed until fully resuspended. Cell debris was centrifuged at 12,000 *g* for 10 min. Immediately, the supernatant was transferred to a 1 ml cuvette, absorbance measured at A_{534} and expressed as [(A_{534} ml^{-1} OD_{600}^{-1}) x 50] (Fineran *et al.,* 2005(a)).

2.10 Quantitative carbapenem and BHL production assays throughout growth

Samples from growth assays were centrifuged as described in section 2.9, supernatants sterilized using 0.22 μm syringe filters and kept on ice up to 6 h. Meanwhile, 400 ml LB agar were poured into 245x245x25 bioassay dishes (Thermo Fisher Scientific). Once the agar was set, 100 ml of an LB top lawn agar containing indicator strains was poured into the bioassay dishes containing set LBA. 100 μl of the β-lactam supersensitive strain *E. coli* ESS was used as the indicator strain for the carbapenem assay, whereas 1 ml of S39006 SP19 was used as the reporter strain for BHL detection (Poulter *et al.,* 2010). When the top agar was set, symmetrical holes were cut using a sterile 0.5 cm core borer. 200 μl of samples for each time point were used to fill the holes. Plates were incubated at 30 ^{o}C. After 16 h, photographs of the bioassay plates were taken, and the disc halo areas of growth inhibition and pigment production for carbapenem and BHL, respectively, were measured using ImageJ (Abràmoff *et al.,* 2004). The data were expressed as [cm^2 OD_{600}^{-1}].

2.11 Carbapenem production and resistance

LBA plates containing a top lawn of *E. coli* ESS were spotted with 10 μl of OD_{600} 1.0 cultures of S39006 gas vesicle mutants, WT and *carA* strains. Plates were incubated O.N. to capture images on the changes of halo inhibition due to carbapenem production. Bioassay LBA plates were covered with molten agar containing *E. coli* ESS as specified in the previous section, whilst LBA Petri dishes were inoculated with 4 ml molten agar and 10 μl of bacteria.

The impact of *Ser39006_3885* (*floR*) on S39006 carbapenem intrinsic resistance was assessed by spotting 10 μl of OD_{600} 1.0 cultures of *P. carotovorum subsp. carotovorum* strains ATTn10 and SM10, and S39006 WT on LBA plates covered with bacterial top lawns prepared by mixing 4 ml LB molten agar with 100 μl of S39006 *floR* or 10 μl *E. coli* ESS.

2.12 Microscopy

Phase contrast microscopy (PCM) images were obtained from cells grown in either solid or liquid cultures. Normalized (OD_{600} 1.0) spots were grown on LB or glucose minimal media with different potassium concentrations. After 16 h of incubation cells were scraped from patches into 5 μl LB or minimal medium on microscope glass slides. Immediately, samples were covered with a glass slip and analysed under oil immersion using an Olympus BX-51 microscope with a 100X lens. Samples from flotation assays were analysed taking 1 μl of samples into 4 μl of either LB or minimal medium with different potassium concentrations. Images were taken with a QICAM monochrome camera adapted to QCapture Pro-6 software.

Transmission electron microscopy (TEM) images were obtained from cells in static liquid cultures after 2 days. Sample preparations were performed as recommended by Ramsay *et al.,* (2011). Briefly, a carbon-coated glow-discharged grid was treated with 0.01% polylysine for 2 min, then 5 μl of undiluted cell suspensions were attached for 10 min and rinsed with dH_2O. Cells were stained with 2 % phosphotungstic acid (pH 7.0) neutralized with KOH. Cell images were obtained using a FEI Tecnai G2 TEM in the Cambridge Advance Imaging Centre, University of Cambridge.

2.13 β- glucuronidase (UidA) and β- galactosidase (LacZ) activity in fusion strains

S39006 strains containing *uidA* or *lacZ* gene fusions were assessed for growth in 25 ml of LB as mentioned in section 2.1. Samples (100 μL) were taken at different time points and kept in 96 well microtitre plates at -80 ^{o}C until assays were performed. Samples were thawed at 37 ^{o}C and 10 μl aliquots were diluted into 90 μl LB and frozen again for no less than 30 min. Thereafter, diluted samples were thawed at room temperature and 10 μl were mixed with 100 μl of either PBS UidA buffer or PBS LacZ. The UidA and LacZ activity (reporter activity), was quantified using a Gemini XPS plate reader fallowing the parameters suggested by Ramsay *et al.* (2011). The reporter activity at each time point was normalized to culture $OD_{600,}$ and expressed as RFU min^{-1} OD_{600}^{-1}.

2.14 Preparation of competent cells

E. coli and S39006 seed cultures were grown as indicated in section 2.4. A seed inoculum (0.5 ml) from a fresh O.N culture was transferred into a 250 ml flask containing 25 ml LB with 375 μl 1 M $MgCl_2$, incubated in a water bath (at 37 ^{o}C for *E. coli* and 30 ^{o}C for S39006), and aerated at 300 rpm. *E. coli* cells were grown to 0.6 OD_{600} and S39006 cells to 0.8 OD_{600}. Cultures were transfer to a pre-chilled 30 ml universal tube and chilled on ice for 1 h. Thereafter, cells were pelleted at 4,500 rpm at 4 ^{o}C for 10 min, and supernatant discarded. Immediately, cells were washed in 10 ml ice-cold water and in 10 % (v/v) glycerol two more times. Cells were pelleted as indicated previously and supernatant discarded after each wash step. *E. coli* cells were resuspended after the final wash step into 1 ml 10 % glycerol, or S39006 into 750 μl 10% glycerol. *E. coli* cells were transferred into pre-chilled 1.5 ml Eppendorf tubes using 200 μl aliquots and kept for up to 6 months.

2.15 DNA transformation by electroporation

Competent cells prepared as described in section 2.14 were used for transformation via electroporation. A mixture of 50 ng of plasmid DNA with either 50 μl of *E. coli* or 100 μl of S39006 was added into 0.2 cm electrode Bio-Rad electroporation cuvettes. A Bio-Rad Gene Pulser was used for electroporation with a pulse controller resistance of 200 Ω, capacitance

25 μFd and voltage 2.5 kV. Bacteria were immediately recovered after pulsing with 1 ml LB for 1 hour at 37 ^{o}C for *E. coli* and 30 ^{o}C for S39006. The recovered cells were pelleted at 8,000 *g* for 5 min and resuspended in 250 μl LB. Finally, 50-100 μl of cells were plated out into appropriate antibiotics and incubated O.N. for selection of transformed colonies.

2.16 Cloning and transformation

All genes cloned were amplified using colony PCR with S39006 (WT) (See Table 2.4 for conditions). Primer sequences and enzyme restriction sites are indicated in Table 2.2. Ser39006_3885 (*floR*) was amplified with primers oAQ32 and oAQ33 for cloning into pQE80*oriT*, oAQ46 and oAQ47 for cloning into pBAD30, and oAQ52 and oAQ53 for cloning into pET19b. Primers oAQ44 and oAQ45 *trkH* were used for amplification of *trkH* and cloning into pBAD30. PCR products were purified and sent for DNA sequencing as indicated previously in section 2.4. PCR and plasmid DNA were double-digested using restriction enzymes, according to the manufacturer protocol (NEB®). The total digestion reaction was run in a 1 % agarose electrophoretic gel for length analysis and separation and size estimates. DNA bands with the expected size insert and vector were cut from the agarose gel and purified using the GeneJet Gel Extraction Kit from Thermo Fisher Scientific. DNA was quantified using a NanoDrop and a 1:4 vector to insert molar ratio was used for 16 h ligation reactions at 16 ^{o}C with T4 DNA ligase (NEB®). Ligation reactions were performed following manufacturer recommendations. Reaction mixtures were heat inactivated at 80 ^{o}C for 10 min and transformed as indicated in section 2.14. pAQY1 and pAQY2 were used to transform S39006 cells, whilst pAQY3 and pAQY4 were transformed into *E. coli* β2163 and *E. coli* DE3, respectively.

2.17 Protein extraction

Cultures for protein analysis were inoculated in 500 ml flasks with 50 ml for TMT-labelling and with 0.2 % arabinose for GvpC immunoblots. Samples for TMT-labelling and GvpC immunoblots were collected at 16 h, normalized to 2.0 OD_{600}, pelleted at 8,000 *g* and 4 ^{o}C, and resuspended in 1.25 ml with CHAPS lysis buffer containing 1X protease inhibitor cocktail set I (Calbiochem) (Coulthurst *et al.,* 2006). The lysis solution was kept on ice and sonicated

for 10 s x 6 cycles (the sonicator was 10 s on and 60 s off per cycle). Cell debris and insoluble material were pelleted at 13,000 *g* and 4 ^{o}C. Supernatants containing soluble protein extracts were transferred to pre-chilled tubes kept at 4 ^{o}C.

For His-tagged FloR purification, cultures of *E. coli* DE3 (pAQY4) were grown in 1 l flasks with 100 ml LB with ampicillin at 37 ^{o}C and shaking at 120 rpm up to 0.6 OD_{600}. Thereafter, temperature was lowered to 20 ^{o}C and heterologous His-tagged FloR expression was induced by adding IPTG and incubating cells for an additional 20 h (Dolan *et al.,* 2017). Cells were collected at 25,000 *g* at 4 ^{o}C for 20 mins. Cells were kept on ice throughout, resuspended in 25 ml lysis buffer and sonicated for 20 s x 5 cycles (the sonicator was 10 s on and 60 s off per cycle). The expression of His-tagged FloR was assessed by Western Blot (Section 2.19).

2.18 Protein quantification and precipitation for TMT and LC-MS/MS proteomics

Cell samples for whole intracellular proteomic analysis were grown as described in sections 2.1, whilst protein extracts were obtained as described in section 2.14. The amount of proteins in the samples was quantified with the DC^{TM} (detergent compatible) Protein Assay from Bio-RAD following the manufacturer's instructions. Thereafter, 100 μg of proteins was diluted with 6 times (volume) of ice-cold acetone and kept at -20^{o}C overnight for precipitation. Samples were sent to the Cambridge Centre for Proteomics (CCP) for procedures described in Appendix, Sections 7.1-4.

2.19 Western Blot

Aliquots of the protein extracts (Section 2.14) were mixed with SDS-PAGE sample buffer to a final volume of 20 μl into 1.5 ml Eppendorf tubes and heated for 10 min at 80 ^{o}C. Proteins were separated using 1D SDS-PAGE by running samples in a 15 % acrylamide gel (resolving gel) (1 mm thick) with 10 lanes, initially through the stacking gel, at 80 mV for 20 min and, later, at 120 mV for 2 h in 1X Electrode Buffer. The gel with the separated proteins was assembled for blotting in a BIO-RAD Mini-PROTEAN Tetra System with an Immobilon-P PVDF membrane (Millipore) and run at 250 mA for 90 min. Then, the PVDF membrane was placed

in 120x120x17 square plate and washed three times for 5 min with Wash Buffer, and blocked with 50 mg ml^{-1} of blocking buffer for 1 h. The antibody hybridization was performed using a rabbit GvpC antibody (for S39006 samples) or an Anti-6-His antibody (for *E. coli* DE3 pAQY4 samples) in blocking solution (1:30000 antibody to blocking solution volume ratio) by mixing for at least 1h. Afterwards, the membrane was washed 4 times for 5min. The secondary antibody hybridization was done with goat IgG (1:30000 IgG to blocking solution volume ratio) for no longer than 40 min. Finally, the membrane was washed 4 times for 5 min. Washing, blocking and hybridization steps were performed on a rotor platform (Red Rotor, Hoefer). Detection was performed with 500 μl each of Detection Reagents (Millipore Develop Kit) at room temperature in a plastic sealed membrane. Bubbles formed after addition of Detection Reagents were removed over the film by pressing the membrane area. The plastic protected membrane was exposed to an X-ray film (Konika Minolta) for 1 min in a dark room using an X-ray film cassette. The X-ray film was developed with fixing (Tatenal Superfix RTU) and developing (Tatenal Roentroll 25 RTU) solutions in dark-room.

2.20 Pressure Nephelometry

The collapse of GVs was monitored using a pressure nephelometer (Holland & Walsby, 2009; Tashiro *et al.,* 2016). Changes in turbidity (nephelometry) caused by gas vesicle collapse were taken after gradual pressure injections of 0.05 MPa using compressed N_2. A blank of 4 ml of media without cells was used to set the millivoltmeter to zero. Afterwards, 0.5 ml of cells from a culture previously grown in LB and left static on the bench for 48 h were added to tubes containing either LB (turgid condition) or LB with 0.35 mM sucrose (hypertonic condition). The tubes were hermetically sealed and the millivoltmeter set to 100. The proportion of gas vesicles remaining after pressure injections and the turgor pressure were calculated as described by Tashiro and co-workers (2016).

Chapter 3
Screening of S39006 gas vesicle mutants

3.1 Potential novel gas vesicle regulators

Gas vesicles accumulate in the cytoplasm and provide distinctive phase brightness to individual cells and white opacity to colonies. S39006 wild type (WT) colonies appear red instead of white opaque due to the production of the prodigiosin pigment. S39006 NWA19 (NWA19) has an in-frame mutation in one of the genes essential for prodigiosin biosynthesis (*pigC*). Random mutagenesis of the non-pigmented strain, NWA19, permitted the identification of mutants with variations in colony opacity due to alterations in gas vesicle production (Ramsay *et al.,* 2011; Lee *et al.,* 2017). The plasmid pKRCPN1 (Monson *et al.,* 2015) was delivered into NWA19 cells by conjugation with *E. coli* β2163. This plasmid contained a transposon cassette composed of a kanamycin resistance gene, Kan^R, for selection of mutants, and a promotorless *lacZ* for construction of reporter gene fusions.

In total, 21 conjugations were set up and 32,432 mutants were screened. Two different colony phenotypes were initially considered for isolation and characterization: transparent and hyper-opaque. Also, it was observed that some colonies had a distinctive colony shape and opacity; these colonies were also isolated and classified as bull's-eye transparent and bull's-eye opaque mutants (Table 3.1). A similar colony phenotype to the bull's-eye transparent mutants was observed in a previous screening for prodigiosin mutants (Paterson, 2013), whilst the bull's-eye opaque had not been investigated before. The genomic insertion site of the TnKRCPN1 transposon was identified in 31 mutants by random primed PCR (RP PCR) reactions and DNA sequencing (Table 3.1). Strains identified as AQY102, 103, 107, 115, 118, 121, 124, 125, 126 and 131 contained transposon insertions in genes uncharacterized for gas vesicle production (Table 3.1). The other strains were not considered novel for this project because their genotypes have been identified in previous, or currently ongoing, investigations in this laboratory.

Mutants AQY44, 54, 74, 75, 108, 112, 117, 122, 138, 142, and 149 had transparent colonies and carried transposon insertions in the gas vesicle gene cluster. The impact of these genes

on gas vesicle formation and flotation was studied previously (Ramsay *et al.,* 2011; Tashiro *et al.,* 2016). Insertions in the ribose kinase gene *rbsK* were identified in the transparent mutants AQY72 and AQY123. Transposon insertions in *rbsK* were reported to have polar effects on *rbsR* transcription, a known regulator of gas vesicle formation (Lee *et al.,* 2017). Insertions in *pigP*, a known prodigiosin, carbapenem and flagella regulator, were identified in three mutants (AQY113, AQY136 and AQY143). Also, mutations in the adenylate cyclase *cyaA*, the transcription factor *crp* and ribonuclease *rph* genes (AQY100, AQY110, 150 and 158) were identified. Mutations in *pigP*, *cyaA*, *crp*, and *rph* were not considered novel for this project because they have been associated with gas vesicle biogenesis by other researchers in this laboratory.

Table 3.1 Identification of transposon insertion sites in S39006 Δ*pigC* mutants.

Strain	Phenotype	Genotype	Insertion orientation relative to gene
AQY44	Transparent	*gvpF1*::TnKRCPN1	Sense
AQY54	Transparent	*gvpV*::TnKRCPN1	Sense
AQY74	Transparent	*gvpA2*::TnKRCPN1	Antisense
AQY75	Transparent	*rbsk*::TnKRCPN1	Same
AQY100	Hyper-opaque	*cyaA*:: TnKRCPN1	Same
AQY102	Bull's-eye transparent	*Ser39006_1186*::TnKRCPN1	Same
AQY103	Bull's-eye opaque	*Ser39006_0591*::TnKRCPN1	Same
AQY107	Hyper-opaque	*trkH:*:TnKRCPN1	Antisense
AQY108	Transparent	*gvpF1*::TnKRCPN1	Sense
AQY110	Hyper-opaque	*crp*::TnKRCPN1	Antisense
AQY112	Transparent	*gvpN*::TnKRCPN1	Sense
AQY113	Transparent	*pigP*::TnKRCPN1	Sense
AQY115	Bull's-eye opaque	*Ser39006_0591*::TnKRCPN1	Sense
AQY117	Transparent	*gvpN*::TnKRCPN1	Sense
AQY118	Bull's-eye transparent	*Ser39006_1185*::TnKRCPN1	Antisense

Table 3.1 continued

Strain	Phenotype	Genotype	Insertion orientation relative to gene.
AQY119	Transparent	*gvpZ*::TnKRCPN1	Antisense
AQY120	Transparent	*gvpA*::TnKRCPN1	Antisense
AQY121	Transparent	*Ser39006_3835:*::TnKRCPN1	Antisense
AQY122	Transparent	*gvrA*::TnKRCPN1	Antisense
AQY123	Transparent	*rsbK*::TnKRCPN1	Antisense
AQY 124	Hyper-opaque	*tufA*:: TnKRCPN1	Antisense
AQY125	Bull's-eye opaque	*Ser39006_3817*::TnKRCPN1	Same
AQY126	Bull's-eye transparent	*Ser39006_1185*::TnKRCPN1	Antisense
AQY131	Transparent	*Ser39006_3835*::TnKRCPN1	Antisense
AQY136	Transparent	*pigP*::TnKRCPN1	Sense
AQY138	Transparent	*gvpV*::TnKRCPN1	Sense
AQY142	Transparent	*gvpW*::TnKRCPN1	Antisense
AQY0143	Transparent	*pigP*::TnKRCPN1	Antisense
AQY149*	Transparent	*gvpN*::TnKRCPN1	Sense
AQY150	Transparent	*rph*::TnKRCPN1	Sense
AQY158	Transparent	*rph*::TnKRCPN1	Sense

*This mutant contains an insertion upstream of the open reading frame.

3.2 S39006 novel gas vesicle mutants display differences in colony and cell morphology, and flotation

Six isolates contained transposon insertions in genes previously uncharacterized (AQY102, 103, 115, 121, 125 and 131); two were highly conserved but have not been reported before to affect gas vesicles (AQY107 and 124), and another two (AQY118 and 126) had insertions in a gene (*Ser39006_1185*) previously identified as *wzt* in a screening for prodigiosin mutants

(Paterson, 2013). Nonetheless, *Ser39006_1185* had not been previously identified in gas vesicle mutant screens (see section 3.2.2).

Mutations in all potential novel regulators were transduced back into NWA19 using phage φOT8; this confirmed that the phenotypes associated with the transposon insertions were reproducible when moved into clean genetic backgrounds (strains without pKRCPN1 or prior to transposon mutagenesis). Thereafter, the mutants obtained were tested for kanamycin resistance and tetracycline sensitivity, and the transposon insertion site was confirmed by sequencing using DNA amplified with specific primers for the transposon and each gene affected. This confirmed that the plasmid was no longer present in the mutants and the transposon was located in the genes previously identified.

3.2.1 AQY121 is defective for gas vesicle production, whilst AQY107 and AQY124 are hyper-producers

Gas vesicle formation and cell buoyancy were assessed in cultures of the mutants considered to have transposon insertions in novel genes (Figure 3.1). Colonies of AQY121 were transparent to the naked eye, whilst AQY107 and AQY124 appeared more opaque (hyper-opaque) compared to the parental strain, NWA19. Nonetheless, it was difficult to obtain images showing the difference among colonies NWA19 and opaque colonies (Figure 3.1.A). To capture the morphological variations associated with gas vesicle production, spots of cultures normalized to 1.0 OD_{600} were patched on LBA (Figure 3.1.B). Samples were also analysed for cell morphology using phase contrast microscopy (PCM) (Figure 3.1.C). The colonies, cell patches and PCM images confirmed that AQY121 was a transparent mutant producing less phase bright structures (gas vesicles). In contrast, patches and individual cells of the hyper-opaque mutant AQY107 were indeed more opaque and they hyper-produced gas vesicles compared to the NWA19 control (Figure 3.1.B-C). Interestingly, the patch from AQY124 did not appear more opaque than NWA19, but it was noticeable that all cells observed in the PCM contained gas vesicles.

WT cells remain buoyant, due to gas vesicles, in LB static cultures (Ramsay *et al.,* 2011). Pictures of AQY121, AQY107 and AQY124 static cultures were taken (Figure 3.1.D). It was

noticed that AQY121 started to sink more compared to NWA19; the top of the AQY121 cultures looked more translucent. In contrast, AQY107 and AQY124 cells remained buoyant and, hence, the culture was turbid throughout the entire liquid column. Furthermore, AQY107 and AQY124 were buoyant for more than 15 days of observation. These observations suggested that AQY121, AQY107 and AQY124 carry mutations in genes modulating gas vesicle production in S39006.

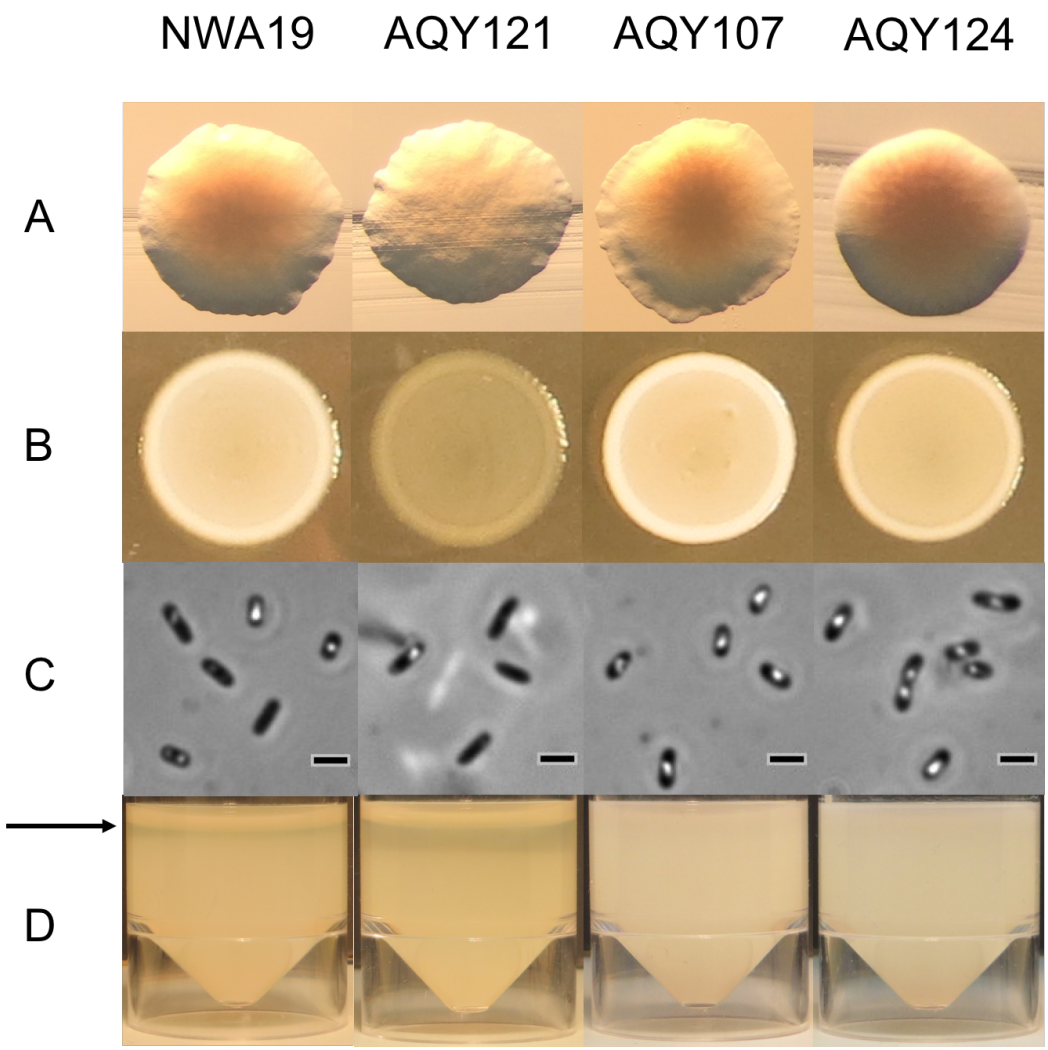

Figure 3.1. Morphology and flotation of S39006 transparent and hyper-opaque mutants. Cultures of NWA19 (Δ*pigC*), AQY121 (*Ser39006_3835*::TnKRCPN1), AQY107 (*trkH*::TnKRCPN1), AQY124 (*tufA*::TnKRCPN1) were used for colony isolation and colonial growth (patch), morphology analysis by PCM and flotation assays in static liquid culture. (**A)** Colony, (**B**) patch and (**C**) PCM images were taken after 16 h of culture. (**D**) Flotation assay images were taken after ten days in static culture. The arrow highlights the zone of the culture that lost cell buoyancy. Only one mutant of each of those sharing the same genotype was considered for this assay and subsequent experiments. Patch and flotation images are representative of three biological replicates. Bars in PCM images from patches correspond to 1 μm.

3.2.2 The bull's-eye mutants produce gas vesicles but fail to remain buoyant

Colonies with distinctive shape and opaqueness distribution were recurrently observed in mutant screens. Mutants AQY102, AQY103, AQY115, AQY118, AQY125 and AQY126 produced rough colonies with a bull's-eye shape (See AQY102 and AQY126 in figure 3.2.A), whilst AQY102, AQY118 and AQY126 looked transparent on the edges, but opaque in the centre of the colony. In contrast, the opaqueness of AQY103, AQY115 and AQY125 mutants was distributed on the bull's-eye colony (See AQY103 and AQY125 in figure 3.2.A). Considering the colony shape and opaqueness distribution, mutants AQY102, AQY118 and AQY126 were classified as bull's-eye transparent mutants, whilst AQY103, AQY115, AQY125 as bull's-eye opaque mutants (Table 3.1).

As in the transparent and hyper-opaque mutants, to study the colony, patch and individual cell morphology, one mutant for each gene resulting in a bull's-eye phenotype was assessed (Figure 3.2). The bull's-eye transparent mutants had a similar patch morphology, but looked less opaque compared to NWA19 patches (Figure 3.2.B). Unexpectedly, it was observed by PCM that cells from the bull's-eye transparent patches still produced gas vesicles. The mutants classified as bull's-eye opaque produced similar patch morphology compared to NWA19. Also, as expected from its colonial phenotype, cells contained gas vesicles.

As with the transparent and hyper-opaque mutants, flotation assays were also done with the bull's-eye mutants (Figure 3.2). Surprisingly, after 3 days of static culture the bull's eye opaque mutants sunk dramatically, whilst the bull's-eye transparent mutants started to sediment moderately but more visible than NWA19. This result suggested that the bull's-eye mutants produce gas vesicles, but did not float, implying that, although gas vesicles are necessary for flotation, they are not sufficient and other factors can influence cell buoyancy.

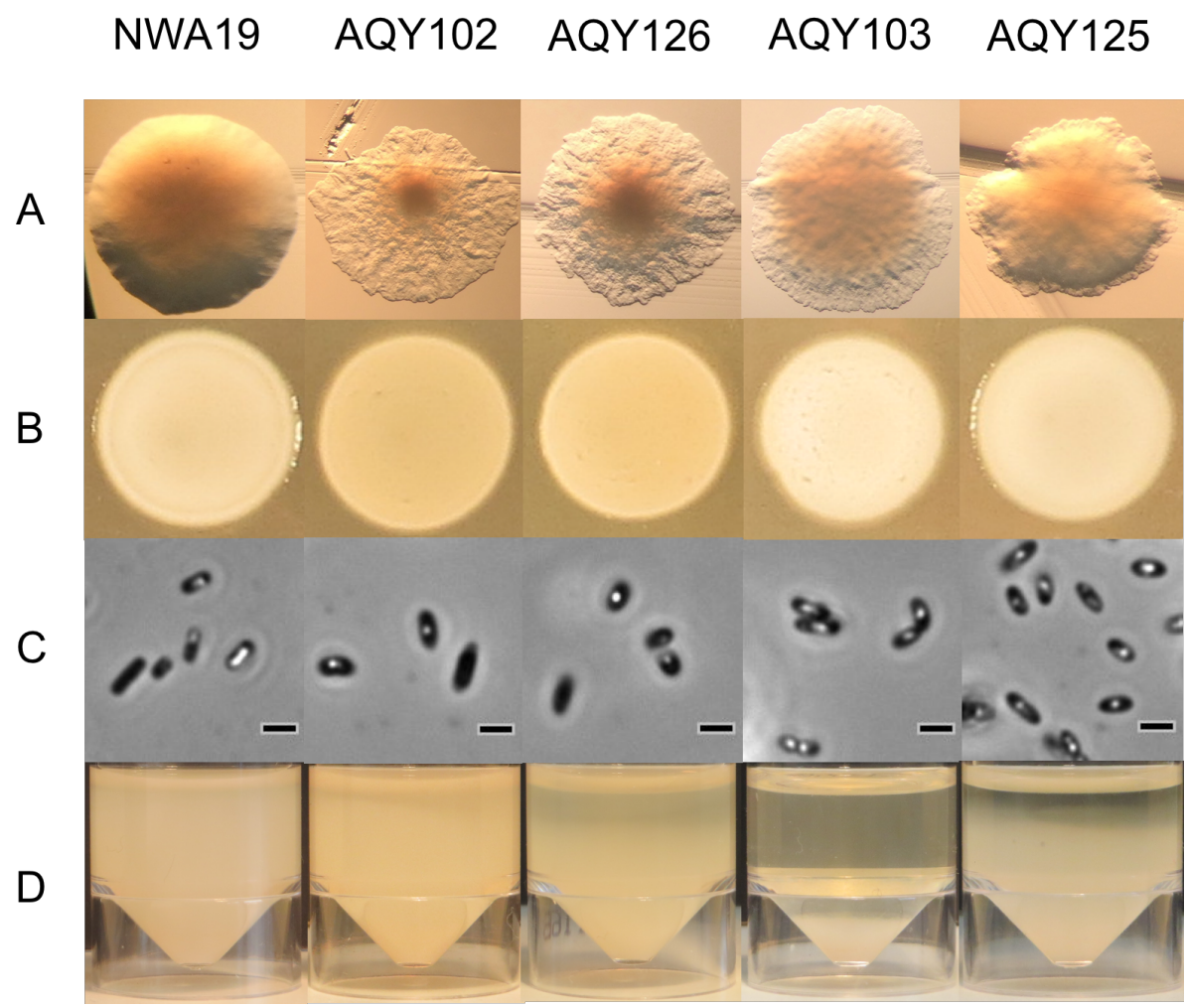

Figure 3.2. Morphology and flotation of S39006 bull's-eye mutants. Cultures of NWA19 (Δ*pigC*), AQY102 (*Ser39006_1186*::TnKRCPN1), AQY126 (*Ser39006_1185*::TnKRCPN1), AQY103 (*Ser39006_0591*::TnKRCPN1) and AQY125 (*Ser39006_3817*::TnKRCPN1) were used for colony isolation and colonial growth (patch), morphology analysis in PCM and flotation in static liquid culture. (**A**) Colony, (**B**) patch and (**C**) PCM images were taken after 16 h of culture. (**D**) Flotation assay images were taken three days after in static incubation. Only one mutant of each of those sharing the same genotype was considered for this assay and further experiments. Patch and flotation images are representative of three biological replicates. Bars in PCM images from patches correspond to 1 μm.

3.3 Bioinformatic analysis of gas vesicle novel mutants

3.3.1 Analysis of the transparent mutants

The transparent mutants AQY121 and AQY131 carried transposons in different sites within a gene annotated as *Ser39006_3835* (Table 3.1; Figure 3.3.A). Both insertions were antisense relative to the direction of transcription of the target gene. Therefore, it was not possible to

study the transcription of this gene using the reporter cassette in the transposon (Monson *et al.,* 2015). The predicted protein coded by *Ser39006_3835* has 272 amino acids, a helix-turn-helix (HTH) DNA binding domain in the N-terminal region of the protein and a DeoR-like sensor domain in the C-terminal region (Figure 3.3.B).

Analysis in the NCBI platform showed that this DeoR family protein has similarities with the glycerol 3-phosphate regulon repressor (GlpR), but the predicted protein from *Ser39006_03835* has only 27% and 26% similarity with GlpR from *E. coli* and *Pseudomonas putida* respectively. Moreover, despite being conserved in closely related bacteria, the predicted *Ser39006_3835* product does not show identity greater than 33% with any known DeoR-like protein previously characterized in enterobacteria (Table 3.2). This suggested that the S39006 gas vesicle regulator protein may represent a new member of the DeoR family.

Comparisons of the *Ser39006_3835* operon with homologues revealed that the genomic organization in upstream genes is conserved to some extent (Figure 3.3.A). None of the genes in the vicinity of *Ser39006_3835* have been characterized in S39006, but similar protein products in *E. coli* are important enzymes in central metabolism. For instance, *Ser39006_3836* contains a 4-hydroxythreonine-4-phosphate dehydrogenase (PdxA)-like domain. PdxA is an enzyme of the pyridoxine (Vitamin B_6) biosynthetic pathway (Laber *et al.,* 1999). Other genes around *Ser39006_3835* are predicted to encode an alcohol dehydrogenase, a sugar epimerase and a glyoxylate reductase, which are proteins involved in carbon metabolism (Table 3.3). Because AQY121 is defective for gas vesicle production and flotation, and *Ser39006_03835* has not been characterized in S39006, or its homologues in other bacteria, this novel mutant represented a good candidate for further study in this project (See Chapter 4).

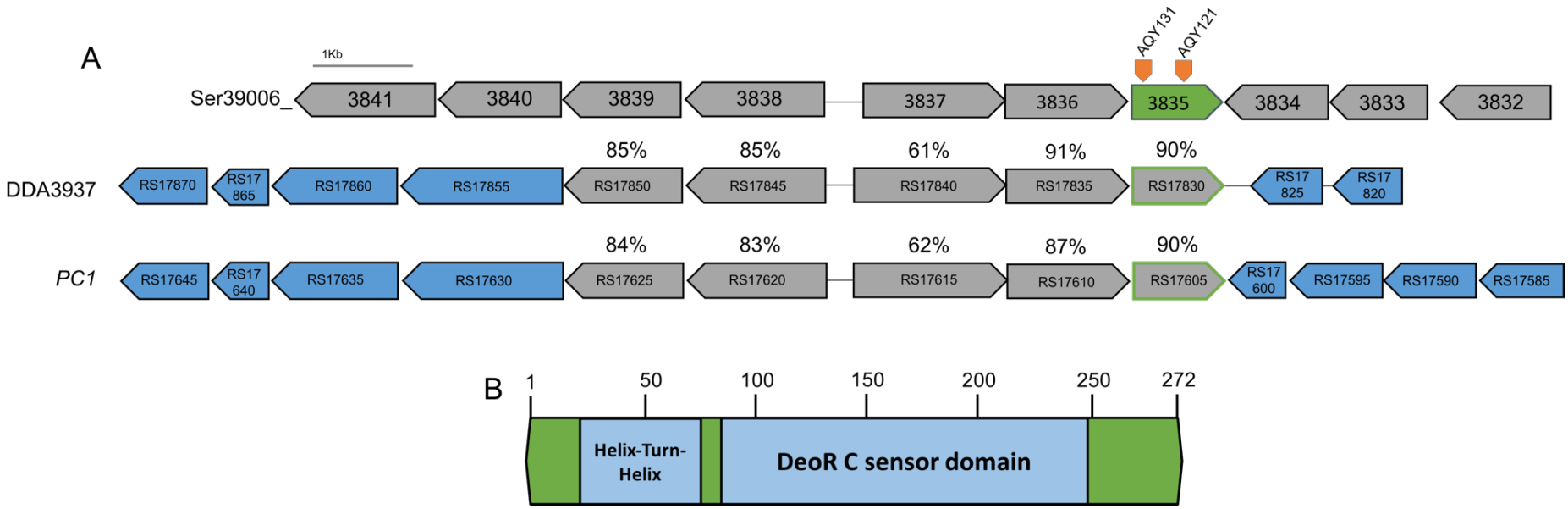

Figure 3.3. Bioinformatic analysis of the transposon insertion site in AQY121 and AQY131 mutants. **A**. Genomic context of the insertion site and comparison with bacteria containing homologues for the gene disrupted. The orange arrows indicate the insertion sites of the transposons in each mutant. The disrupted gene and its homologues are highlighted in green. Homologues are represented in grey filled arrows. The percentage of similarity is indicated above each homologue. The genes highlighted in blue indicate that the genes do not have homology with the ones in S39006. Genes from S39006 are represented with the prefix S39006_ and a suffix number indicated in each gene. Likewise, for genes from *Dickeya dadantii* 3937 (DDA3937) and *Pectobacterium carotovorum* subsp. *carotovorum* strain PC1 (PC1) **B**. The number of amino acids and identification of conserved domains in the predicted protein encoded by *Ser39006_3835.*

Table 3.2. BLASTP of predicted amino acid sequence encoded by gene *Ser39006_3835.*

Organism	Description	Max score	Query cover	E value	Ident	Accession
Serratia sp. ATCC 39006	DeoR/GlpR transcriptional regulator	551	100%	0	**99%**	WP_021017094.1
Dickeya chrysanthemi	DeoR/GlpR transcriptional regulator	506	100%	1E-180	**90%**	WP_033575450.1
Brenneria goodwinii	DeoR/GlpR transcriptional regulator	504	98%	5E-180	**92%**	WP_048637539.1
Dickeya dadantii	DeoR/GlpR transcriptional regulator	500	97%	3E-178	**90%**	WP_033112081.1
Dickeya sp. 2B12	DeoR/GlpR transcriptional regulator	499	100%	6E-178	**89%**	WP_033569127.1
Dickeya solani	DeoR/GlpR transcriptional regulator	498	99%	2E-177	**89%**	WP_057084174.1
Dickeya dadantii 3937	Glycerol-3-phosphate regulon repressor	498	96%	3E-177	**90%**	ADM99999.1
Dickeya sp. NCPPB 3274	DeoR/GlpR transcriptional regulator	498	99%	3E-177	**89%**	WP_042861035.1
Dickeya	DeoR/GlpR transcriptional regulator	497	99%	7E-177	**89%**	WP_049842472.1
Dickeya dianthicola	DeoR/GlpR transcriptional regulator	496	100%	9E-177	**89%**	WP_029729738.1
Escherichia coli K-12 substr. MC4100	GlpR transcriptional regulator *	90.5	92%	3e-26	**27%**	CDJ73449.1
Pseudomonas putida KT2440	DNA-binding transcriptional repressor GlpR*	82.0	83%	3e-23	**26%**	NP_743235.1
Escherichia coli K-12 substr. MG1655	transcriptional repressor of the aga regulon, AgaR*	135	91%	7e-43	**33%**	NP_417600.1
Escherichia coli K-12 substr. MG1655	transcriptional repressor for the L-ascorbate utilization divergent operon, UlaR*	89.0	94%	1e-25	**28%**	NP_418612.1
Escherichia coli K-12 substr. MC4100	DNA-binding transcriptional repressor, DeoR*	67.8	86%	6e-18	**26%**	CDJ71281.1
Escherichia coli	DeoT*	14.6	26%	3.4	**23%**	AHW84543.1

* Characterized DeoR family proteins.

Table 3.3. Description of predicted proteins encoded by *Ser39006_3835*, and up/downstream genes.

Gene ID	Description
S39006_3832	ROK-family transcriptional repressor
S39006_3833	Transcriptional regulator, LacI family
S39006_3834	Aldose 1-epimerase
S39006_3835	Transcriptional regulator, DeoR family
S39006_3836	4-hydroxythreonine-4-phosphate dehydrogenase
S39006_3837	Four-carbon acid sugar kinase family protein
S39006_3838	Class IV iron-containing alcohol dehydrogenase
S39006_3839	Class I aldolase, member of the dihydrodipicolinate synthase family
S39006_3840	Glyoxylate reductase
S39006_3841	Sugar phosphate permease

3.3.2 Analysis of the hyper-opaque mutants

Two mutants classified as hyper-opaque contained antisense (non-fusion) transposon insertions in genes that were found to be highly conserved. The genes truncated in AQY107 and AQY124 encode the predicted potassium transporter, TrkH, and the translation

elongation factor Tu, EF-Tu, respectively (Table 3.1) (Figure 3.4) (Tables 3.4 and 3.5). Interestingly, these genes have been widely studied in bacteria but never reported as cell buoyancy regulators (Levin & Zhou, 2014; Widjaja *et al.,* 2017). The genomic locus flanking the transposon in AQY107 was also conserved in *E. coli* (Figure 3.4.A). Nonetheless, it seemed that *trkH* is bordered by genes that are unrelated to its function. Downstream of *trkH* is a gene (*hemG*) predicted to code for a flavodoxin involved in the synthesis of the iron complex heme. Also, an operon containing the 16S rRNA (*rrsA*), the isoleucine (*ileT*) and alanine (*alaT*) tRNAs genes was found downstream of the *trkH* operon. Upstream of *trkH* were identified genes predicted to encode proteins for fatty acid oxidation (FadA and FadB), peptide hydrolysis (PepQ) and unknown functions (YigZ).

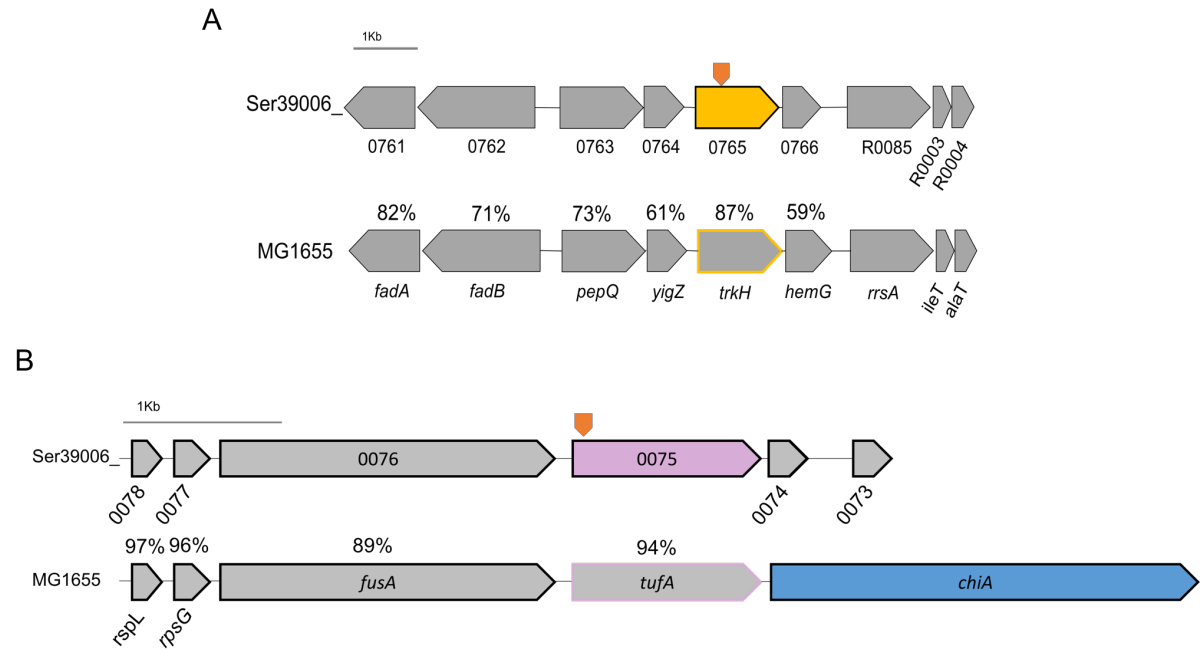

Figure 3.4. Bioinformatic analysis of the transposon insertion site in hyper-opaque mutants AQY107 (A) and AQY124 (B). A-B. Genomic context of the insertion sites and comparison with bacteria containing homologues for the disrupted genes. The orange arrows indicate the insertion sites of the transposons in each mutant. The disrupted gene and its homologues are highlighted in yellow and light purple for AQY107 and AQY124 respectively. Homologues are represented by grey filled arrows. The percentage of identity of the encoded proteins is indicated above each homologue. The gene highlighted in blue indicates that it does not have homology with any genes in S39006; this gene encodes an endochitinase. Genes from S39006 are represented with the prefix S39006_ and a suffix number indicated for each gene, whilst the genes from *E. coli* K12 MG155 (MG155) are identified with letters.

Table 3.4. BLASTP of predicted amino acid sequence encoded by gene *Ser39006_0765*.

Organism	Description	Max score	Query cover	E value	Ident	Accession
Serratia sp. ATCC 39006	Trk system potassium transporter TrkH	965	100%	0	**100%**	WP_021014040.1
Brenneria goodwinii	Trk system potassium transporter TrkH	855	100%	0	**91%**	WP_048637054.1
Dickeya zeae	Trk system potassium transporter TrkH	853	100%	0	**91%**	WP_012882952.1
Brenneria goodwinii	Trk system potassium transporter TrkH	852	100%	0	**91%**	WP_095835323.1
Dickeya zeae	Trk system potassium transporter TrkH	852	100%	0	**91%**	WP_019844070.1
Lonsdalea britannica	Trk system potassium transporter TrkH	851	100%	0	**91%**	WP_085650798.1
Dickeya chrysanthemi	Trk system potassium transporter TrkH	851	100%	0	**92%**	WP_040002877.1
Lonsdalea quercina	Trk system potassium transporter TrkH	851	100%	0	**91%**	WP_026738407.1
Dickeya dianthicola	Trk system potassium transporter TrkH	850	100%	0	**91%**	WP_024107680.1
Dickeya zeae	Trk system potassium transporter TrkH	850	100%	0	**91%**	WP_016943417.1

Table 3.5. BLASTP of predicted amino acid sequence encoded by gene *Ser39006_0075.*

Organism	Description	Max score	Query cover	E value	Ident	Accession
Serratia sp. ATCC 39006	elongation factor Tu	798	100%	0	**99%**	WP_021013352.1
Dickeya	MULTISPECIES: elongation factor Tu	791	100%	0	**98%**	WP_012882957.1
Dickeya paradisiaca Ech703	translation elongation factor Tu	790	100%	0	**98%**	ACS84214.1
Dickeya solani	elongation factor Tu	789	100%	0	**98%**	WP_026595308.1
Dickeya zeae	elongation factor Tu	789	100%	0	**98%**	WP_019845203.1
Dickeya	MULTISPECIES: elongation factor Tu	788	100%	0	**98%**	WP_013315919.1
Dickeya dianthicola	elongation factor Tu	787	99%	0	**98%**	WP_047100555.1
Lonsdalea quercina	elongation factor Tu	786	100%	0	**97%**	WP_027063854.1
Dickeya sp. B16	elongation factor Tu	786	99%	0	**98%**	WP_049842493.1
Dickeya chrysanthemi Ech1591	translation elongation factor Tu	785	100%	0	**97%**	ACT05209.1

EF-Tu is encoded by *tfuA* and in S39006 this gene was found downstream of conserved genes predicted to be involved in RNA translation, such as S12 and S7 30S ribosomal proteins and the elongation factor G genes, *rspL, rspG* and *fusA*. Immediately downstream is a gene not obviously related to mRNA processing, but encoding a predicted bacterioferritin (*Ser39006_0074*) (Figure 3.4.B). Given that the transposon in pKRCPN1 is composed of a large sequence containing the *lacZ* reporter and kanamycin resistance genes, initially, it was considered that the hyper-opaque phenotypes in AQY107 and AQY124 were caused by polar effects on *hemG* and the predicted bacterioferritin gene *Ser39006_0074*, respectively. Both genes are predicted to produce iron sequestering proteins. It therefore seemed possible that AQY107 and AQY124 connected gas vesicle regulation and iron storage. However, data discussed in chapter 5 suggested that this was not the case for AQY107.

3.3.3 Analysis of the bull's-eye transparent mutants

Bioinformatic analysis of AQY102, AQY118 and AQY126 revealed that the mutants classified as bull's-eye transparent mutants had insertions in the same operon (Figure 3.5.A). Two independent insertions in mutants AQY118 and AQY126 were located in a gene (*Ser39006_1185*) predicted to encode a protein containing two domains related to Wzt-like proteins. Wzt is an ATP-dependent O-antigen polysaccharide (O-PS) binding and transporter protein in *E. coli* O9a (Cuthberston *et al.,* 2010). The transposon in AQY102 disrupted the *Ser39006_1185* downstream gene (*Ser39006_1186*). This gene is predicted to encode a protein with a class I S-adenosylmethionine (SAM)-dependant methyltransferase domain (Figure 3.5.C). Proteins with SAM-methyltransferase domains modify a variety of molecules, such as proteins, DNA, RNA, lipids and lipopolysaccharide (LPS), among others (Martin & McMillan, 2002; Schubert *et al.,* 2003; Steiner *et al.,* 2008). BLAST analysis revealed that the proteins are conserved in different bacteria from different phyla, such as proteobacteria and firmicutes (Tables 3.6 and 3.7). Interestingly, upstream genes are predicted to encode proteins involved in LPS synthesis, whilst the last gene of the operon *Ser39006_1187* was predicted to encode a protein with no well known domains.

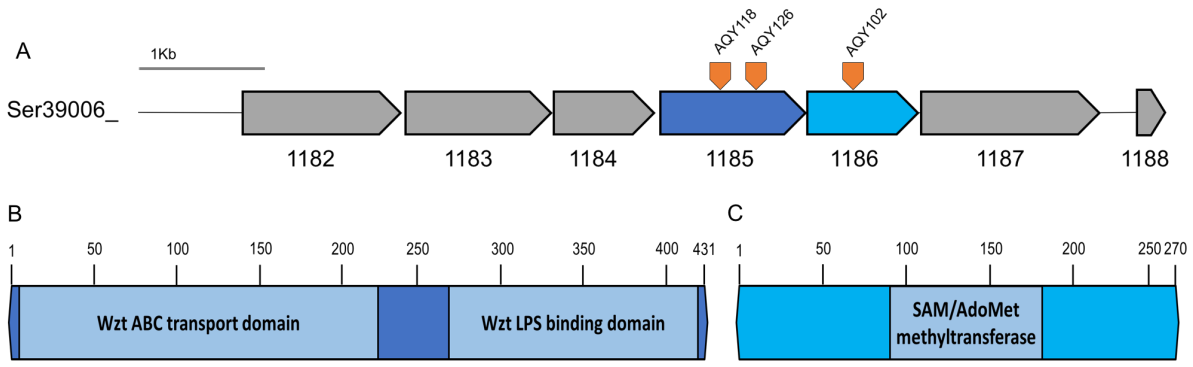

Figure 3.5. Bioinformatic analysis of the transposon insertion site in bull's-eye transparent mutants AQY102, AQY118 and AQY126. **A**. Genomic context of the insertion sites. The orange arrow indicates the transposon insertion site in each mutant. The disrupted genes are highlighted in light blue for AQY102 and dark blue for AQY118 and AQY126. Upstream and downstream genes are represented as grey filled arrows. Genes are annotated with the prefix S39006_ and a suffix number indicated for each gene. The number of amino acids and Identification of conserved domains in the predicted protein encoded by (**B**) *Ser39006_1185* and (**C**) *Ser39006_1186.*

Table 3.6. BLASTP of predicted amino acid sequence encoded by gene *Ser39006_1185*.

Organism	Description	Max score	Query cover	E value	Ident	Accession
Serratia sp. ATCC 39006	Teichoic-acid-transporting ATPase	887	100%	0	**100%**	ESN63777.1
Yersinia massiliensis	ABC transporter ATP-binding protein	488	98%	3.00E-168	**55%**	WP_019210536.1
Yersinia enterocolitica	ABC transporter ATP-binding protein	474	98%	1.00E-162	**56%**	WP_083159349.1
Yersinia aldovae	ABC transporter	472	98%	3.00E-162	**56%**	CNH03684.1
Endozoicomonas montiporae	ABC transporter ATP-binding protein	470	99%	4.00E-161	**55%**	WP_051789262.1
Endozoicomonas montiporae	ABC transporter ATP-binding protein	469	99%	4.00E-161	**54%**	WP_082211563.1
Pantoea dispersa	ABC transporter ATP-binding protein	434	98%	3.00E-147	**50%**	WP_058775754.1
Erwinia gerundensis	ABC transporter ATP-binding protein	433	98%	1.00E-146	**49%**	WP_067432063.1
Francisella sp. TX077310	ABC transporter ATP-binding protein	374	99%	2.00E-123	**43%**	WP_072711611.1
Pseudomonas thermotolerans	ABC transporter ATP-binding protein	329	99%	4.00E-106	**42%**	WP_017938050.1

Table 3.7. BLASTP of predicted amino acid sequence encoded by gene *Ser39006_1186.*

Organism	Description	Max score	Query cover	E value	Ident	Accession
Serratia sp. ATCC 39006	class I SAM-dependent methyltransferase	562	100%	0	**100%**	WP_021014456.1
Yersinia aldovae	class I SAM-dependent methyltransferase	257	91%	2.00E-82	**52%**	WP_049632745.1
Yersinia enterocolitica	class I SAM-dependent methyltransferase	256	91%	4.00E-82	**52%**	WP_083159348.1
Endozoicomonas montiporae	methyltransferase domain-containing protein	253	95%	4.00E-81	**50%**	WP_082211564.1
Pseudomonas stutzeri	class I SAM-dependent methyltransferase	250	82%	5.00E-80	**51%**	WP_081002779.1
Yersinia massiliensis	class I SAM-dependent methyltransferase	250	91%	1.00E-79	**49%**	WP_019210535.1
Sporomusa ovata	class I SAM-dependent methyltransferase	216	84%	1.00E-66	**50%**	WP_081658617.1
Sporomusa ovata DSM 2662	methyltransferase domain containing protein	215	81%	2.00E-66	**51%**	EQB27007.1
Candidatus accumulibacter sp. BA-92	putative S-adenosylmethionine-dependent methyltransferase	177	81%	3.00E-51	**39%**	EXI78676.1
Xanthomonas campestris	class I SAM-dependent methyltransferase	159	71%	3.00E-44	**39%**	WP_042599032.1

3.3.4 Analysis of the bull's-eye opaque mutants

In contrast to the bull's-eye transparent isolates, not all the transposon insertions in the bull's-eye opaque mutants were located in genes from the same operon (Figure 3.6.A and 3.7). Nonetheless, BLAST analysis revealed that these genes and other genes in their operons might also code for proteins related to LPS synthesis and transport (Table 3.8 and 3.9). AQY103 and AQY115 were disrupted for the same gene (*Ser39006_0591*). This gene was predicted to code for a conserved protein with a Wzy-like C-terminal domain (Figure 3.6.B). Wzy is an inner membrane protein that catalyses the addition of glycans into the LPS chain (Cuthberston *et al.,* 2010). The gene disrupted (*Ser39006_3817*) in mutant AQY125 was annotated as a "polysaccharide biosynthesis protein". Nevertheless, some homology with a putative O-PS flippase from *Dickeya chrysanthemi* was also detected in the BLASTP analysis

(Table 3.9). It seemed that the bull's-eye mutants had insertions in genes involved in outer membrane architecture.

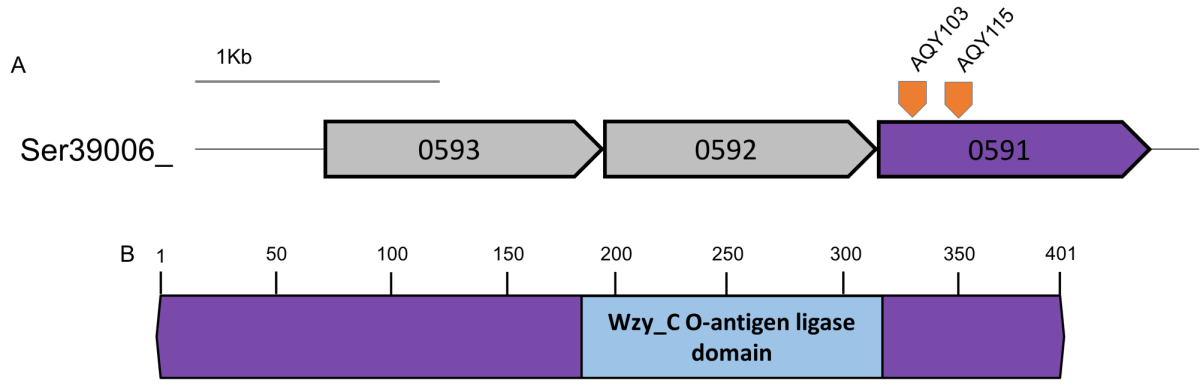

Figure 3.6. Bioinformatic analysis of the transposon insertion site in bull's-eye opaque mutants AQY103 and AQY115. **A**. Genomic context of the transposon insertions. The orange arrow indicates the transposon insertion site in each mutant. The disrupted gene is highlighted in purple. Upstream genes are represented as grey filled arrows. Genes are annotated with the prefix S39006_ and a suffix number indicated for each gene. **B.** Amino acid length and Identification of conserved domains in the predicted protein encoded by *Ser39006_0591*.

Table 3.8. BLASTP of predicted amino acid sequence encoded by gene *Ser39006_0591*.

Organism	Description	Max score	Query cover	E value	Ident	Accession
Serratia sp. ATCC 39006	hypothetical protein	814	100%	0	**100%**	WP_021013866.1
Dickeya dadantii	polymerase	569	99%	0	**67%**	WP_038912220.1
Dickeya chrysanthemi	O-antigen ligase domain-containing protein	561	99%	0	**69%**	WP_015848249.1
Dickeya	MULTISPECIES: polymerase	556	99%	0	**68%**	WP_038663487.1
Dickeya sp. NCPPB 3274	polymerase	552	99%	0	**68%**	WP_042861533.1
Dickeya zeae	polymerase	547	99%	0	**66%**	WP_038902985.1
Dickeya solani	teichuronic acid biosynthesis protein TuaE	547	99%	0	**67%**	WP_022631695.1
Dickeya dianthicola	polymerase	541	99%	0	**68%**	WP_024109316.1
Dickeya sp. S1	polymerase	541	99%	0	**69%**	WP_049855323.1
Dickeya	MULTISPECIES: polymerase	539	99%	0	**69%**	WP_038920562.1

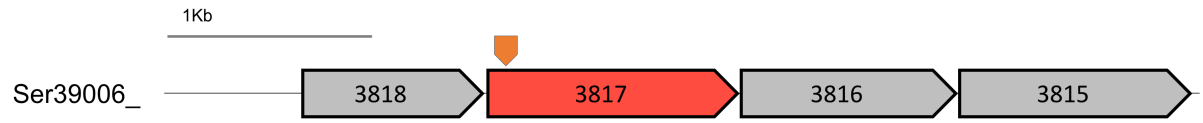

Figure 3.7. Bioinformatic analysis of the transposon insertion site in bull's-eye opaque mutant AQY125. Genomic context of the transposon insertion. The orange arrow indicates the transposon insertion site in AQY125. The disrupted gene is highlighted in red. Upstream and downstream genes are represented as grey filled arrows. Genes are annotated with the prefix S39006_ and a suffix number indicated for each gene.

Table 3.9. BLASTP of predicted amino acid sequence encoded by gene *Ser39006_3817*.

Organism	Description	Max score	Query cover	E value	Ident	Accession
Serratia sp. ATCC 39006	polysaccharide biosynthesis protein	792	100%	0.0	**100%**	WP_021017076.1
Escherichia coli	hypothetical protein	298	98%	4.00E-96	**42%**	WP_001131242.1
Escherichia coli	O139 family O-antigen flippase	297	98%	1.00E-95	**42%**	WP_063085470.1
Escherichia coli	hypothetical protein	296	98%	1.00E-95	**42%**	WP_097339650.1
Escherichia coli	hypothetical protein	296	98%	1.00E-95	**42%**	WP_097309871.1
Escherichia coli	hypothetical protein	232	66%	6.00E-72	**40%**	WP_001352378.1
Escherichia coli	hypothetical protein	231	66%	1.00E-71	**40%**	WP_085456984.1
Escherichia coli T426	hypothetical protein EBAG_02099	217	57%	6.00E-67	**42%**	OSL94296.1
Escherichia coli	hypothetical protein	74.7	47%	9.00E-13	**30%**	WP_001257278.1
Escherichia	MULTISPECIES: hypothetical protein	62	46%	2.00E-08	**27%**	WP_016262108.1

3.4 Bull's-eye mutants exhibit cellular aggregation

PCM analysis of single cells showed a distinctive conglomeration of cells in some mutants (Figure 3.8). Samples from NWA19, transparent (AQY121) and hyper-opaque (AQY107 and AQY124) mutants showed that cells remained dispersed after slide preparation for microscopy imaging. In contrast, the bull's-eye transparent (AQY102 and AQY126) and opaque (AQY103 and AQY 125) mutants produced large clusters of cells.

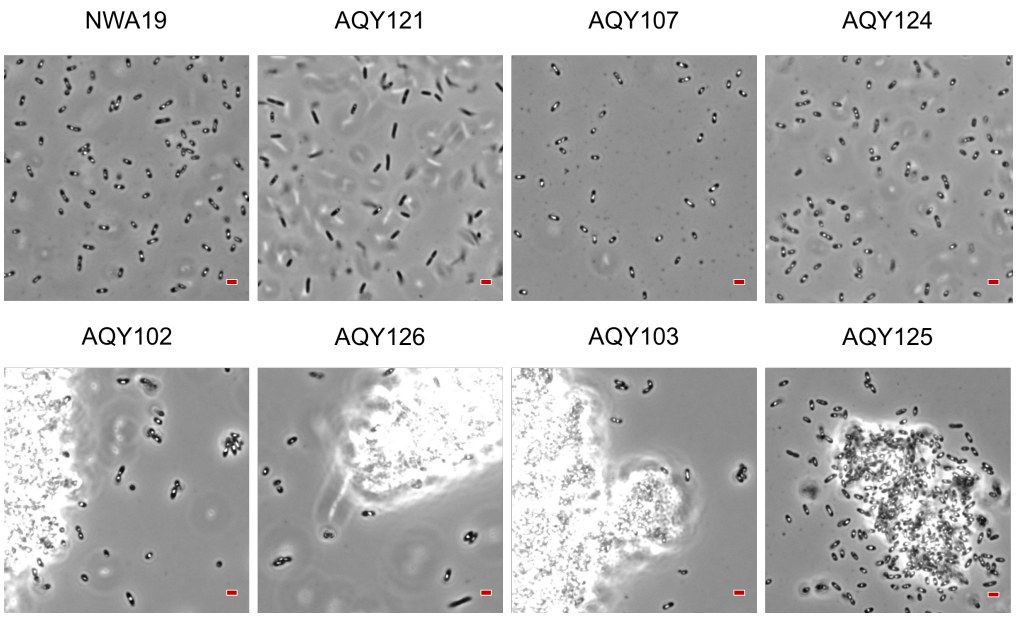

Figure 3.8. Cell aggregation in S39006 mutants. PCM images of NWA19 (Δ*pigC*), AQY121 (*Ser39006_3835*::TnKRCPN1), AQY107 (*trkH*::TnKRCPN1), AQY124 (*tufA*::TnKRCPN1), AQY102 (*Ser39006_1186*::TnKRCPN1), AQY126 (*Ser39006_1185*::TnKRCPN1), AQY103 (*Ser39006_0591*::TnKRCPN1) and AQY125 (*Ser39006_3817*::TnKRCPN1) samples from patches. Bars correspond to 1 μm.

3.5 Mutations in novel gas vesicle regulators might be pleiotropic

Gas vesicle production involves pleiotropic regulators also affecting secondary metabolism and motility (Ramsay *et al.,* 2011; Lee *et al.,* 2017). As NWA19 is prodigiosin negative, the gas vesicle mutants derived from this strain were not assessed for pigment production. Nevertheless, NWA19 still produced a carbapenem and flagella. Therefore, antibiotic activity and motility of the gas vesicle mutants were assessed (Figures 3.9 and 10). The production of the carbapenem was completely abolished in the transparent mutant AQY121, whilst hyper-opaque mutants AQY107 and AQY124 seemed to produce less antibiotic than NWA19. The bull's-eye transparent mutants AQY102 and AQY126 had similar antibiotic activity compared to NWA19. Interestingly, although the bull's-eye opaque mutants produced less antibiotic than NW19, the deficiency was more pronounced in mutant AQY125.

The swimming motility assay confirmed that the mutants found in this project were pleiotropic (Figure 3.10). The transparent mutant AQY121 produced a bigger swimming halo whilst the bull's-eye mutants were non-motile. The hyper-opaque mutants showed reduced flagellar motility compared to NWA19. Observations after 48 h of incubation showed that the "bull's-eye" transparent mutants produced minor swimming halos, whilst the bull's-eye opaque were non-motile.

Overall, the results in this chapter indicate that the *deoR*-like gene disrupted in AQY121 encodes a highly pleiotropic regulator that might be involved in positive regulation of gas vesicles and carbapenem production, while repressing flagellar motility in the WT strain. The potassium transporter, *trkH*, and the elongation factor Tu genes disrupted in hyper-opaque mutants AQY107 and AQY124, respectively, might be important negative gas vesicle regulators, but with moderate positive impacts on antibiotic production and flagellar motility. The genes disrupted in bull's-eye mutants might regulate the production of LPS molecules that affect cell organization and colony morphology, but also cell buoyancy, antibiotic production and flagellar motility.

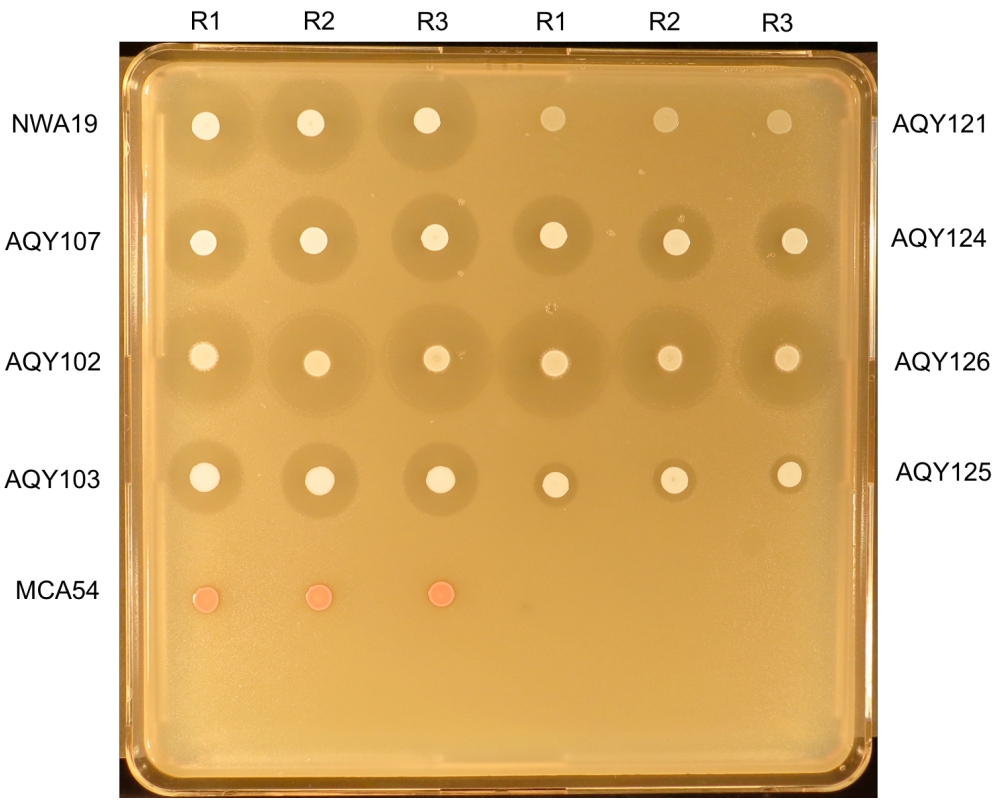

Figure 3.9. Carbapenem production in S39006 mutants. The halo of inhibition corresponds to the carbapenem activity of normalized (OD_{600} 1.0) NWA19 (Δ*pigC*), AQY121 (*Ser39006_3835*::TnKRCPN1), AQY107 (*trkH*::TnKRCPN1), AQY124 (*tufA*::TnKRCPN1), AQY102 (*Ser39006_1186*::TnKRCPN1), AQY126 (*Ser39006_1185*::TnKRCPN1), AQY103 (*Ser39006_0591*::TnKRCPN1) and AQY125 (*Ser39006_3817*::TnKRCPN1) patches on a top lawn of *E. coli* SS (ESS). MC54 (*carA* mutant) was used as a negative control. R1, R2 and R3 correspond to independent replicates for the strains assessed.

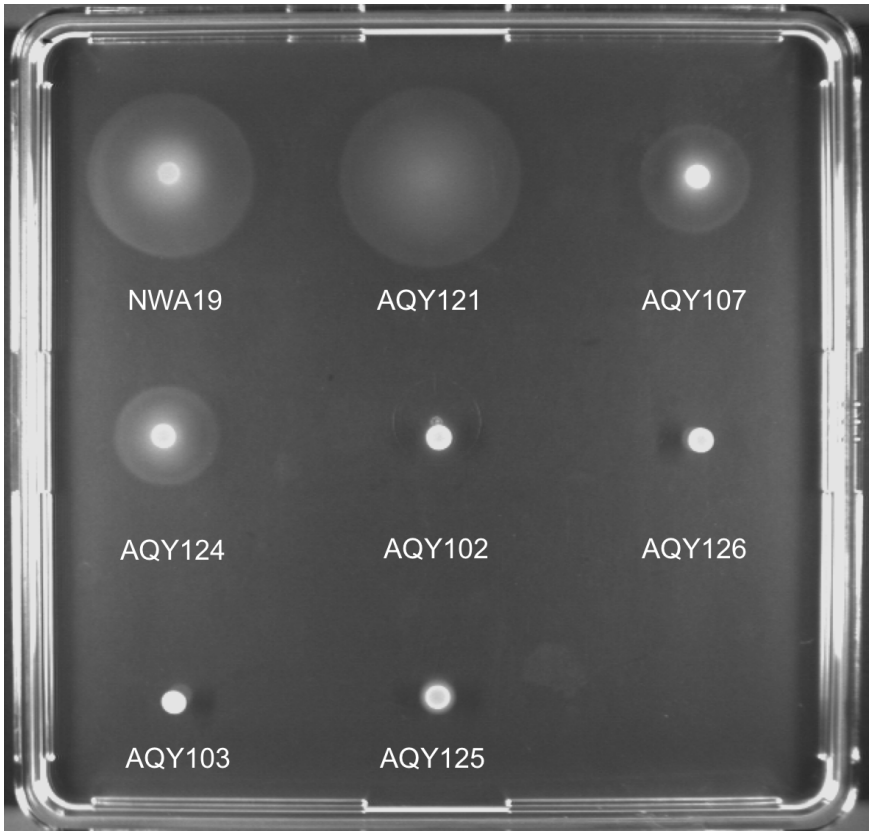

Figure 3.10. Swimming motility in S39006 mutants. Swimming halo of normalized (OD_{600} 1.0) NWA19 (Δ*pigC*), AQY21 (*Ser39006_3835*::TnKRCPN1), AQY107 (*trkH*::TnKRCPN1), AQY124 (*tufA*::TnKRCPN1), AQY102 (*Ser39006_1186*::TnKRCPN1), AQY126 (*Ser39006_1185*::TnKRCPN1), AQY103 (*Ser39006_0591*::TnKRCPN1) and AQY125 (*Ser39006_3817*::TnKRCPN1) spots after 16 h of culture. The image is representative of three biological replicates.

3.6 Discussion

Random mutagenesis with plasmid-transposon hybrids is an effective tool for rapid genetic screening in Gram-negative bacteria (Dennis & Zyltra. 1998). Mutagenesis experiments with the plasmid PKRCPN1 allowed the identification of gas vesicle structural and regulatory genes by random insertion in the S39006 genome (Ramsay *et al.,* 2011; Monson *et al.,* 2015; Lee *et al.,* 2017). Analysis of mutants in this project revealed defects in some genes previously studied and confirmed a proof of principle of random mutagenesis. More importantly, novel regulatory genes were also identified.

The phenotypic characterization of the different gas vesicle mutants showed that the mutations were pleiotropic. Notably, *Ser39006_3885*, a *deoR*-like gene characterized in this study, might be an important regulator of cell buoyancy, motility and secondary metabolism. Members from the DeoR family are transcription repressors known for regulating multiple phenotypes in bacteria by releasing promoter regions after allosteric binding with phosphorylated sugars in their sensor domain (Mortensen *et al.,* 1989; Garcés *et al.,* 2008). Studies in different bacteria confirm that regulators of the DeoR family control multiple phenotypes, including motility, antibiotic production and resistance, LPS synthesis, cell differentiation, osmotic and temperature stress response, in addition to carbon, fatty-acid, nucleotide, deoxynucleotide and peptide metabolism (Saxild *et al.,*1996; Ramos-Aires *et al.,* 2004; Elgrably-Weiss *et al.,* 2006; Ulanova *et al.,* 2013; Wang *et al*., 2014). However, this work is the first report of a DeoR regulator involved in gas vesicle and β–lactam antibiotic production. The demonstrated impact and phenotypic versatility of *Ser39006_3885* suggest that it is a global transcriptional regulator, similar to PigP and PhoB in S39006. Therefore, a detailed analysis of this mutant was conducted (see Chapter 4).

The mutant AQY107 was identified as carrying a transposon insertion in the low affinity potassium transporter gene, *trkH*. The Trk potassium uptake system is highly conserved in bacteria and works in a multiunit complex comprising the transmembrane protein TrkH (an extra copy known as TrkG is found in *E. coli*), the NAD^+ and NADH binding peripheral protein TrkA and the ATP-binding protein TrkE (Bossemeyer *et al.,* 1989; Dosch *et al.,* 1991; Harms *et al.,* 2001). Trk is involved in transporting extracellular potassium when high concentrations are available; it facilitates osmoregulation but has also been reported to influence virulence factor production and antibiotic resistance in Gram negative pathogens (Epstein *et al.,* 1986; Parra-Lopez *et al.,* 1994; Su *et al.,* 2009; Alkhuder *et al.,* 2010; Valente & Xavier, 2015).

The transposon insertion in the *trkH* homologue in S39006 caused hyper-production of gas vesicles, long-lasting floatation, reduced flagellar motility and, apparently, antibiotic production. Regulation of gas vesicle and antibiotic production via *trkH* had not been reported before. Recently, the role of TrkA-gated potassium efflux pumps in *Bacillus subtilis* biofilms involving potassium-dependent attraction of free motile cells was reported (Humphries *et al.,*

2017). Nonetheless, how extracellular potassium controls flagellar motility has not been established.

The hyper-opaque mutant AQY124 contained an insertion in one of the two gene copies coding for the elongation factor Tu. Although this mutant was hyper-buoyant, it showed reduced swimming motility and carbapenem production (Figure 3.1, 3.9 and 3.10). EF-Tu has been mainly studied for its role in delivering amino acyl-tRNAs into the ribosome A site, a crucial process in protein synthesis. Enterobacteria, such as *E. coli* and *Salmonella*, carrying defects in EF-Tu are viable, but slow growers (Hughes, 1990; Zuurmond *et al.,* 1999). This may also be the case in AQY124 and could explain why patches did not look as hyper-opaque as the AQY107 patches (Figure 3.1.B). Besides its crucial role in protein synthesis, *in vitro* experiments suggested that EF-Tu acts as a chaperone protecting unfolded and denatured proteins (Caldas *et al.,* 1998) Moreover, curiously it has been reported that EF-Tu can be bound to the outer surface, outer membrane vesicles and fibronectin in *Acinetobacter baumanii,* and toxins that are essential in Type VI secretion-based defence in *P. aeruginosa* (Dallo *et al.,* 2012; Whitney *et al.,* 2015). It seems that EF-Tu may play multiple roles in bacteria; nonetheless, its role in motility, cell buoyancy and secondary metabolism regulation have not been studied. EF-Tu may be an important chaperone interacting with other regulators involved in gas vesicle, flagella and antibiotic production.

Six of the 32 transposon mutants identified in this project showed a distinctive colony shape, here classified as bull's-eye, due to insertions in genes predicted to be important for outer membrane LPS architecture (Table 3.1). Mutants AQY103, AQY115 and AQY125 may be impaired for LPS biosynthesis, AQY118 and AQY126 for transport, and AQY102 for methylation. Alterations in the outer LPS layer in other proteobacteria, such as *Vibrio cholerae* O1 and *Myxococcus xanthus*, also result in distinctive colony morphologies (Morris *et al.,* 1996; Bowden & Kaplan, 1998). Nonetheless, little is known about how LPS determines colonial growth and morphology in bacteria.

In addition to the distinctive colony shape (compared to WT), the bull's-eye mutants showed cell buoyancy and motility limitations, whilst the bull's-eye opaque mutants also appeared to be defective for carbapenem production. The bull's-eye transparent mutants in this study

have similar colony shape to three S39006 mutants (TPP31, TPP38 and TPL531) studied previously for prodigiosin production (Paterson, 2013). Double mutants TPP31 and TPP38 had insertions in the same gene affected for mutants AQY118 and AQY126 (*Ser39006_1185*) in addition to insertions in *ygfX* (Previously annotated as *pigV*). Paterson (2013) refers to *Ser39006_1185* as *wzt*; however, BLASTP analysis of the predicted amino acid sequence from *Ser39006_1185* showed only 40% and 54% identity and similarity, respectively with the characterized Wzt from *E. coli* N24c serotype O9. Given the phenotypic impact and moderate homology of its protein product with Wzt, *Ser39006_1185* was not referenced in this work as *wzt.* More important is that the TPP31 and TPP38 mutants showed reduced prodigiosin production compared to a single *ygfX* mutant, suggesting that the protein encoded by *Ser39006_1185* bypasses YgfX regulation (Paterson, 2013). This supports the idea that the LPS genes found in this study are pleiotropic, not only affecting cell shape but also cell buoyancy, motility and antibiotic production.

Mutant TPL531 had transposon insertions in *ygfX* and the anti- σ^E (sigma factor E) protein gene *rseA* instead of *Ser39006_1185* (Paterson, 2013). The mutation in *rseA* increased the reporter activity in a *ygfX*::*lacZ* fusion strain. RseA is a sequestering protein controlling σ^E, which is an outer membrane stress response regulator that facilitates the expression of multiple genes coding for outer membrane proteins (OMPs), and LPS synthesis and transport proteins (Rhodius *et al.,* 2005). Therefore, it may be possible that *rseA*- σ^E dependent LPS production controls prodigiosin through YgfX. It is also possible that YfgX-dependent pathway affects other phenotypes in S39006. Recently, a study revealed that the YgfX has an impact on S39006 motility, and that it is also regulated by the post-transcriptional regulator RsmA and the flagella master regulator FlhDC (Hampton *et al.,* 2016). Further investigations on the impact of LPS genes, *ygfX, rseA* and σ^E on gas vesicle, flagella and antibiotic production would help to understand the connection between outer cell membrane assembly and genetic regulation in S39006.

Flotation assays showed that LPS mutants precipitated after 3 days (Figure 3.2.D). Interestingly however, PCM images of individual cells showed that bull's-eye mutants still produce phase bright structures (gas vesicles). This suggested that, although gas vesicles are essential, other components (LPS) are also necessary for cell buoyancy. Also, PCM images

revealed that bull's-eye mutant cells stuck to each other forming abnormal cell clusters (Figure 3.8). Mutations in different LPS genes may result in altered outer membrane architectures that affect cell buoyancy in S39006. This rare conglomeration of cells may have increased their density and, therefore, led to precipitation. Bacteria can modify their outer membrane architecture, through O-PS modification, to adapt and shape their interactions with the environment (Lerouge & Vanderleyden, 2002). Cell aggregation has been reported as a distinctive strategy facilitating loss of buoyancy after sulphide depletion in the photosynthetic, purple gas vacuolated bacterium *Lamprocystis purpurea* comb. nov. (previously classified as *Amoebobacter purpureus*) (Overmann & Pfenning, 1992). Moreover, enteropathogenic *E. coli* mutants defective for secretion of polysaccharides comprising an O-antigen rich capsule fail to float, compared to a WT strain, in artificial buoyancy conditions (Peleg *et al.,* 2005). Therefore it appears that the regulation of LPS assembly on the bacterial surface may be an important control mechanism for cell buoyancy in S39006.

Transduction with φOT8 permitted the mobilization of each transposon insertion from the mutants into the NWA19 parental strain. φOT8 is an effective broad-host range phage depending on flagella for infection (Evans *et al.,* 2010); φOT8 resistant mutants cannot swim. Furthermore, experiments in a "paralysed" S39006 mutant, *motA*, which produces flagella but remains non-motile suggested that φOT8 requires functional flagella rather than just the flagellar structure itself. Here, it was shown that flagellar motility was altered to different degrees in the transparent, hyper-opaque, bull's-eye transparent and bull's-eye opaque mutants (Section 3.5 and Figure 3.10).

The hyper-motility of AQ121 explains its sensitivity to φOT8 infection. Also, although AQY107 and AQY124 showed reduced swimming motility, residual flagellar activity was sufficient for transduction. In contrast, the bull's-eye mutants had more dramatic defects in swimming motility than the other mutants. The bull's-eye transparent mutants showed moderate swimming halos after 48 h of incubation, whilst the bull's-eye opaque mutants did not (Section 3.5). Because it was possible to transduce the mutations from the bull's-eye opaque mutants, their motility deficiency is not caused by an absolute impairment in flagellar assembly or rotation. Previous reports in *Salmonella enterica* serovar Typhimurium and *Proteus mirabilis* showed that mutations in genes (such as *waaL* and *wzx*) involved in LPS

synthesis and transport affect swarming motility (Toguchi *et al.,* 2000; Morgenstein *et al.,* 2010). Another study in *E. coli* showed that mutations in different genes involved in LPS synthesis have different impacts on *flhDC* expression and in both swimming and swarming motilities (Girgis *et al.,* 2007). It is possible that the LPS mutants have impacts on motility through YgfX and FlhDC, as discussed previously. Nonetheless, given that *flhC* and flagella rotation are essential for φOT8 infection in S39006 (Evans *et al.,* 2010), the flagellar activity may be significantly active in the bull's-eye mutants for phage infection but nor for effective swimming motility. Possibly, similar to the early sedimentation seen in the flotation assays (Figure 3.2.D), the impaired swimming motility was caused by the cellular aggregation. This abnormal cell aggregation may impede free-living buoyant and motile phases in the bull's-eye mutants.

Chapter 4
FloR: a novel DeoR family regulator controlling flotation, secondary metabolism and motility

Random transposon mutagenesis of the prodigiosin defective strain, S39006 LacA Δ*pigC* (NWA19), enabled identification of potential regulators of gas vesicle production (Chapter 3). Mutant AQY121 carried a transposon insertion in a previously uncharacterized gene annotated as *Ser39006_3835* predicted to encode a DeoR-like transcriptional factor. The mutation in this gene disrupted the formation of phase bright structures (gas vesicles) and flotation, but also carbapenem production and swimming motility. *Ser39006_3835* was referred to as *floR* (**flo**tation **r**egulator).

4.1 *floR* controls gas vesicle production

To continue studying the effect of *floR* on gas vesicle formation, the mutation from AQY121 was transduced into S39006 LacA (WT). TEM Images of WT and *floR* mutant cells confirmed that the mutation in *floR* caused reduction in gas vesicle production leading to reduced buoyancy and lack of phase bright structures observed in AQY121 (S39006 LacA Δ*pigC floR*::TnKRCPN1) in previous assays (Figure 4.1, see also Figure 3.1, Chapter 3). Gas vesicles confer opacity on S39006 colonies, and so the absence of gas vesicles observed in TEM analysis explained the translucent phenotype observed in colonies and patches of the *floR* mutant. To confirm the role of *floR* on gas vesicle formation, *floR* was cloned into the arabinose inducible expression vector, pBAD30, to construct the plasmid pAQY2 and used for complementation of the *floR* mutant. Ectopic expression of *floR* in LB with 0.2 % arabinose restored production of gas vesicles in the mutants (Figure 4.2).

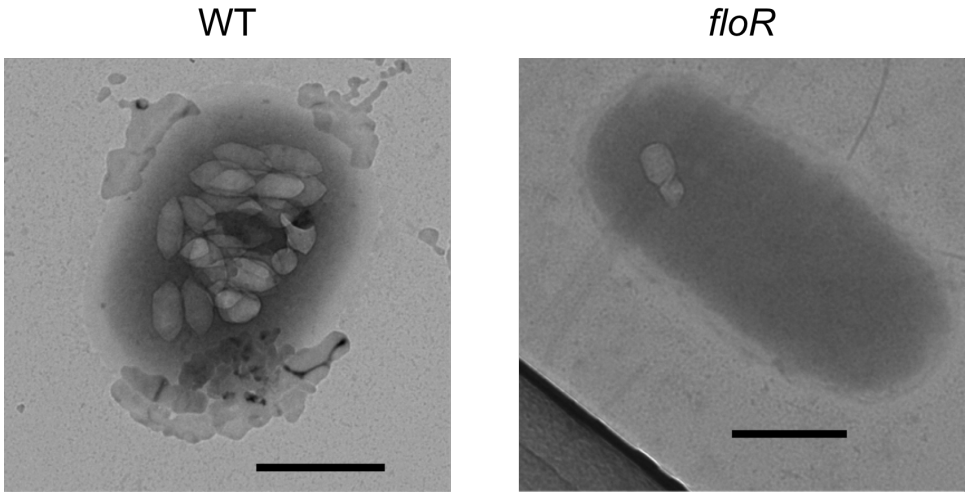

Figure 4.1. TEM images of WT and the *floR* mutant. TEM image of a WT single cell showing gas vesicles clustered in the cytoplasm and a *floR* mutant single cell mutant showing loss of gas vesicles. Scale bars correspond to 500 nm.

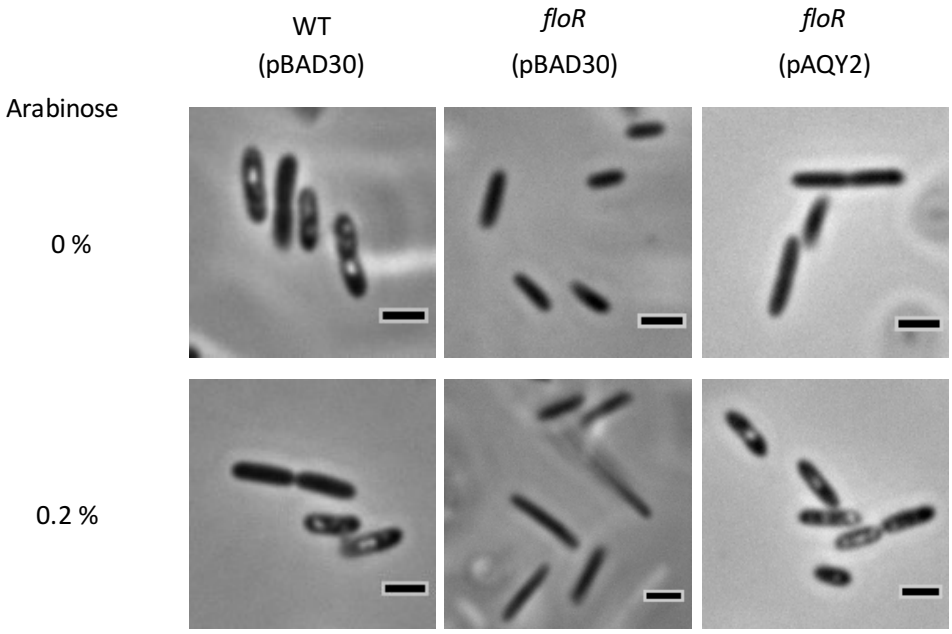

Figure 4.2 Complementation of the *floR* mutant gas vesicle formation. PCM Images of *floR* mutant cells carrying an empty vector (pBAD30) and pAQY2 (pBAD30 + *floR*), and grown in LB plates +/- arabinose. Images are representative of three biological replicates. Scale bars correspond to 1 μm.

4.2 FloR regulates the expression of the gas vesicle gene cluster

The synthesis of gas vesicles depends on the expression of several genes from the contiguous *gvpA1-gvpY* and *gvrA-gvrC* operons (Ramsay *et al.,* 2011; Tashiro *et al.,* 2016). Therefore, the mutation in *floR* was transduced into reporter strains with fusions to promoters of the *gvpA1-gvpY* and *gvrA-gvrC* operons; *gvpA1*::*uidA* and *gvrA*::*uidA* (Ramsay *et al.,* 2011; Monson *et al.,* 2016; Lee *et al.,* 2017). The β-glucuronidase (UidA) reporter activity throughout growth showed that the transcription of *gvpA1-gvpY* and *gvrA-gvrC* operons was significantly reduced in the *floR* mutant (see ANOVA analysis in Figure 4.3 and 4.4). Complementation of the *floR* mutant with pAQY2 significantly stimulated the expression of the gas vesicle gene operons above the levels observed in the mutant carrying an empty vector (pBAD30), and similar to the controls (*gvpA1*::*uidA* and *gvrA*::*uidA*) (Figures 4.3 and 4.4). Given the impacts on gas vesicle production and gene expression, *floR* was considered a positive regulator of gas vesicle formation and flotation operating through the expression of *gvpA1-gvpY* and *gvrA-gvrC* operons.

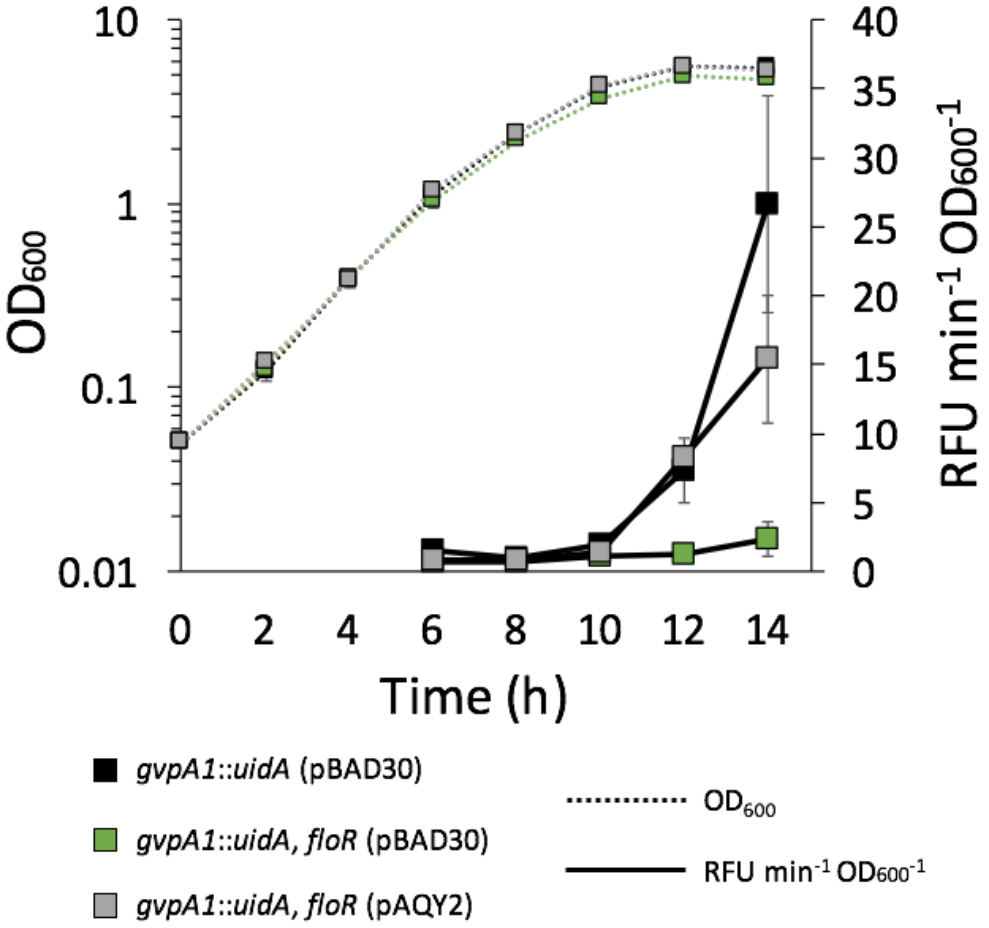

Figure 4.3. Complementation of *gvpA1* expression in the *floR* mutant. Cell density (OD_{600}, dotted lines) and gene expression (RFU min^{-1} OD_{600}^{-1}, continuous lines) were measured throughout growth in LB with 0.2 % arabinose. Complementation for *gvpA1*::*uidA* reporter activity in the *floR* mutant was assessed by ectopic expression with pAQY2 (grey box). The reporter strain and *floR* mutant containing the empty vector were used as controls, black and green respectively. The data represent the average and standard deviation (error bars) of three biological replicates. **ANOVA two-factor analysis of the β-glucuronidase reporter activity** from 6 to 14 h of growth in *gvpA1*::*uidA* (pBAD30) and *gvpA1*::*uidA*, *floR* (pBAD30) found $F=45.75 > F_{crit} = 4.35$, $p= 1.40*10^{-6}$; in *gvpA1*::*uidA*, *floR* (pBAD30) and *gvpA1*::*uidA*, *floR* (pAQY2) $F=55.15 > F_{crit} = 4.35$, $p= 3.60*10^{-7}$; and in *gvpA1*::*uidA* (pBAD30) and *gvpA1*::*uidA*, *floR* (pAQY2) $F=4.60 > F_{crit} = 4.35$, $p= 0.044$.

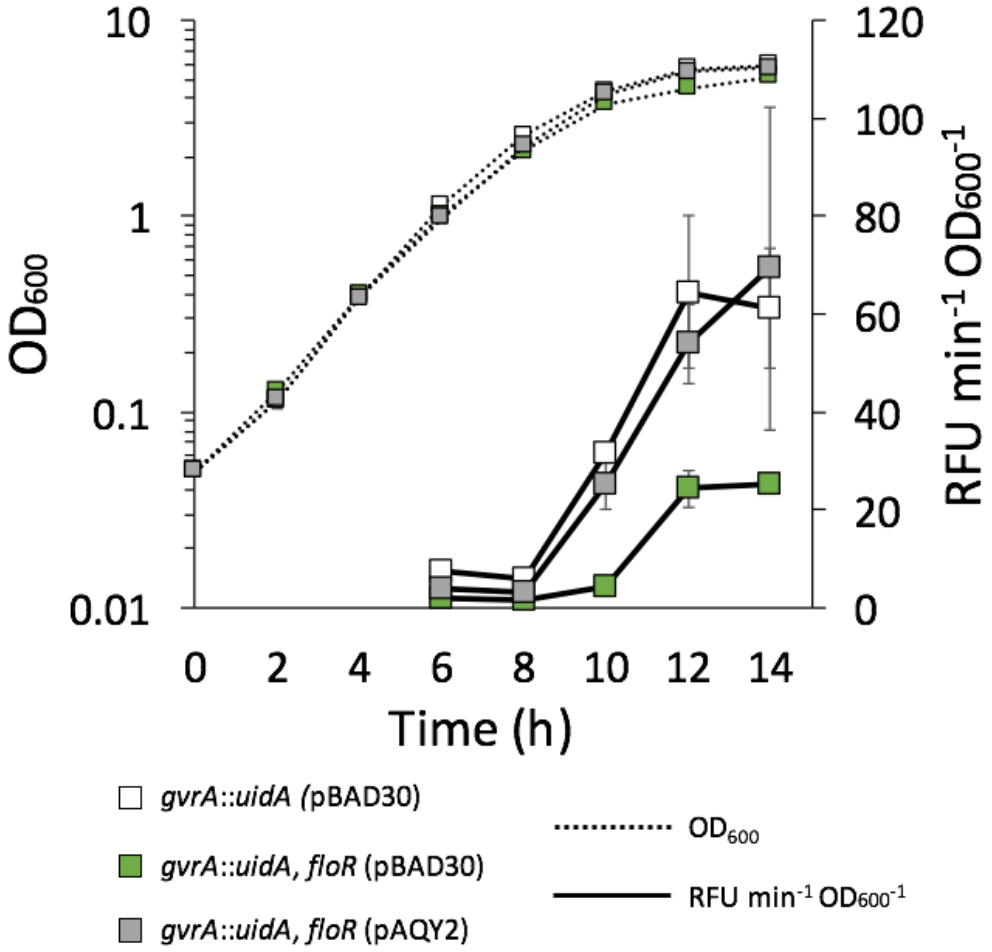

Figure 4.4. Complementation of *gvrA* expression in the *floR* mutant. Cell density (OD_{600}, dotted lines) and gene expression (RFU min^{-1} OD_{600}^{-1}, continuous lines) were measured throughout growth in LB with 0.2 % arabinose. Complementation for *gvrA*::*uidA* reporter activity in the *floR* mutant was assessed by ectopic expression with pAQY2 (grey box). The reporter strain and *floR* mutant containing the empty vector were used as controls, white and green respectively. The data represent the average and standard deviation (error bars) of three biological replicates. **ANOVA two-factor analysis of the *β*-glucuronidase reporter activity** from 6 to 14 h of growth in *gvrA*::*uidA* (pBAD30) and *gvrA*::*uidA*, *floR* (pBAD30) found $F = 92.74 > F_{crit} = 4.35$, $p = 5.94*10^{-9}$; in *gvrA*::*uidA*, *floR* (pBAD30) and *gvrA*::*uidA*, *floR* (pAQY2) $F = 0.41 < F_{crit} = 4.35$, $p = 0.53$; and in *gvrA*::*uidA* (pBAD30) and *gvrA*::*uidA*, *floR* (pAQY2) $F = 24.35 > F_{crit} = 4.35$, $p = 7.97*10^{-6}$.

4.3 *floR* is a pleiotropic regulatory gene controlling secondary metabolism and motility

Colonies and patches of WT and gas vesicle reporter strains were red on LB plates due to the production of prodigiosin. The transduction of the mutation in *floR* from the prodigiosin-defective strain AQY121 into the WT, *gvpA1*::*uidA* and *gvrA*::*uidA* strains enabled assessment of the impact of *floR* on pigment production. In addition to the gene reporter activity in the *gvpA1*::*uidA* strains, samples for quantitation of prodigiosin production throughout growth were taken (Figure 4.5). The *floR* mutant carrying an empty vector showed significantly reduced levels of prodigiosin production from mid exponential to stationary growth phase, whilst the complemented mutant recovered production observed in the *gvpA1*::*uidA* strain carrying an empty vector (See ANOVA analysis in Figure 4.5 legend). This result confirmed that *floR* is also an important regulator for the production of the antimicrobial pigment, prodigiosin.

In Chapter 3 (Figures 3.9 and 3.10, section 3.5) it was shown that the transposon insertion in AQY121 impaired carbapenem production, while increasing swimming motility. These phenotypes were reproduced in the *floR* mutants obtained after transduction of the transposon insertion into the WT background strain (Figures 4.6 and 4.7). WT S39006 produced a clear halo of inhibition on the β-lactam supersensitive strain *E. coli* ESS. In contrast, patches of the *floR* mutant did not show antibiotic activity; similar to the carbapenem negative control strain MC54 (Figure 4.6). Ectopic expression of *floR* in the mutant confirmed that this regulator also controls swimming motility (Figure 4.7). The mutant with an empty vector produced greater swimming halos, whilst the complemented mutant displayed a similar swimming phenotype to that of WT. Given the impact of *floR* on gas vesicles, carbapenem and prodigiosin production and swimming motility, and the confirmation by complementation, it was clear that *floR* is an important pleiotropic regulator connecting cell buoyancy, motility and secondary metabolism.

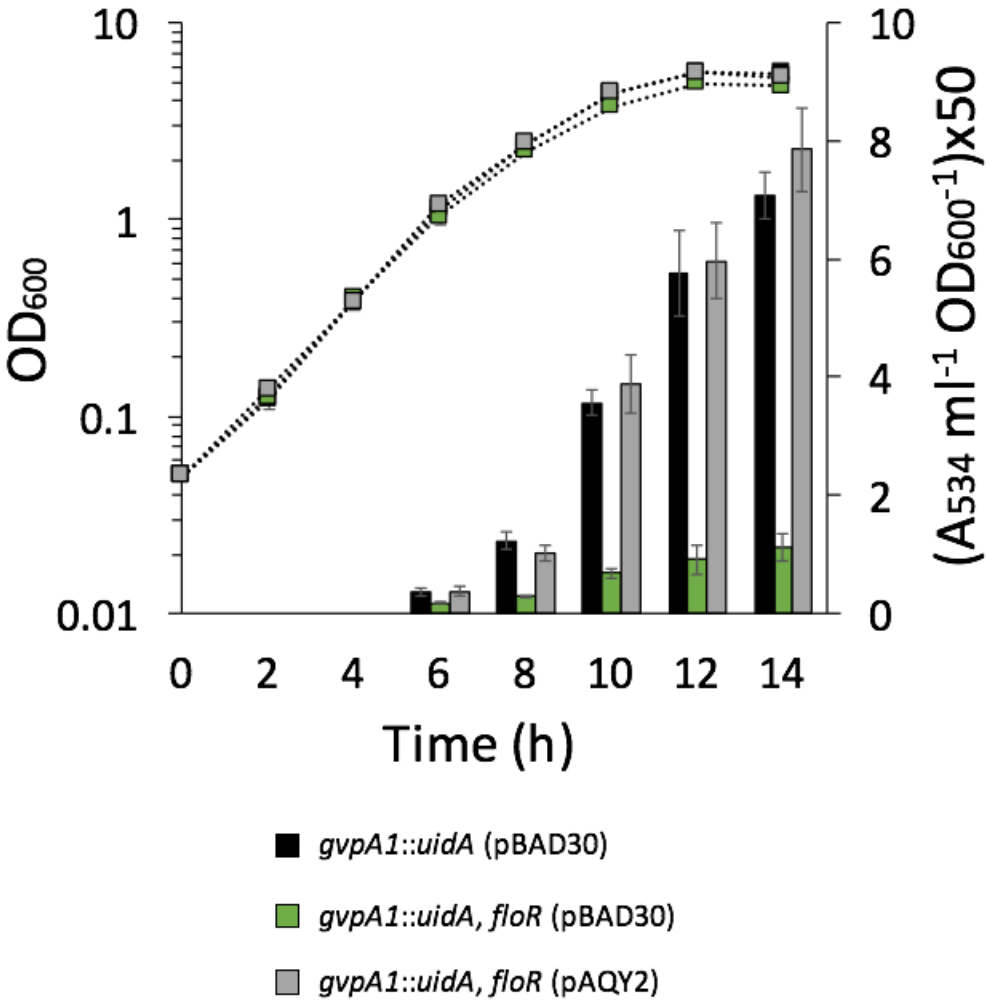

Figure 4.5. Prodigiosin production in the *floR* mutant. Cell density (OD_{600}, dotted lines) and prodigiosin production ((A534 ml^{-1} OD_{600}^{-1})X50, bars) were measured throughout growth in LB with 0.2 % arabinose. Complementation for pigment production in the *floR* mutant was obtained by ectopic expression with pAQY2 (grey bar). The reporter strain and *floR* mutant containing the empty vector were used as controls, black and green respectively. The data represent the average and standard deviation (error bars) of three biological replicates. ANOVA two-factor analysis of the prodigiosin production from 6 to 14 h of growth in *gvpA1*::*uidA* (pBAD30) and *gvpA1*::*uidA*, *floR* (pBAD30) found $F = 769.25 > F_{crit} = 4.35$, $p = 1.95*10^{-17}$; in *gvpA1*::*uidA*, *floR* (pBAD30) and *gvpA1*::*uidA*, *floR* (pAQY2) $F=1.94 < F_{crit} = 4.35$, $p= 0.19$; and in *gvpA1*::*uidA* (pBAD30) and *gvpA1*::*uidA*, *floR* (pAQY2) $F=592.85 > F_{crit} = 4.35$, $p= 2.45*10^{-16}$.

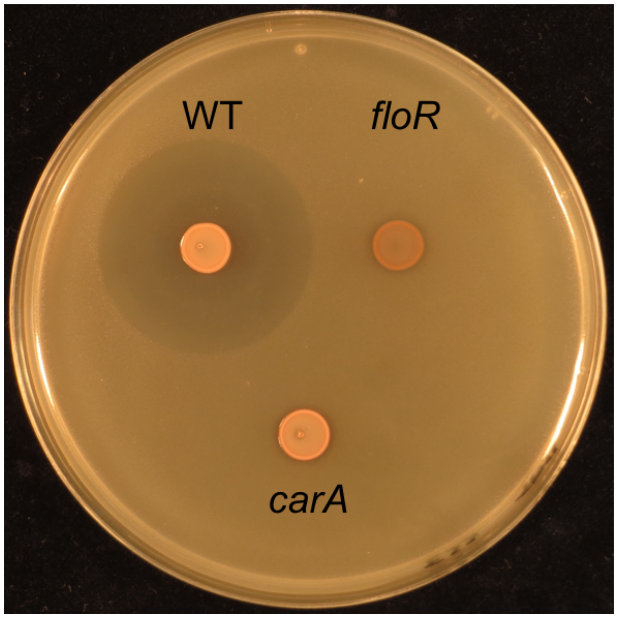

Figure 4.6. Carbapenem production after transduction of the mutation in *floR* into WT. Cultures were spotted on a top lawn containing the β-lactam supersensitive strain *E. coli* ESS. The *carA* mutant, MC54, was used as negative control. Images are representative of three biological replicates.

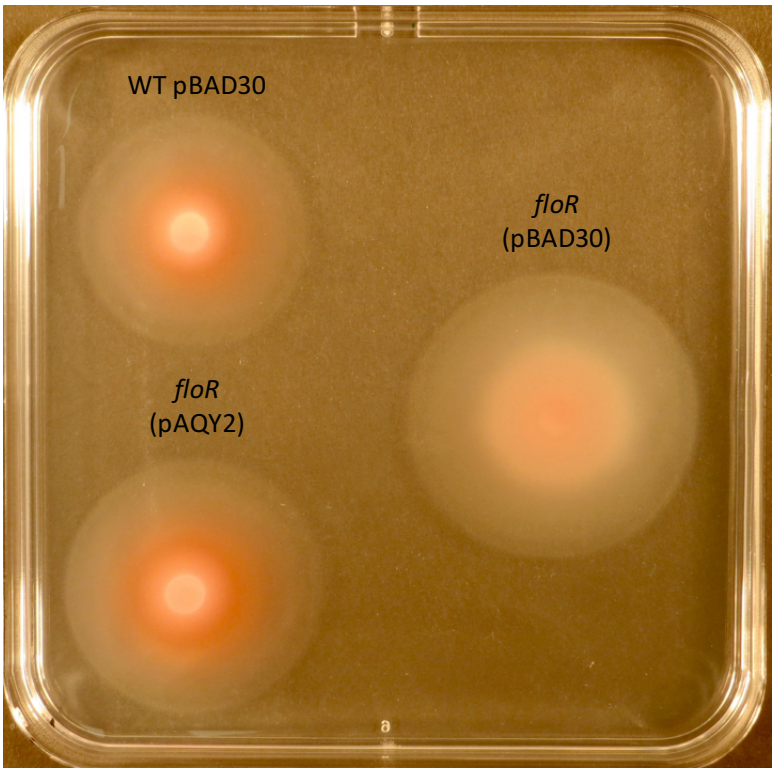

Figure 4.7. Swimming motility assay of the *floR* mutant. Complementation of swimming motility in the *floR* mutant was assessed by ectopic expression in the pAQY2 containing strain. The WT and mutant strains containing the empty vector were used as controls. The Image is representative of three biological replicates

4.4 Gas vesicle gene expression in microaerophilic conditions is *floR*-dependent

A previous study showed that S39006 cells grown in microaerophilic conditions exhibited increased transcription of the *gvpA1-gvpY* operon, compared to aerated cultures (Ramsay *et al.,* 2011). Therefore, oxygen depletion is considered an important input stimulating the production of gas vesicles. Strains carrying the mutation in *floR* were assessed for oxygen-dependent gas vesicle gene expression. The β-glucuronidase reporter activity in the *floR* mutant background under reduced aeration showed that both *gvpA1-gvpY* and *gvrA-gvrC* operons were significantly down-regulated (Figures 4.8 and 4.9). This suggested that the genetic pathway depending on growth in aerated conditions requires *floR* to stimulate the gas vesicle production.

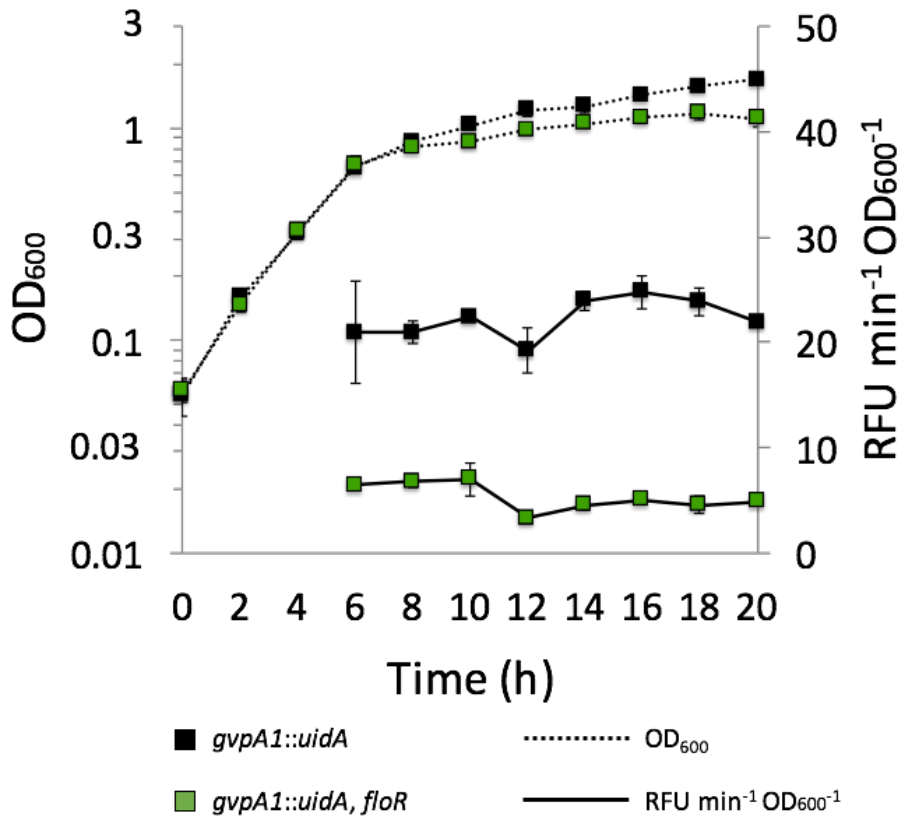

Figure 4.8. *gvpA1* promoter activity in the *floR* mutant under microaerophilic conditions. Cell density (OD_{600}, dotted lines) and gene expression (RFU min^{-1} OD_{600}^{-1}, continuous lines) were measured throughout growth in LB and reduced aeration. The data represent the average and standard deviation (error bars) of three biological replicates. ANOVA two-factor analysis of the β-glucuronidase reporter activity from 6 to 14h of growth in *gvpA1*::*uidA* and *gvpA1*::*uidA*, *floR* found $F = 1419.89 > F_{crit} = 4.15$, $p = 4.38*10^{-28}$.

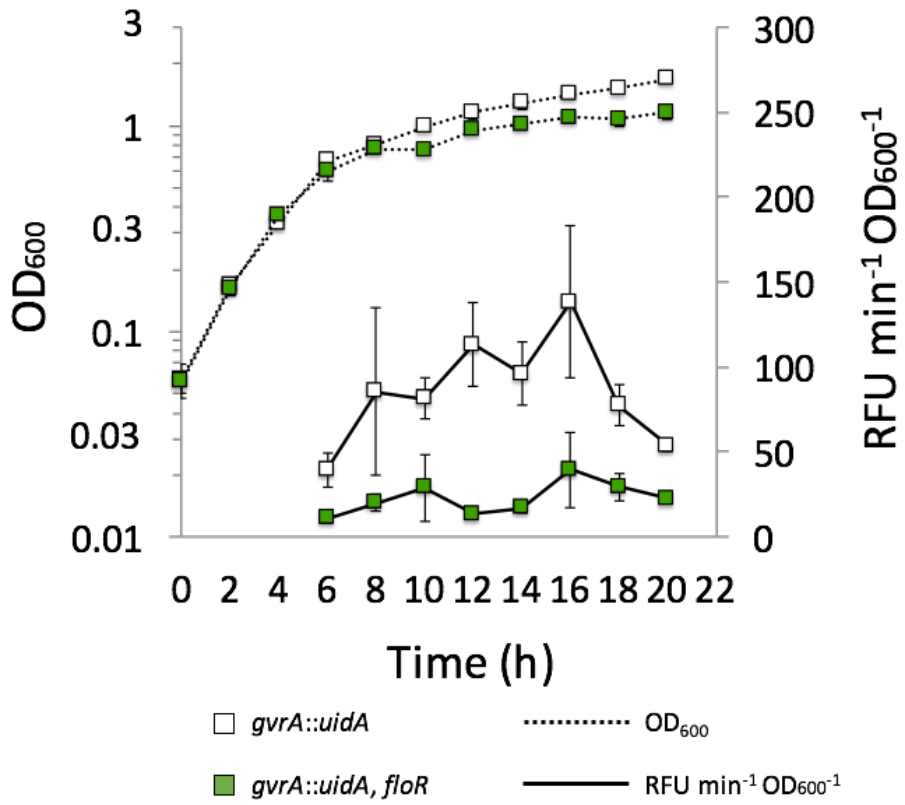

Figure 4.9. *gvrA* promoter activity in the *floR* mutant under microaerophilic conditions. Cell density (OD_{600}, dotted lines) and gene expression (RFU min^{-1} OD_{600}^{-1}, continuous lines) were measured throughout growth in LB and reduced aeration. The data represent the average and standard deviation (error bars) of three biological replicates. ANOVA two-factor analysis of the β-glucuronidase reporter activity from 6 to 14 h of growth in *gvrA*::*uidA* and *gvrA*::*uidA*, *floR* found $F = 112.70 > F_{crit} = 4.15, p = 5.20*10^{-12}$.

4.5 TMT labelling and LC-MS/MS quantitation and sequencing of intracellular proteins confirms that *floR* is a pleiotropic regulator

The identification of the transposon insertion in AQY121 and subsequent bioinformatic analysis showed that *floR* is the last gene in an operon (See figure 3.3, chapter 3), and the genes 3' of *floR* were transcribed convergently. Therefore, it was not expected that the transposon insertion in *floR* could cause any polar effects on downstream genes. Complementation of *gvpA1* and *gvrA* promoter activity, phase bright structures, pigment production, and swimming motility under ectopic expression of *floR* suggested that other genes are not involved in the phenotypes affected in the *floR* mutant. FloR was predicted to

be part of a family of transcriptional repressors controlling the expression of genes involved in central metabolic pathways (See chapter 3, section 3.2.1). Therefore, it was considered important to study the global impact of the *floR* mutation by identifying and quantifying the intracellular proteome of the *floR* mutant, because this would allow the identification of any other regulatory components under *floR* control.

Differences in gene expression for gas vesicle formation and antibiotic production between the WT and different mutants (including the *floR* strains) were observed between mid-exponential and stationary growth phase in cells incubated for 14-20 hours (Ramsay *et al.,* 2011; Lee *et al.,* 2017). Therefore, cell samples from WT and the *floR* mutant cultures were taken at stationary growth phase and normalized for optical density prior to protein extraction. This procedure was done in collaboration with Chin Mei Lee, a Ph.D student working on the characterization of S39006 *rbsR*::TnKRCPN1. The purified protein samples were sent for tandem mass tagging (TMT) of peptides with 10 isobaric reporters (TMT-10plex) in the Cambridge Centre for Proteomics (CCP) for separation, sequencing and quantitation via liquid chromatography and mass spectrophotometry (LC-MS/MS) of the intracellular proteomes. Four WT replicates, three from the *floR* mutant and the other three from S39006 *rbsR*::TnKRCPN1 were sent for analysis to allow complete usage of the 10 reporters provided in the TMT-10plex analysis.

Previous bioinformatic analysis of the whole genome sequence revealed that 4,413 protein-encoding genes are present in S39006 (Fineran *et al.,* 2013). The sequence of S39006 ORFs were uploaded for public access in www.ecogene.org and https://www.ncbi.nlm.nih.gov/gene. Moreover, the amino acid sequences for the predicted proteins are accessible through different databases websites, such as https://www.ncbi.nlm.nih.gov/protein/ , and http://www.uniprot.org, among others. The databases allowed comparative analyses of the peptides labelled with TMT reagents to determine the abundance of the labelled proteins in the *floR* and WT strains.

The TMT labelling efficiency in the experiment was 82% and 2410 proteins were identified in the *floR* mutant, this corresponds to approximately 55% of the predicted proteins encoded

by genomic ORFs. Differential expression analysis (DEA) with linear models for microarray data (LIMMA) showed that the expression of 802 proteins was significantly altered in the *floR* mutant, *P*-value <0.05 (Figure 4.10). 395 of the 802 differentially expressed proteins were up-regulated, whilst 407 were down-regulated in the *floR* mutant. Figure 4.11 showed that most of the proteins produced with significant differences in the *floR* mutant had low *P*-values. Pearson coefficient correlations (PCC) between replicates show that samples from bacteria with the same genotype had linear associations with R-values close to 1, whilst comparisons between replicates from different strains present lower R-values (Figure 4.12). This indicated that samples (WT and the *floR* mutant) had differential proteome profiles. Also, DEA with LIMMA permitted a principal component analysis (PCA) between samples and visualisation of protein abundance variation. Samples of the *floR* mutant in PCA were separated from WT samples, whilst replicates for each samples were located close to each other (Figure 4.13). In summary, a high frequency of identified proteins with significant low *P*-values, a linear correlation between replicates and a clear separation of samples in PCA confirmed that the mutation in *floR* caused many changes in the S39006 proteome.

Figure 4.10. Volcano plot of the *floR* mutant proteome. Relation between the fold change and adjusted *P*-values of 2410 protein identified and quantified (blue dots) by TMT and LC-MS/MS. The position of proteins involved in gas vesicle production (GvpA1, GvpG, GvpH, GvrA and GvrC), carbapenem (CarA) and prodigiosin production (PigA, PigB, PigC and PigH), and flagellar motility (FilfC, FilF, FlgD and FlgE) are highlighted in red dots. The proteins significantly up and down-regulated are located to the right and left of the Y-axis, respectively, and above the dashed line (*P*=0.05). The fold change of the proteins below the dashed line was not considered statistically significant.

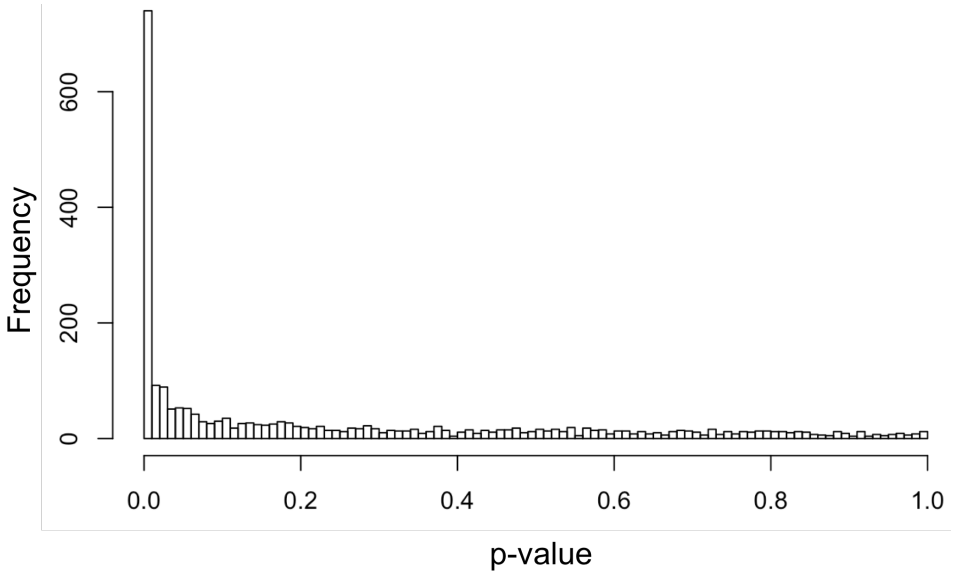

Figure 4.11. *P*-value distribution of the proteome quantitation in the *floR* mutant. Bars represent the frequency of *P*-values in protein fold change between WT and the *floR* mutant.

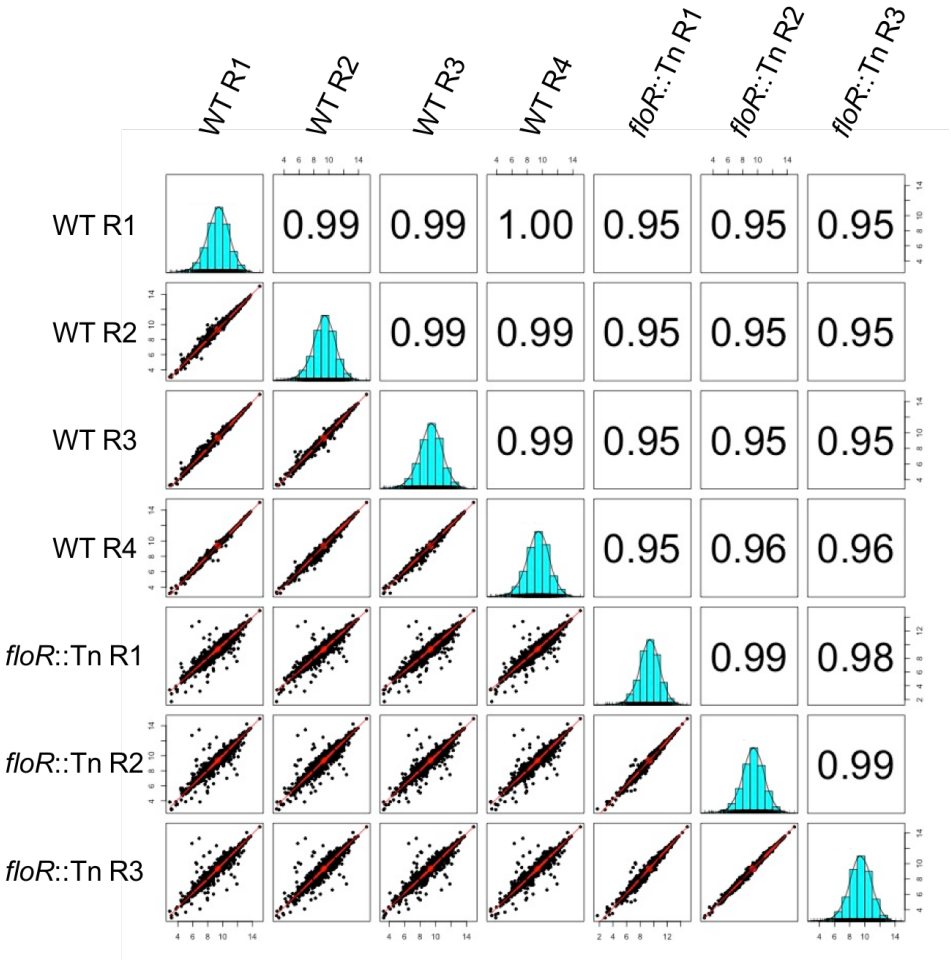

Figure 4.12. Pearson correlation coefficients between replicates of WT and the *floR* mutant. Four WT and three *floR* mutant replicates were included in the TMT and LC-MS/MS analysis.

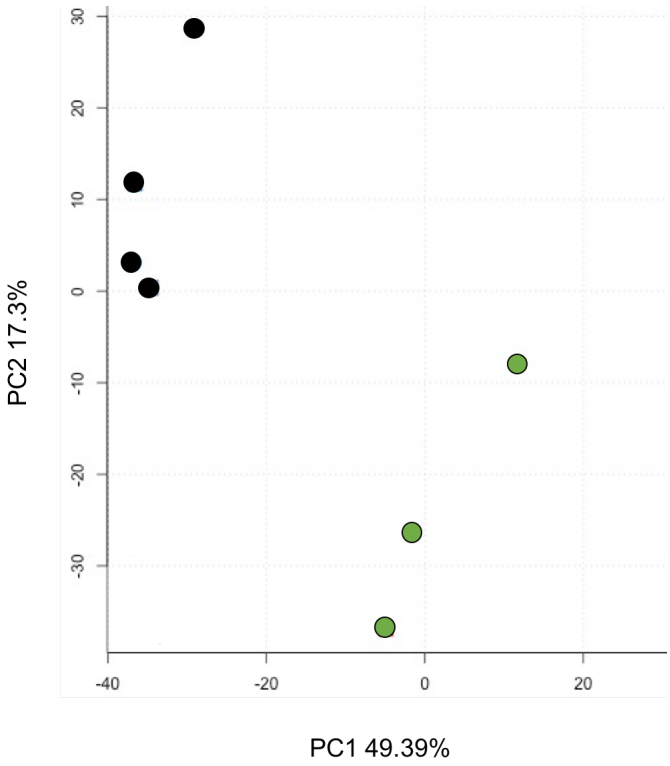

Figure 4.13. Principal component analysis (PCA) of replicates of WT and the *floR* mutant. Black dots represent WT samples and green dots *floR*. Four WT and three *floR* mutant replicates were included in the TMT and LC-MS/MS analysis.

The quantitation and sequencing of the intracellular proteome in the WT and *floR* mutant confirmed that the mutation in *floR* had negative impacts on the expression of the gas vesicle gene cluster (Figure 4.14). 11 of the 19 proteins encoded by the gas vesicle gene cluster were produced in significantly lower amounts in the *floR* mutant. The affected proteins were: structural proteins GvpA1, GvpC, GvpF1, GvpG and GvpN (necessary for gas vesicles shape), regulatory proteins GvrA and GvrB, and proteins with unknown function that are not considered essential for gas vesicle formation, such as GvpW, GvpY, GvpH and GvpZ. Although three other proteins were detected, they did not have significant changes when compared to WT samples. These were: the structural protein GvpF2 and proteins of unknown function GvpK and GvpX. 5 proteins were not detected in the DEA LIMMA analysis: the structural proteins GvpA2, GvpA3 GvpF3, and GvpV (necessary for gas vesicle shape) and the regulatory protein, GvrC (Figure 4.14). Overall, the quantitation and identification of the proteins encoded by the *gvpA-gvpY* and *gvrA-gvrC* operons confirmed previous results showing the impact of *floR* on gas vesicle gene expression (Section 4.2). Moreover, this experiment

supported the idea that FloR regulates gas vesicle production through control of the cognate regulators GvrA, GvrB and GvrC.

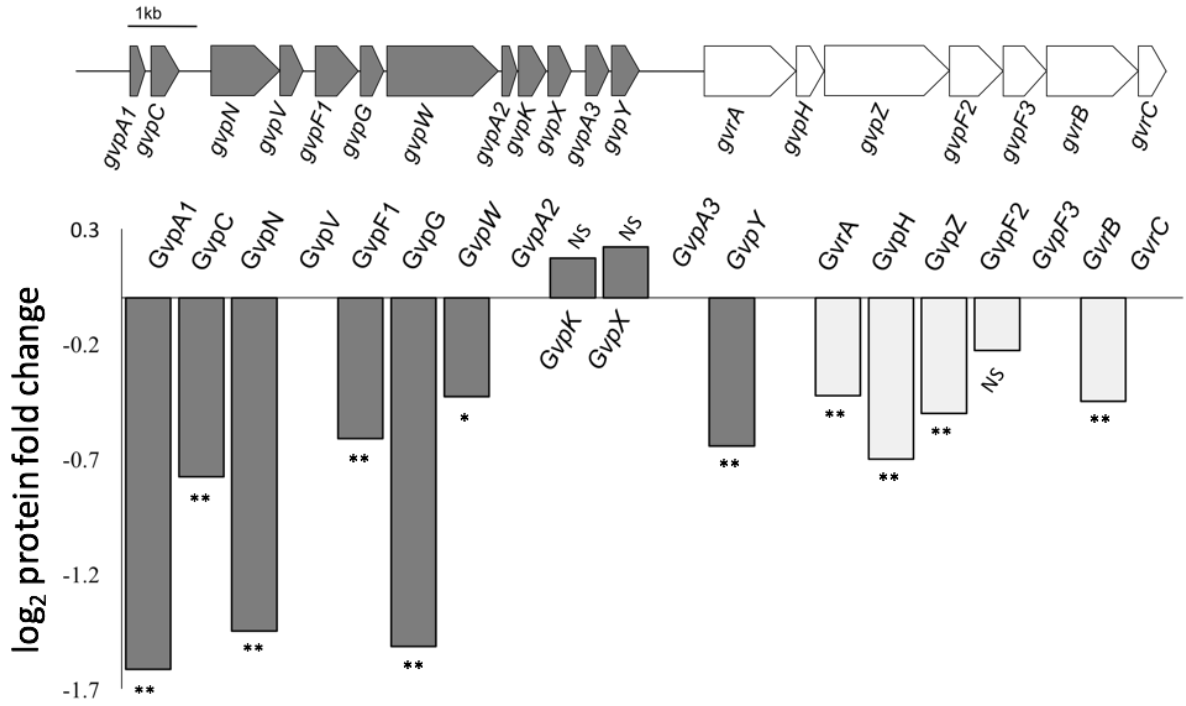

Figure 4.14. Fold change production of gas vesicle proteins in the *floR* mutant. Bars represent the difference in production of gas vesicles between WT and the *floR* mutant samples. Stars represent adjusted P- values: ** ($p<0.01$), * ($p<0.05$) and NS (not significant change). Gas vesicles proteins undetected in the TMT and LC-MS/MS analysis are represented as empty spaces (without bars).

In section 4.3, it was shown that the mutation in *floR* affected antibiotic production and swimming motility (Figures 4.5, 4.6 and 4.7). As with the proteins encoded by the gas vesicle gene cluster, the proteins from the prodigiosin and carbapenem operons were down-regulated in the *floR* mutant (Table 4.1). Proteins from both the 4-methoxy-2-2'-bipyrrole-5-carbaldehyde (MBC) and 2-methyl-3-n-amyl-pyrrole (MAP) parallel pathways for prodigiosin production were produced in significantly lower amounts compared to those in WT.

The reduced production of the carbapenem biosynthetic enzymes CarA, CarB and CarC explains the impaired antibiotic activity of the *floR* mutant (Table 4.1). The proteins providing intrinsic resistance to carbapenem, CarF and CarG, were also detected in lower amounts in the mutant. These proteins are essential in *P. carotovorum* to avoid suicide during carbapenem production (McGowan *et al.,* 1996). The resistance of the *floR* mutant to

exogenous carbapenem production from the carbapenem producer strain *P. carotovorum* ATTn10 was tested (Figure 4.15. A negative control for carbapenem sensitivity with a WT top lawn confirmed that S39006 is resistant to exogenous antibiotic (Figure 4.15.A), whilst a positive control showed that *P. carotovorum* ATTn10 produced the antibiotic (Figure 4.15.C). Unexpectedly, given the reduced production of CarF and CarG (Table 4.1), the *floR* mutant still retained intrinsic resistance to exogenous carbapenem (Figure 4.15.B). This implies that although CarF and CarG production was low, there is still sufficient to provide carbapenem resistance.

Table 4.1. Fold change of proteins from the carbapenem and prodigiosin genetic cluster in the *floR* mutant.

Uniprot code	Protein	$\log_2$ fold change	Adjusted *P*-value
Q5W271	PigA	-1.24	**
Q5W270	PigB	-1.28	**
Q5W269	PigC	-0.90	**
V3V8I0	PigD	-1.11	**
V3TT95	PigE	-1.14	**
V3TX75	PigF	-1.65	**
V3TQH2	PigG	-1.40	**
Q5W264	PigH	-1.52	**
V3V8I5	PigI	-1.34	**
Q5W262	PigJ	-0.25	*
V3T1Z2	CarA	-4.55	**
V3TL74	CarB	-2.49	**
V3TSU2	CarC	-3.41	**
V3T1Y6	CarF	-0.33	**
V3TL70	CarG	-1.32	**

** ($p<0.01$), * ($p<0.05$).

In contrast to proteins involved in gas vesicle, carbapenem and prodigiosin production, several proteins involved in flagellar motility were overexpressed in the *floR* mutant (Table 4.2). Specifically, proteins involved in flagellum structure (FlgH, FlgK, FlgL, FlhA, FliC, FliD and FliP), in assembly (FlgA, FlgD and FliH), and rotation (FliG FliN and YcgR) were detected. Also, others proteins predicted as chemotactic response regulators were identified as up-regulated. This result supported previous observations on the hyper-motility of the *floR* mutant (Figure 4.7). The surfactant synthesis protein RhlA was also detected in high amounts

in the *floR* mutant (Table 4.2). Both flagella and surfactant production are essential for swarming motility in S39006 (Williamson *et al.,* 2008). To investigate further the role of *floR* on swarming motilty, samples of WT and *floR* mutants were spotted into semisolid LBA. Figure 4.16 confirms that the *floR* mutant is a hyper-active swarmer.

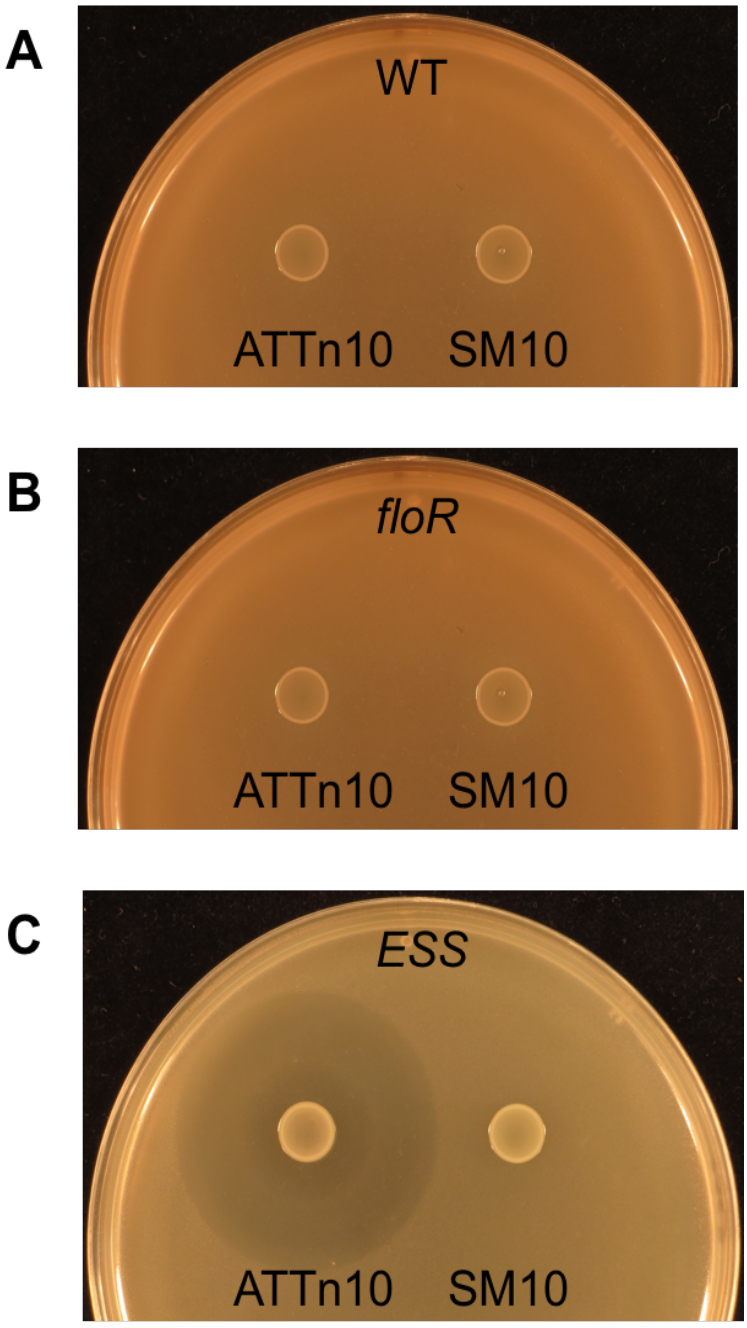

Figure 4.15. Carbapenem sensitivity in the *floR* mutant. The carbapenem producer *P. carotovorum* ATTn10 and the carbapenem mutant *P. carotovorum* SM10 were spotted on top lawns containing (**A**) WT, (**B**) the *floR* mutant and (**C**) the β-lactam supersensitive strain *E. coli* ESS. All images are representative of three biological replicates.

Table 4.2. Fold change of proteins involved in swimming and swarming motility.

Uniprot code	Name/ description	log_2 fold change	Adjusted *P*- value
V3TN54	**FlgD**/Basal-body rod modification protein	1.74	**
V3TRY0	**FliH**/Flagellar assembly protein	1.27	**
V3TWW5	Putative Methyl-accepting chemotaxis sensory transducer	1.15	**
V3SYE9	Putative Methyl-accepting chemotaxis sensory transducer	1.15	**
V3TTZ2	Putative Methyl-accepting chemotaxis sensory transducer	1.10	**
V3TPD4	Putative Methyl-accepting chemotaxis sensory transducer	1.04	**
V3TKC4	**FlgL**/Flagellar hook-associated protein 3	1.01	**
V3T139	**FlgK**/Flagellar hook-associated protein 1	0.98	**
V3T157	Putative Methyl-accepting chemotaxis sensory transducer	0.98	**
V3V2S0	**FliC**/Flagellin	0.92	**
V3U027	**RhlA**/Surfactant synthesis protein	0.89	**
V3TW17	Putative Methyl-accepting chemotaxis sensory transducer	0.85	**
V3V2S3	**FliF**/Flagella M Ring	0.84	**
V3V2U3	**FlgE**/Flagellar hook protein	0.82	**
V3V681	Putative Methyl-accepting chemotaxis sensory transducer	0.78	**
V3TRZ2	**FlgH**/Flagellar L-ring protein	0.77	**
V3TU64	Putative Methyl-accepting chemotaxis sensory transducer	0.75	**
V3TUR3	Putative Methyl-accepting chemotaxis sensory transducer	0.70	**
V3TPS5	Putative Methyl-accepting chemotaxis sensory transducer	0.67	**
V3TN65	Putative Methyl-accepting chemotaxis sensory transducer	0.66	**
V3TN31	**FliD**/Flagellar hook-associated protein 2	0.64	**
V3TS04	**CheB**/Chemotaxis response regulator protein-glutamate methylesterase	0.64	**
C5J9G8	**FlhA**/Flagellar biosynthesis protein	0.62	**
V3V2V4	**CheZ**/Protein phosphatase-flagellar motor control protein	0.61	**
V3TKE3	Chemotaxis protein methyltransferase	0.60	**
V3TJP2	Putative Methyl-accepting chemotaxis sensory transducer	0.57	**
V3UZI2	Putative Methyl-accepting chemotaxis sensory transducer	0.58	**
V3TU01	Putative Methyl-accepting chemotaxis sensory transducer	0.53	**
V3TN36	**FliG**/Flagellar motor switch protein	0.52	**
V3V2V9	**CheW**/Chemotaxis receptor signal protein	0.49	**
V3TRY4	**FliM**/Flagellar motor switch protein	0.48	**
V3T147	**FlgA**/Flagella basal body P-ring formation protein	0.47	**
V3V2P8	Putative Methyl-accepting chemotaxis sensory transducer	0.42	**
V3TK75	Putative Methyl-accepting chemotaxis sensory transducer	0.42	**
V3U0B9	**YcgR**/Flagellar brake protein	0.34	*
V3TKC0	**FliN**/Flagellar motor switch protein	0.32	**
V3V2T2	**FliP**/Flagellar biosynthetic protein	0.22	*
V3T0D6	Putative Methyl-accepting chemotaxis sensory transducer	0.21	**
V3T3B2	Putative Methyl-accepting chemotaxis sensory transducer	0.19	**
V3T563	Putative Methyl-accepting chemotaxis sensory transducer	0.19	**
V3T144	**FlgF**/Flagellar basal body protein	0.16	NS
V3T133	Flagellar protein similar to MopB (71.5% *P. carotovorum* subp. *carotovorum*) and FliO (57.5% *Yersinia frederiksenii*)	0.15	NS
V3TN48	**FlgI**/Flagellar P-ring protein	0.043	NS
V3TRX7	**FliS**/Flagellar chaperone	-0.17	NS
V3V9I7	Putative Methyl-accepting chemotaxis sensory transducer	-0.18	NS
V3TZH1	Putative Methyl-accepting chemotaxis sensory transducer	-0.26	**

*($p<0.05$), **($p<0.01$), NS($p>0.05$)

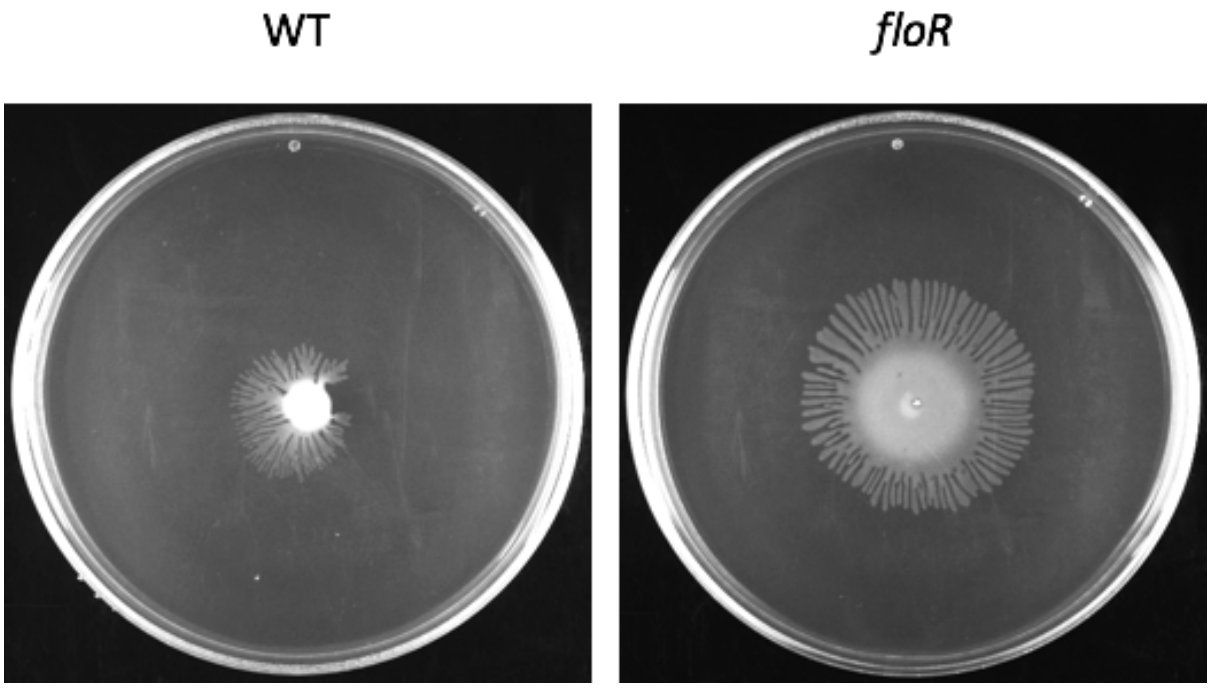

Figure 4.16. Swarming motility assay in the *floR* mutant. All images are representative of three biological replicates.

4.6 FloR is a master regulator

Previous studies identified the transcription factor PigP as a master regulator affecting multiple genes involved in antibiotic production and motility (Fineran *et al.,* 2005(a); Williamson *et al.,* 2008). Similar to *floR*, *pigP* mutants are defective for carbapenem and prodigiosin production, but hyper-active for flagellar motility. Thus, it was reasonable to hypothesize that *floR* dependent regulation was connected to other regulators affecting the phenotypes studied before. Searches were done for regulators previously characterized in S39006 among the 2410 proteins identified from the TMT LC-MS/MS experiment (See Chapter 1, sections 1.4, 1.6 and 1.4, and Figure 1.5). Table 4.3 summarizes the regulatory proteins identified in the *floR* mutant and their phenotypes in S39006, and Figure 4.17 represents the previously known regulatory network of the proteins significantly altered. The HexA and GntR *E. coli* homologues, PigU and PigT respectively, were up-regulated, whilst the mRNA binding protein RsmA, the sigma factor (σ^{38}) RpoS, the periplasmic phosphate binding protein PstS and SylA-like transcription regulator Rap were all down-regulated in the mutant. Other regulatory proteins detected, such as PstA, SdhE, PigZ, Hfq, PigP and PigS did not show significant changes in the *floR* mutants.

Table 4.3. Fold change of pleiotropic regulators in the *floR* mutant.

Name	log_2 fold change	Adjusted *P*-value	Description	GV	FM	Car	Pig	BHL	Reference
PigU	**0.66**	**	*E. coli* HexA homologue (LysR-family). This protein contains a N-terminal HTH binding domain.			+	+		Fineran *et al.,* 2005(b); Wilf *et al.,* 2013
PigT	**0.25**	**	*E. coli* GntR homologue. This protein is a transcriptional activator sensitive to gluconate repression		+		+		Fineran *et al.,* 2005(a)
PstA	**0.21**	NS	Phosphate transport system permease protein				-		Slater *et al.,*2003
SdhE	**0.15**	NS	Flavinylation factor		+		+		Hampton *et al.*, 2016
PigZ	**0.11**	NS	TetR family transcriptional repressor , controls the expression of the ZrpADBC pump		Swi+, Swa-	+	-		Gristwood *et al.*, 2008
Hfq	**-0.04**	NS	sRNAs chaperone			+	+		Wilf *et al.,* 2013; Wilf *et al.,* 2013
PigP	**-0.06**	NS	N-terminal HTH (lambda repressor family)		-	+	+		Fineran *et al.,* 2005(b)
PigS	**-0.21**	Ns	ArsR-family transcriptional regulator, HTH.				+		Fineran *et al.,* 2005(b)
RsmA	**-0.40**	**	RNA-binding protein	+	-	-	-		Ramsay *et* al., 2011; Wilf *et al.*, 2013
RpoS	**-0.49**	**	Stationary phase sigma factor subunit of RNA polymerase		-	-	-		Wilf *et al.*, 2012; Wilf *et al.*, 2013
PstS	**-0.52**	**	Phosphate-binding protein			-	-	-	Slater *et al.,*2003
Rap	**-2.08**	**	SylA-like transcriptional regulator		-	+	+		Thomson *et al.,* 1997

*(p<0.05), **(p<0.01), NS(p>0.05), GV (gas vesicles), FM (flagellar motility), Swi (Swimming motility), Swa (swarming motility), Pig (prodigiosin), BHL (N-butanoyl-Lhomoserine lactone), + (upregulation), - (downregulation), NS (not significant change detected), empty (not assessed yet).

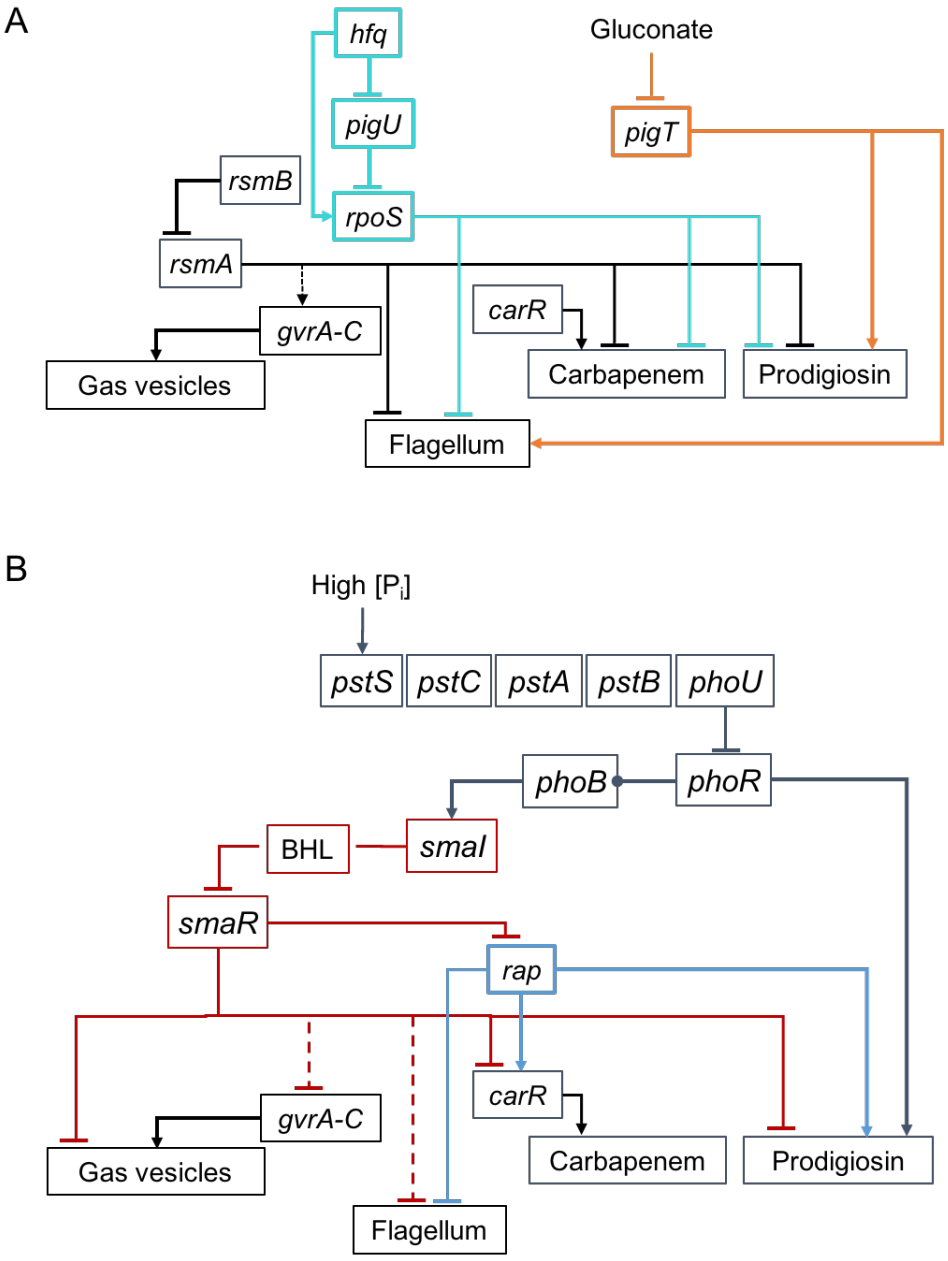

Figure 4.17. Network of known regulators of gas vesicles, flagellum, carbapenem and prodigiosin production affected in the *floR* mutant. A. The *rsmA-rsmB* dependent regulatory pathway is highlighted in black lines, *pigU-rpoS* in cyan and gluconate-*pigT* in orange. **B.** The orthophosphate-*pstSCAB-phoU-phoBR* regulatory pathway is highlighted in dark blue, QS in red and *rap* in light blue. Continuous lines indicate direct regulation, whilst discontinuous indirect. Arrows and perpendicular lines indicate activation and inactivation respectively, whilst the lines ending in a solid circle indicate regulation thought to be through phosphorylation. See description in text for detailed information.

4.6.1 FloR regulates gas vesicles via RsmA-*rsmB* and PigU-RpoS

RsmA is a positive regulator of the *gvpA1-gvpY* and *gvrA-gvrC* operons (Ramsay *et al.,* 2011) (Table 4.3, figure 4.15.A and section 1.4.3). It, therefore, seemed possible that FloR controlled gas vesicle production through RsmA positive regulation. To test this hypothesis, the mutation in *floR* was transduced into a *rsmA*::*uidA* fusion strain, and the β-glucuronidase activity and cell morphology assessed (Figures 4.18.A and 4.19). The reporter activities in the *rsmA*::*uidA* and *rsmA*::*uidA*, *floR* strains did not show significant differences (Figure 4.18.A). It was also observed that, similar to the *rsmA*::*uidA* and *floR* single mutants, the *rsmA*::*uidA*, *floR* strain lost the ability to produce phase bright structures (gas vesicles) (Figure 4.19). Therefore, it was still plausible that the gas vesicle loss in the *floR* mutants was caused by down-regulation of RsmA, and FloR controlled the RsmA levels through post-transcriptional regulatory pathways.

The small RNA *csrB* (a *rsmB* homologue) binds to CsrA (a RsmA homologue) in *E. coli* to antagonize its mRNA binding activity (Romeo, 1998). Furthermore, experiments in S39006 showed that disruption of *rsmB* causes overexpression of the gas vesicle operons (Ramsay *et al.,* 2011) (Figure 4.17.A and Section 1.4.3). This suggested that FloR could be affecting RsmA-dependent control of gas vesicles through *rsmB*. The mutation in *floR* was transduced into an *rsmB*::*uidA* strain and the reporter activity and morphology assessed. Figure 4.18.B shows that the mutation in *floR* up-regulated the β-glucuronidase activity. This suggested that FloR inhibits *rsmB* expression and, thus, affected *rsmB*-post-transcriptional repression of RsmA to enable the production of gas vesicles. In contrast, PCM analysis of *rsmB*::*uidA* and *rsmB*::*uidA, floR* strains showed that, whilst most *rsmB* mutants produced phase bright structures, the mutation in *floR* bypassed the *rsmB* mutant phenotype. If *floR*-dependent gas vesicle production were solely controlled through the RsmA-*rsmB* pathway, some gas vesicle production would be expected in the *rsmB, floR* double mutant. The absence of phase bright structures in the *rsmB*::*uidA, floR* strains suggested that FloR-dependent regulation of gas vesicles was not exclusively under *rsmB* or RsmA control.

Previous studies in S39006 showed that *rpoS* was a negative regulator of flagella, prodigiosin and carbapenem production (Wilf & Salmond, 2012; Wilf *et al.,* 2013) (Figure 4.17.A).

Moreover, gene expression assays and proteomic analysis in S39006 confirmed that the RNA binding protein, Hfq, aided by sRNAs, promotes directly the translation of *rpoS* mRNA, and *rpoS* transcription indirectly through inhibition of PigU (Wilf *et al.,* 2011; Wilf *et al.,* 2013) (Figure 4.17.A and sections 1.6.2, 1.6.3 and 1.7.3). Interestingly, the *floR* mutant showed overexpression of PigU and reduction of RpoS levels, whilst Hfq production did not vary significantly (Table 4.3). This result suggested that *floR* regulates PigU and RpoS without affecting Hfq expression. To assess the impact of *floR* on the PigU-RpoS pathway, the mutation in *floR* was transduced into a *rpoS*::*uidA* strain and the reporter activity and cell morphology measured (Figures 4.18.C and 4.19). The β-glucuronidase activity in the *rpoS*, *floR* double mutant was lower than in the *rpoS* single mutant; this supported the idea that FloR regulates the expression of the sigma factor. Surprisingly, the *rpoS*::*uidA* mutant did not produce phase bright structures (Figure 4.19). The *rpoS*-dependent regulation of gas vesicles has not been reported in S39006. Taking together the proteomics data, plus the transcription reporter assay and cell morphology observations in PCM, these results suggest that FloR controls gas vesicles via inhibition of PigU for RpoS expression, in addition to the *rsmB*-RsmA pathway.

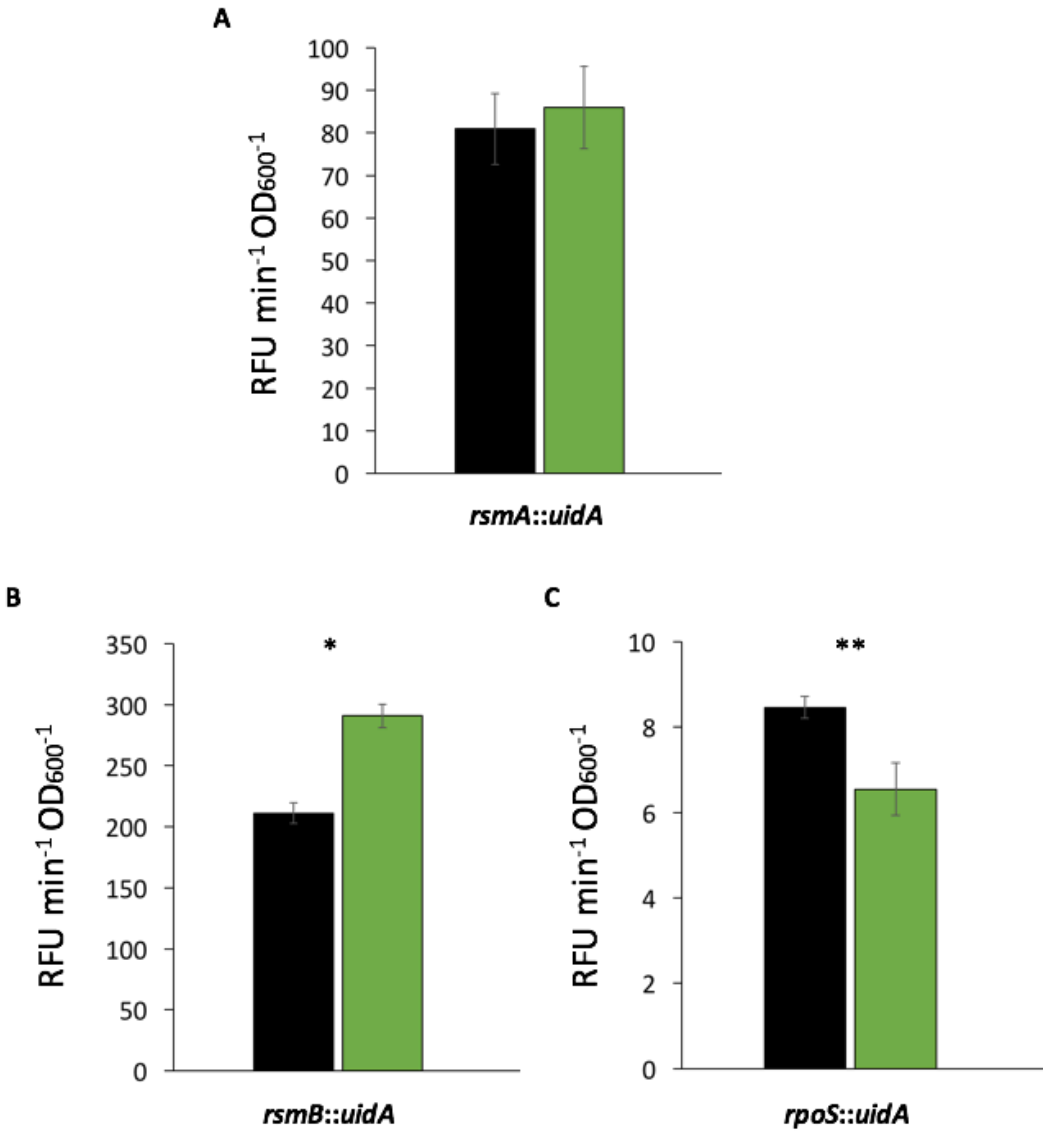

Figure 4.18. Effect of *floR* mutation on *rsmA*, *rsmB* and *rpoS* expression. Black bars represent the β-galactosidase activity (UidA) in (**A**) *rsmA*::*uidA,* (**B**) *rsmB*::*uidA,* and (**C**) *rpoS*::*uidA* single mutants, and green bars the UidA activity in fusion strain with the *floR* mutation. Samples were taken after 12h of growth. The data represent the average and standard deviation (error bars) of three biological replicates. *p<0.05 and ** p<0.01

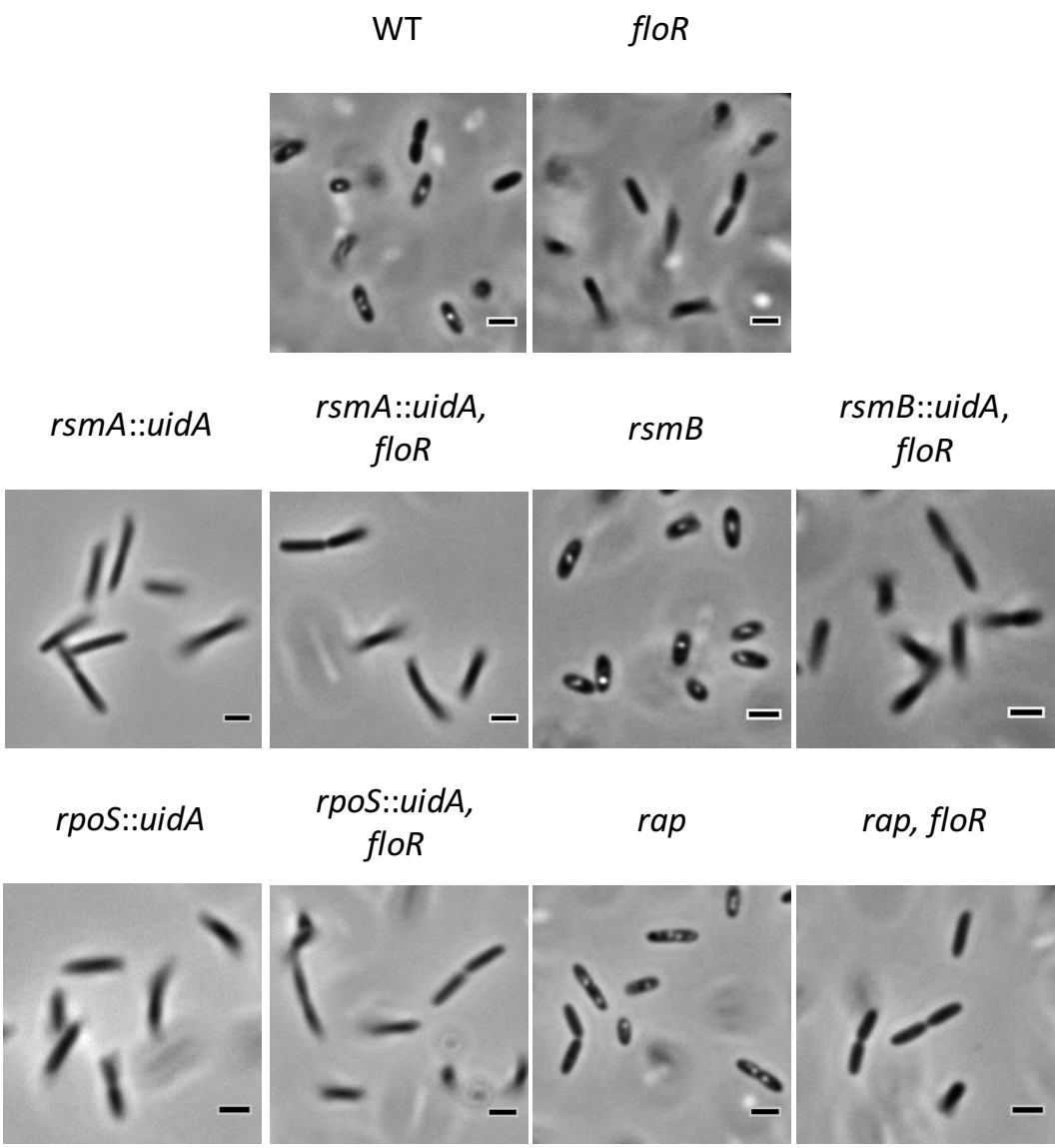

Figure 4.19. PCM analysis of *floR*- (*rsmA, rsmB*, *rpoS*, *rap*) double mutants. Scale bars correspond to 1 μm.

4.6.2 FloR stimulates antibiotic production through *rap* regulation

The mutation in *floR* caused overexpression of PigU, PigT (positive regulators of carbapenem and prodigiosin) and reduced production of RsmA, RpoS and PstS, which are negative regulators (Table 4.3). This implied that the overexpression of PigU, PigT and the inhibition of RsmA, RpoS, PstS should lead to carbapenem and prodigiosin production above WT levels. However, this was not observed in the phenotypic characterization of the *floR* mutant (Figures 4.5 and 4.6, Table 4.1). The prodigiosin and carbapenem production, and the

intracellular proteome quantitation and sequencing suggested that FloR was a positive regulator of antibiotic production (Figures 4.5 and 4.6, Table 4.1).

The reduction in antibiotic production in the *floR* mutant could be explained by the down-regulation (-2.1 protein log fold change) of Rap, a positive antibiotic regulator (Table 4.3). It seemed that Rap regulation of prodigiosin and carbapenem was dominant over PigU, PigT, RsmA, Rpos and PstS in the *floR* mutant. To test this hypothesis, prodigiosin was extracted from *rap, rsmA* and *rpoS* single mutants and double (*rap, floR; rsmA, floR*; *rpoS, floR*) mutants (Figure 4.20). Prodigiosin production in the *rap* and *rap, floR* mutant strains was significantly reduced (10 times) compared to the WT and the single *floR* mutant. Furthermore, there was no significant difference between the *rap* and *rap, floR* mutants. This implied that neither the PigU and PigT overexpression nor the down-regulation of RsmA, RpoS and PstS in the *floR* mutant could bypass the prodigiosin phenotype caused by the mutation in *rap*.

Interestingly, prodigiosin production in the *rsmA*::*uidA* and *rpoS*::*uidA,* and *rsmA*::*uidA, floR* and rpoS::uidA, *floR* strains was up-regulated compared to WT and the single *floR* mutant (Figure 4.20). Contrary to prodigiosin production in *rap* and *rap*, *floR* mutants, the *rsmA*::*uidA*, *floR* and *rpoS*::*uidA, floR* mutants show significantly reduced prodigiosin production when compared to *rsmA*::*uidA* and *rpoS*::*uidA* single mutants. As the mutation in *rap* was not bypassed by the mutation in *floR*, contrary to the *rsmA* and *rpoS* mutants, it may be reasonable to conclude that *rap*-dependent antibiotic regulation is dominant in the *floR* regulatory network.

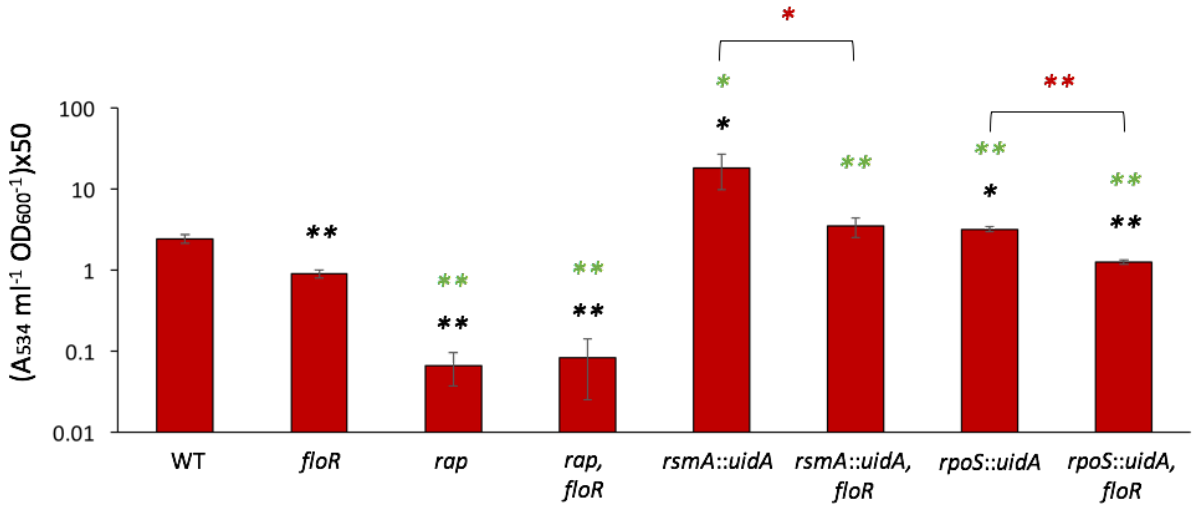

Figure 4.20. Prodigiosin production in *floR*- (*rsmA, rsmB*, *rpoS*, *rap*) double mutants. Bars represent the average production of prodigiosin and error bars the standard deviation of three biological replicates. *p<0.05 and ** p<0.01. Black stars represent statistical differences when compared to WT, green stars when compared to *floR* and red stars between samples indicated in brackets.

4.6.3 FloR affects BHL production

In high extracellular P_i concentrations, the orthophosphate (P_i) transport and response complex PstSCAB-PhoU inhibits activation of the PhoBR two-component system, whilst at low P_i concentrations PhoR autophosphorylates and activates PhoB (Hsieh & Wanner, 2010). The phosphorylated transcription factor, PhoB, enhances expression of the QS autoinducer (BHL) synthase gene, *smaI,* and the carbapenem and prodigiosin biosynthetic operons (Slater *et al.,* 2003 and Gristwood *et al.,* 2009) (Figure 4.17.B and section 1.7.2). Therefore, mutations in *pstSCAB-phoU* essentially mimic low P_i conditions and result in elevated BHL and antibiotic production. The proteomic analysis showed that the *floR* mutant had reduced production of PstS, the phosphate binding component of the PstSCAB-PhoU system (Table 4.3). To corroborate the negative impact on PstS levels in the *floR* mutant, the production of the QS autoinducer was assessed throughout growth with a BHL sensor strain (SP19) (Figure 4.21). The *floR* mutant significantly overproduced BHL at late exponential and stationary growth phase (See ANOVA analysis in Figure 4.21 legend).

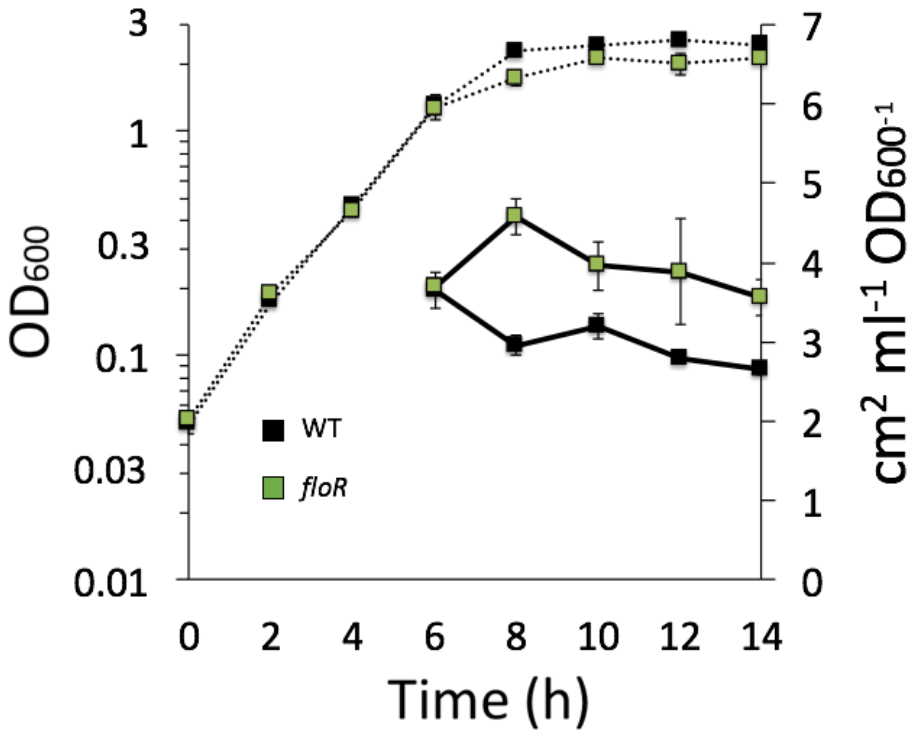

Figure 4.21. BHL production in the *floR* mutant. Cell growth is represented in dashed lines and BHL production in continuous lines. The data represent the average and standard deviation (error bars) of three biological replicates. ANOVA two-factor analysis of BHL detection in WT and the *floR* mutant supernatants taken from 6 to 14 h of growth: $F = 79.43 > F_{crit} = 4.35$, $p = 2.11*10^{-8}$.

4.7 FloR regulates its own operon and the expression of proteins involved in carbon metabolism

floR was a gene initially annotated as Ser39006_3835 and predicted to encode a DeoR-like transcriptional regulator (Figure 3.3, section 3.2.1). Previously studied members of the DeoR family commonly repress the expression of operons involved in central metabolism (Chapter 3, Section 3.6). Moreover, genes upstream of *floR* were predicted to encode proteins related to carbon metabolism (Table 3.3, Section 3.2.1). The abundance of proteins encoded in the *floR* operon was assessed in the TMT and LC-MS/MS quantitation and sequencing data. First, it was clear that the proteins encoded by genes upstream of *floR* (Ser39006_3836 and Ser39006_3837) were overexpressed and among those most highly expressed (Table 4.4). Also, the proteins from the upstream operon were found to be among the most abundant in the *floR* mutant (Figure 4.22.A, Table 4.4). In contrast, the levels of proteins encoded by genes downstream of *floR* were not altered. This suggested that FloR may repress its own operon

by a negative feedback loop mechanism and upstream genes probably by divergent transcription repression (Figure 4.22.B).

Other proteins among those most up-regulated in the *floR* mutant supported the idea that this regulator is involved in carbon metabolism control. For instance, a glucose 1-phosphatase homologue (V3T1I6), the ribose dehydrogenase RbsD (V3TQM9), the aerobic C4-dicarboxylate transporter DctA (V3TU23) and other uncharacterised proteins with conserved domains related to carbohydrates hydrolysis, recognition and transport were found highly expressed (Table 4.4). Other proteins with conserved domains apparently unrelated to carbohydrate utilisation were also overexpressed. This includes proteins involved in flagellar motility and chemotaxis; an uncharacterised XRE-like transcriptional regulator (V3TP78), proteins containing domains for protein modification (V3TN35), and amidohydrolase activity (V3TWN8).

Bioinformatic analysis of proteins down-regulated by the mutation in *floR* was also done (Table 4.5). As expected, proteins from the carbapenem, prodigiosin and gas vesicle clusters were identified among the most affected proteins. Other proteins related to central metabolism were also noted, such as a 3-dehydro-L-gulonate-6-phosphate decarboxylase (V3V772) homologue and an acyl-coA dehydrogenase (V3T1L7). In addition, other proteins such as an uncharacterized IclR-like transcription factor (V3TWM7) and a predicted protein chaperone of the small heat shock (HSP20) family (V3VBC1) were identified (Table 4.5).

Table 4.4. "Top hit" proteins increased in the *floR* mutant.

	Uniprot code	log_2 fold change	Adjusted *P*-value	Name	Gene	Organism with closest homologue protein/ identity score	Conserved domains	NCBI code
1	V3TKK5	6.54	**	Uncharacterized protein	Ser39006_3838	*Dickeya zeae* %85	Class IV iron-containing alcohol dehydrogenase	WP_021017097.1
2	V3TPE5	6.22	**	Uncharacterized protein	Ser39006_3839	*Dickeya solani* 86%	Class I aldolase, member of the dihydrodipicolinate synthase family	WP_021017098.1
3	V3SYI3	3.36	**	Uncharacterized protein	Ser39006_3836	*Pectobacterium carotovorum* 90%	PdxA-family	WP_021017095.1
4	V3SYI9	3.35	**	Uncharacterized protein	Ser39006_3841	*Erwinia typographi* 90%	Sugar phosphate permease	WP_021017100.1
5	V3THV3	3.13	**	Uncharacterized protein	Ser39006_3840	*Erwinia billingiae* 84%	D-isomer specific 2-hydroxyacid dehydrogenase, NAD binding domain	WP_021017099.1
6	V3UZX5	2.88	**	Uncharacterized protein	Ser39006_3837	*P. carotovorum* 63%	Four-carbon acid sugar kinase family protein	WP_021017096.1
7	V3TN35	2.35	*	Uncharacterized protein	Ser39006_0546	bacteria symbiont BFo1 of *Frankliniella occidentalis* 64%	Disulfide oxidoreductase/Thioredoxin like protein	WP_021013820.1
8	V3T0L2	2.13	*	Uncharacterized protein	Ser39006_3038	*D. zeae* 78%	N-terminal carbohydrate binding (Isoamylase) and C-terminal putative esterase domains	WP_021016300.1
9	V3TN54	1.74	**	FlgD	Ser39006_3185	*P. carotovorum* 72%	Flagellar basal body rod modification protein	WP_021016446.1
10	V3T1I6	1.63	*	Glucose-1-phosphatase	Ser39006_3333	*Hafnia alvei* 74%	Histidine phosphatase superfamily	WP_021016594.1
11	V3U1M2	1.53	NS	Uncharacterized protein	Ser39006_0148	*P. carotovorum* 99%	Pectate lyase	WP_021013424.1
12	V3TI12	1.41	**	Uncharacterized protein	Ser39006_3900	*Lonsdalea quercina* 85%	Small subunit of acetolactate synthase	WP_021017159.1
13	V3TQM9	1.40	**	RsbD	*rbsD*	*Dickeya dadantii* 88%	D-ribose pyranose/furanose isomerase	WP_021013778.1
14	V3TNR5	1.34	**	Uncharacterized protein	Ser39006_4200	*Pectobacterium atrosepticum* strain SCRI 1043 *72%*	Alpha/beta hydrolase of unknown function	ESN61171.1
15	V3TS81	1.31	**	Uncharacterized protein	Ser39006_1019	*Dickeya dianthicola 71%*	Short-chain dehydrogenase	WP_021014290.1
16	V3TQD2	1.28	**	Uncharacterized protein	Ser39006_2621	*Enterobacter sp. EGD-HP1* 45%	Non-conserved domain	WP_021015883.1

*($p<0.05$), **($p<0.01$), NS($p>0.05$)

Table 4.4 continued

	Uniprot code	log_2 fold change	Adjusted *P*-value	Name	Gene	Organism with closest homologue protein/ identity score	Conserved domains	NCBI code
17	V3TRY0	1.27	**	FliH	Ser39006_3166	*D. dadantii* 70%	Flagellar assembly protein H	ESN62241.1
18	V3TU23	1.24	**	DctA	Ser39006_0359	*Dickeya paradisiaca* 88%	C4-dicarboxylate transporter	WP_021013636.1
19	V3TWW5	1.15	**	Methyl-accepting chemotaxis protein II	Ser39006_1275	*Rahnella aquatilis* 85%	Methyl-accepting chemotaxis protein II	WP_021014544.1
20	V3SYE9	1.15	**	Methyl-accepting chemotaxis protein I	Ser39006_3796	*D. dadantii* 68%	Methyl-accepting chemotaxis protein I	WP_021017055.1
21	V3TTZ2	1.10	**	Methyl-accepting chemotaxis protein II	Ser39006_2536	*Brenneria sp. EniD312* 70%	Methyl-accepting chemotaxis protein II	WP_021015799.1
22	V3TKX2	1.09	**	Uncharacterized protein	Ser39006_3966	*Yersinia massiliensis* 70%	Periplasmic sugar-binding domain of uncharacterized ABC-type transport systems	WP_021017222.1
23	V3TIS3	1.06	**	Uncharacterized protein	Ser39006_2622	*Kosakonia sacchari* 58%	Non-conserved domain	ESN61697.1
24	V3TPD4	1.04	**	methyl-accepting chemotaxis protein II	Ser39006_0996	*Dickeya chrysanthemi* 79%	Methyl-accepting chemotaxis protein II	WP_021014267.1
25	V3TKC4	1.01	**	FlgL	Ser39006_3177	*Pectobacterium wasabiae* 66%	Flagellar hook-associated protein	WP_021016438.1
26	V3T139	0.98	**	FlgK	Ser39006_3178	*Dickeya sp.* NCPPB 3274 72%	Flagellar hook-associated protein	WP_021016439.1
27	V3T157	0.98	**	Methyl-accepting chemotaxis protein I	Ser39006_3198	*D. chrysanthemi* 78%	methyl-accepting chemotaxis protein I	WP_021016459.1
28	V3TP78	0.97	**	Putative transcriptional regulator	Ser39006_3545	*Pectobacterium betavasculorum* 81%	Helix-turn-helix XRE-family like protein-(No related to PigP)	WP_037381924.1
29	V3TN09	0.95	**	Uncharacterized protein	Ser39006_3135	*Brenneria goodwinii* 59%	Non-conserved domain	WP_021016396.1
30	V3VCC6	0.93	**	Uncharacterized protein	Ser39006_2503	*Serratia sp. ATCC 39006* 95%	Caudovirales tail fibre assembly protein, lambda gpK	WP_021015766.1
31	V3V2S0	0.92	**	FliC	Ser39006_3159	*Yersinia kristensenii* 78%	Flagellin	WP_021016420.1
32	V3TWN8	0.91	**	Uncharacterized protein	Ser39006_2484	*D. solani* 78%	Amidohydrolase family domain	ESN65075.1
33	V3TL18	0.90	**	Uncharacterized protein	Ser39006_4003	*L. quercina* 70%	RND (Resistance, Nodulation, and cell Division) family efflux transporter	WP_021017262.1

*($p<0.05$), **($p<0.01$), NS($p>0.05$)

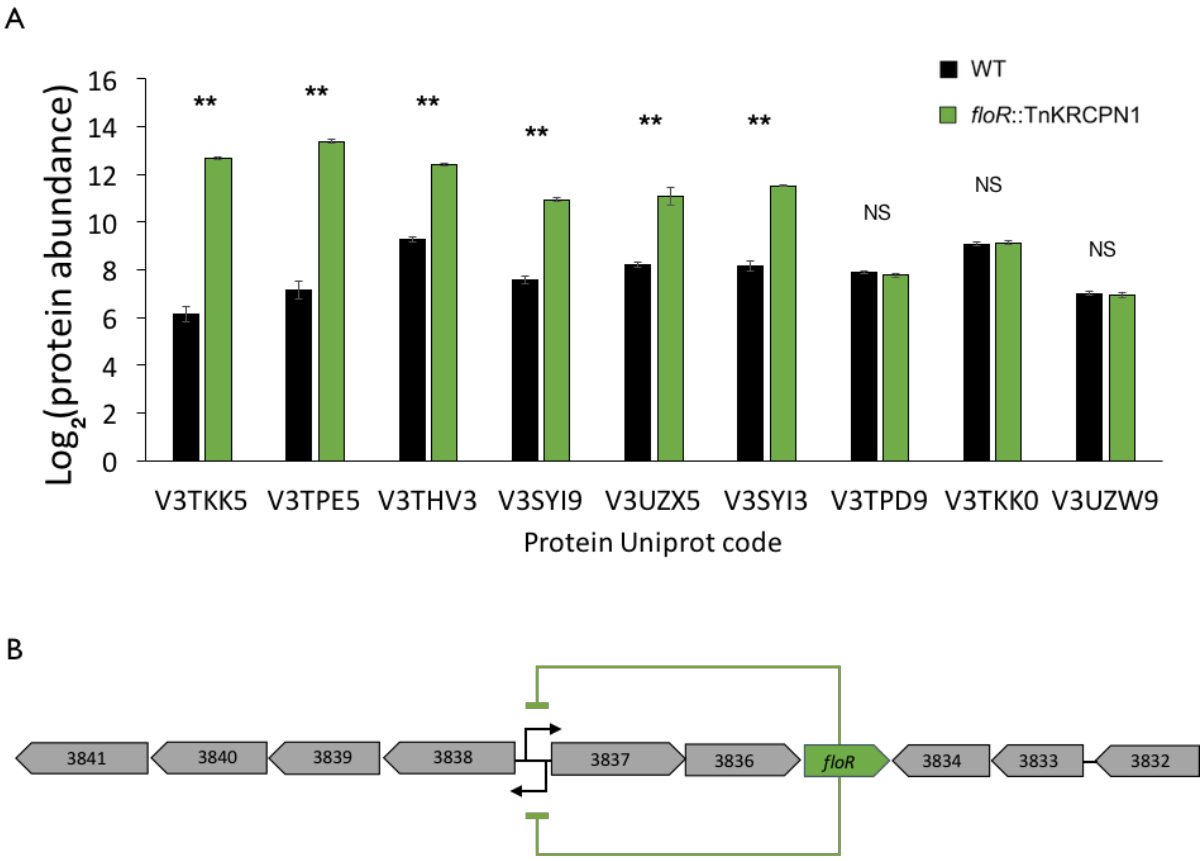

Figure 4.22. Effect of *floR* on the expression of upstream genes. A. Abundance of proteins encoded by genes Ser39006_3841 (V3TKK5), Ser39006_3840 (V3TPE5), Ser39006_3839 (V3THV3), Ser39006_3838 (V3SY19), Ser39006_3837 (V3UZX5), Ser39006_3836 (V3SYI3), Ser39006_3834 (V3TDP9), Ser39006_3833 (V3TKK0), Ser39006_3832 (V3UZW9) in WT and the *floR* mutant. Stars represent adjusted P- values: ** ($p<0.01$), * ($p<0.05$) and NS (not significant change) **B.** Model representing negative feedback loop and divergent regulation by FloR.

Table 4.5. "Top hit" proteins decreased in the *floR* mutant.

	Uniprot code	log_2 fold change	Adjusted *P*-value	Name	Gene	Organism with closest homologue protein/ identity score	Conserved domains	NCBI code
1	V3T1Z2	-4.55	**	CarA	*carA*	*P. betavasculorum* 75%	Carbapenem synthetase	WP_021016744.1
2	V3TMA8	-3.89	**	Uncharacterized protein	Ser39006_2925	*Yersinia frederiksenii* 86%	Non-conserved domains	WP_021016187.1
3	V3TSU2	-3.41	**	CarC	*carC*	*P. carotovorum* 92%	Carbapenem synthetase	WP_021016742.1
4	V3TT94	-2.98	**	Uncharacterized protein	Ser39006_2301	*B. goodwinii 68%*	Amidase	WP_021015566.1
5	V3TR50	-2.91	**	Uncharacterized protein	Ser39006_2926	*Yersinia ruckeri ATCC 29473 66%*	Non-conserved domains	WP_021016188.1
6	V3TNB8	-2.63	**	Uncharacterized protein	Ser39006_4090	*Amphritea atlantica* 68%	Leucine Zipper domain	WP_021017349.1
7	V3V772	-2.58	**	3-dehydro-L-gulonate-6-phosphate decarboxylase	Ser39006_0988	*B. goodwinii* 79%	Orotidine 5'-phosphate decarboxylase	WP_021014259.1
8	V3TL74	-2.49	**	CarB	*carB*	*P. carotovorum* 82%	Carboxymethylproline synthase	WP_021016743.1
9	V3TW95	-2.25	**	Uncharacterized protein	Ser39006_2349	*D. diatnhocola 68%*	Non-conserved domains	WP_021015613.1
10	V3TJT5	-2.08	**	Rap	*rap*	*D. dianthicola* 95%	Regulator of antibiotic production	WP_021016279.1
11	V3TSG6	-1.73	**	Uncharacterized protein	Ser39006_3361	*Paenibacillus sp. Leaf* 39%	Non-conserved domains	WP_021016622.1
12	V3VBC1	-1.72	**	Uncharacterized protein	Ser39006_2188	*D. zeae* 72%	Small heat shock protein (HSP20) family.	WP_021015453.1
13	V3TX75	-1.65	**	PigF	*pigF*	*Serratia plymuthica* 85%	4-hydroxy-2,2'-bipyrrole-5-carbaldehyde (HBC) methyltransferase	WP_021014644.1
14	M9WML5	-1.61	**	GvpA1	*gvpA1*	*Syntrophaceae bacterium 99%*	Gas vesicle structural protein A (homologue 1)	WP_021013972.1.
15	V3V3C2	-1.60	**	Hypothetical protein	Ser39006_3359	No homologues in other microorganisms	Non-conserved domains	WP_021016620.1
16	Q5W264	-1.52	**	PigH	*pigH*	*Serratia sp. YD25* 78%	4-hydroxy-2,2'-bipyrrole-5-methanol synthase	WP_021014646.1.

*(p<0.05), **(p<0.01), NS(p>0.05)

Table 4.5 continued

	Uniprot code	log_2 fold change	Adjusted *P*-value	Name	Gene	Organism with closest homologue protein/ identity score	Conserved domains	NCBI code
17	V3TXT5	-1.52	**	Uncharacterized protein	Ser39006_0232	*Halomonas sp. CSM-2* 63%	Class I SAM-dependent methyltransferase	WP_021013508.1
18	M9WPV0	-1.51	**	GvpG	*gvpG*	*Psychromonas ingrahamii* (strain 37)53%	Gas vesicle protein G	WP_021013978.1
19	M9WR86	-1.45	**	GvpN	*gvpN*	*Syntrophaceae bacterium* 59%	AAA (ATPase) domain	WP_021013974.1.
20	V3TQH2	-1.40	**	PigG	*pigG*	Serratia marcescens 79%	acyl carrier protein	WP_021014645.1.
21	V3TWM7	-1.40	**	Uncharacterized protein	Ser39006_1170	*Escherichia coli* 76%	IclR like trascriptional regulator	WP_021014439.1
22	V3V8I5	-1.34	**	PigI	*pigI*	*S. marcescens* 68%	D-alanine--poly(Phosphoribitol) ligase	WP_021014647.1.
23	V3V8G8	-1.33	**	Uncharacterized protein	Ser39006_1363	*Brenneria goodwinii* %82	Acyl CoA acyltransferase	WP_021014632.1
24	V3TL70	-1.32	**	CarG	*carG*	*P. carotovorum* 69%	Non-conserved domains	WP_021016738.1.
25	Q5W270	-1.27	**	PigB	*pigB*	*Serratia marcescens* 73%	Oxidoreductase	WP_021014640.1.
26	V3TKU7	-1.25	**	Uncharacterized protein	Ser39006_3357	*Desulfotomaculum acetoxidans* 55%	NHL repeat unit of beta-propeller proteins.	WP_021016618.1
27	Q5W271	-1.24	**	PigA	*pigA*	*Serratia marcescens* 80%	Flavoprotein desaturase	WP_021014639.1.
28	V3T1L7	-1.17	**	Uncharacterized protein	Ser39006_3363	*Scytonema tolypothrichoides* 46%	Acyl CoA dehydorgenase	WP_084297647.1
29	V3TIC1	-1.14	**	Hypothetical protein	Ser39006_3364	*S. plymuthica* 73%	Non-conserved domains	WP_021017264.1
30	V3TT95	-1.14	**	PigE	*pigE*	*S. marcescens* 86%	Acetylornithine transaminase	WP_021014643.1.
31	V3V8I0	-1.11	**	PigD	*pigD*	*S. plymuthica 86%*	Thiamine diphosphate dependent-3-acetyloctanal synthase	WP_021014642.1
32	V3TLA4	-1.10	**	Hypothetical protein	Ser39006_3517	*D. paradisiaca* 55%	Non-conserved domains	WP_021016778.1
33	V3TSG2	-1.09	**	Hypothetical protein	Ser39006_3356	*Bradyrhizobium sp. ORS 375* 34%	Non-conserved domains	WP_021016617.1

*(p<0.05), **(p<0.01), NS(p>0.05)

4.8 Bioinformatic analysis of the upstream intergenic sequence of the *floR* operon

floR is predicted to encode a transcriptional repressor and its mutation caused the overexpression of proteins encoded from upstream genes and from different operons. This prompted analysis of intergenic sequence upstream of the *floR* operon using BPROM, a tool for prediction of bacterial promoters, to identify potential transcription initiation sites and -10 and -35 boxes for the transcription of the divergent operons (Figure 4.23.A). MEME was also used to search for shared motifs in four regulatory sequences of the operons encoding the ten most overexpressed proteins in the *floR* mutant (See Table 4.4). The sequence logo illustrating the consensus motif with the highest score and the occurrence of each nucleotide in it is shown in Figure 4.23.B. The MEME analysis identified a potential 22bp binding sequence overlapping the transcription initiation site and the -10 box next to the *floR* operon (Figure 4.23.A). However, the motif found could not be considered significant because error values (E-values) for the motifs were above 0.05. A motif comparison (Tomtom) with databases of binding sequences of bacterial transcription factors suggested similarities with the binding sequences of RsbR, CRP and PhoB transcription factors. Nonetheless, the E-values of the motif-motif comparisons were above 0.05. Experimental simulations for motif *de novo* findings and motif-motif comparisons consider a search significant with E-values equal or lower than 0.05 and 0.01, respectively (Bailey & Elkan, 1994, Gupta *et al.,* 2007).

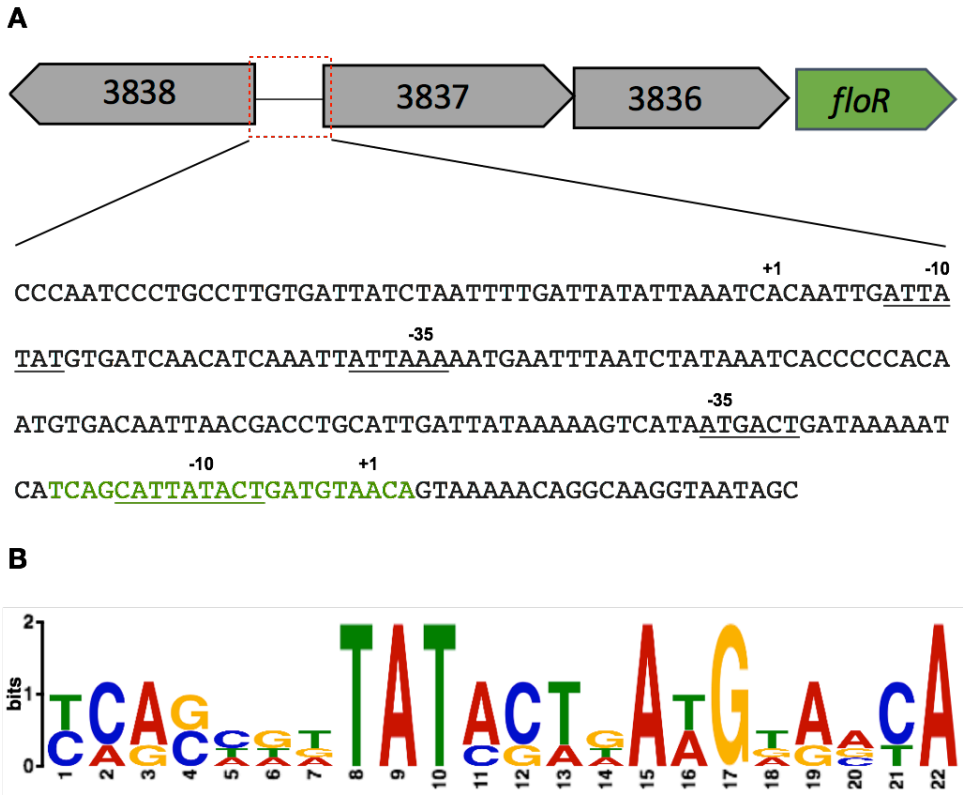

Figure 4.23. Analysis of *floR* operon upstream intergenic sequence. A. The intergenic region (red dotted box) contains two predicted transcription sites (+1), -10 and -35 boxes (underlined sequences), presumably, for divergent expression of upstream and downstream operons. A conserved binding motif among the promoter regions of the genes encoding proteins highly expressed in the TMT and LC-MS/MS experiment was detected (green nucleotides). **B.** Sequence logo illustrating the degree (bits) of conservation of each nucleotide in the predicted binding motif.

4.9 Discussion

4.9.1 Gas vesicle and pleiotropic gene regulation by FloR

The results in this chapter suggested that FloR acts through *rsmB*-RsmA and PigU-RpoS to regulate gas vesicle production (Figure 4.18 and 4.24, Table 4.3). RsmA-dependent regulation of gas vesicles, but also flagellar motility, has been reported previously in S39006 (Williamson *et al.,* 2008; Ramsay *et al.,* 2011; Wilf *et al.,* 2013). Experiments in *E. coli* showed that the *rsmB* homologue (*csrB*) forms a large monomeric complex which sequesters multiple CsrA (RsmA) proteins to inhibit its post-transcriptional regulatory functions (Liu *et al.,* 1997; Babitzke & Romeo. 2007). The transcription assays using *rsmB*::*uidA* reporter fusions suggest that *rsmB* is overexpressed in the *floR* mutant (Figure 4.18.B). Therefore, it is likely that loss

of gas vesicles and flagellar hyper-motility are caused by *rsmB*-mediated inhibition of the RsmA activity. Nonetheless, the post-translational modulation of RsmA by *rsmB* does not explain the reduced RsmA levels in the proteomic experiments (Table 4.3). Although it was reported that *rsmB* degradation increases in *P. carotovorum rsmA* mutants (Chaterjjee *et al.,* 2007), it is unknown whether *rsmB* overexpression stimulates RsmA degradation. Possibly, FloR regulates RsmA levels through alternative pathways to *rsmB* involving protein degradation.

The regulation of gas vesicle formation by the stationary phase sigma factor, RpoS, represents a new finding in S39006 (Section 4.6.1). A previous report showed that RpoS is a negative regulator of flagellar motility in S39006 (Wilf & Salmond, 2012). Therefore, it is likely that FloR acts through RpoS to regulate both flagellar motility and cell buoyancy (Figure 4.24.A). Interestingly, *rpoS* and *rsmA* mutants present similar gas vesicle, flagellar, carbapenem and prodigiosin phenotypes (Figure 4.24.A). The connection between RpoS and RsmA pathways has not been studied in S39006. Nonetheless, previous investigations in *E. coli* showed that RpoS facilitates the transcription of the *rsmA*-homologue, *csrA*, whilst CsrA induces RpoS proteolysis (Yakhnin *et al.,* 2011; Park *et al.,* 2017). Given that *rsmA* transcription was not altered in the *floR* mutant (Figure 4.16.A), the RpoS negative feedback regulation via CsrA observed in *E. coli* may not occur in S39006.

Other regulators, such as LrhA and PigU (HexA-like regulators), inhibit the expression of RpoS to control multiple phenotypes in *E. coli* and S39006 (Peterson *et al.,* 2006; Wilf *et al.,* 2012) (Figure 4.17.A). Proteomic analysis, qPCR and EMSA assays in previous investigations suggest that the RNA-chaperone Hfq induces *rpoS* expression indirectly through *pigU* inhibition and directly by binding to the *rpoS* mRNA ladder (Wilf *et al.,* 2013; Figure 4.17). Although the Hfq levels were similar to the WT strains in the *floR* mutant, PigU was found to be up-regulated (Table 4.3). FloR may inhibit *pigU* expression to promote *rpoS* transcription through Hfq-independent pathways. It is also possible that FloR controls Hfq-dependent regulation of RpoS by impacting the transcription of small RNAs, such as *dsrA* and *rprA*. Small RNAs help Hfq to stabilise and protect transcripts from degradation, and increase translation (McCullen *et al.,* 2010; Soper *et al.,* 2010).

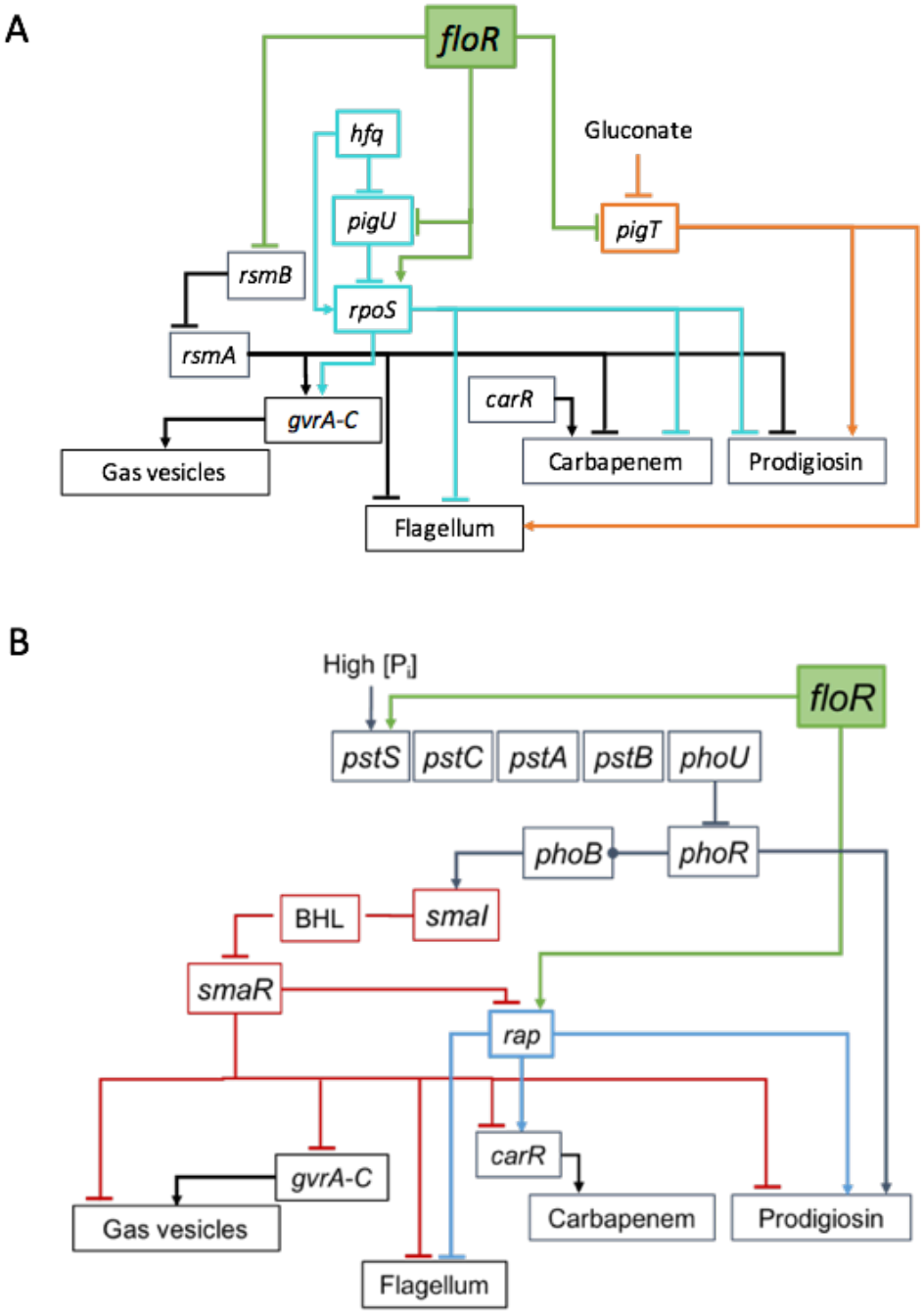

Figure 4.24. Model of *floR*-dependent regulation in the network. A. FloR regulation of *rsmA*/*rsmB*, *pigU*/*rpoS* and *pigT*-dependent pathways. **B.** FloR regulation of *pstS,* QS and *rap* dependent pathways. Lines ending in arrows indicate positive regulation, whilst perpendicular lines indicate negative regulation. See text for detailed information.

Ramsay and co-workers (2011) showed that gas vesicles were mostly produced at late-exponential and stationary phase via QS regulation. Given the loss of gas vesicles in *rpoS* mutants and its role in stationary phase gene regulation, it is possible that RpoS is also essential for gas vesicle formation at high-cell densities. Both QS and RpoS are positively

regulated by Hfq in S39006 (Wilf *et al.,* 2011; Wilf *et al.,* 2013) (See Chapter 1, section 1.7.3 and Figure 1.4). Moreover, other investigations in *Pseudomonas aeruginosa* and *Pseudomonas fluorescens* suggested that RpoS controls QS regulation by helping their LuxR-homologues to recognize multiple promoter regions (Schuster *et al.,* 2004; Liu *et al.,* 2018) Interestingly, proteomics and BHL detection assays in the *floR* mutant suggests that FloR inhibits BHL production through up-regulation of the phosphate binding protein PstS (Section 4.6.3, Table 4.3, Figures 4.21 and 4.24). Therefore, it is possible that FloR is connected through multiple regulators to tightly control (positively and negatively) gene expression in stationary phase.

In addition to proteomics, phenotypic assays suggested that FloR positive regulation of antibiotic production is caused mostly through Rap instead of RsmA-*rsmB*, PigU-RpoS, PigT and PstS-SmaI-dependent pathways (Sections 4.3, 4.6.1 and 4.6.2, and Figures 4.20 and 4.24). In contrast, FloR inhibition of flagellar motility may be the result of positive regulation on RsmA, RpoS and Rap, and negative on PigT, instead of PstS-SmaI (Figure 4.24). Overall, the results presented here suggests that FloR is major regulator modulating multiple networks in S39006 for cell buoyancy, motility and secondary metabolism.

4.9.2 Carbon metabolism and pleitropic regulation by FloR

The proteomic data suggested that FloR represses its own operon to control its own expression along with genes encoding an uncharacterized four-carbon kinase and a PdxA-like protein (Figure 4.22A and Table 4.4). PdxA (4-hydroxythreonine-4-phosphate dehydrogenase) is part of the pyridoxal-5-phosphate (Vitamin B6) pathway, which utilises D-erythose-4-phosphate as precursor (Laber *et al.,* 1999). D-erythose-4-phosphate is also an intermediate of the pentose phosphate pathway (PPP). Thus, it is possible that the FloR-regulated four-carbon kinase encoded by Ser39006_3837 and the PdxA-like protein encoded by Ser39006_3836 are involved in the utilisation of four carbon-metabolites to control biosynthetic pathways, such as PPP and Vitamin B6.

The synthesis of other proteins involved in central metabolism was also altered in the *floR* mutant (Section 4.7). The ribose operon regulator RbsR and the CsrD homologue, PigX, in

S39006 also regulate the expression of enzymes involved in carbon utilisation, such as ribose dehydrogenase, RbsD and glycerol kinase, GlpK (Lee *et al.,* 2017; Fineran *et al.,* 2007). Furthermore, the RsmA/*rsmB* homologues CsrA/*csrB* and the sigma factor RpoS are involved in glycolysis, glycogen biosynthesis, gluconeogenesis and acetate metabolism control in *E. coli* (Romeo *et al.,* 1993; Sabnis *et al.,* 1995; Romeo, 1998; Wei *et al.,* 2000, Potts *et al.,* 2017). This study and others on *rbsR, rsmA/rsmB* and *pigX* mutants indicate that S39006 is a potential model organism for understanding how bacteria connect carbon metabolism and cell buoyancy, motility and secondary metabolism regulation.

The connection between the catabolism of high energy carbohydrates, such as glucose, and pleiotropic regulation has been studied in different Gram-negative bacteria (Saier, 1998; Nanchen *et al.,* 2008; Stella *et al.,* 2008; Kalivoda *et al.,* 2010; Shimada *et al.,* 2011). In *Serratia marcescens*, glucose-depleted conditions induce the production of the secondary messenger cAMP to activate CRP-dependent gene expression of catabolic genes, and stimulate swimming motility (Botsford & Harman, 1992; Stella *et al.,* 2008). In contrast, glucose down-regulates flagellar motility by inhibiting the expression of the adenylate cyclase gene, *cyaA*, involved in cAMP synthesis (Stella *et al.,* 2008). Glucose inhibition of swimming motility may be important in bacteria to remain in environments with high quality carbon substrates, whilst cAMP-CRP-dependent activation of motility might help to migrate from environments limited in energy resources (Zhao *et al.,* 2007; Stella *et al.,* 2008). Interestingly, mutants defective in genes involved in carbon metabolism regulation, such as *rsmA*, *rpoS, rbsR* and *floR* showed contrasting flagella and gas vesicle phenotypes. Furthermore, although cell movement via gas vesicles is limited to a vertical plane, it has been proposed as a cost/effective ("cheap") mechanism for migration compared to flagellar motility (Walsby, 1994). Therefore, S39006 may repress motility and stimulate gas vesicle production by FloR in environments with low energy carbon sources to float and rise up without investing energy in flagellar rotation.

Contrary to motility regulation, both glucose and cAMP have negative impacts on prodigiosin production in *S. marcescens*. Moreover, glucose inhibits prodigiosin production in *crp* mutants. This suggests that glucose also controls pigment production through CyaA-cAMP-CRP independent pathways (Kalivoda *et al.,* 2010). Prodigiosin has been proposed as a

metabolic sink for “energy-spilling” when ATP concentrations are high (Haddix *et al.,* 2008). Given that cAMP is high during glucose-depletion, cAMP-dependent repression of prodigiosin production has been suggested as a strategy to avoid “energy-spilling” during starvation (Kalivoda *et al.,* 2010). Possibly, catabolic regulators, such as FloR, stimulate prodigiosin production in environments with alternative carbon substrates (i.e four-carbon sugars) to bypass the cAMP-CRP pathway.

4.9.3 FloR-dependent regulation of gas vesicles in a low aerated environment

Experiments investigating microaerophilic conditions suggested that FloR regulation is essential for cell buoyancy in low oxygen concentrations (Section 4.4). Probably, oxygen depletion in cultures of the *floR* mutant did not stimulate the activity of the *gvpA1* promoter because the intrinsic gas vesicle regulators GvrA, GvrB, GvrC were down-regulated. More importantly, FloR may facilitate migration, aided by gas vesicles, to environments with optimal oxygen concentrations and energy resources. Exposure to oxygen-rich environments in facultative bacteria, such as S39006, results in a higher energetic yield from catabolic pathways (Tran & Unden, 1998).

4.9.4 Intracellular proteomic profile of the *floR* mutant

TMT 10-plex and LC-MS/MS sequencing and quantitation of the Intracellular proteome identified 802 proteins differentially expressed (*P* value <0.05) in the *floR* mutant. The proteomic data confirmed the results on gas vesicle formation, antibiotic production and motility. Furthermore, the proteomic analysis permitted targeting the regulatory and catabolic pathways affected by the mutation in *floR*. Previous experiments in *pigX* and *hfq* mutants using 2D-DiGE (difference in gel) analysis and iTRAQ 4-plex with LC-MS/MS, respectively, also identified proteins involved in carbon utilization (Fineran *et al.,* 2007; Wilf *et al.,* 2013). Nonetheless, more proteins were identified in this research using TMT and LC-MS/MS; 530 proteins in the *floR* mutant with a cut-off of *P* value<0.01 compared to 33 and 486 in S39006 *pigX*::mini-Tn*5*Sm/Sp and S39006 Δ*hfq* mutants, respectively. The total protein match was also higher in the *floR* mutant proteome analysis; 2410 compared to 1369 in the *hfq* mutant. Interestingly, previous comparative studies with shotgun proteomics suggested

that iTRAQ 4-plex peptide-labelling resulted in a larger peptide-spectrum match, compared to TMT 6-plex and iTRAQ 8-plex (Pichler *et al.,* 2010). This suggest that the number of isobaric reporters that determines the number of channels (samples or replicates) for multiplexing is important; the higher the plex, the total number of proteins identified decreases. Nonetheless, the sampling time could explain the difference in proteins identified between the *floR* and S39006 Δ*hfq* mutants. Wilf and co-workers (2013) took samples for protein extraction after 10 h of growth, whilst samples in this project where taken at 16 h.

Bioinformatic analysis from the proteomic experiment presented in this project revealed that 45% of the proteins predicted from whole genome sequencing were not identified. Several factors could explain this result: (i) detection limitations from the TMT and LC-MS/MS analysis, (ii) the protein extraction analysed in the experiment corresponded only to intracellular proteins; the secreted proteome was excluded, and (iii) gene-silencing effects dependent on growth conditions. For instance, significant variations in the global proteome profile of *E. coli* occur when grown in complex media (i.e. LB), with an excess of glucose, under stress conditions or in different growth phases (Schimdt *et al.,* 2016)

It is also possible that some proteins were not detected due to ineffective peptide quantitation. Although the LC-MS/MS analysis revealed that the peptide tagging efficiency was high, 15% of the peptides could not be identified in all the replicates of the experiment; this may be the case with gas vesicle proteins GvpV and GvrC (Figures 4.14). Also, it is likely that peptides from proteins such as GvpA2, GvpA3 and GvpF3 were missing because the peptide match was assigned to homologous proteins GvpA1, GvpF1 and GvpF2.

Some proteins from the carbapenem and prodigiosin operons could not be detected in the TMT and LC-MS/MS experiment. For instance, CarD, CarE, CarH and PigO, which are proteins that are not essential for antibiotic production. In contrast, all the essential proteins detected were down-regulated in the *floR* mutant. This confirmed the observations on carbapenem and prodigiosin production (Figures 4.5 and 4.6). The proteins involved in intrinsic resistance to carbapenem (CarF and CarG) were also negatively affected in the *floR* mutant (Table 4.1). The protein quantitation revealed that the carbapenem biosynthetic proteins are 2.5 to 4.5 (log) fold down-regulated, whilst CarF and CarG 0.3 and 1.3 (log) fold. The resistance to

exogenous carbapenem in the *floR* mutant (Figure 4.15) suggests, that, despite the reduction of CarF and CarG levels, the proteins are still functional. Perhaps, the down-regulation of Rap in the *floR* mutant does not affect the biosynthetic and resistance proteins similarily. Moreover, *carF* and *carG* expression is under control of an internal promoter within *carD*, in addition to the *carA* promoter (Coulthurst *et al.,* 2005). Thus, it is possible that in the *floR* mutant *carF* and *carG* expression is still active due to other transcriptional regulators acting through the internal promoter in *carD*.

Chapter 5
TrkH regulates potassium-dependent control of gas vesicles, prodigiosin production, and turgor pressure in *Serratia*

The gas vesicle mutant AQY107 had a transposon in the low affinity potassium transporter gene, *trkH*, (Chapter 3). This mutant was classified as a gas vesicle hyper-producer because colonies and patches appeared more opaque than the parental strain (NWA19) (Chapter 3, Section 3.2.1 and Figure 3.1.B). Also, PCM images showed that all AQY107 cells contained phase-bright structures and cells in static liquid cultures remained buoyant over time, whilst some NWA19 cells did not produce gas vesicles and would sink to the bottom of the liquid culture (Figure 3.1.C and D). Phenotypic assays suggested that the mutation in *trkH* also affected flagellar motility and carbapenem antibiotic production (Figures 3.9 and 3.10). This chapter presents further details on the role of *trkH* in cell buoyancy, motility and secondary metabolism.

5.1 Expression of *trkH* down-regulates gene expression for gas vesicle formation

To confirm that *trkH* regulates gas vesicle production, phage transduction was used to transfer the *trkH* mutation into WT cells and reporter fusion strains for the *gvpA1-gvpY* and *gvrA-gvrC* operons. Thereafter, the cell morphology of the WT and the *trkH* mutant was assessed in TEM. The *trkH* mutants contained densely packed gas vesicles, compared to WT cells (Figure 5.1). This supported previous observations in the AQY107 mutant for gas vesicle formation under PCM.

To assess the impact of *trkH* on the expression of the gas vesicle operons, *gvpA1-gvpY* and *gvrA-gvrC*, the reporter activity in *gvpA1*::*uidA* and *gvrA*::*uidA* reporter fusion strains carrying the *trkH* mutation was assessed. The UidA activity in the *gvpA1*::*uidA*, *trkH* strain was higher at late-exponential and stationary phase compared to the control strain (*gvpA1*::*uidA*) (Figure 5.2). In contrast, the *trkH* mutation did not alter the expression of *gvrA* (Figure 5.3). These results indicated that the potassium transporter was important for control of gas vesicle

formation in S39006 through down-regulation of *gvpA1-gvpY* operon expression, but not the *gvrA-gvrC* operon.

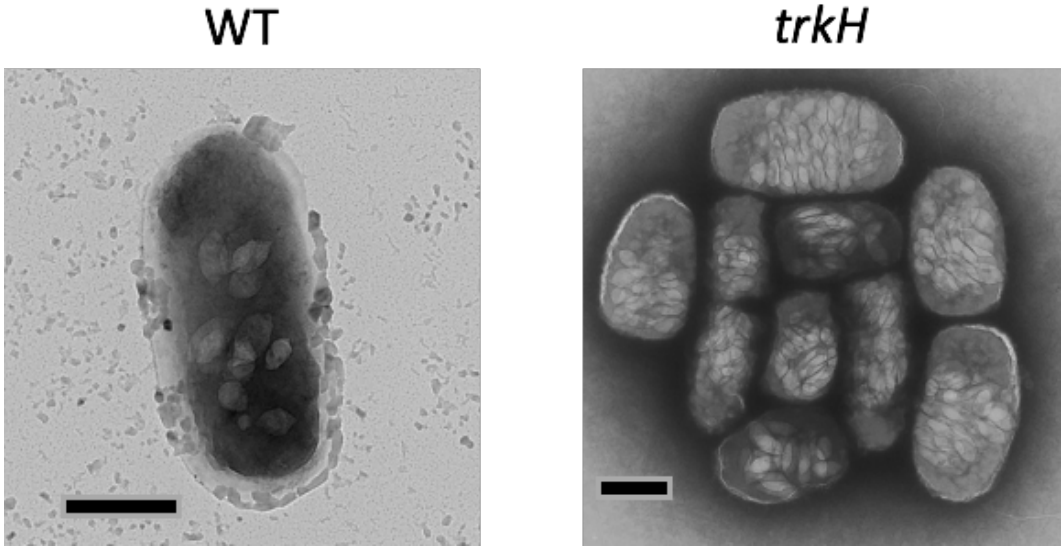

Figure 5.1. Gas vesicle formation in the *trkH* mutant. TEM images of a WT single cell (left) and a group of *trkH* mutants (right). Scale bars correspond to 500 nm.

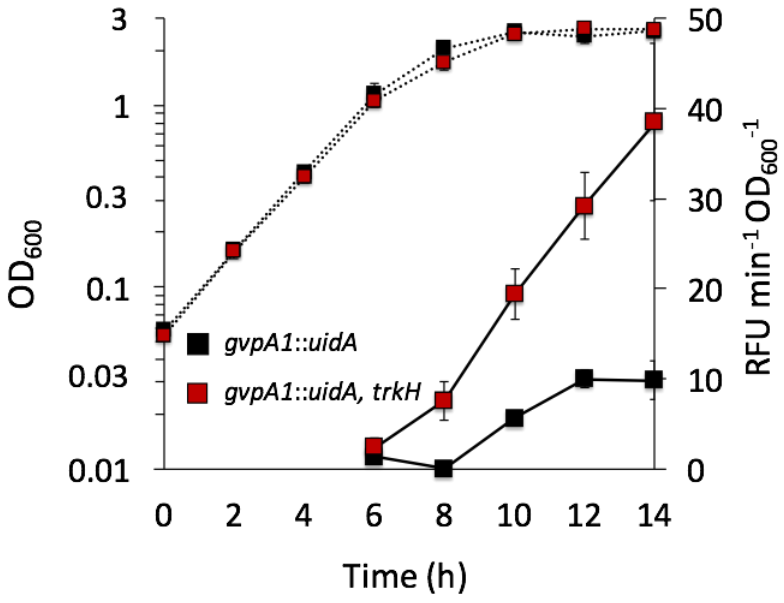

Figure 5.2. *gvpA1* expression in the *trkH* mutant. Cell density (OD_{600}, dotted lines) and gene expression (RFU min^{-1} OD_{600}^{-1}, continuous lines) were measured throughout growth in LB. The data represent the average and standard deviation (error bars) of three biological replicates. **ANOVA two-factor analysis of the *β*-glucuronidase reporter activity** from 6 to 14 h of growth in *gvpA1*::*uidA* and *gvpA1*::*uidA*, *trkH* found $F = 86.86 > F_{crit} = 4.35$; *p*-value $1.02*10^{-8}$.

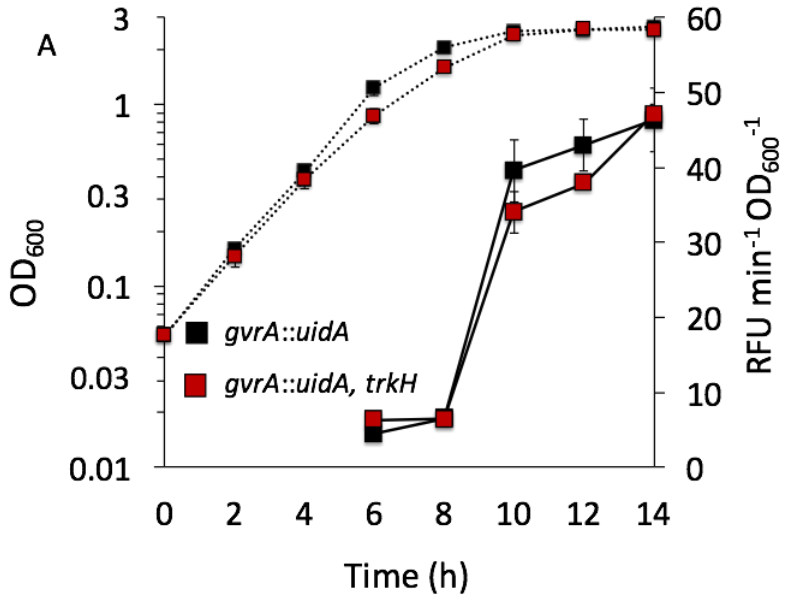

Figure 5.3. *gvrA* expression in the *trkH* mutant. Cell density (OD_{600}, dotted lines) and gene expression (RFU min^{-1} OD_{600}^{-1}, continuous lines) were measured throughout growth in LB. The data represent the average and standard deviation (error bars) of three biological replicates. **ANOVA two-factor analysis of the *β*-glucuronidase reporter activity** from 6 to 14 h of growth in *gvrA*::*uidA* and *gvrA*::*uidA*, *trkH* found $F = 3.17 > F_{crit} = 4.35$; *p*-value 0.09.

Mutations in some genes in the *gvrA-gvrC* operon result in loss of gas vesicle production (Tashiro *et al.,* 2016), whilst the *trkH* mutation leads to hyper-production of gas vesicles through up-regulation of the *gvpA1-gvpY* operon. Thus, whether the *trkH* mutation could bypass the mutation in essential genes for gas vesicle formation in *gvrA-gvrC* operon was assessed. Figure 5.4 shows the patch and cell morphology for double *gvrA*,*trkH*; *gvpF2*, *trkH*; *gvpF3,trkH*; *gvrB*, *trkH;* and *gvrC*, *trkH* mutants. This showed that the mutation in *trkH* did not bypass the phenotype caused by the loss of genes from the *gvrA-gvrC* operon. Moreover, although *trkH* did not affect promoter activity of the *gvrA-gvrC* operon, the hyper-production of gas vesicles in the *trkH* background required the expression of the structural and regulatory genes in this operon.

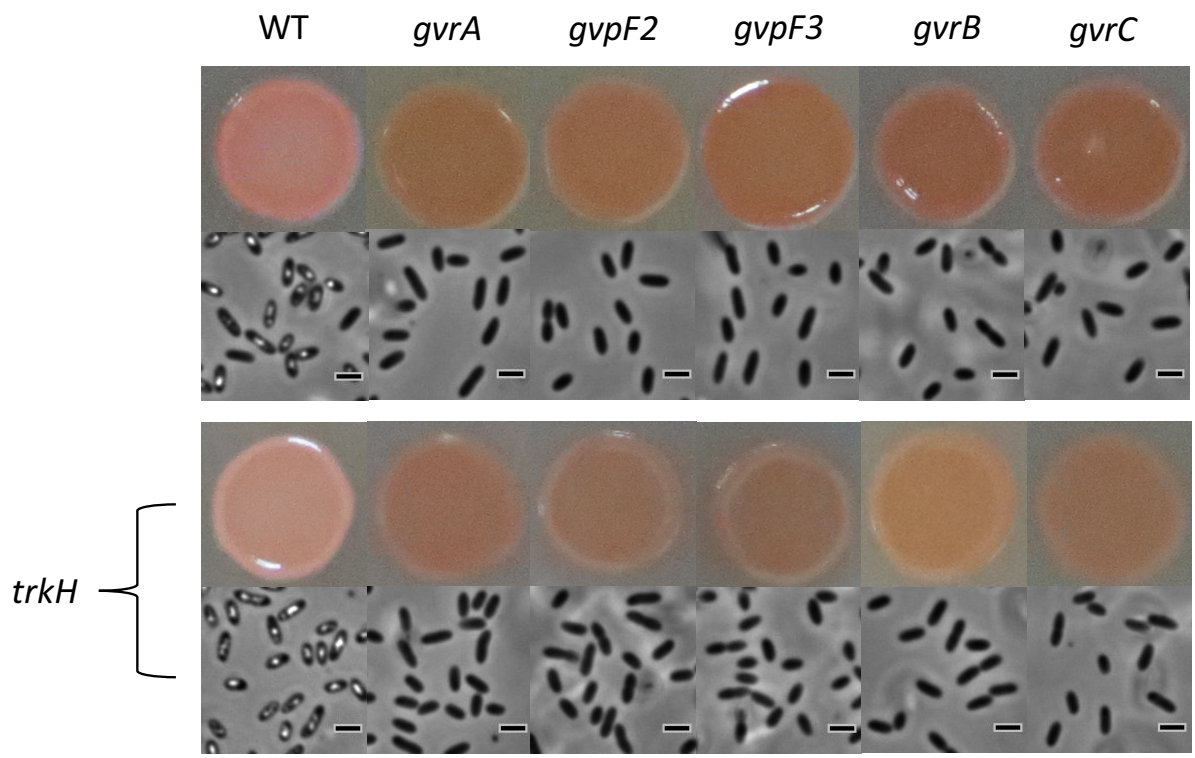

Figure 5.4. Gas vesicle production in *trkH*, (*gvrA*; *gvpF2*; *gvpF3*; *gvrB* and *gvrC*) double mutants. Patch and cell morphology in PCM of double mutants for *trkH* and genes essential for gas vesicle formation from the *gvrA-gvrC* operon. Images are representative of three biological replicates. Scale bars correspond to 1 μm

To confirm the impact of *trkH* on gas vesicle production, the mutant gene was complemented in trans. Ectopic expression under control of an arabinose-inducible promoter in the *trkH* mutant resulted in significantly reduced *gvpA1* transcription compared with the mutant carrying an empty vector (Figure 5.5.A). Furthermore, the transcription of *gvpA1* in the complemented mutant was similar to that in the control strain (*gvpA*1::*uidA*). The production of GvpC, a protein encoded from the *gvpA1-gvpAY* operon and important for gas vesicle structure strengthening, was also assessed in a Western Blot. As expected, the *trkH* mutant carrying an empty vector showed hyper-production of GvpC, whilst this was reduced in the complemented mutant (Figure 5.5.B). These results were corroborated by analyzing the formation of phase-bright structures. Cells complemented for *trkH* lost gas vesicle production (Figure 5.6). Taking all these results together, it can be concluded that *trkH* is a negative regulator of gas vesicle production and expression of genes in the *gvpA1-gvpY* operon.

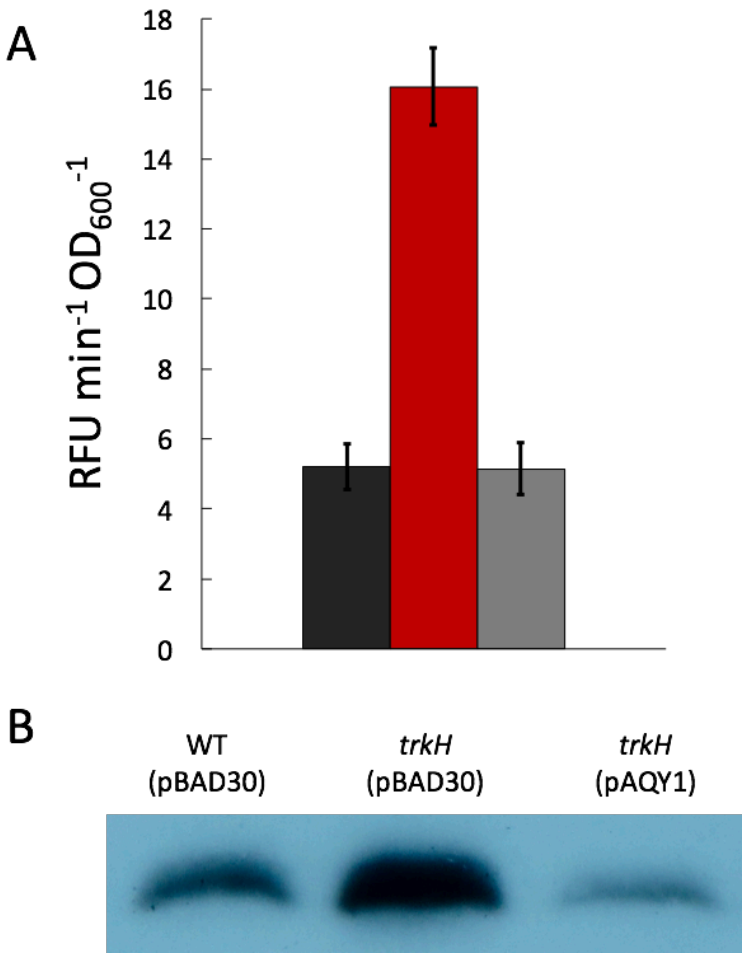

Figure 5.5. Impact of *trkH* on gene expression. A. Complementation of *gvpA1* expression in the *trkH* mutant. The expression in the reporter strains *gvpA1*::*uidA* and *gvpA1*::*uidA*, *trkH* containing the empty vector (pBAD30) are represented in black and red bars, respectively. The *trkH* mutant was tested for complementation with pAQY1 in the *gvpA1*::*uidA*, *trkH* strains (grey bar). The data represent the average and standard deviation (error bars) of three biological replicates. **B.** Immunodetection of GvpC (See Chapter 2, section 2.19). The image is representative of three biological replicates.

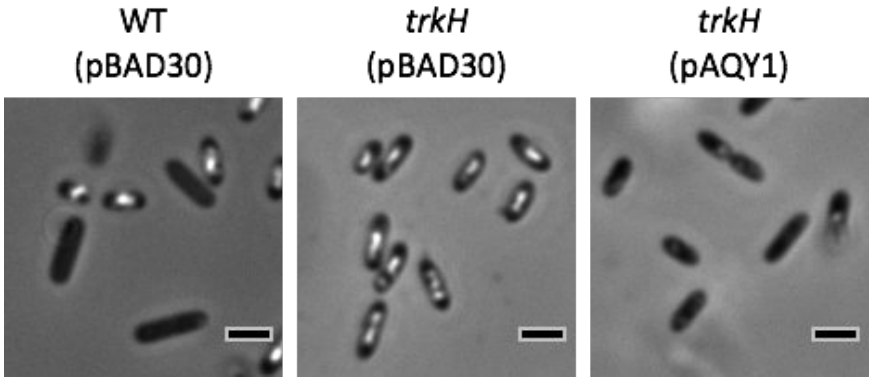

Figure 5.6. Complementation of the *trkH* mutant gas vesicle production. Scale bars correspond to 1 μm. Images are representative of three biological replicates.

5.2 Environmental potassium controls gas vesicle gene expression and morphogenesis through TrkH

TrkH is a low-affinity potassium uptake protein active at relatively high concentrations compared to other systems in *E. coli* (Rhoads *et al.,* 1976; Schlösser *et al.,* 1995). Hence, gene expression, flotation and gas vesicle formation was measured in the WT and *trkH* mutant strains grown in minimal media with different potassium concentrations (0.25, 2.5 and 25 mM KCl). Mid-to-high concentrations of KCl (2.5 and 25 mM) had similar negative impacts on the β-glucuronidase reporter activity throughout growth in the *gvpA1*::*uidA* strain, whilst in lower (0.25 mM) KCl concentrations the reporter activity was significantly higher at stationary phase (Figure 5.7.A). This suggested that high extracellular potassium is an environmental cue for negative regulation of the *gvpA1-gvpY* operon.

To assess the role of *trkH* on potassium-dependent regulation of gene expression, the *gvpA1* transcription activity was measured in the *trkH* background under different extracellular potassium concentrations. The reporter activity in *gvpA1*::*uidA* and *gvpA1*::*uidA, trkH* strains remained the same throughout growth in 0.25 mM KCl (Fig. 5.6..B). In contrast, the β-glucuronidase activity increased significantly in the *trkH* mutant in 2.5 and 25 mM KCl from mid-exponential phase (Figure 5.7.C and D). The effect of potassium and the *trkH* mutation on gas vesicle gene expression was confirmed by measuring the UidA activity in minimal media supplemented with potassium phosphate buffer as an alternative K^+ source to KCl (Fig. 5.8). Similar to *gvpA1* expression assays in minimal media with KCl, the reporter activity did not vary in mutant cells grown in a low potassium concentration, whilst the transcription of *gvpA1* increased in *trkH* mutants grown in relatively high potassium concentrations. These results suggested that the mutation in *trkH* mimics the effect of depleted potassium conditions in S39006. Furthermore, they indicate that *trkH* facilitates potassium-dependent down-regulation of gas vesicle formation in mid-to-high potassium concentrations.

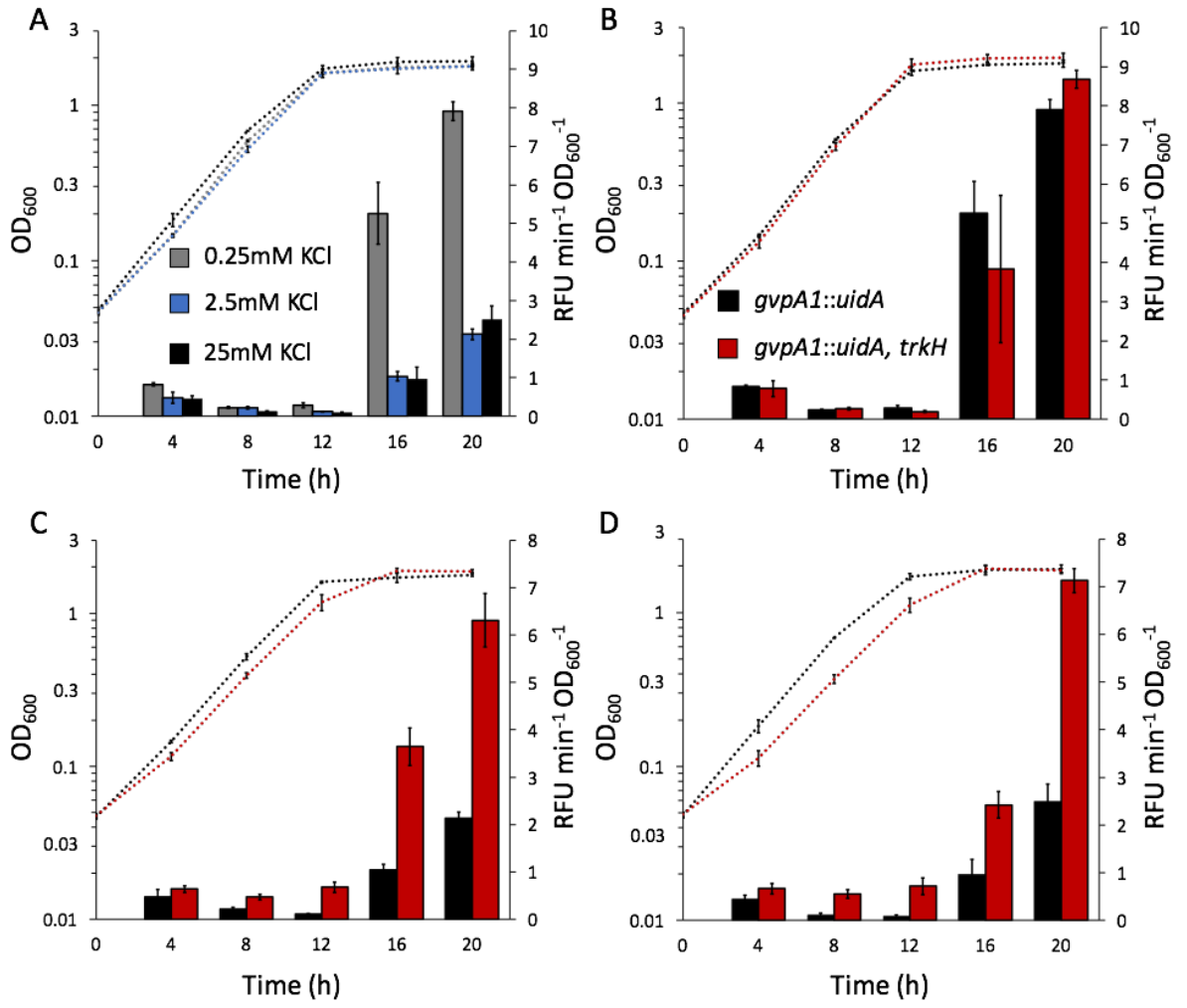

Figure 5.7. Effect of potassium on *gvpA1* expression throughout growth. Growth (dotted lines) was measured as OD_{600} and gene reporter activity (bars) as RFU min^{-1} OD_{600}^{-1}. **A.** Growth and reporter activity in the *gvpA1*::*uidA* strain grown in minimal media supplemented with 0.25 mM, 2.5 mM and 25 mM KCl. ANOVA analysis of the β-glucuronidase reporter activity from 2 to 20 h in cells grown in 0.25 and 2.5 mM KCl found $F = 73.30 > F_{crit} = 4.08$; *p*-value $1.39*10^{-10}$; in 0.25 and 25 mM KCl $F = 69.38 > F_{crit} = 4.08$; *p*-value $2.84*10^{-10}$; and in 2.5 and 25 mM KCl $F = 0.59 < F_{crit} = 4.08$; *p*-value 0.45. **B-D.** Growth and reporter activity in *gvpA1*::*uidA* (black) and *gvpA1*::*uidA trkH* (red) strains in minimal media supplemented with (**B**) 0.25 mM, (**C**) 2.5 mM and (**D**) 25 mM KCl. ANOVA analysis of the β-glucuronidase reporter activity from 2 to 20 h of growth with (**B**) 0.25 mM: $F = 0.12 < F_{crit} = 4.08$; *p*-value 0.73, (**C**) 2.5 mM: $F = 518.89 > F_{crit} = 4.08$; *p*-value $1.61*10^{-24}$ and (**D**) 25 mM KCl: $F = 521.89 > F_{crit} = 4.08$; *p*-value $1.45*10^{-24}$. The data represent the average and standard deviation (error bars) of three biological replicates

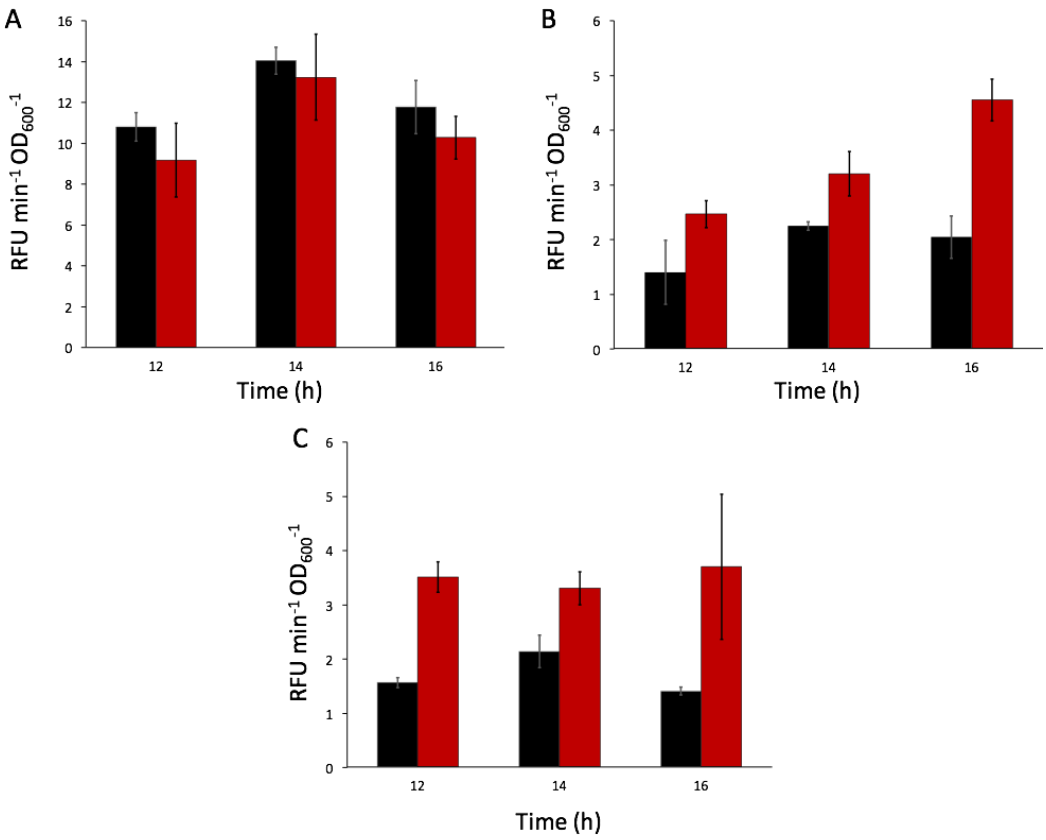

Figure 5.8. *gvpA1* expression in minimal media with an alternate potassium source to KCl. Cells were grown in minimal media at final concentrations of (**A**), 0.14 mM, (**B**) 1.4 mM and (**C**) 14 mM K^+ using minimal medium with potassium phosphate salts instead of KCl as a source of K^+. ANOVA analysis of the β-glucuronidase reporter activity from 12 to 16 h of growth with (**A**) 0.14 mM found $F = 4.08 < F_{crit} = 4.74$; p-value 0.066; (**B**) in 1.4 mM $F = 70.87 > F_{crit} = 4.74$; p-value $2.22*10^{-6}$, and (**C**) in 14 mM KCl: $F = 42.57 > F_{crit} = 4.74$; p-value $2.83*10^{-5}$. The data represent the average and standard deviation (error bars) of three biological replicates.

PCM analysis in cells grown in minimal media with different potassium concentrations corroborated the observations on the effect of extracellular potassium and *trkH* in *gvpA1* expression. Figure 5.9 shows that gas vesicle formation was absent throughout growth in WT cells at 2.5 mM KCl. In contrast, *trkH* mutants grown under the same conditions formed gas vesicles at exponential phase (10 h). In low KCl concentrations these structures were detected at stationary phase in both WT and mutant cells. Flotation assays using minimal media and cell morphology analysis in PCM, supported previous results (Figure 5.10). WT and *trkH* mutant cells remained buoyant and produced phase-bright structures in a low potassium concentration. As expected, the *trkH* mutant grown in relatively high potassium concentrations mimicked the phenotypes observed in potassium-depleted conditions, whilst the WT cells did not produce gas vesicles, or float.

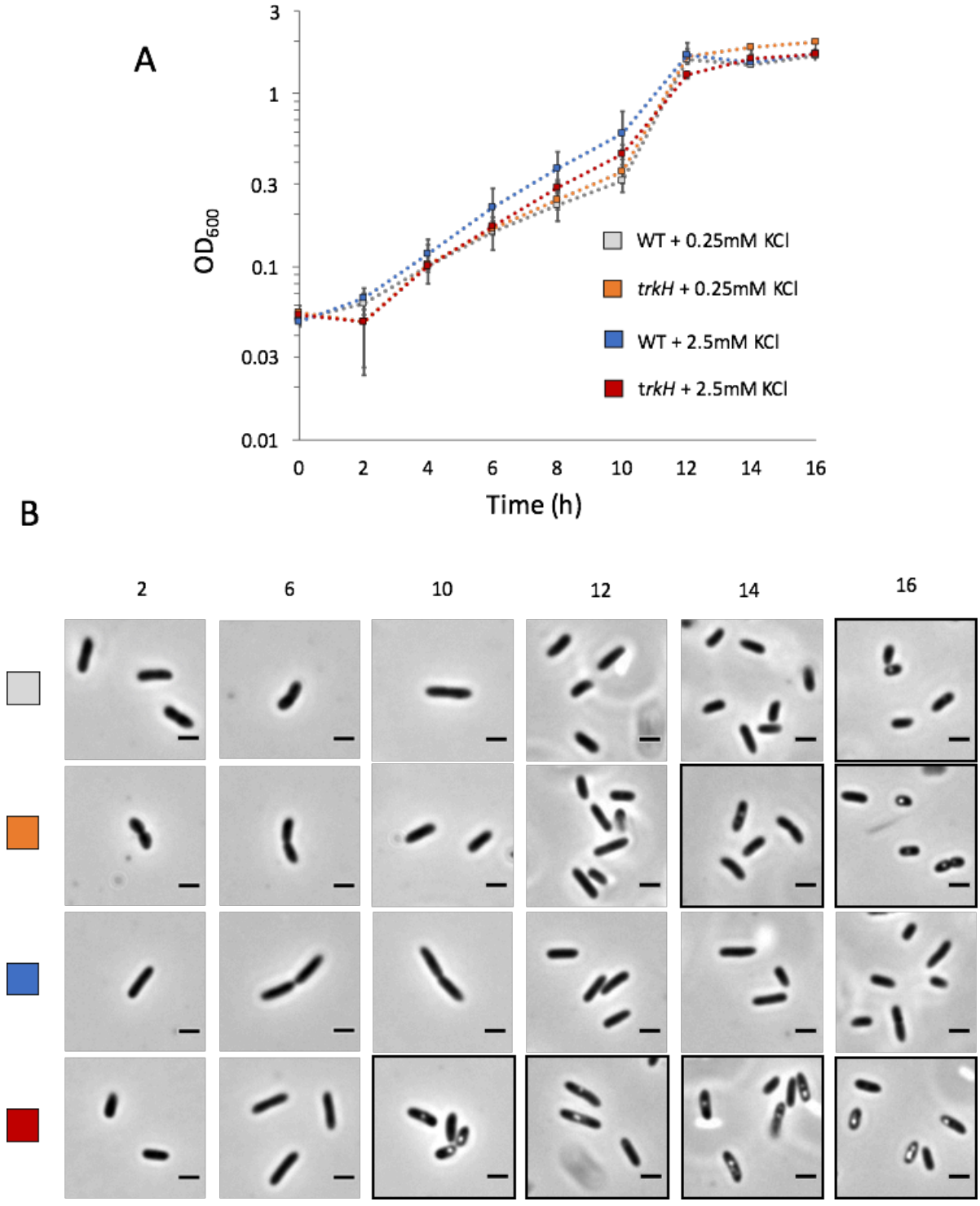

Figure 5.9. Effect of potassium on gas vesicle formation in WT and *trkH* strains. (**A**) Growth and (**B**) gas vesicle formation throughout time in WT and *trkH* mutant cells grown in the presence of 0.25 mM and 2.5 mM KCl. Images of cells with phase-bright structures are framed with black lines. PCM images were taken immediately after OD_{600} measurements. The data in growth assays represent the average and standard deviation (error bars) of three biological replicates.

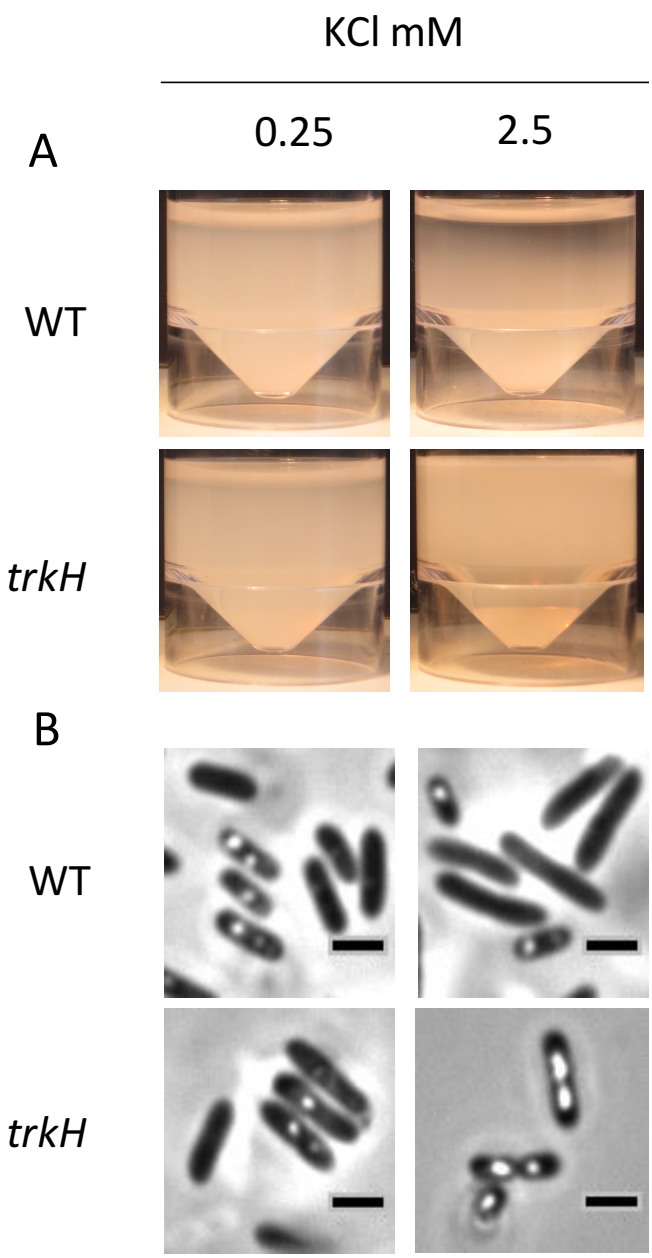

Figure 5.10. Effect of potassium on flotation and gas vesicle formation. WT and *trkH* mutant cells grown in minimal media with 0.25 mM or 2.5 mM KCl. **A.** Flotation assay. **B**. PCM of cells grown in solid medium. Scale bars correspond to 1 μm. Images are representative of three biological replicates.

5.3 The *trkH* mutation bypasses microaerophilic regulation of gas vesicles

Similar to the impact of the *trkH* mutation, microaerophilic conditions up-regulate the transcription of the *gvpA1-gvpY* operon, but not *gvrA-gvrC,* in S39006 (Ramsay *et al.,* 2011). Therefore, it was considered possible that oxygen and potassium availability affect the same regulatory pathway for gas vesicle regulation. If so, it would not be expected that the *trkH*

mutation would bypass the *gvpA1* expression affects in microaerophilic conditions. Figure 5.11 shows that the β-glucuronidase activity in cultures under microaerophilic conditions was higher in the *trkH* mutant than in WT cells. This result suggested that potassium repression of gas vesicles via TrkH is active in microaerophilic conditions and independent of the regulatory pathways controlling the oxygen response for cell buoyancy.

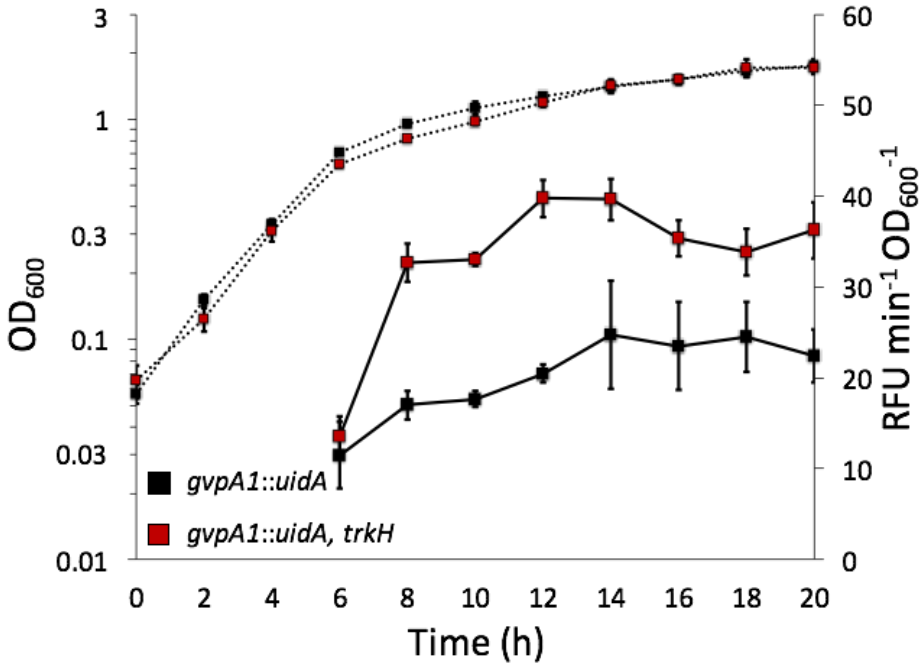

Figure 5.11. *gvpA1* expression in the *trkH* mutant under microaerophilic conditions. Growth (dotted lines) was measured as OD_{600} and reporter activity (continuous lines) as RFU min^{-1} OD_{600}^{-1}. Black boxes correspond to the *gvpA1*::*uidA* strain whereas red boxes to the reporter fusion strain carrying the mutation in *trkH*. ANOVA analysis of the β-glucuronidase reporter activity from 6 to 20 h of growth found $F = 86.86 > F_{crit} = 4.35$; *p*-value $1.02*10^{-8}$. The data represent the average and standard deviation (error bars) of three biological replicates.

5.4 The mutation in *trkH* is pleiotropic

Previous experiments in the prodigiosin negative *trkH* mutant AQY107 suggested that the mutation in *trkH* is pleiotropic (Chapter 3, section 3.5). Therefore, swimming motility, prodigiosin and carbapenem production was assessed in the mutant strain obtained after transduction of the *trkH* mutation into a WT strain. The *trkH* mutant showed reduced flagellar motility when compared to WT, while ectopic expression of *trkH* restored swimming motility

(Figure 5.12.A). This result suggested that TrkH is an important element enabling potassium-dependent positive regulation of motility in S39006.

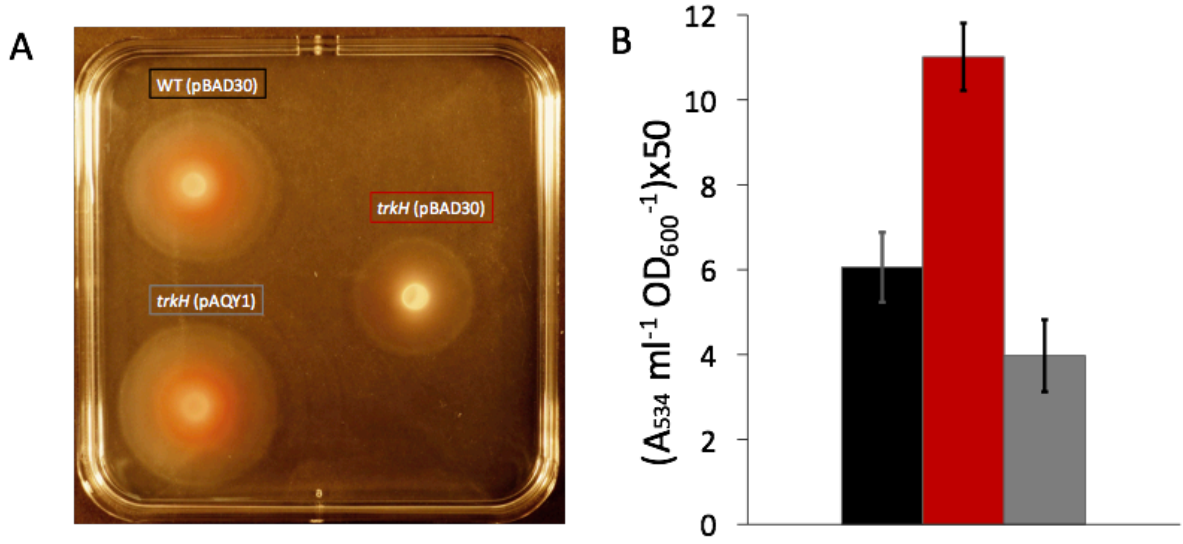

Figure 5.12 Motility and pigment production in the *trkH* mutant. Complementation of (**A**) swimming motility and (**B**) prodigiosin production (A534 ml^{-1} OD_{600}^{-1}) in the *trkH* mutant. The WT (black) and *trkH* (red) mutant carrying an empty vector were used as controls. *trkH* mutants were complemented with pAQY1 in *trkH* cells (grey). (**A**) The image is representative of three biological replicates. (**B**) The data represent the average and standard deviation (error bars) of three biological replicates.

The extraction of prodigiosin from WT and mutant samples in stationary growth phase showed that pigment production was up-regulated in the *trkH* background (Figure 5.12.B). More importantly, complementation experiments in the mutant demonstrated that the expression of *trkH* restored prodigiosin production. The effect of extracellular potassium on prodigiosin production was also assessed. Pigment production in a low potassium concentration was similar in the WT and mutant strains. In contrast, it was reduced at higher potassium concentrations in WT samples and up-regulated in the *trkH* mutant (Fig. 5.13.A). Furthermore, the reporter activity in a strain with a gene fusion in the prodigiosin biosynthetic operon (*pigA*::*lacZ*) indicated that high extracellular potassium concentrations down-regulate gene expression (Fig. 5.13.A). These results suggest that potassium uptake through TrkH inhibits the *pigA* promoter activity in the control of prodigiosin biosynthesis.

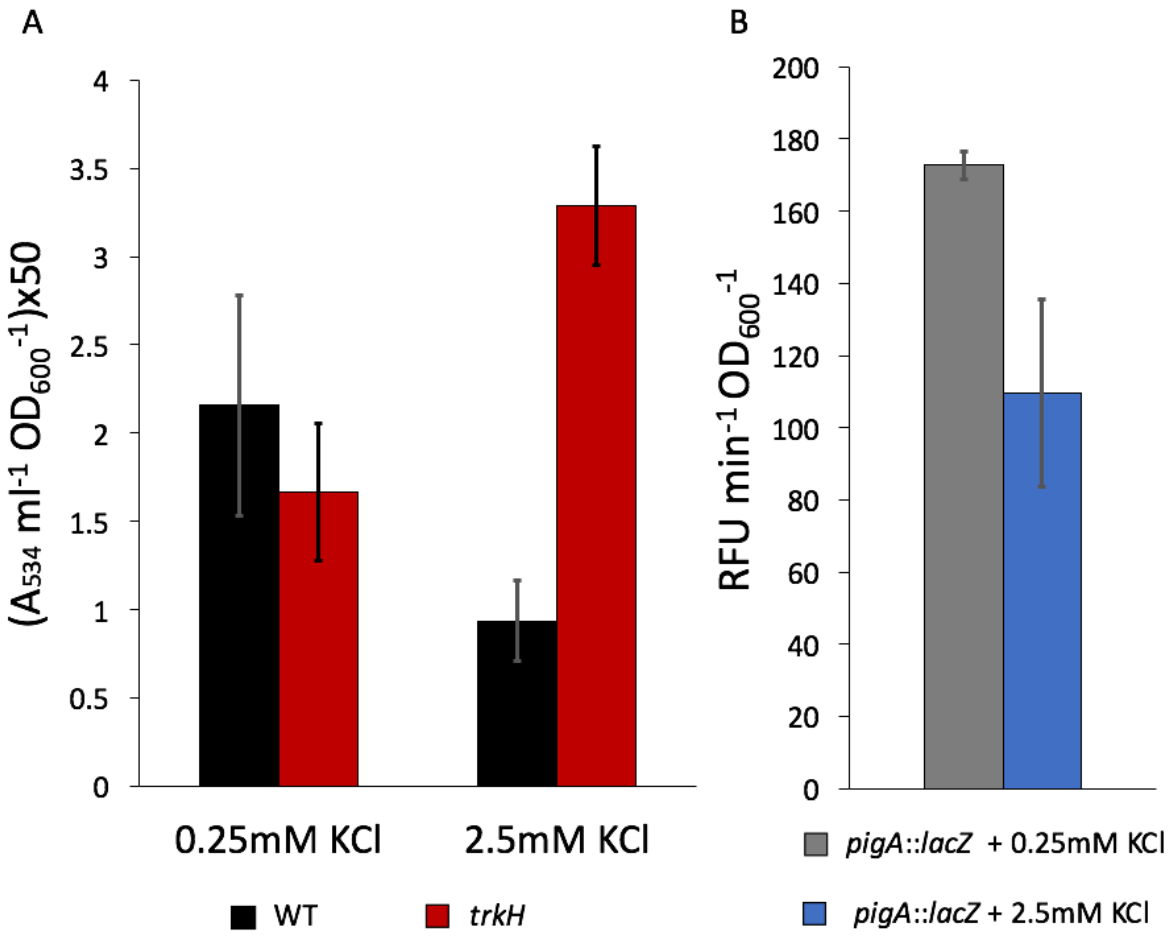

Figure 5.13. Potassium-dependent regulation of prodigiosin production and *pigA* expression. A. Pigment production of WT and *trkH* cells cultured at different potassium concentrations. **B**. Activity of *pigA*::*lacZ* reporter fusion was measured in cells grown in different potassium concentrations. The data in A and B represent the average and standard deviation (error bars) of three biological replicates.

Carbapenem antibiotic production was measured previously in cell patches of the prodigiosin defective and *trkH* mutant strain, AQY107 (Chapter 3, Figure 3.9). Although antibiotic activity was not abolished, it appeared to be reduced compared to the parental strain (NWA19). In contrast, a semiquantitative assay for carbapenem production using culture supernatants did not show significant changes between the WT and *trkH* mutant (Figure 5.14.A-B). Neither antibiotic production in supernatants nor the transcription activity from the promoter of the carbapenem biosynthetic operon were affected significantly in cultures grown in minimal medium with different potassium concentration (Figure 5.15.C and D). These experiments confirmed that the mutation in *trkH* did not affect carbapenem production.

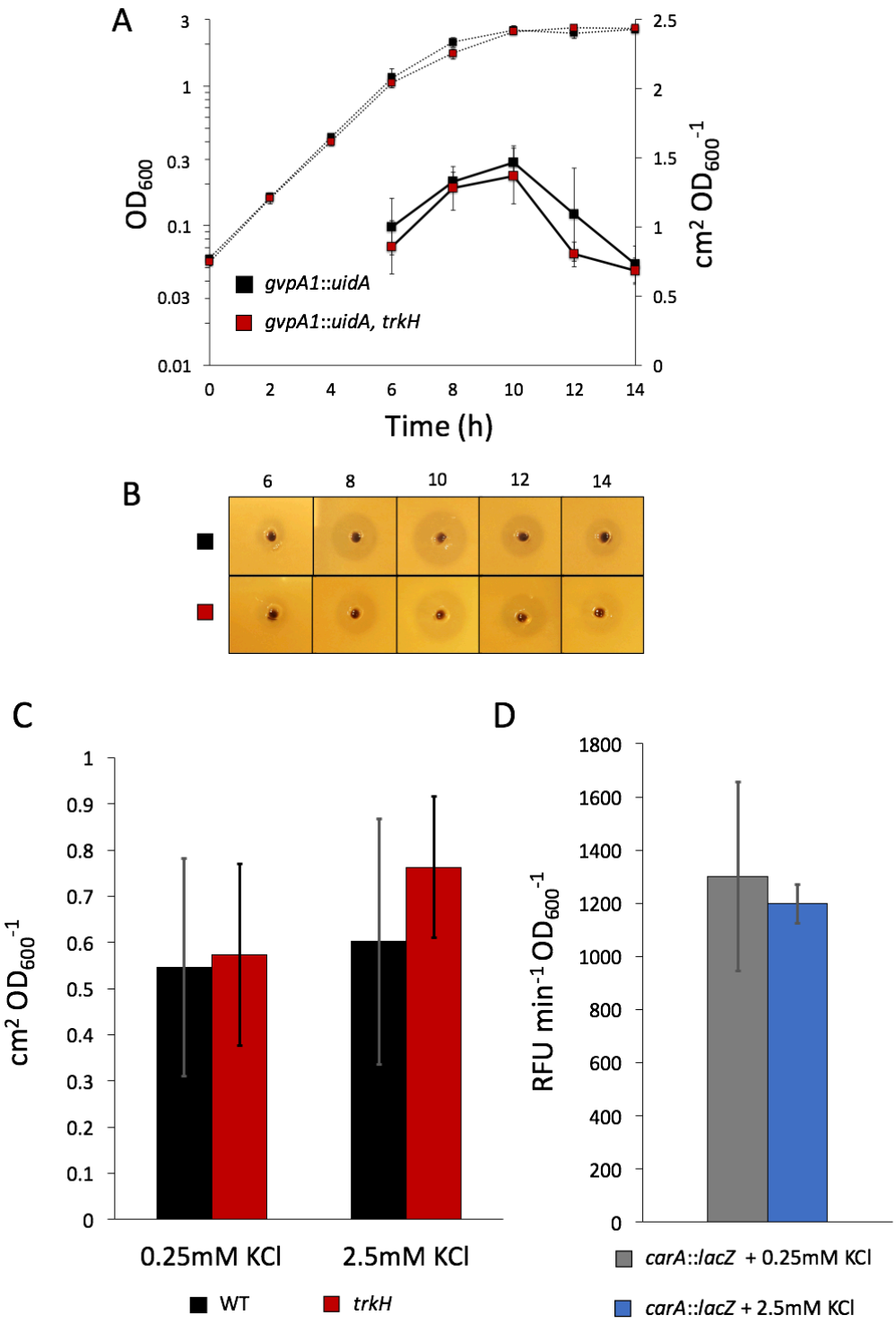

Figure 5.14. Potassium effect on carbapenem production and *carA* expression. A. Carbapenem production in mid exponential and stationary phase (6 to 14 h) of *gvpA1*::*uidA* and *gvpA1*::*uidA*, *trkH* strains grown in LB. **B.** Halos of inhibition of *E. coli* ESS from *gvpA1*::*uidA* (black) and *gvpA1*::*uidA*, *trkH* (red) supernatants taken from 6 to 14 h. Images are representative of three biological replicates. **C.** Carbapenem production from WT and *trkH* mutant cultures grown at different potassium concentrations. **D.** Activity of *carA*::*lacZ* reporter in cells grown at different potassium concentrations. The data in A, C and D represent the average and standard deviation (error bars) of three biological replicates.

5.5. TrkH does not control gas vesicle production through known pathways

To identify other components involved in the potassium-dependent response, the transcription of different gas vesicle, motility and prodigiosin regulator genes was measured. First, the reporter activity was assessed in *smaI, smaR, pigP*, *pigQ*, *pigR*, *pigS*, *pigX* and *ygfX* fusion strains grown in minimal media with different KCl concentrations (Figure 5.15.). Then in *rsmA* and *rsmB* fusion strains carrying the *trkH* mutation grown in LB (Figure 5.16). Also, the production of the QS autoinducer (BHL) in both complex and minimal media was measured (Figure 5.17). QS molecule production and all transcriptional reporter fusions evaluated appeared unaffected.

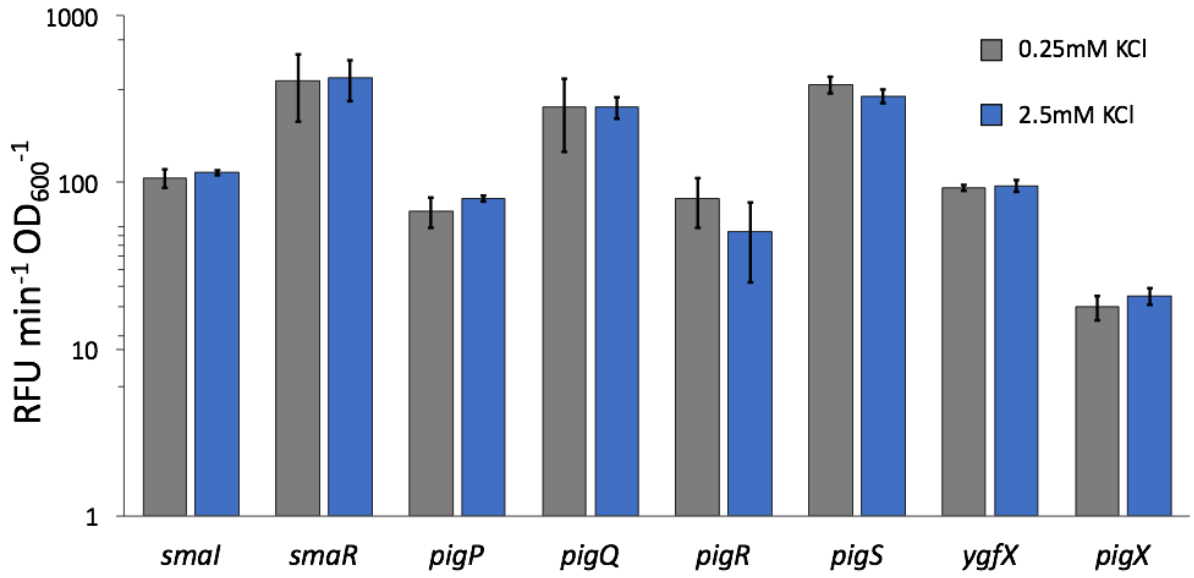

Figure 5.15. Expression of prodigiosin regulators under different concentrations of potassium. Gene reporter activity was measured in cultures of LIS (*smaI*::*lacZ*), HSPIG67 (*pigP*::*lacZ*), HSPIG17 (*pigQ*::*lacZ*), HSPIG23 (*pigR*::*lacZ*), HSPIG26 (*pigS*::*lacZ*), HSPIG46 (*ygfX*::*lacZ*), and ROP4 (*pigX*::*lacZ*) grown in minimal media supplemented with 0.25 mM and 2.5 mM KCl. The data represent the average and standard deviation (error bars) of three biological replicates.

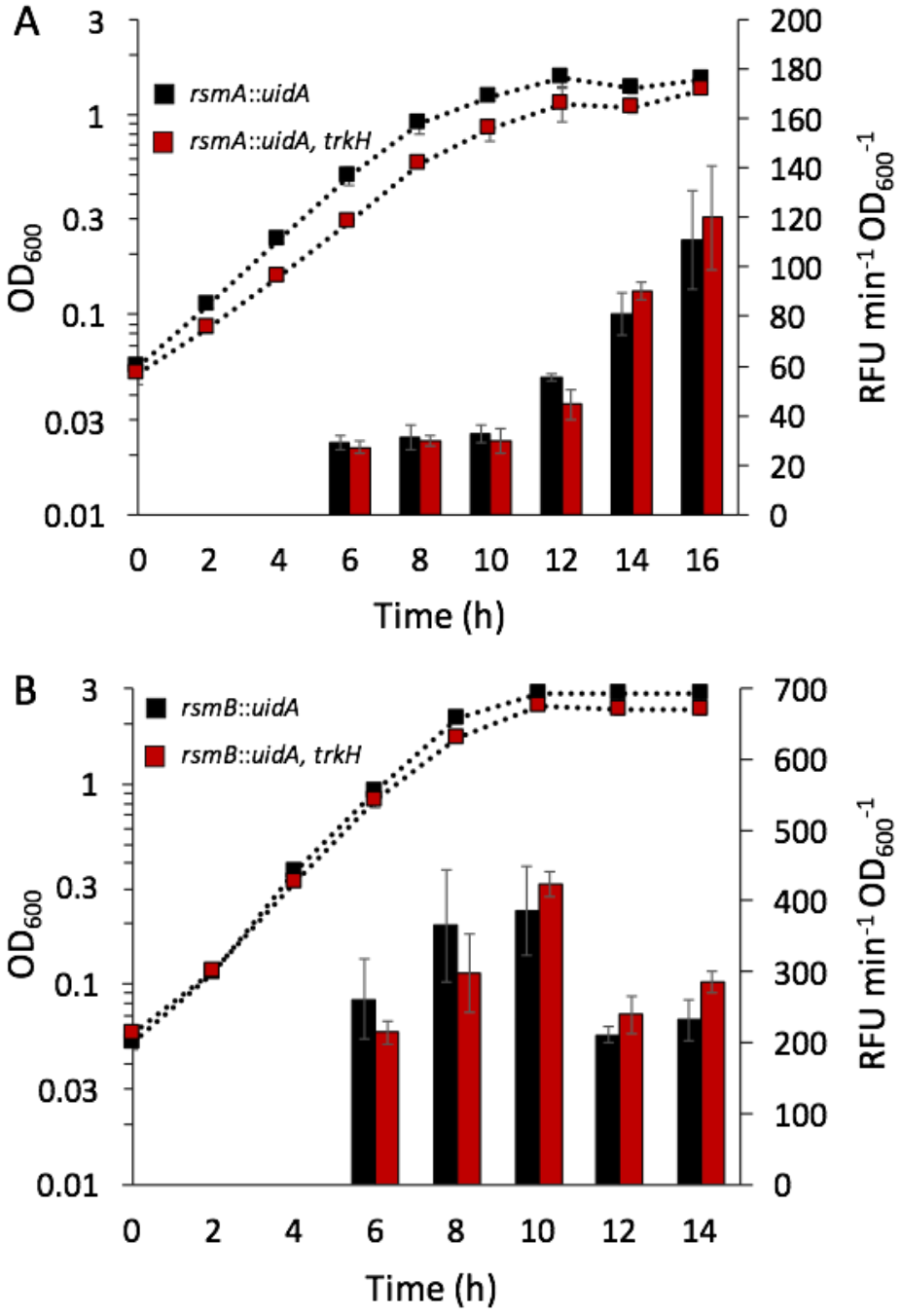

Figure 5.16. Effect of *trkH* on *rsmA* and *rsmB* transcription. Growth (dotted lines) and gene reporter acctivity (bars) in (**A**) *rsmA*::*uidA* and (**B**) *rsmB*::*uidA* fusion strains carrying the *trkH* mutation. Cells were grown in LB media. The data represent the average and standard deviation (error bars) of three biological replicates.

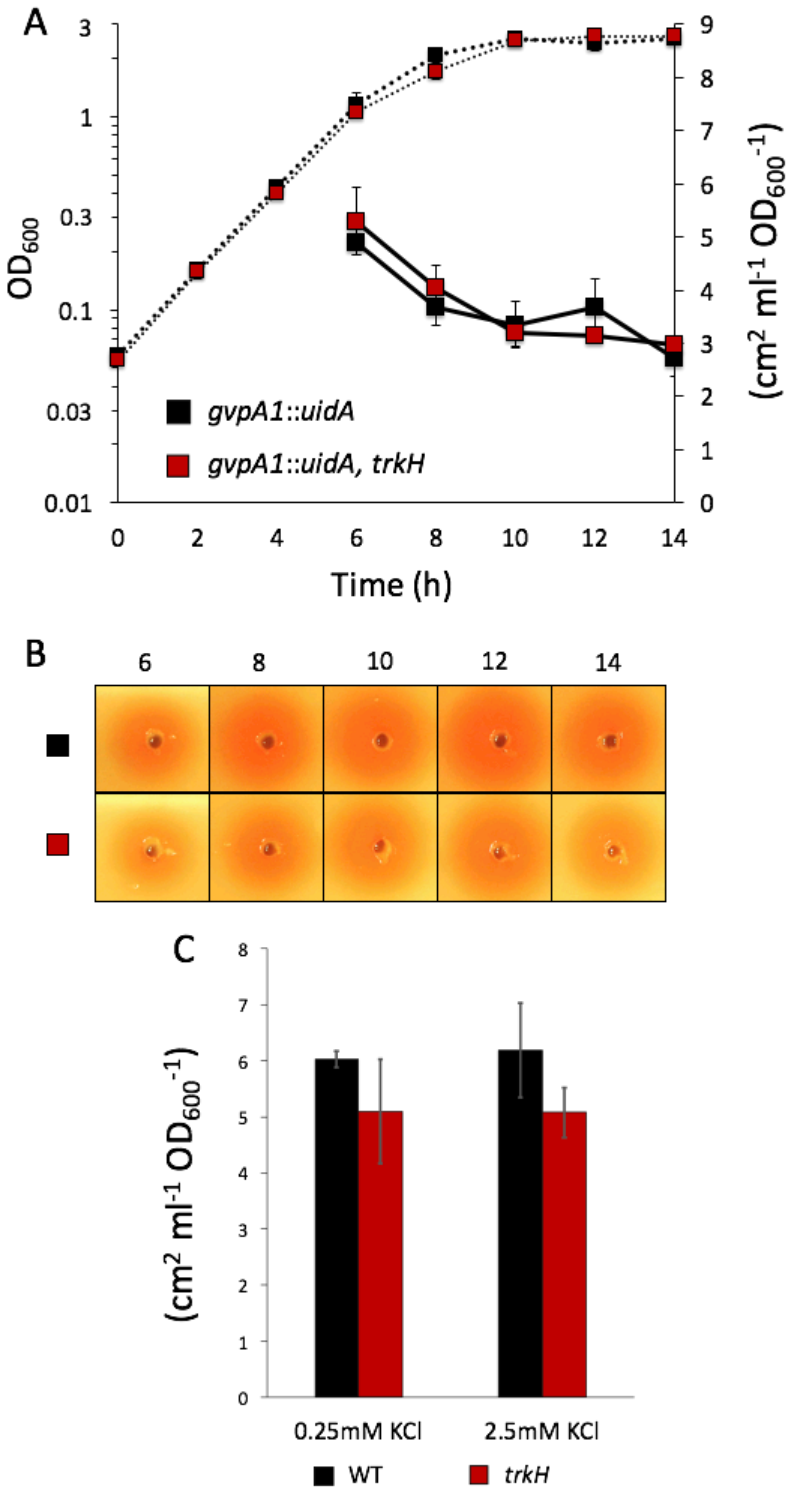

Figure 5.17. Effect of *trkH* and potassium on QS autoinducer production. A. BHL production throughout mid, late-exponential and stationary phase in LB media. **B.** Induction of prodigiosin production in the BHL reporter strain SP19 using *gvpA1*::*uidA* (black box) and *gvpA1*::*uidA*, *trkH* (red box) mutant supernatants taken from samples throughout growth (A). Images are representative of three biological replicates. **C**. BHL production at stationary phase in minimal media with either 0.25 mM KCl or 2.5 mM KCl. The data in A and C represent the average and standard deviation (error bars) of three biological replicates.

Since the *trkH* mutation and variations in extracellular potassium did not alter carbapenem production, nor the transcription of known pleiotropic regulators, the TrkH-dependent pathway was considered to play a comparatively minor role in the hierarchy of S39006 gene regulation. To test this hypothesis, the *trkH* mutation was transduced into a mutant defective for the PigW/PigQ two-component system. A previous study showed that mutations in *pigW* and *pigQ* were bypassed by mutations in other regulators, such as *rsmA* and *rpoS* (Williamson *et al.,* 2008; Wilf *et al.,* 2012). Similar to the *trkH* mutant, gene expression assays in a *pigQ* mutant suggested that the PigW/PigQ two-component system down-regulates gas vesicle production in S39006 (Ramsay *et al.,* 2011). Moreover, PigW/PigQ affects motility and prodigiosin production, but not carbapenem production (Fineran *et al.,* 2005(a); Williamson *et al.,* 2008). Thus, the expression of *gvpA1*, prodigiosin production and swimming motility in *trkH-pigW* double mutants could allow assessment of how representative the potassium-dependent regulation is in S39006. Figure 5.18.A shows that single and double mutants up-regulated *gvpA1* expression to similar levels. In contrast, the prodigiosin production in double mutants bypassed both *trkH* and *pigW* single mutations, and restored the WT levels (Figure 5.18.B). Interestingly, the *pigW* mutation bypassed the flagellar phenotype observed in the *trkH* background to completely abolish swimming motility (Fig. 5.18.C). These results suggested that the two-component system is espistatic over TrkH-dependent flagellar motility regulation, but not on the other phenotypes. It is possible that TrkH is under control of other major pleiotropic regulators, but also involved in controlling other minor regulators specific for cell buoyancy and prodigiosin production in S39006.

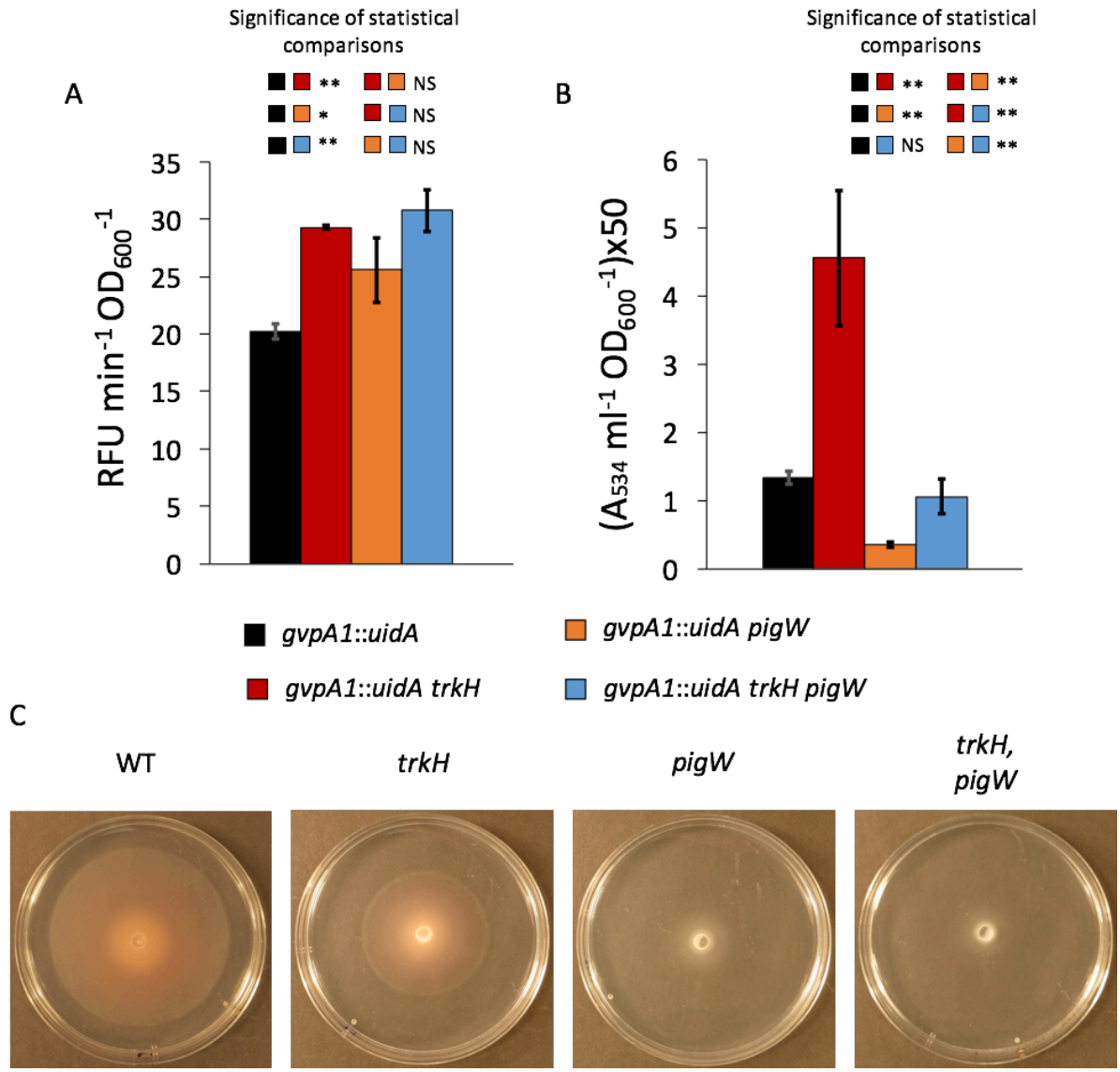

Figure 5.18. Characterization of *pigW-trkH* double mutants. A. Expression of *gvpA1.* **B.** Prodigosin production. The data represent the average and standard deviation (error bars) of three biological replicates, * $p < 0.05$, ** $p < 0.01$, NS: Not significant. **C.** Swimming motility. Images are representative of three biological replicates.

5.6 The mutation in *trkH* affects cell turgor pressure

Pressure nephelometry experiments in the cyanobacterium *Anabaena flos-aquae* showed that potassium uptake increased turgor pressure and, hence, caused gas vesicle collapse (Allison & Walsby, 1981). Given that TrkH facilitates potassium uptake in S39006, cell turgor was expected to be reduced in the *trkH* mutant. Therefore, the collapse of gas vesicles was assessed in LB (turgid medium) and LB with sucrose (hypertonic medium) in the mutant

(Chapter 1, Section 1.3). The difference between the mean critical collapse pressure (when 50% of the gas vesicles collapse) in turgid and hypertonic cultures of WT and *trkH* cells showed that turgor pressure in WT samples was similar to previous measurements (Tashiro *et al.,* 2016), whilst significantly reduced in the *trkH* mutant (Fig. 5.19.A and B). This is an interesting result and the first report demonstrating and quantifying *in vivo* the impact of *trkH* on turgor pressure

To confirm that the reduction on turgor pressure was caused by the mutation in *trkH*, the nephelometry experiment was also done with the *pigW* single and *trkH-pigW* double mutants, which also up-regulated gas vesicle production. Turgor pressure in the *pigW* background did not change compared to WT, whilst in the double mutant it was reduced as in the *trkH* single mutant (Figure 5.19.C and D). This implied that gas vesicle hyper-production does not affect the turgor pressure measurement. Moreover, the pressure nephelometry experiment suggested that potassium uptake through TrkH controls gas vesicle via cell turgor regulation, and by transcriptional control of the *gvpA1-gvpY* operon.

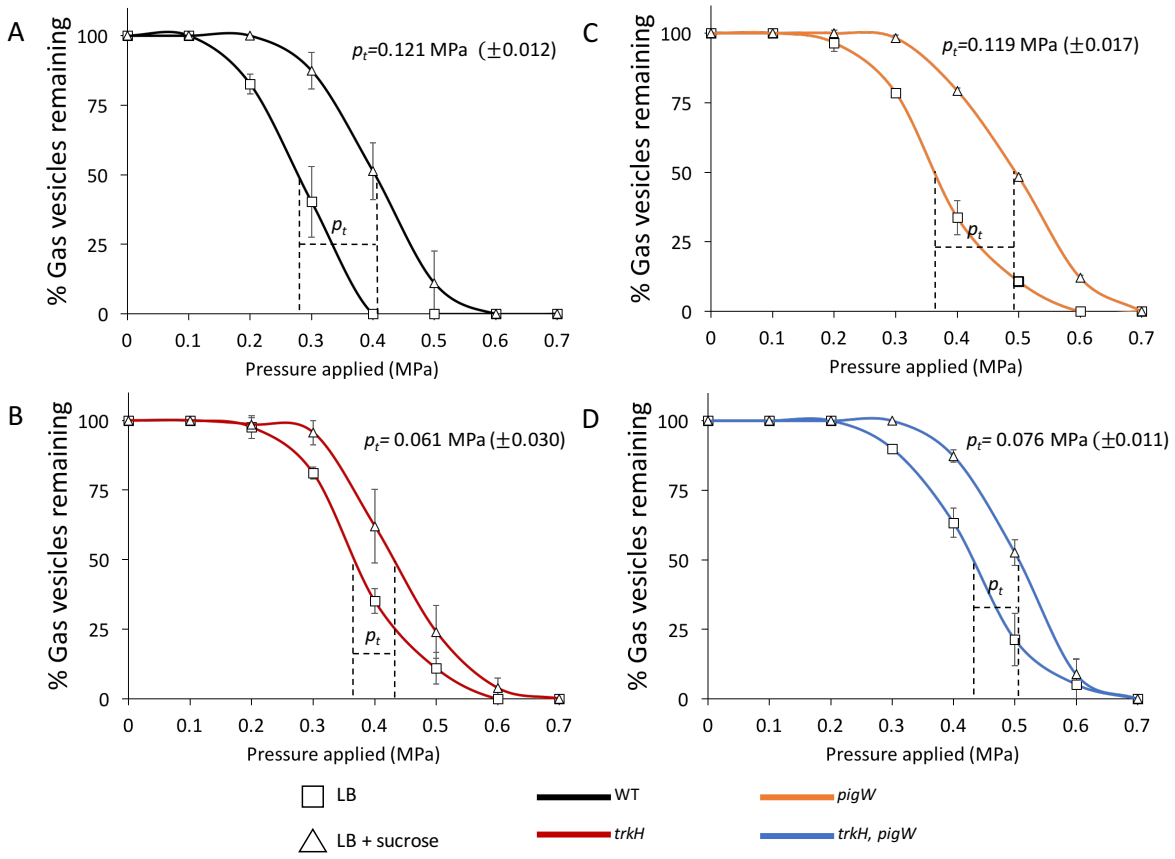

Figure 5.19. Turgor pressure measurements in the *trkH* mutant. Pressure nephelometry of (**A**) WT; (**B**) *trkH;* (**C**) *pigW* and (**D**) *trkH, pigW* mutant cultures was performed in turgid (LB) and hypertonic (LB + sucrose) conditions. Turgor pressure (p_t) is indicated for each strain. The data represent the average and standard deviation (error bars, ±) of three biological replicates.

5.7 Discussion

The experiments in this study led to the discovery that extracellular potassium uptake via the TrkH transporter is an environmental input for cell buoyancy, motility and secondary metabolism regulation in S39006. Potassium is known as an important abiotic factor affecting cell turgor, membrane potential, intracellular pH and metabolism (Tokuda *et al.,* 1981; Epstein, 2003; Gundlach *et al.,* 2017). Also, some reports showing how potassium modulates bacterial behavior have been published. For instance, potassium flux through the Trk system influences protein secretion, virulence, and resistance to antimicrobial peptides and aminoglycoside antibiotics in bacterial pathogens of man and plants (Groisman *et al.,* 1992; Laasik *et al.,* 2005; Su *et al.,* 2009; Castañeda-García *et al.,* 2011; Lázár *et al.,* 2013; Valente & Xavier *et al.,* 2016).

In S39006 extracellular potassium and TrKH down-regulate the production of the linear trypirrole pigment, prodigiosin. Two gene copies of *trkA*, one of the components of the Trk system which works as a cytoplasmic gate for potassium uptake, are located immediately upstream from a large operon involved in the synthesis of both linear and cyclic prodiginines in *Streptomyces coelicolor* (Cerdeño *et al.,* 2001). Interestingly, the authors reported that *trkA* is not essential for prodiginine production but "affected the titre in liquid media". In this study, it was demonstrated that ectopic expression of *trkH* in the mutant restored prodigiosin production to WT levels. Moreover, high extracellular potassium concentrations inhibit prodigiosin production and the expression from the *pigA* promoter, which regulates the prodigiosin biosynthetic operon in S39006.

Gas vesicle formation and cell buoyancy in S39006 were stimulated in potassium depleted conditions but inhibited in high extracellular potassium concentrations. In *Anabaena flos-aquae*, potassium uptake is a light-dependent regulatory mechanism for gas vesicle collapse (Allison & Walsby, 1981). Light exposure increased intracellular K^+ and turgor pressure sufficiently to extinguish cell buoyancy. S39006 is a heterotrophic bacterium, rather than photosynthetic. Furthermore, the experiments in this investigation showed that extracellular potassium on its own down-regulates gas vesicle production. Nonetheless, TrkH expression

and function may be under control of other regulatory components to connect the potassium-dependent response to other inputs, such as metabolic states and carbon source availability.

TrkA and TrkE, the intracellular components of the Trk system, drive TrkH-dependent potassium uptake by binding to NAD^+/NADH and ATP, respectively (Schlosser *et al.,*1993; Deller *et al.,* 2015). Therefore, it is likely that the metabolic status of the cell affects TrkH functionality. This potential connection between potassium transport and central metabolism may explain why prodigiosin production is affected in *trkH* mutants. As discussed in Chapter 4, although the natural physiological role of prodigiosin is not completely clear, it has been considered an "energy spilling" molecule involved in reduction of ATP levels in the cell (Haddix *et al.,* 2008). Therefore, potassium uptake though TrkH may down-regulate prodigiosin production to maintain ATP available.

TrkH also affected flagellar motility in S39006. The role of potassium in motility was reported previously in a Gram-positive bacterium. A recent publication showed that TrkA regulates potassium-dependent communication between *Bacillus subtillis* biofilm and free motile cells (Humphries *et al.,* 2017). Non motile cells produce electrical waves by pumping out potassium to "call" free cells, but also to communicate within the biofilm (Prindle *et al.,* 2015). Humphries and collaborators (2017) proposed a mechanism for flagellar motility regulation in which high extracellular potassium concentrations in the vicinity of the biofilm cause membrane depolarization in motile cells to increase potassium influx. The osmotic shift leads to cell hyperpolarization and, hence, the proton motive force increases and powers flagellar rotation. Considering that *trkH* expression up-regulates flagellar motility, it is possible that potassium-dependent electrical communication for motility control also occurs in S39006.

Flagellar motility is ecologically versatile compared to migration driven by gas vesicles. Swimming cells can twitch and move around in different directions, whilst gas vesicle producing bacteria are limited to upwards movement. Some prokaryotes produce both gas vesicles and flagella (Pfeifer, 2012). Nonetheless, most of them, including S39006, seem to regulate their production to be mutually exclusive. Potassium rich environments may favor swimming behavior due to their capacity to generate the proton motive force, whilst potassium depleted environments stimulate gas vesicle formation to provide an alternative

mechanism of migration in low energy status. Despite the limitations of buoyant migration, gas vesicles facilitate longstanding and sustainable vertical movement that may be useful for reaching potassium rich environments (Walsby, 1994).

Interestingly, flagellar motility and gas vesicles oppositely regulated in S39006 through RsmA, *rsmB, pigQ* and *pigX* (Ramsay *et al.,* 2011). Valente and Xavier (2016) showed that Trk-dependent control of virulence occurs under transcriptional regulation of *rsmB* in *Pectobacterium wasabiae*. Nonetheless, the transcription activity throughout growth of reporter strains with chromosomal fusions showed that TrkH does not affect *rsmA*, *rsmB, pigQ* or *pigX* transcription in S39006. Gene expression assays with reporter strains and phenotypic assays also suggested that the potassium-dependent regulation of gas vesicles, motility and prodigiosin does not occur through transcription control of other known major regulators, such as PigP or QS.

Other investigations in the Gram-positive pathogen, *Streptococcus pneumoniae* showed that the *trkH* mutant down-regulates the production of the secondary messenger, cyclic-di-AMP (c-di-AMP) (Zarrella *et al.,* 2018). Interestingly, previous reports demonstrated that high affinity potassium transport systems are inhibited by c-di-AMP binding to cytoplasmic and membrane associated proteins, such as the sensor kinase KdpD (Bai *et al.,* 2014; Moscoso *et al.,* 2016). This suggests that TrkH may stimulate c-di-AMP production to block transport systems that are active at low potassium concentrations (i.e. the Kdp system).

In low extracellular potassium concentrations, the Trk system is not active and *E. coli* survives using uptake systems with relative high and moderate affinity (Kdp and Kup (TrkD) respectively) compared to TrkH (Rhoads *et al.,* 1976; Bossemeyer *et al.,* 1989) Bioinformatic analysis using whole genome sequence revealed that S39006 contains both *kdp* and *kup*, in addition to *trkH*. It is likely that S39006 survives at low potassium concentrations using higher potassium affinity systems. Expression of the *kdpFABC* operon encoding the transporter subunits is under osmolarity regulation in *E. coli* (Laimins *et al.,* 1981). The sensor kinase KdpD phosphorylates the effector protein KdpE to activate *kdpFABC* transcription when turgor pressure is reduced after environmental potassium depletion (Epstein, 1992; Epstein, 2003). Previous investigations showed that mutants defective in components of the Trk system

expressed actively the *kdpFACB* operon at high extracellular potassium concentrations (Rhoads *et al.,* 1976; Siarot *et al.,* 2017). Here, it was demonstrated that a mutation in *trkH* mimics low extracellular potassium conditions for gas vesicle gene expression and prodigiosin production, but pressure nephelometry experiments also indicated that TrkH is a positive regulator of turgor pressure. It is possible that Trk system activity at high extracellular potassium concentrations increases potassium flux, c-di-AMP and turgor pressure to repress the KdpD/KdpE two-component system in S39006. Potassium dependent modulation of the sensor kinase, KdpD, and the transcription factor, KdpE, may be involved in pleiotropic regulation in S39006. A similar mechanism of regulation was reported for phosphate-dependent regulation in S39006. Mutants defective for expression of the phosphate transport system *pstSCAB*, mimic low phosphate conditions. This resulted in activation of the two component system PhoB/PhoR for up-regulation of QS, carbapenem and prodigiosin production (Slater *et al.,* 2003; Gristwood *et al.,* 2009).

Chapter 6
Final Discussion

Random transposon mutagenesis of the prodigiosin-negative strain, NWA19, followed by a comprehensive screening of gas vesicle mutants, random primed PCR and DNA sequencing, led to discovery of novel regulators for cell buoyancy in S39006 (See Chapter 3). Mutations in seven genes were found to affect colony opacity. The mutant classified as transparent contained a transposon insertion in a gene encoding a DeoR family transcription regulator, and lost production of phase bright structures (gas vesicles) and buoyancy. Two hyper-opaque mutants produced more gas vesicles, as seen in PCM, and remained buoyant longer that the WT. These mutants contained an insertion in genes predicted to encode either the low affinity potassium transporter TrkH or the elongation factor EF-Tu. A third group of mutants classified in this investigation as bull's-eye mutants had mutations in operons related to LPS synthesis or transport. Surprisingly, although these mutants produced gas vesicles, they sank after a few days of static culture. This indicated that gas vesicle formation is necessary, but not sufficient, for cell buoyancy.

The experiments in Chapter 4 showed that FloR (the Deor family transcriptional regulator) controls cell buoyancy, flagellar motility, carbapenem and prodigiosin production in S39006. Proteomic analysis suggested that FloR is a master regulator involved also in central metabolism and acting through different regulatory components. These include the phosphate uptake regulon PstSCAB-PhoU, the QS system SmaI/SmaR, the SylA-like regulator Rap, the gluconate sensor PigT, the post-transcriptional regulators RsmA and *rsmB*, the HexA-like regulator PigU, and the stationary phase and stress response sigma factor RpoS. Phenotypic and gene expression assays in *floR* mutants showed that the loss of gas vesicles is caused by up-regulation of *rsmB* and PigU, which inhibit RsmA activity and *rpoS* expression, respectively (Figure 6). Furthermore, proteomics and gene expression assays suggested that FloR controls gas vesicle formation via transcription regulation of the *gvrA-gvrC* operon. Given than RsmA and RpoS inhibit flagellar motility, their down-regulation in the *floR* mutant also explains the hyper-motility observed in swimming and swarming assays. The reduced production of Rap, and overproduction of PigT and the QS autoinducer (caused presumably

by down-regulation of PstS) also explained the increased motility in the mutant. In contrast, Rap appeared to be a dominant regulator for carbapenem and prodigiosin production, compared to negative regulators such as RsmA and RpoS. Figure 6 shows a model for the FloR regulatory pathway described in this research.

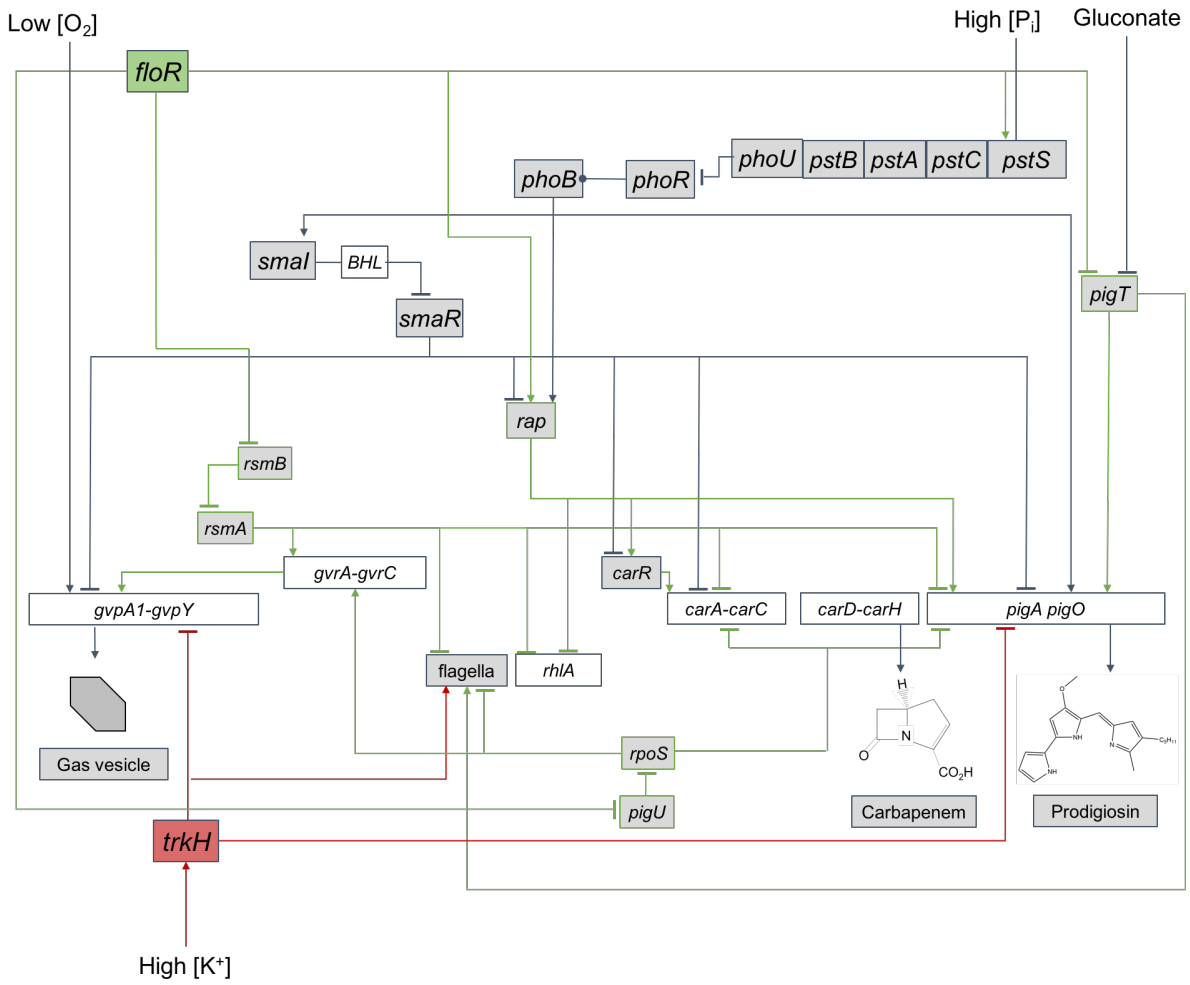

Figure 6. Model of FloR and potassium-dependent genetic regulation for cell buoyancy, flagellar motility, carbapenem and prodigiosin production. The FloR and potassium-dependent regulatory pathways are highlighted in green and red, respectively. Lines ending in arrows indicate induction, whilst lines ending in circles and perpendicular lines represent phosphorylation and negative regulation, respectively.

The characterization of the mutation in *trkH* led to the to discovery that potassium uptake via the transporter TrkH is a negative regulatory input for gas vesicle and prodigiosin production (Figure 6). In contrast, complementation of *trkH* mutants in swimming assays suggested that potassium influx stimulates flagellar motility. Gene expression assays with reporter fusion strains showed that extracellular potassium down-regulates gas vesicles by impacting *gvpA1-*

gvpY operon expression, rather than *gvrA-gvrC.* Also, the promoter activity of the prodigiosin biosynthetic operon, *pigA-pigO*, was affected negatively in high potassium concentrations. In addition, pressure nephelometry assays confirmed that TrkH regulates turgor pressure. This technique allowed *in vivo* quantification of the effects of TrkH on turgor pressure. Interestingly, the mutation in *trkH* did not affect the expression of the small RNA, *rsmB*, which was reported in another bacterium to be involved in the potassium-dependent control of virulence via TrkH. Other regulators involved in pleiotropy and in prodigiosin production were unaltered in different potassium concentrations. The transduction mechanism for the extracellular potassium response in S39006 remains unknown.

Considering that the mutation in *trkH* mimicked extracellular low potassium concentrations, transcriptomics and proteomics with mutants for the Trk system would allow comprehensive observations on the metabolic and genetic state of the cell under potassium-depleted conditions. More importantly, multi-omics would permit the identification and analysis of transcriptional and post-transcriptional regulatory components that may be under TrkH regulation. As discussed in Chapter 5, other systems and intracellular regulators reported in other bacteria as controlling the potassium-dependent response could be involved in the TrkH-dependent regulon in S39006. Therefore, future experiments using site directed mutagenesis should target higher affinity potassium uptake systems such as *trkD* and *kdpFABC*, and the two-component system genes *kdpD/kdpE*. In the future, random transposon mutagenesis of NWA19 and WT strains experiments, followed by screening for gas vesicle and prodigiosin mutants, respectively, grown on minimal media plates supplemented with low concentrations of potassium (i.e. 0.25mM KCl) may uncover cryptic regulators for gas vesicle and prodigiosin production repressed under high potassium conditions.

Further experiments to study FloR-dependent regulation would be interesting. Site directed mutagenesis using homologous recombination to construct *floR*::*lacZ* reporter fusions could be used to assess *floR* transcription in cells grown in different carbon sources and carrying mutations in other major pleiotropic regulators, such as *pigP* and *hfq*. Given that the proteomic data suggest that FloR controls its own operon, complementation experiments using ectopic expression of *floR* in a *floR*::*lacZ* fusion strain would confirm if the negative

feedback loop regulation occurs. Also, other factors affecting *floR* could be identified by random transposon mutagenesis in the *floR*::*lacZ* strain, using blue/white screening on LB plates supplemented with Xgal. The loss or enhancement of β-galactosidase activity in these colonies would suggest that a *floR* regulator was disrupted.

DeoR-like transcription factors such as DeoR, GlpR, SugR, UlaR among others, are also susceptible to allosteric modulation by phosphorylated metabolites, such as deoxyribose-5-phosphate, glycerol-3-phosphate, fructose-1-6 bisphosphate, fructose-6-phosphate and glucose-6-phosphate, and L-ascorbate-6-phosphate (Mortensen *et al.,* 1989; Gaigalat *et al.,* 2007; Garces *et al.,* 2008). These effectors affect the DNA binding affinity of the regulators and, hence, their transcription activity. Moreover, these ligands are metabolic intermediates related to the operons and pathways controlled by the DeoR-like regulators. Chip-seq using purified protein samples may help to identify the effectors, promoters and DNA motifs interacting with FloR. This would allow identification of operons and regulators are directly controlled by FloR, but also enable targeting of metabolic pathways and effectors that modulate its activity. Thereafter, **e**lectrophoretic **m**obility **s**hift **a**ssays (EMSA) with purified FloR, DNA probes and potential effectors could be performed.

In this work an attempt to purify FloR was made. Immunoblotting with a His-tag antibody in whole cell protein samples corroborated FloR expression after heterologous expression in *E. coli* (Figure 7.1, Appendix). Previous analysis of the predicted amino acid sequence of FloR suggested that this protein has a molecular weight 30KDa. The western blot corroborated this prediction (Figure 7.1, Appendix). Unfortunately, due to time limitation, the protein purification process could not be followed further.

Other strategies were considered in parallel to experiments with FloR purified samples. Gene expression assays and proteomics suggested that FloR regulates gas vesicles and motility through *rsmB*, and antibiotic production through Rap. The transcriptional activity of *rap*, *pigQ, and pigX* regulators was assessed using promoter fusions after heterologous expression of *floR* (Figure 7.2, Appendix). Interestingly, the reporter activity remained unaltered in the strains supplemented with arabinose and carrying a vector with *floR* (pAQY2). In the future, if changes were observed in the reporter activity of the promoter fusion DNA pull-down

assays with cell extracts (such as promoter trapping and reverse ChIP) could be performed in samples from the WT and *floR* mutant. This would allow examination of the regulatory protein complexes bound to the promoter regions and amino acid sequencing could confirm if FloR was present in these complexes.

Unfortunately, the role of EF-Tu and LPS-related genes in gas vesicle production could not be studied in detail due to time limitation. However, as discussed in Chapter 3, EF-Tu and LPS biogenesis proteins have been associated with several physiological effects in other bacteria, in addition to mRNA processing and outer membrane architecture, respectively. For instance, EF-Tu is known to interact with toxins involved in the Type VI secretion system (Whitney *et al.,* 2015). Give the preliminary data showing links between EF-Tu, LPS biosynthesis and gas vesicle production, complementation assays should be performed to confirm the regulatory and physiological roles of these genes in the gas vesicle phenotype. In addition to the phenotypic analysis, gene expression and proteomics experiments should be with these mutants and LPS electrophoretic profiles assays would help determine if the outer membrane changes dramatically in the bull's-eye mutants. Also, co-immunoprecipitation (Co-IP) with an EF-Tu antibody would be useful to determine if this elongation factor interacts with any other proteins involved in gas vesicle regulation.

Overall, this study discovered new regulatory components involved in production of gas vesicles, flagella, and the carbapenem and prodigiosin antibiotics. In principle, this new information may be exploitable in the biotechnological applications of gas vesicles, or carbapenem and prodiginine bioactive molecules as proposed previously (Coulthurst *et al.,* 2005; Williamson *et al.,* 2006; Farhadi *et al.,* 2018). This investigation has expanded previous studies on S39006 showing that cell buoyancy is under tight regulation of biotic and abiotic factors, including carbon metabolism, population density and oxygen availability (Ramsay *et al.,* 2011; Tashiro *et al.,* 2016; Lee *et al.,* 2017). This work also supports previous reports discussing the physiological and ecological importance of gas vesicles and flagella in various bacterial systems (Walsby, 1994; Wiliamson *et al.,* 2008, Pfeifer, 2012). The regulation of gas vesicles, flagella, carbapenem and prodigiosin by multiple environmental inputs (potassium in particular), surface components (LPS in particular), plus intracellular response regulators (transcriptional regulators; FloR and RpoS)) and housekeeping components (i.e EF-Tu)

indicates the physiological complexity and adaptive capacity of 39006. The first study of S39006 described its isolation from roots and stems of halophytic plants and salt marsh channel waters, in which brackish water would flood the surface periodically and alter the water column depth continuously (Parker *et al.,* 1982). The strain was first studied by the Squibb Chemical Company in New Jersey, USA, for its ability to make carbapenem antibiotic. Fortunately, from our perspective, this environmental strain adapted readily to domestic life in UK laboratories and, still, 36 years later, continues to reveal new fascinating information on the genetics and molecular biology of diverse physiological processes in a simple enterobacterium.

References

Abràmoff, M. D., Magalhães, P. J., & Ram, S. J. (2004). Image processing with ImageJ. *Biophotonics international*, *11*(7), 36-42.

Alkhuder, K., Meibom, K. L., Dubail, I., Dupuis, M., & Charbit, A. (2010). identification of *trkH*, encoding a potassium uptake protein required for *Francisella tularensis* systemic dissemination in mice. *PLoS ONE*, *5*(1), e8966.

Allison, E. M., & Walsby, A. E. (1981). The role of potassium in the control of turgor pressure in a gas-vacuolate blue-green alga. *Journal of Experimental Botany*, *32*(1), 241–249.

Arnoldi, M., Fritz, M., Bäuerlein, E., Radmacher, M., Sackmann, E., & Boulbitch, A. (2000). Bacterial turgor pressure can be measured by atomic force microscopy. *Physical Review E*, *62*(1), 1034.

Atkinson, S., & Williams, P. (2009). Quorum sensing and social networking in the microbial world. *Journal of the Royal Society, Interface*, *6*(40), 959–78.

Babitzke, P., & Romeo, T. (2007). CsrB sRNA family: sequestration of RNA-binding regulatory proteins. *Current Opinion in Microbiology*, *10*(2), 156–163.

Bai, Y., Yang, J., Zarrella, T. M., Zhang, Y., Metzger, D. W., & Bai, G. (2014). Cyclic di-AMP impairs potassium uptake mediated by a cyclic di-AMP binding protein in *Streptococcus pneumoniae*. *Journal of Bacteriology*, *196*(3), 614-623.

Bailey, T. L., & Elkan, C. (1994). Fitting a mixture model by expectation maximization to discover motifs in biopolymer, 28-36.

Bainton, N. J., Bycroft, B. W., Chhabra, S. R., Stead, P., Gledhill, L., Hill, P. J., … Williams, P. (1992). A general role for the *lux* autoinducer in bacterial cell signalling: control of antibiotic biosynthesis in *Erwinia*. *Gene*, *116*(1), 87–91.

Battesti, A., Majdalani, N., & Gottesman, S. (2011). The RpoS-Mediated General Stress Response in *Escherichia coli*. *Annu. Rev. Microbiol*, *65*, 189–213.

Benjamini, Y., & Hochberg, Y. (1995). Controlling the false discovery rate: a practical and powerful approach to multiple testing. *Journal of the royal statistical society. Series B (Methodological)*, 289-300.

Berg, G. (2000). Diversity of antifungal and plant-associated *Serratia plymuthica* strains. *Journal of Applied Microbiology*, *88*(6), 952–960.

Boratyn, G. M., Schäffer, A. A., Agarwala, R., Altschul, S. F., Lipman, D. J., & Madden, T. L. (2012). Domain enhanced lookup time accelerated BLAST. *Biology direct*, *7*(1), 12.

Botsford, J. L., & Harman, J. G. (1992). Cyclic AMP in prokaryotes. *Microbiological Reviews*, *56*(1), 100–22.

Bowden, M. G., & Kaplan, H. B. (1998). The *Myxococcus xanthus* lipopolysaccharide O-antigen is required for social motility and multicellular development. *Molecular Microbiology*, *30*(2), 275–284.

Brown, L., & Elliott, T. (1996). Efficient translation of the RpoS sigma factor in *Salmonella typhimurium* requires host factor I, an RNA-binding protein encoded by the *hfq* gene. *Journal of Bacteriology*, *178*(13), 3763–70.

Buchholz, B. E. E., Hayes, P. k., & Walsby, A. E. (1993). The distribution of the outer gas vesicle protein, GvpC, on the *Anabaena* gas vesicle, and its ratio to GvpA. *Journal of General Microbiology*, *139*(10), 2353–2363.

Caldas, T. D., El Yaagoubi, A., & Richarme, G. (1998). Chaperone properties of bacterial elongation factor EF-Tu. *Journal of Biological Chemistry*, *273*(19), 11478-11482

Carver, T., Harris, S. R., Berriman, M., Parkhill, J., & McQuillan, J. A. (2011). Artemis: an integrated platform for visualization and analysis of high-throughput sequence-based experimental data. *Bioinformatics*, *28*(4), 464-469.

Castaneda-Garcia, A., Do, T. T., & Blazquez, J. (2011). The K^+ uptake regulator TrkA controls membrane potential, pH homeostasis and multidrug susceptibility in *Mycobacterium smegmatis*. *Journal of Antimicrobial Chemotherapy*, *66*(7), 1489–1498.

Cerdeño, A. M., Bibb, M. J., & Challis, G. L. (2001). Analysis of the prodiginine biosynthesis gene cluster of *Streptomyces coelicolor* A3(2): new mechanisms for chain initiation and termination in modular multienzymes. *Chemistry & Biology*, *8*(8), 817–829.

Chatterjee, A., Cui, Y., & Chatterjee, A. K. (2002). RsmA and the quorum-sensing signal, N-[3-oxohexanoyl]-L-homoserine lactone, control the levels of *rsmB* RNA in *Erwinia carotovora* subsp. *carotovora* by affecting its stability. *Journal of Bacteriology*, *184*(15), 4089–95.

Chekabab, S. M., Jubelin, G., Dozois, C. M., & Harel, J. (2014). PhoB activates *Escherichia coli* O157: H7 virulence factors in response to inorganic phosphate limitation. *PloS one*, *9*(4), e94285.

Coulthurst, S. J., Barnard, A. M. L., & Salmond, G. P. C. (2005). Regulation and biosynthesis of carbapenem antibiotics in bacteria. *Nature Reviews. Microbiology*, *3*(4), 295–306.

Coulthurst, S. J., Kurz, C. L., & Salmond, G. P. C. (2004). *luxS* mutants of *Serratia* defective in autoinducer-2-dependent "quorum sensing" show strain-dependent impacts on virulence and production of carbapenem and prodigiosin. *Microbiology*, *150*(6), 1901–1910.

Coulthurst, S. J., Lilley, K. S., & Salmond, G. P. C. (2006). Genetic and proteomic analysis of the role of *luxS* in the enteric phytopathogen, *Erwinia carotovora*. *Molecular Plant Pathology*, *7*(1), 31–45.

Cox, A. R. J., Thomson, N. R., Bycroft, B., Stewart, G. S. A. B., Williams, P., & Salmond, G. P. C. (1998). A pheromone-independent CarR protein controls carbapenem antibiotic synthesis in the opportunistic human pathogen *Serratia marcescens*. *Microbiology*, *144*(1), 201–209.

Cui, Y., Chatterjee, A., & Chatterjee, A. K. (2001). Effects of the Two-Component System Comprising GacA and GacS of *Erwinia carotovora* subsp. *carotovora* on the Production of Global Regulatory *rsmB* RNA, Extracellular Enzymes, and $Harpin_{Ecc}$. *Molecular Plant-Microbe Interactions*, *14*(4), 516–526.

Cuthbertson, L., Kos, V., & Whitfield, C. (2010). ABC transporters involved in export of cell surface glycoconjugates. *74*(3), 341–362.

Dallo, S. F., Zhang, B., Denno, J., Hong, S., Tsai, A., Haskins, W., … Weitao, T. (2012). Association of *Acinetobacter baumannii* EF-Tu with cell surface, outer membrane vesicles, and fibronectin. *The Scientific World Journal*, *2012*, 1–10.

Danevčič, T., Borić Vezjak, M., Tabor, M., Zorec, M., & Stopar, D. (2016). Prodigiosin induces autolysins in actively grown *Bacillus subtilis* Cells. *Frontiers in Microbiology*, *7*, 27.

DasSarma, S., Arora, P., Lin, F., Molinari, E., & Yin, L. R. (1994). Wild-type gas vesicle formation requires at least ten genes in the *gvp* gene cluster of *Halobacterium halobium* plasmid pNRC100. *Journal of Bacteriology*, *176*(24), 7646–52.

De Fernandez, M. F., Eoyang, L., & August, J. T. (1968). Factor fraction required for the synthesis of bacteriophage Qβ-RNA. *Nature*, *219*(5154), 588–590.

Deller, M. C., Johnson, H. A., Miller, M. D., Spraggon, G., Elsliger, M.-A., Wilson, I. A., & Lesley, S. A. (2015). Crystal structure of a two-subunit TrkA octameric gating ring assembly. *PLOS ONE*, *10*(3), e0122512.

Demarre, G., Guérout, A. M., Matsumoto-Mashimo, C., Rowe-Magnus, D. a., Marlière, P., & Mazel, D. (2005). A new family of mobilizable suicide plasmids based on broad host range R388 plasmid (IncW) and RP4 plasmid (IncPα) conjugative machineries and their cognate *Escherichia coli* host strains. *Research in Microbiology*, *156*(2), 245–255.

Deng, Y., Sun, M., & Shaevitz, J. W. (2011). Direct measurement of cell wall stress stiffening and turgor pressure in live bacterial cells. *Physical Review Letters*, *107*(15), 158101.

Dennis, J. J., & Zylstra, G. J. (1998). Plasposons: modular self-cloning minitransposon derivatives for rapid genetic analysis of gram-negative bacterial genomes. *Applied and Environmental Microbiology*, *64*(7), 2710–5.

Deziel, E., Lépine, F., Milot, S., & Villemur, R. (2003). *rhlA* is required for the production of a novel biosurfactant promoting swarming motility in *Pseudomonas aeruginosa*: 3-(3-hydroxyalkanoyloxy) alkanoic acids (HAAs), the precursors of rhamnolipids. *Microbiology*, *149*(8), 2005–2013.

Dolan, S. K., Bock, T., Hering, V., Owens, R. A., Jones, G. W., Blankenfeldt, W., & Doyle, S. (2017). Structural, mechanistic and functional insight into gliotoxin bis-thiomethylation in *Aspergillus fumigatus*. *Open Biology*, *7*(2), 160292.

Dosch, D. C., Helmer, G. L., Sutton, S. H., Salvacion, F. F., & Epstein, W. (1991). Genetic analysis of potassium transport loci in *Escherichia coli*: evidence for three constitutive systems mediating uptake potassium. *Journal of Bacteriology*, *173*(2), 687–96.

Elgrably-Weiss, M., Schlosser-Silverman, E., Rosenshine, I., & Altuvia, S. (2006). DeoT, a DeoR-type transcriptional regulator of multiple target genes. *FEMS Microbiology Letters*, *254*(1), 141–148.

Englert, C., Krüger, K., Offner, S., & Pfeifer, F. (1992). Three different but related gene clusters encoding gas vesicles in halophilic archaea. *Journal of Molecular Biology*, *227*(2), 586–592.

Epstein, W. (1986). Osmoregulation by potassium transport in *Escherichia coli*. *FEMS Microbiology Letters*, *39*(1–2), 73–78.

Epstein, W. (1992). Kdp, a bacterial P-type ATPase whose expression and activity are regulated by turgor pressure. *Acta Physiologica Scandinavica. Supplementum*, *607*, 193–9.

Epstein, W. (2003). The roles and regulation of potassium in bacteria. *Progress in Nucleic Acid Research and Molecular Biology*, *75*, 293–320.

Evans, T. J., Crow, M. a., Williamson, N. R., Orme, W., Thomson, N. R., Komitopoulou, E., & Salmond, G. P. C. (2010). Characterization of a broad-host-range flagellum-dependent phage that mediates high-efficiency generalized transduction in, and between, *Serratia* and *Pantoea*. *Microbiology*, *156*(1), 240–247.

Farewell, A., Kvint, K., & Nyström, T. (1998). Negative regulation by RpoS: a case of sigma factor competition. *Molecular Microbiology*, *29*(4), 1039–1051.

Farhadi, A., Ho, G., Kunth, M., Ling, B., Lakshmanan, A., Lu, G. J., … Shapiro, M. G. (2018). Recombinantly expressed gas vesicles as nanoscale contrast agents for ultrasound and hyperpolarized MRI. *AIChE Journal*, *64*(8), 2927–2933.

Figueroa-Bossi, N., Schwartz, A., Guillemardet, B., D'Heygère, F., Bossi, L., & Boudvillain, M. (2014). RNA remodeling by bacterial global regulator CsrA promotes Rho-dependent transcription termination. *Genes & Development*, *28*(11), 1239–51.

Fineran, P. C., Slater, H., Everson, L., Hughes, K., & Salmond, G. P. C. (2005) (a). Biosynthesis of tripyrrole and β-lactam secondary metabolites in *Serratia*: Integration of quorum sensing with multiple new regulatory components in the control of prodigiosin and carbapenem antibiotic production. *Molecular Microbiology*, *56*(6), 1495–1517.

Fineran, P. C., Everson, L., Slater, H., & Salmond, G. P. C. (2005). A GntR family transcriptional regulator (PigT) controls gluconate-mediated repression and defines a new, independent pathway for regulation of the tripyrrole antibiotic, prodigiosin, in *Serratia*. *Microbiology*, *151*(12), 3833–3845.

Fineran, P. C., Iglesias Cans, M. C., Ramsay, J. P., Wilf, N. M., Cossyleon, D., McNeil, M. B., … Salmond, G. P. C. (2013). Draft genome sequence of *Serratia* sp. strain ATCC 39006, a model bacterium for analysis of the biosynthesis and regulation of prodigiosin, a carbapenem, and gas vesicles. *Genome Announce*, *1*(6), e01039-13.

Fineran, P. C., Williamson, N. R., Lilley, K. S., & Salmond, G. P. C. (2007). Virulence and prodigiosin antibiotic biosynthesis in *Serratia* are regulated pleiotropically by the GGDEF/EAL domain protein, PigX. *Journal of Bacteriology*, *189*(21), 7653–7662.

Fuller, N. J., West, N. J., Marie, D., Yallop, M., Rivlin, T., Post, A. F., & Scanlan, D. J. (2005). Dynamics of community structure and phosphate status of picocyanobacterial populations in the Gulf of Aqaba, Red Sea. *Limnology and Oceanography*, *50*(1), 363-375

Gaigalat, L., Schlüter, J.-P., Hartmann, M., Mormann, S., Tauch, A., Pühler, A., & Kalinowski, J. (2007). The DeoR-type transcriptional regulator SugR acts as a repressor for genes encoding the phosphoenolpyruvate: sugar phosphotransferase system (PTS) in *Corynebacterium glutamicum*. *BMC Molecular Biology*, *8*(1), 104.

Garces, F., Fernández, F. J., Gómez, A. M., Pérez-Luque, R., Campos, E., Prohens, R., … Vega, M. C. (2008). Quaternary structural transitions in the DeoR-Type repressor UlaR control transcriptional readout from the L-ascorbate utilization regulon in *Escherichia coli*. *Biochemistry*, *47*(44), 11424–11433.

Gatto, L., & Lilley, K. S. (2012). MSnbase-an R/Bioconductor package for isobaric tagged mass spectrometry data visualization, processing and quantitation. *Bioinformatics*, *28*(2), 288–289.

Girgis, H. S., Liu, Y., Ryu, W. S., & Tavazoie, S. (2007). A comprehensive genetic characterization of bacterial motility. *PLoS Genetics*, *3*(9), e154.

Gristwood, T., Fineran, P. C., Everson, L., Williamson, N. R., & Salmond, G. P. C. (2009). The PhoBR two-component system regulates antibiotic biosynthesis in *Serratia* in response to phosphate. *BMC Microbiology*, *9*, 112.

Groisman, E. A., Parra-Lopez, C., Salcedo, M., Lipps, C. J., & Heffron, F. (1992). Resistance to host antimicrobial peptides is necessary for *Salmonella* virulence. *Proceedings of the National Academy of Sciences of the United States of America*, *89*(24), 11939–43.

Gundlach, J., Herzberg, C., Hertel, D., Thürmer, A., Daniel, R., Link, H., & Stülke, J. (2017). Adaptation of *Bacillus subtilis* to life at extreme potassium limitation. *mBio*, *8*(4), e00861-17.

Gupta, S., Stamatoyannopoulos, J. A., Bailey, T. L., & Noble, W. (2007). Quantifying similarity between motifs. *Genome Biology*, *8*(2), R24

Guzman, L. M., Belin, D., Carson, M. J., & Beckwith, J. (1995). Tight regulation, modulation, and high-level expression by vectors containing the arabinose PBAD promoter. *Journal of Bacteriology*, *177*(14), 4121–30.

Haddix, P. L., Jones, S., Patel, P., Burnham, S., Knights, K., Powell, J. N., & LaForm, A. (2008). Kinetic analysis of growth rate, ATP, and pigmentation suggests an energy-spilling function for the pigment prodigiosin of *Serratia marcescens*. *Journal of Bacteriology*, *190*(22), 7453–63.

Hampton, H. G., McNeil, M. B., Paterson, T. J., Ney, B., Williamson, N. R., Easingwood, R. A., ... & Fineran, P. C. (2016). CRISPR-Cas gene-editing reveals RsmA and RsmC act through FlhDC to repress the SdhE flavinylation factor and control motility and prodigiosin production in *Serratia*. *Microbiology*, *162*(6), 1047-1058.

Harms, C., Domoto, Y., Celik, C., Rahe, E., Stumpe, S., Schmid, R., … Bakker, E. P. (2001). Identification of the ABC protein SapD as the subunit that confers ATP dependence to the K^+ -uptake systems Trk H and Trk G from *Escherichia coli* K-12. *Microbiology* (Vol. 147).

Heeb, S., & Haas, D. (2001). Regulatory roles of the GacS/GacA two-component system in plant-associated and other Gram-negative bacteria. *Molecular Plant-Microbe Interactions*, *14*(12), 1351–1363.

Holland, D. P., & Walsby, A. E. (2009). Digital recordings of gas-vesicle collapse used to measure turgor pressure and cell–water relations of cyanobacterial cells. *Journal of Microbiological Methods*, *77*(2), 214–224.

Hsieh, Y.-J., & Wanner, B. L. (2010). Global regulation by the seven-component Pi signaling system. *Current Opinion in Microbiology*, *13*(2), 198–203.

Hughes, D. (1990). Both genes for EF-Tu in *Salmonella typhimurium* are individually dispensable for growth. *Journal of Molecular Biology*, *215*(1), 41–51.

Humphries, J., Xiong, L., Liu, J., Prindle, A., Yuan, F., Arjes, H. A., … Süel, G. M. (2017). Species-independent attraction to biofilms through electrical signalling. *Cell*, *168*(1–2), 200–209.e12.

Hyytiäinen, H., Montesano, M., & Palva, E. T. (2001). Global regulators ExpA (GacA) and KdgR modulate extracellular enzyme gene expression through the RsmA-*rsmB* system in *Erwinia carotovora* subsp. *carotovora*. *Molecular Plant-Microbe Interactions: MPMI*, *14*(8), 931–938.

Jenal, U., & Malone, J. (2006). Mechanisms of cyclic-di-GMP signaling in bacteria. *Annual Review of Genetics*, *40*(1), 385–407.

Kalivoda, E. J., Stella, N. A., Aston, M. A., Fender, J. E., Thompson, P. P., Kowalski, R. P., & Shanks, R. M. Q. (2010). Cyclic AMP negatively regulates prodigiosin production by *Serratia marcescens*. *Research in Microbiology*, *161*(2), 158–167.

Laasik, E., Ojarand, M., Pajunen, M., Savilahti, H., & Mäe, A. (2005). Novel mutants of *Erwinia carotovora* subsp. *carotovora* defective in the production of plant cell wall degrading enzymes generated by Mu transpososome-mediated insertion mutagenesis. *FEMS Microbiology Letters*, *243*(1), 93–99.

Laber, B., Maurer, W., Scharf, S., Stepusin, K., & Schmidt, F. S. (1999). Vitamin B_6 biosynthesis: formation of pyridoxine 5'-phosphate from 4-(phosphohydroxy)-l-threonine and 1-deoxy-d-xylulose-5-phosphate by PdxA and PdxJ protein. *FEBS Letters*, *449*(1), 45-48.

Laimins, L. A., Rhoads, D. B., & Epstein, A. W. (1981). Osmotic control of *kdp* operon expression in *Escherichia coli* (potassium transport/lac fusion/turgor pressure). *Genetics*, *78*(1), 464–468.

Lázár, V., Pal Singh, G., Spohn, R., Nagy, I., Horváth, B., Hrtyan, M., … Pál, C. (2013). Bacterial evolution of antibiotic hypersensitivity. *Molecular Systems Biology*, *9*(1), 700.

Lee, C. M., Monson, R. E., Adams, R. M., & Salmond, G. P. C. (2017). The LacI–Family Transcription Factor, RbsR, is a pleiotropic regulator of motility, virulence, siderophore and antibiotic production, gas vesicle morphogenesis and flotation in *Serratia*. *Frontiers in Microbiology*, *8*(September), 1678.

Leng, Y., Vakulskas, C. A., Zere, T. R., Pickering, B. S., Watnick, P. I., Babitzke, P., & Romeo, T. (2016). Regulation of CsrB/C sRNA decay by EIIA^{Glc} of the phosphoenolpyruvate: carbohydrate phosphotransferase system. *Molecular Microbiology*, *99*(4), 627–639.

Lerouge, I., & Vanderleyden, J. (2002). O-antigen structural variation: mechanisms and possible roles in animal/plant–microbe interactions. *FEMS Microbiology Reviews*, *26*(1), 17–47.

Liu, M. Y., & Romeo, T. (1997). The global regulator CsrA of Escherichia coli is a specific mrna-binding protein. *Journal of Bacteriology*, *179*(14), 4639–4642.

Liu, X., & Matsumura, P. (1994). The FlhD/FlhC complex, a transcriptional activator of the Escherichia coli flagellar class II operons. *Journal of Bacteriology*, *176*(23), 7345-7351.

Liu, X., Ji, L., Wang, X., Li, J., Zhu, J., & Sun, A. (2018). Role of RpoS in stress resistance, quorum sensing and spoilage potential of *Pseudomonas fluorescens*. *International Journal of Food Microbiology*, *270*, 31–38.

Martin, J. L., & McMillan, F. M. (2002). SAM (dependent) I AM: the S-adenosylmethionine-dependent methyltransferase fold. *Current Opinion in Structural Biology*, *12*(6), 783–93.

Martiny, A. C., Coleman, M. L., & Chisholm, S. W. (2006). Phosphate acquisition genes in *Prochlorococcus* ecotypes: evidence for genome-wide adaptation. *Proceedings of the National Academy of Sciences*, *103*(33), 12552-12557.

Matilla, M. A., Leeper, F. J., & Salmond, G. P. C. (2015). Biosynthesis of the antifungal haterumalide, oocydin A, in *Serratia* , and its regulation by quorum sensing, RpoS and Hfq. *Environmental Microbiology*, *17*(8), 2993–3008.

Matilla, M. a., Stöckmann, H., Leeper, F. J., & Salmond, G. P. C. (2012). Bacterial biosynthetic gene clusters encoding the anti-cancer haterumalide class of molecules: Biogenesis of the broad spectrum antifungal and anti-oomycete compound, oocydin A. *Journal of Biological Chemistry*, *287*(46), 39125–39138.

Mauzy, C. A., & Hermodson, M. A. (1992). Structural homology between *rbs* repressor and ribose binding protein implies functional similarity. *Protein Science*, *1*, 843–849.

McAlister, G. C., Nusinow, D. P., Jedrychowski, M. P., Wühr, M., Huttlin, E. L., Erickson, B. K., ... & Gygi, S. P. (2014). MultiNotch MS3 enables accurate, sensitive, and multiplexed detection of differential expression across cancer cell line proteomes. *Analytical chemistry*, *86*(14), 7150-7158

McCullen, C. A., Benhammou, J. N., Majdalani, N., & Gottesman, S. (2010). Mechanism of positive regulation by DsrA and RprA small noncoding RNAs: pairing increases translation and protects *rpoS* mRNA from degradation. *Journal of Bacteriology*, *192*(21), 5559–71.

McGowan, S. J., Barnard, A. M., Bosgelmez, G., Sebaihia, M., Simpson, N. J., Thomson, N. R., ... & Salmond, G. P. C. (2005). Carbapenem antibiotic biosynthesis in Erwinia carotovora is regulated by physiological and genetic factors modulating the quorum sensing-dependent control pathway. *Molecular microbiology*, *55*(2), 526-545.

McGowan, S. J., Sebaihia, M., Porter, L. E., Stewart, G. S., Williams, P., Bycroft, B. W., & Salmond, G. P. C. (1996). Analysis of bacterial carbapenem antibiotic production genes reveals a novel beta-lactam biosynthesis pathway. *Molecular Microbiology*, *22*(3), 415–26.

McNeil, M. B., Clulow, J. S., Wilf, N. M., Salmond, G. P. C., & Fineran, P. C. (2012). SdhE is a conserved protein required for flavinylation of succinate dehydrogenase in bacteria. *The Journal of Biological Chemistry*, *287*(22), 18418–28.

McNeil, M. B., Hampton, H. G., Hards, K. J., Watson, B. N. J., Cook, G. M., & Fineran, P. C. (2014). The succinate dehydrogenase assembly factor, SdhE, is required for the flavinylation and activation of fumarate reductase in bacteria. *FEBS Letters*, *588*(3), 414–421.

Miller, J. H. (1972). *Experiments in molecular genetics*. Cold Spring Harbor Laboratory.

Money, N. P. (2008). Insights on the mechanics of hyphal growth. *Fungal Biology Reviews*, *22*(2), 71–76.

Monson, R. E., Tashiro, Y., & Salmond, G. P. C. (2016). Overproduction of individual gas vesicle proteins perturbs flotation, antibiotic production and cell division in the enterobacterium *Serratia* sp. ATCC 39006. *Microbiology (United Kingdom)*, *162*(9), 1595–1607.

Monson, R., Smith, D. S., Matilla, M. A., Roberts, K., Richardson, E., Drew, A., … Salmond, G. P. C. (2015). A plasmid-transposon hybrid mutagenesis system effective in a broad range of enterobacteria. *Frontiers in Microbiology*, *6*, 1442.

Morgenstein, R. M., Clemmer, K. M., & Rather, P. N. (2010). Loss of the *waaL* O-antigen ligase prevents surface activation of the flagellar gene cascade in *Proteus mirabilis*. *Journal of Bacteriology*, *192*(12), 3213–21.

Morris Jr, J. G., Sztein, M. B., Rice, E. W., Nataro, J. P., Losonsky, G. A., Panigrahi, P., ... & Johnson, J. A. (1996). *Vibrio cholerae* 01 can assume a chlorine-resistant rugose survival form that is virulent for humans. *Journal of Infectious Diseases*, *174*(6), 1364-1368.

Mortensen, L., Dandanell, G., & Hammer, K. (1989). Purification and characterization of the *deoR* repressor of *Escherichia coli*. *The EMBO Journal*, *8*(1), 325–331.

Moscoso, J. A., Schramke, H., Zhang, Y., Tosi, T., Dehbi, A., Jung, K., & Gründling, A. (2016). Binding of cyclic di-AMP to the *Staphylococcus aureus* sensor kinase KdpD occurs via the universal stress protein domain and downregulates the expression of the Kdp potassium transporter. *Journal of Bacteriology*, *198*(1), 98-110

Mukherjee, A., Cui, Y., Ma, W., Liu, Y., & Chatterjee, A. K. (2000). hexA of *Erwinia carotovora* ssp. *carotovora* strain Ecc71 negatively regulates production of RpoS and *rsmB* RNA, a global regulator of extracellular proteins, plant virulence and the quorum-sensing signal, N-(3-oxohexanoyl)- l-homoserine lactone. *Environmental Microbiology*, *2*(2), 203–215.

Nanchen, A., Schicker, A., Revelles, O., & Sauer, U. (2008). Cyclic AMP-dependent catabolite repression is the dominant control mechanism of metabolic fluxes under glucose limitation in *Escherichia coli*. *Journal of Bacteriology*, *190*(7), 2323–30.

Ng, W. L., & Bassler, B. L. (2009). Bacterial quorum sensing network architectures. *Annual Review of Genetics*, *43*(1), 197–222.

Numan, M., Bashir, S., Mumtaz, R., Tayyab, S., Rehman, N. U., Khan, A. L., … Al-Harrasi, A. (2018). Therapeutic applications of bacterial pigments: a review of current status and future opportunities. *3 Biotech*, *8*(4), 207.

Offner, S., Hofacker, A., Wanner, G., & Pfeifer, F. (2000). Eight of fourteen *gvp* genes are sufficient for formation of gas vesicles in halophilic archaea. *Journal of Bacteriology*, *182*(15), 4328–36.

Osawa, M., & Erickson, H. P. (2018). Turgor pressure and possible constriction mechanisms in bacterial division. *Frontiers in Microbiology*, *9*, 111.

Overmann, J., & Pfennig, N. (1992). Bouyancy regulation and aggregate formation in *Amoebobacter purpureus* from Mahoney Lake. *FEMS Microbiology Letters*, *101*(2), 67–69.

Pandey, R., Chander, R., & Sainis, K. (2009). Prodigiosins as anti cancer agents: living upto their name. *Current Pharmaceutical Design*, *15*(7), 732–741.

Papireddy, K., Smilkstein, M., Kelly, J. X., Shweta, Salem, S. M., Alhamadsheh, M., … Reynolds, K. A. (2011). Antimalarial activity of natural and synthetic prodiginines. *Journal of Medicinal Chemistry*, *54*(15), 5296–5306.

Park, H., McGibbon, L. C., Potts, A. H., Yakhnin, H., Romeo, T., & Babitzke, P. (2017). Translational repression of the RpoS antiadapter IraD by CsrA is mediated via translational coupling to a short upstream open reading frame. *mBio*, *8*(4), e01355-17.

Parker, W. L., Rathnum, M. L., Wells, J. S., Trejo, W. H., Principe, P. a, & Sykes, R. B. (1982). SQ 27,860, a simple carbapenem produced by species of *Serratia* and *Erwinia*. *The Journal of Antibiotics*, *35*(6), 653–660.

Parra-Lopez, C., Lin, R., Aspedon, A., & Groisman, E. A. (1994). A *Salmonella* protein that is required for resistance to antimicrobial peptides and transport of potassium. *The EMBO Journal*, *13*(17), 3964–72.

Paterson, T. J. (2013). Regulation of the conserved hypothetical operon *sdhEygfX* and its control of cellular processes (Doctoral dissertation, University of Otago).

Patterson-Fortin, L. M., Vakulskas, C. A., Yakhnin, H., Babitzke, P., & Romeo, T. (2013). Dual posttranscriptional regulation via a cofactor-responsive mRNA leader. *Journal of Molecular Biology*, *425*(19), 3662–3677.

Peleg, A., Shifrin, Y., Ilan, O., Nadler-Yona, C., Nov, S., Koby, S., … Rosenshine, I. (2005). Identification of an *Escherichia coli* operon required for formation of the O-antigen capsule. *Journal of Bacteriology*, *187*(15), 5259–66.

Peterson, C. N., Carabetta, V. J., Chowdhury, T., & Silhavy, T. J. (2006). LrhA regulates *rpoS* translation in response to the Rcs phosphorelay system in *Escherichia coli*. *Journal of Bacteriology*, *188*(9), 3175–81.

Pfeifer, F. (2012). Distribution, formation and regulation of gas vesicles. *Nature Reviews Microbiology*, *10*(10), 705–715.

Pichler, P., Köcher, T., Holzmann, J., Mazanek, M., Taus, T., Ammerer, G., & Mechtler, K. (2010). Peptide labeling with isobaric tags yields higher identification rates using iTRAQ 4-Plex compared to TMT 6-Plex and iTRAQ 8-Plex on LTQ Orbitrap. *Analytical Chemistry*, *82*(15), 6549–6558.

Potts, A. H., Leng, Y., Babitzke, P., & Romeo, T. (2018). Examination of Csr regulatory circuitry using epistasis analysis with RNA-seq (Epi-seq) confirms that CsrD affects gene expression via CsrA, CsrB and CsrC. *Scientific Reports*, *8*(1), 5373.

Potts, A. H., Vakulskas, C. A., Pannuri, A., Yakhnin, H., Babitzke, P., & Romeo, T. (2017). Global role of the bacterial post-transcriptional regulator CsrA revealed by integrated transcriptomics. *Nature Communications*, *8*(1), 1596.

Poulter, S., Carlton, T. M., Su, X., Spring, D. R., & Salmond, G. P. C. (2010). Engineering of new prodigiosin-based biosensors of *Serratia* for facile detection of short-chain N-acyl homoserine lactone quorum-sensing molecules. *Environmental Microbiology Reports*, *2*(2), 322–328.

Prindle, A., Liu, J., Asally, M., Ly, S., Garcia-Ojalvo, J., & Süel, G. M. (2015). Ion channels enable electrical communication in bacterial communities. *Nature*, *527*(7576), 59–63.

R Core Team (2012) "R: a language and environment for statistical computing", Vienna, Austria: R Foundation for Statistical Computing.

Ramos-Aires, J., Plésiat, P., Kocjancic-Curty, L., & Köhler, T. (2004). Selection of an antibiotic-hypersusceptible mutant of *Pseudomonas aeruginosa*: identification of the GlmR transcriptional regulator. *Antimicrobial Agents and Chemotherapy*, *48*(3), 843–51.

Ramsay, J. P., Williamson, N. R., Spring, D. R., & Salmond, G. P. C. (2011). A quorum-sensing molecule acts as a morphogen controlling gas vesicle organelle biogenesis and adaptive flotation in an enterobacterium. *Proceedings of the National Academy of Sciences of the United States of America*, *108*(36), 14932–14937.

Rhoads, D. B., Waters, F. B., & Epstein, W. (1976). Cation transport in *Escherichia coli*. VIII. Potassium transport mutants. *The Journal of General Physiology*, *67*(3), 325–41.

Rhodius, V. A., Suh, W. C., Nonaka, G., West, J., & Gross, C. A. (2005). Conserved and Variable Functions of the σE Stress Response in Related Genomes. *PLoS Biology*, *4*(1), e2.

Rojas, E. R., & Huang, K. C. (2018). Regulation of microbial growth by turgor pressure. *Current Opinion in Microbiology*, *42*, 62–70.

Romeo, T. (1998). Global regulation by the small RNA-binding protein CsrA and the non-coding RNA molecule CsrB. *Molecular Microbiology*, *29*(6), 1321–1330.

Romeo, T., Gong, M., Liu, M. Y., & Brun-Zinkernagel, A. M. (1993). Identification and molecular characterization of *csrA*, a pleiotropic gene from *Escherichia coli* that affects glycogen biosynthesis, gluconeogenesis, cell size, and surface properties. *Journal of Bacteriology*, *175*(15), 4744–55.

Sabnis, N. A., Yang, H., & Romeo, T. (1995). Pleiotropic regulation of central carbohydrate metabolism in *Escherichia coli* via the gene *csrA*. *The Journal of Biological Chemistry*, *270*(49), 29096–104.

Saier, M. H. (1998). Multiple mechanisms controlling carbon metabolism in bacteria. *Biotechnology and Bioengineering*, *58*(2–3), 170–174.

Saxild, H. H., Andersen, L. N., & Hammer, K. (1996). Dra-nupC-pdp operon of Bacillus subtilis: nucleotide sequence, induction by deoxyribonucleosides, and transcriptional regulation by the *deoR*-encoded DeoR repressor protein. *Journal of Bacteriology*, *178*(2), 424–34.

Schlosser, A., Hamann, A., Bossemeyer, D., Schneider, E., & Bakker, E. P. (1993). NAD^+ binding to the *Escherichia coli* K^+ -uptake protein TrkA and sequence similarity between TrkA and domains of a family of dehydrogenases suggest a role for NAD^+ in bacterial transport. *Molecular Microbiology*, *9*(3), 533–543.

Schlosser, A., Meldorf, M., Stumpe, S., Bakker, E. P., & Epstein, W. (1995). TrkH and its homolog, TrkG, determine the specificity and kinetics of cation transport by the Trk system of *Escherichia coli*. *Journal of Bacteriology*, *177*(7), 1908–1910.

Schmidt, A., Kochanowski, K., Vedelaar, S., Ahrné, E., Volkmer, B., Callipo, L., … Heinemann, M. (2016). The quantitative and condition-dependent *Escherichia coli* proteome. *Nature Biotechnology*, *34*(1), 104–110.

Schubert, H. L., Blumenthal, R. M., & Cheng, X. (2003). Many paths to methyltransfer: a chronicle of convergence. *Trends in biochemical sciences*, *28*(6), 329-335

Schuster, M., Hawkins, A. C., Harwood, C. S., & Greenberg, E. P. (2004). The *Pseudomonas aeruginosa* RpoS regulon and its relationship to quorum sensing. *Molecular Microbiology*, *51*(4), 973–985.

Shimada, T., Fujita, N., Yamamoto, K., & Ishihama, A. (2011). Novel roles of cAMP receptor protein (CRP) in regulation of transport and metabolism of carbon sources. *PLoS ONE*, *6*(6), e20081.

Shomar, H., Gontier, S., van den Broek, N. J., Mora, H. T., Noga, M. J., Hagedoorn, P. L., & Bokinsky, G. (2018). Metabolic engineering of a carbapenem antibiotic synthesis pathway in *Escherichia coli*. *Nature Chemical Biology*, 1.

Shukla, H. D., & DasSarma, S. (2004). Complexity of gas vesicle biogenesis in *Halobacterium* sp. strain NRC-1: identification of five new proteins. *Journal of Bacteriology*, *186*(10), 3182–6.

Siarot, L., Toyazaki, H., Hidaka, M., Kurumisawa, K., Hirakawa, T., Morohashi, K., & Aono, T. (2017). A novel regulatory pathway for K+ uptake in the legume symbiont *azorhizobium caulinodans* in which TrkJ Represses the *kdpFABC* operon at high extracellular K+ concentrations. *Applied and Environmental Microbiology*, *83*(19), AEM.01197-17.

Sivertsen, A. C., Bayro, M. J., Belenky, M., Griffin, R. G., & Herzfeld, J. (2010). Solid-state NMR characterization of gas vesicle structure. *Biophysical Journal*, *99*(6), 1932–1939.

Slater, H., Crow, M., Everson, L., & Salmond, G. P. C. (2003). Phosphate availability regulates biosynthesis of two antibiotics, prodigiosin and carbapenem, in *Serratia* via both quorum-sensing-dependent and -independent pathways. *Molecular Microbiology*, *47*(2), 303–320.

Smyth, G. K. Limma: linear models for microarray data. Bioinformatics and computational biology solutions using R and bioconductor. Edited by: Gentleman R, Carey V, Dudoit S, Irizarry R, Huber W. 2005.

Soper, T., Mandin, P., Majdalani, N., Gottesman, S., & Woodson, S. A. (2010). Positive regulation by small RNAs and the role of Hfq. *Proceedings of the National Academy of Sciences of the United States of America*, *107*(21), 9602–7.

Spory, A., Bosserhoff, A., von Rhein, C., Goebel, W., & Ludwig, A. (2002). Differential regulation of multiple proteins of Escherichia coli and *Salmonella enterica* serovar Typhimurium by the transcriptional regulator SlyA. *Journal of Bacteriology*, *184*(13), 3549–59.

Steiner, K., Novotny, R., Werz, D. B., Zarschler, K., Seeberger, P. H., Hofinger, A., ... & Messner, P. (2008). Molecular basis of S-layer glycoprotein glycan biosynthesis in *Geobacillus stearothermophilus*. *Journal of Biological Chemistry*, *283*(30), 21120-21133.

Stella, N. A., Kalivoda, E. J., O'Dee, D. M., Nau, G. J., & Shanks, R. M. Q. (2008). Catabolite repression control of flagellum production by *Serratia marcescens*. *Research in Microbiology*, *159*(7–8), 562–8.

Su, J., Gong, H., Lai, J., Main, A., & Lu, S. (2009). The potassium transporter Trk and external potassium modulate *Salmonella enterica* protein secretion and virulence. *Infection and Immunity*, *77*(2), 667–75.

Tashiro, Y., Monson, R. E., Ramsay, J. P., & Salmond, G. P. C. (2016). Molecular genetic and physical analysis of gas vesicles in buoyant enterobacteria. *Environmental Microbiology*, *18*(4), 1264–1276.

Tegel, H., Tourle, S., Ottosson, J., & Persson, A. (2010). Increased levels of recombinant human proteins with the *Escherichia coli* strain Rosetta(DE3). *Protein Expression and Purification*, *69*(2), 159–167.

Thomson, N. R., Cox, a, Bycroft, B. W., Stewart, G. S., Williams, P., & Salmond, G. P. C. (1997). The *rap* and *hor* proteins of *Erwinia*, *Serratia* and *Yersinia*: a novel subgroup in a growing superfamily of proteins regulating diverse physiological processes in bacterial pathogens. *Molecular Microbiology*, *26*(3), 531–544.

Thomson, N. R., Crow, M. a., McGowan, S. J., Cox, a., & Salmond, G. P. C. (2000). Biosynthesis of carbapenem antibiotic and prodigiosin pigment in *Serratia* is under quorum sensing control. *Molecular Microbiology*, *36*(3), 539–556.

Tichy, E. M., Hardwick, S. W., Luisi, B. F., & Salmond, G. P. C. (2017). 1.8 Å resolution crystal structure of the carbapenem intrinsic resistance protein CarF. *Acta Crystallographica Section D Structural Biology*, *73*(7), 549–556.

Tichy, E. M., Luisi, B. F., & Salmond, G. P. C. (2014). Crystal structure of the carbapenem intrinsic resistance protein CarG. *Journal of Molecular Biology*, *426*(9), 1958–1970.

Toguchi, A., Siano, M., Burkart, M., & Harshey, R. M. (2000). Genetics of swarming motility in *Salmonella enterica* serovar Typhimurium: critical role for lipopolysaccharide. *Journal of Bacteriology*, *182*(22), 6308–21.

Tokuda, H., Nakamura, T., & Unemoto, T. (1981). Potassium ion is required for the generation of ph-dependent membrane potential and ΔpH by the marine bacterium *vibrio alginolyticus*. *Biochemistry*, *20*(14), 4198-4203

Tong, S., Porco, A., Isturiz, T., & Conway, T. (1996). Cloning and molecular genetic characterization of the Escherichia coli *gntR*, *gntK*, and *gntU* genes of GntI, the main system for gluconate metabolism. *Journal of Bacteriology*, *178*(11), 3260–9.

Tran, Q. H., & Unden, G. (1998). Changes in the proton potential and the cellular energetics of Escherichia coli during growth by aerobic and anaerobic respiration or by fermentation. *European Journal of Biochemistry*, *251*(1–2), 538–543.

Tsai, C. S., & Winans, S. C. (2010). LuxR-type quorum-sensing regulators that are detached from common scents. *Molecular Microbiology*, *77*(5), 1072–1082.

Tsui, H. C., Feng, G., & Winkler, M. E. (1997). Negative regulation of *mutS* and *mutH* repair gene expression by the Hfq and RpoS global regulators of *Escherichia coli* K-12. *Journal of Bacteriology*, *179*(23), 7476–87.

Tsui, H.-C. T., Leung, H.-C. E., & Winkler, M. E. (1994). Characterization of broadly pleiotropic phenotypes caused by an *hfq* insertion mutation in *Escherichia coli* K-12. *Molecular Microbiology*, *13*(1), 35–49.

Ulanova, D., Kitani, S., Fukusaki, E., & Nihira, T. (2013). SdrA, a new DeoR family regulator involved in *Streptomyces avermitilis* morphological development and antibiotic production. *Applied and Environmental Microbiology*, *79*(24), 7916–21.

Valente, R. S., & Xavier, K. B. (2015). The trk potassium transporter is required for rsmb-mediated activation of virulence in the phytopathogen *Pectobacterium wasabiae*. *Journal of Bacteriology*, *198*(2), 248–55.

Valentin-Hansen, P., Eriksen, M., & Udesen, C. (2004). The bacterial Sm-like protein Hfq: a key player in RNA transactions. *Molecular Microbiology*, *51*(6), 1525–1533.

Walderhaug, M. O., Polarek, J. W., Voelkner, P., Daniel, J. M., Hesse, J. E., Altendorf, K., & Epstein, W. (1992). KdpD and KdpE, proteins that control expression of the *kdpABC* operon, are members of the two-component sensor-effector class of regulators. *Journal of Bacteriology*, *174*(7), 2152–9.

Walsby, A. E. (1971). The pressure relationships of gas vacuoles. *Proceedings of the Royal Society B: Biological Sciences*, *178*(1052), 301–326.

Walsby, A. E. (1994). Gas vesicles. *Microbiological Reviews*, *58*(1), 94–144.

Wang, F., Ren, N. N., Luo, S., Chen, X. X., Mao, X. M., & Li, Y.Q. (2014). DptR2, a DeoR-type auto-regulator, is required for daptomycin production in *Streptomyces roseosporus*. *Gene*, *544*(2), 208–215.

Wang, Z., Li, B., Zhou, L., Yu, S., Su, Z., Song, J., … Lu, D. (2016). Prodigiosin inhibits Wnt/β-catenin signaling and exerts anticancer activity in breast cancer cells. *Proceedings of the National Academy of Sciences of the United States of America*, *113*(46), 13150–13155.

Wei, B. L., Brun-Zinkernagel, A.-M., Simecka, J. W., Prüß, B. M., Babitzke, P., & Romeo, T. (2001). Positive regulation of motility and *flhDC* expression by the RNA-binding protein CsrA of Escherichia coli. *Molecular Microbiology*, *40*(1), 245–256.

Wei, B., Shin, S., LaPorte, D., Wolfe, A. J., & Romeo, T. (2000). Global regulatory mutations in *csrA* and *rpoS* cause severe central carbon stress in *Escherichia coli* in the presence of acetate. *Journal of Bacteriology*, *182*(6), 1632–40.

Whitehead, N. A., Barnard, A. M. L., Slater, H., Simpson, N. J. L., & Salmond, G. P. C. (2001). Quorum-sensing in Gram-negative bacteria. *FEMS Microbiology Reviews*, *25*(4), 365–404.

Whitney, J. C., Quentin, D., Sawai, S., LeRoux, M., Harding, B. N., Ledvina, H. E., ... & Raunser, S. (2015). An interbacterial $NAD(P)^+$ glycohydrolase toxin requires elongation factor Tu for delivery to target cells. *Cell*, *163*(3), 607-619.

Wilf, N. M., & Salmond, G. P. C. (2012). The stationary phase sigma factor, RpoS, regulates the production of a carbapenem antibiotic, a bioactive prodigiosin and virulence in the enterobacterial pathogen *Serratia* sp. ATCC 39006. *Microbiology*, *158*(3), 648–658.

Wilf, N. M., Reid, A. J., Ramsay, J. P., Williamson, N. R., Croucher, N. J., Gatto, L., … Salmond, G. P. C. (2013). RNA-seq reveals the RNA binding proteins, Hfq and RsmA, play various roles in virulence, antibiotic production and genomic flux in *Serratia* sp. ATCC 39006. *BMC Genomics*, *14*(1), 822.

Wilf, N. M., Williamson, N. R., Ramsay, J. P., Poulter, S., Bandyra, K. J., & Salmond, G. P. C. (2011). The RNA chaperone, Hfq, controls two *luxR*-type regulators and plays a key role in pathogenesis and production of antibiotics in *Serratia* sp. ATCC 39006. *Environmental Microbiology*, *13*(10), 2649–2666.

Williamson, N. R., Fineran, P. C., Gristwood, T., Chawrai, S. R., Leeper, F. J., & Salmond, G. P. C. (2007). Anticancer and immunosuppressive properties of bacterial prodiginines. *Future Microbiology*. *Future Medicine*, *6*(2), 605-618.

Williamson, N. R., Fineran, P. C., Ogawa, W., Woodley, L. R., & Salmond, G. P. C. (2008). Integrated regulation involving quorum sensing, a two-component system, a GGDEF/EAL domain protein and a post-transcriptional regulator controls swarming and RhlA-dependent surfactant biosynthesis in *Serratia*. *Environmental Microbiology*, *10*(5), 1202–1217.

Williamson, N. R., Simonsen, H. T., Ahmed, R. A. A., Goldet, G., Slater, H., Woodley, L., … Salmond, G. P. C. (2005). Biosynthesis of the red antibiotic, prodigiosin, in *Serratia*: identification of a novel 2-methyl-3-n-amyl-pyrrole (MAP) assembly pathway, definition of the terminal condensing enzyme, and implications for undecylprodigiosin biosynthesis in *Streptomyces*. *Molecular Microbiology*, *56*(4), 971–989.

Williamson, N. R., Fineran, P. C., Leeper, F. J., & Salmond, G. P. C. (2006). The biosynthesis and regulation of bacterial prodiginines. *Nature Reviews Microbiology*, *4*(12), 887

Wolfe, A. J., & Visick, K. L. (2008). Get the message out: cyclic-Di-GMP regulates multiple levels of flagellum-based motility. *Journal of Bacteriology*, *190*(2), 463–75.

Wu, R., Zhang, R., Zagnitko, O., Dementieva, I., Maltzev, N., Watson, J. D., … Joachimiak, A. (2003). Crystal structure of *Enterococcus faecalis* SlyA-like transcriptional factor. *The Journal of Biological Chemistry*, *278*(22), 20240–4.

Xu, B. Y., Dai, Y. N., Zhou, K., Liu, Y. T., Sun, Q., Ren, Y. M., ... & Zhou, C. Z. (2014). Structure of the gas vesicle protein GvpF from the cyanobacterium *Microcystis aeruginosa*. *Acta Crystallographica Section D*, *70*(11), 3013-3022

Yakhnin, H., Yakhnin, A. V., Baker, C. S., Sineva, E., Berezin, I., Romeo, T., & Babitzke, P. (2011). Complex regulation of the global regulatory gene *csrA*: CsrA-mediated translational repression, transcription from five promoters by Eσ70 and EσS, and indirect transcriptional activation by CsrA. *Molecular Microbiology*, *81*(3), 689–704.

Zarrella, T. M., Metzger, D. W., & Bai, G. (2018). Stress suppressor screening leads to detecting regulation of cyclic di-AMP homeostasis by a Trk-family effector protein in *Streptococcus pneumoniae*. *Journal of Bacteriology*, JB-00045

Zhao, K., Liu, M., & Burgess, R. R. (2007). Adaptation in bacterial flagellar and motility systems: from regulon members to “foraging”-like behavior in *E. coli*. *Nucleic Acids Research*, *35*(13), 4441–4452.

Zuurmond, A.-M., Rundlöf, A.-K., & Kraal, B. (1999). Either of the chromosomal *tuf* genes of *E. coli* K-12 can be deleted without loss of cell viability. *Molecular and General Genetics*, *260*(6), 603–607.

Appendix

7. TMT labelling, LC-MS/MS and Bioinformatics analysis of S39006 *floR* mutant proteome

This protocol was kindly provided by Dr. Mike Deery from the Cambridge Centre for Proteomics.

7.1 TMT labelling

TMT 10plex labelling was performed following manufacturer's instructions (Thermo Fisher Scientific). Four independent replicates of WT protein samples were labelled with TMT tags 126, 127N, 127C, 128N, whilst three replicates of S39006 *floR* protein samples with 128C, 129N and 129C. All protein samples were combined and cleaned using a Sep-Pak C18 cartridge.

7.2 High-pH first dimension reverse-phase fractionation

The following LC conditions were used for the fractionation of the TMT samples: desalted peptides were resuspended in 0.1 ml 20 mM ammonium formate (pH 10.0) + 4 % (v/v) acetonitrile. Peptides were loaded onto an Acquity bridged ethyl hybrid C18 UPLC column (Waters; 2.1 mm i.d. x 150 mm, 1.7 µm particle size), and profiled with a linear gradient of 5-60 % acetonitrile + 20 mM ammonium formate (pH10.0) over 60 min, at a flow-rate of 0.25 ml min^{-1}. Chromatographic performance was monitored by sampling eluate with a diode array detector (Acquity UPLC, Waters) scanning between wavelengths of 200 and 400 nm. Samples were collected in 1 min increments and reduced to dryness by vacuum centrifugation.

7.3 LC-MS/MS

Dried fractions from the high pH reverse-phase separations were resuspended in 30 μl of 0.1 % formic acid and placed into a glass vial. 1 μl of each fraction was injected by the HPLC

autosampler and separated by the LC method detailed below. A total of 10 combined fractions were analysed by LC-MS/MS.

LC-MS/MS experiments were performed using a Dionex Ultimate 3000 RSLC nanoUPLC (Thermo Fisher Scientific Inc, Waltham, MA, USA) system and a Lumos Orbitrap mass spectrometer (Thermo Fisher Scientific Inc, Waltham, MA, USA). Peptides were loaded onto a pre-column (Thermo Scientific PepMap 100 C18, 5mm particle size, 100A pore size, 300 mm i.d. x 5mm length) from the Ultimate 3000 auto-sampler with 0.1 % formic acid for 3 min at a flow rate of 10 μl min^{-1}. After this period, the column valve was switched to allow elution of peptides from the pre-column onto the analytical column. Separation of peptides was performed by C18 reverse-phase chromatography at a flow rate of 300 nl min^{-1} using a Thermo Scientific reverse-phase nano Easy-spray column (Thermo Scientific PepMap C18, 2mm particle size, 100A pore size, 75 mm i.d. x 50cm length). Solvent A was water + 0.1 % formic acid and solvent B was 80 % acetonitrile, 20 % water + 0.1 % formic acid. The linear gradient employed was 2-40 % B in 93 min. (Total LC run time was 120 min including a high organic wash step and column re-equilibration).

The eluted peptides from the C18 column LC eluant were sprayed into the mass spectrometer by means of an Easy-Spray source (Thermo Fisher Scientific Inc.). All *m/z* values of eluting peptide ions were measured in an Orbitrap mass analyzer, set at a resolution of 120,000 and were scanned between *m/z* 380-1500 Da. Data dependent MS/MS scans (Top Speed) were employed to automatically isolate and fragment precursor ions by collision-induced dissociation (CID, Normalised Collision Energy (NCE): 35 %) which were analysed in the linear ion trap. Singly charged ions and ions with unassigned charge states were excluded from being selected for MS/MS and a dynamic exclusion window of 70 seconds was employed. The top 10 most abundant fragment ions from each MS/MS event were then selected for a further stage of fragmentation by Synchronous Precursor Selection (SPS) MS3 (McAlister *et al.,* 2014) in the HCD high energy collision cell using HCD (High energy Collisional Dissociation, (NCE: 65 %). The *m/z* values and relative abundances of each reporter ion and all fragments (mass range from 100-500 Da) in each MS3 step were measured in the Orbitrap analyser, which was set at a resolution of 60,000. This was performed in cycles of 10 MS3 events before the Lumos

instrument reverted to scanning the *m/z* ratios of the intact peptide ions and the cycle continued.

7.4 Bionformatic Analysis

Proteome Discoverer v2.1 (Thermo Fisher Scientific) and Mascot (Matrix Science) v2.6 were used to process raw data files. Data were aligned with the UniProt *Serratia sp. ATCC 39006* database, in addition to using the common repository of adventitious proteins (cRAP) v1.0. Protein identification allowed an MS tolerance of ± 10 ppm and an MS/MS tolerance of ± 0.8Da ppm along with permission of up to 2 missed tryptic cleavages. Quantification was achieved by calculating the sum of centroided reporter ions within a ± 2 millimass unit (mmu) window around the expected *m/z* for each of the four TMT reporter ions.

All comparative analyses were performed with the R statistical language (R Core Team, 2012). The R package MSnbase (Gatto & Lilley, 2012) was used for processing proteomics data. Briefly, this entailed missing value removal (instances where a protein was identified but not quantified in all channels were rejected from further analysis), log2-transformation of the raw data, followed by sample normalization; utilizing the 'diff.median' method in MSnbase (this translates all sample columns so that they all match the grand median). Protein differential abundance was evaluated using the Limma package (Smyth, 2005). Differences in protein abundances were statistically determined using the Student's t-test with variances moderated by Limma's empirical Bayes method. P-values were adjusted for multiple testing by the Benjamini Hochberg method (Benjamini & Hochberg, 1995).

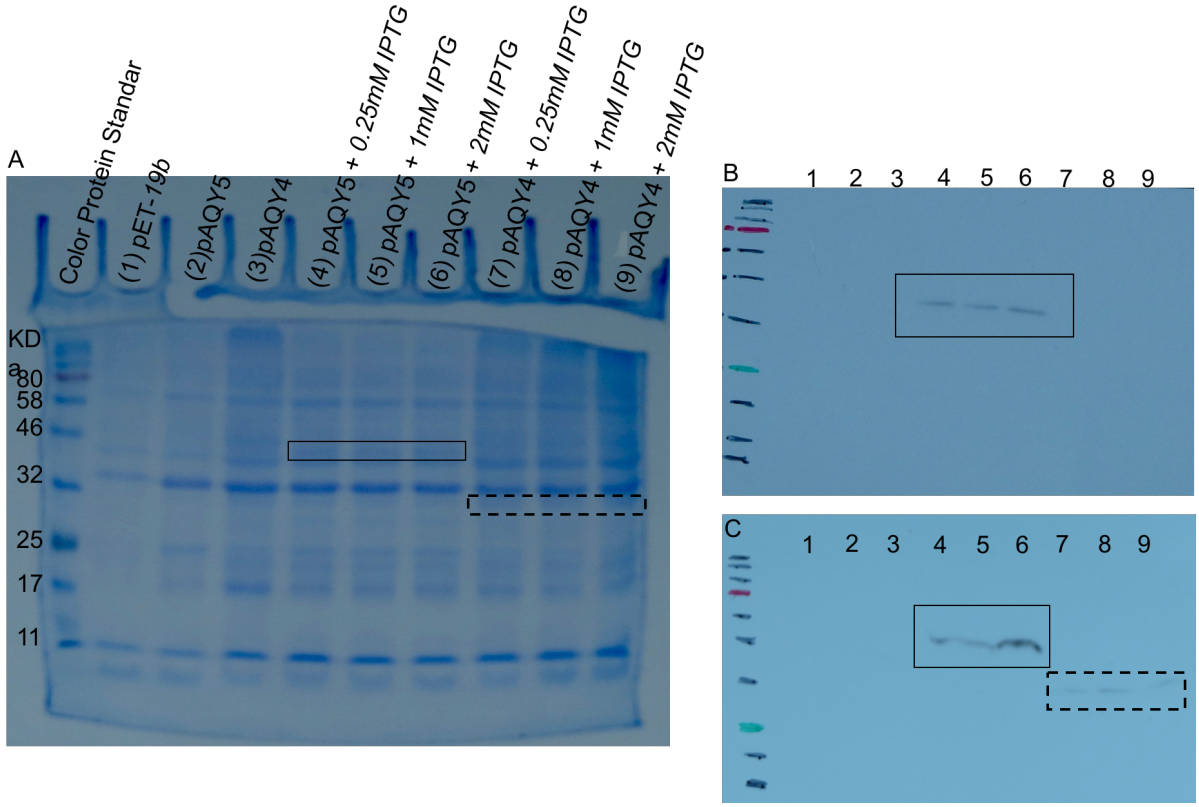

Figure 7.1. SDS gel and western blots from *E. coli* expressing His-tagged Orf1187 and FloR. Samples in wells 1 to 3 were treated with 50mM sodium phosphate buffer (pH: 7.8), 0.3 M NaCl and 1X protease inhibitor, grown for 8h and protein expression was induced after 4h with 2mM IPTG. Samples in wells 4 to 9 were grown similarly, treated with an alternative Lysis Buffer (50 mM Tris HCl pH: 8, 200 mM NaCl, 10 % glycerol, 1 mM imidazole and 1X protease inhibitor) and induced with different IPTG concentrations (see image). **A.** SDS page showing whole-cell soluble protein pattern, zones corresponding to the proteins detected in western blots (B and C) are continuous lines (for Orf1187) and dashed lines (FloR). Western blots with (B) 5 μl and (C) 20 μl of samples previously described.

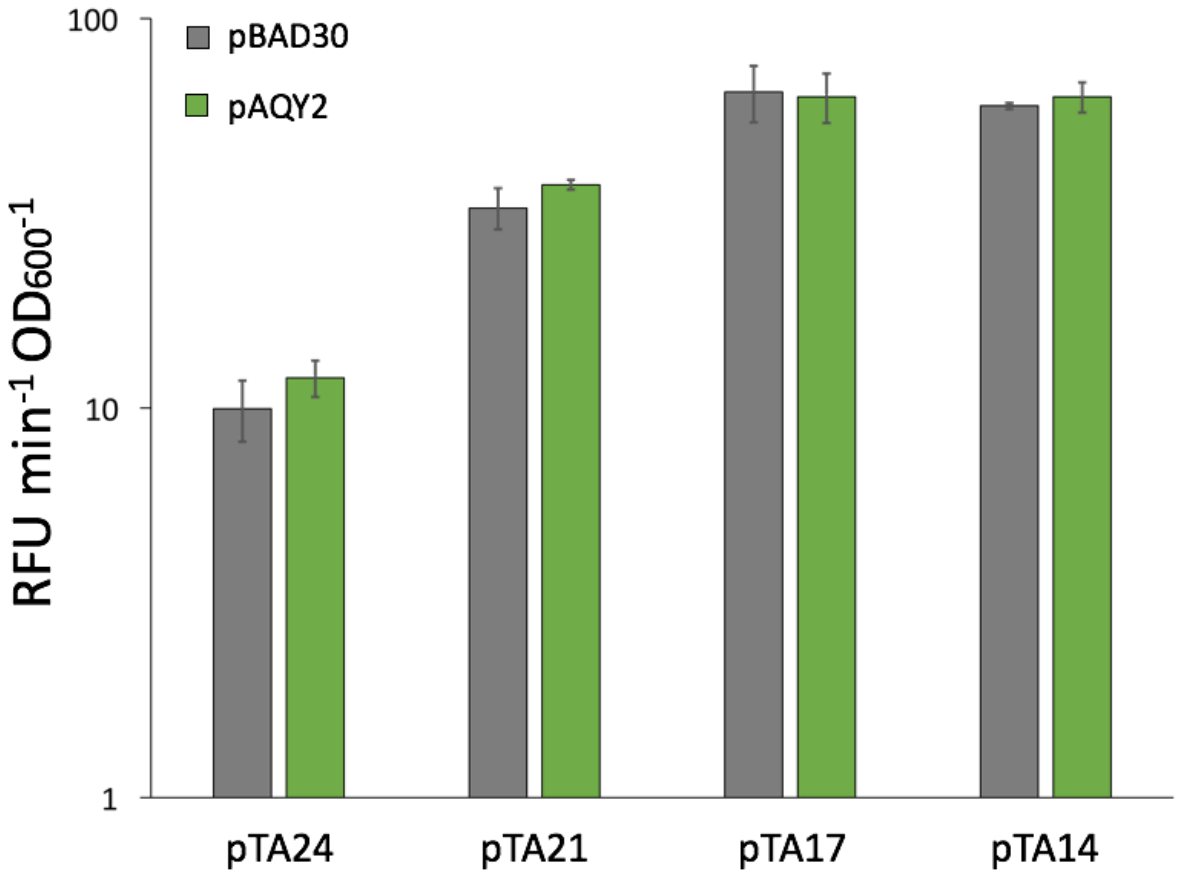

Figure 7.2. Activity of the *pigX*, *pigQ*, *smaR* and *rap* promoters under FloR heterologous expression. The β Galactosidase activity was measured in *E. coli* DH5α carrying plasmids with a *lacZ* reporter fusion under control of the *pigX*, *pigQ*, *smaR* and *rap* promoters (pTA24, pTA21 and pTA17 and pTA14, respectively) from S39006 with either pBAD30 or pAQY2 (pBAD30 + *floR*). The data represent the average and standard deviation (error bars) of three biological replicates.